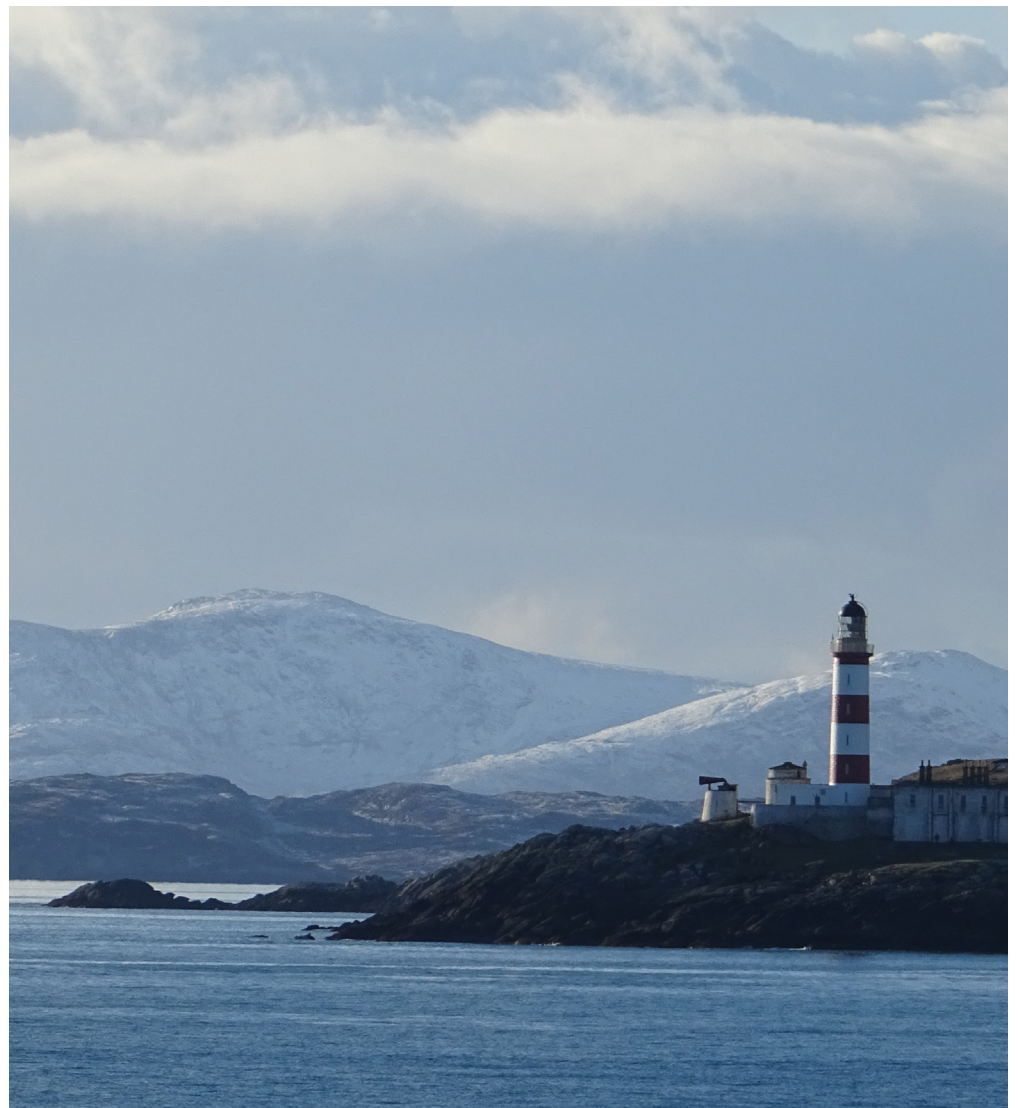


# ICES Report on Ocean Climate 2020

Volume 356 | November 2022

ICES COOPERATIVE  
RESEARCH REPORT

RAPPORT  
DES RECHERCHES  
COLLECTIVES



## International Council for the Exploration of the Sea Conseil International pour l'Exploration de la Mer

H. C. Andersens Boulevard 44–46  
DK-1553 Copenhagen V  
Denmark  
Telephone (+45) 33 38 67 00  
Telefax (+45) 33 93 42 15  
[www.ices.dk](http://www.ices.dk)  
[info@ices.dk](mailto:info@ices.dk)

Series editor: Emory Anderson  
Prepared under the auspices of ICES Working Group on Ocean Hydrography (WGOH)

ISBN number: 978-87-7482-975-1

ISSN number: 2707-7144

Cover image: © Crown Copyright / Marine Scotland. All rights reserved.

This document has been produced under the auspices of an ICES Expert Group or Committee.  
The contents therein do not necessarily represent the view of the Council.

© 2022 International Council for the Exploration of the Sea.

This work is licensed under the Creative Commons Attribution 4.0 International License (CC BY 4.0). For citation of datasets or conditions for use of data to be included in other databases, please refer to ICES data policy.



# ICES Cooperative Research Report

Volume 356 | November 2022

## ICES Report on Ocean Climate

### Editors

Cesar González-Pola • Karin M. H. Larsen • Paula Fratantoni •  
Agnieszka Beszczynska-Möller

Recommended format for purpose of citation:

González-Pola, C., Larsen, K. M. H., Fratantoni, P., and Beszczynska-Möller, A.  
(Eds.). 2022. ICES Report on ocean climate 2020. ICES Cooperative Research  
Reports Vol. 356. 121 pp. <https://doi.org/10.17895/ices.pub.19248602>



**ICES**  
**CIEM**

International Council for  
the Exploration of the Sea  
Conseil International pour  
l'Exploration de la Mer

# Contents

I	Foreword .....	i
1	Introduction .....	1
	Highlights for the North Atlantic 2020 .....	1
	Highlights for the North Atlantic atmosphere in winter 2019/2020 .....	2
	Initial outlook for 2021 .....	2
2	Summary of upper ocean conditions in 2020 .....	3
	2.1 <i>In situ</i> stations and sections.....	3
	2.2 Sea surface temperature.....	9
	2.3 ARGO gridded temperature and salinity fields .....	10
	2.3.1 ISAS: Gridded temperature and salinity fields.....	10
	2.3.2 Highlights of 2020 .....	11
	2.3.3 Surface layers .....	12
	Seasonal patterns of T/S 2020 anomaly.....	12
	Seasonal cycle and monthly anomalies.....	14
	Interannual variability and long-term tendency .....	15
	Mixed-layer depth.....	16
	2.3.4 Intermediate and deep layers .....	18
	2.4 Subpolar Gyre Index.....	19
3	The North Atlantic atmosphere .....	22
	3.1 The North Atlantic Oscillation NAO index .....	22
	3.2 Sea level pressure and wind speed .....	23
	3.3 Surface air temperature .....	27
	3.4 Outlook beyond 2020.....	27
4	Detailed area descriptions, part I: The upper ocean .....	29
	Introduction.....	29
	4.1 West Greenland .....	31
	4.2 Labrador Sea .....	33
	Oceanographic monitoring of the Labrador Sea .....	34
	Deep convection, water ventilation, and hydrographic trends .....	35
	Hydrographic changes in the Labrador Sea over the past 80 years .....	37
	Conclusion .....	37
	4.3 Newfoundland-Labrador Shelf .....	38
	4.4 Gulf of St. Lawrence .....	41
	4.5 Scotian Shelf .....	43
	4.6 Northeast US continental shelf .....	46
	4.7 Icelandic waters .....	52
	4.8 Bay of Biscay and the Iberian Coast .....	55
	4.9 Gulf of Cadiz .....	58

4.10	Canary Basin .....	60
4.11	Southwest Approaches .....	62
4.12	Celtic Seas .....	65
4.13	Rockall Trough.....	66
4.14	Hatton-Rockall Basin .....	68
4.15	Iceland Basin .....	69
4.16	Irminger Sea .....	70
4.17	Faroese waters and the Faroe Shetland Channel .....	72
4.18	North Sea .....	76
	Annual conditions .....	77
	Summer conditions .....	79
4.19	Skaggerak, Kattegat, and the Baltic Sea .....	81
4.20	Norwegian Sea .....	85
4.21	Barents Sea .....	88
4.22	Fram Strait.....	90
5	Detailed area descriptions, part II: The intermediate and deep ocean .....	95
	Introduction.....	95
5.1	Nordic Seas.....	96
5.1.1	Greenland Sea .....	96
5.1.2	Norwegian Sea .....	97
5.1.3	Iceland Sea .....	99
5.2	North Atlantic.....	99
5.2.1	Iceland-Scotland Ridge overflow waters.....	99
5.2.2	Iceland Basin .....	100
5.2.3	Rockall Trough.....	102
5.2.4	Irminger Basin .....	102
5.2.5	Labrador Basin.....	103
5.2.6	West Iberian margin.....	105
5.2.7	Gulf of Cadiz .....	108
5.2.8	Canary Basin .....	109
	References.....	111
	Annex 1: Contact information for authors by section.....	114
	Annex 2: List of abbreviations and acronyms .....	119

## I Foreword

We are very pleased to present the International Council for the Exploration of the Sea (ICES) report on ocean climate (IROC) 2020. The IROC production is a credit to the tireless efforts and long-term commitment of the international experts who are members of the ICES Working Group on Oceanic Hydrography (WGOH). This report provides a combined analysis of the ocean-hydrography observations that are regularly collected at multiple stations in the ICES regions of the North Atlantic and its adjacent seas. The best possible overview of ocean changes is presented based on measurements of temperature and salinity over time, with several time-series dating back from multiple decades to over a century.

The Covid-19 pandemic affected the IROC 2020 service delivery, due to continued disruptions and travel restrictions in many countries that hampered ocean observing activities. Expert group members encountered varying challenges, including personal experiences (e.g. school closures), impacts on data-collection efforts, and issues accessing oceanographic sites. During the COVID-19 pandemic, WGOH meetings were held online, with virtual gatherings in spring and autumn 2021. These online meetings provided the opportunity for more members to engage in discussions. WGOH welcomed five new members from Germany, Ireland, and UK in 2021. While the WGOH membership (61) has increased, we would like to extend our heartfelt gratitude to colleagues who stepped down recently. In particular, special thanks to Penny Holliday [National Oceanographic Centre (NOC), UK] and Holger Klein (Federal Maritime and Hydrographic Agency, Germany) for their many years of service organizing oceanographic campaigns and providing highly valued contributions to the IROC and wider WGOH activities.

We envisage that 2022 will be a dynamic year for WGOH members, with the upcoming UN Decade of Ocean Science for Sustainable Development endorsed conference “ICES/NAFO 4th Decadal Variability of the North Atlantic and its Marine Ecosystems: 2010–2019 Symposium” scheduled for 26–28 April in Bergen, Norway. The expert group will also co-convene two sessions at the ICES Annual Science Conference in September 2022 on “Oceanography and ecosystems in the North Atlantic: Science and operational services” (theme session) and “Advancing the pathways for oceanography to ecosystem science and advice” (network session). Finally, we also plan a number of other activities including efforts to improve the IROC content (e.g. standardized maps), document the protocols for data analysis in each region, continue to identify and respond to our stakeholder needs, and increase our efforts to work with the wider global ocean observing community.

The IROC was written by the following WGOH members and collaborators: Jon Albretsen (IMR, Bergen, Norway); Wilken-Jon von Appen (AWI, Bremerhaven, Germany); Barbara Bex (MSS, Aberdeen, UK); Agnieszka Beszczynska-Möller (IOPAN, Sopot, Poland); Léon Chafik (MISU, Stockholm, Sweden); Boris Cisewski (TI-SF, Bremerhaven, Germany); Caroline Cusack (Marine Institute, Galway, Ireland); Frédéric Cyr (DFO, St. John’s, Newfoundland, Canada); Eoghan Daly (ICRAG, Ireland); Magnus Danielsen (MFRI, Iceland); Damien Desbruyères (Ifremer/LOPS, Brest, France); Angelika Dummermuth (MARUM, Germany); Stephen Dye (Cefas, Lowestoft, UK); Almudena Fontán (AZTI, San Sebastian, Spain); Paula Fratantoni (NOAA, Woods Hole, MA, USA); Peter Galbraith (DFO, Mont-Joli, Quebec, Canada); César González-Pola (IEO, Gijón, Spain); Hjálmar Hátún (FAMRI, Tórshavn, Faroes); David Hebert (DFO, Dartmouth, Nova Scotia, Canada); Jenny Hindson (MSS, Aberdeen, UK); Billy Hunter (AFBI, UK); Randi Ingvaldsen (IMR, Bergen, Norway); Sam Jones (SAMS, Oban, UK); Johannes Karstensen (GEOMAR, Germany); Dagmar Kieke (IUP, Germany); Manuela Köllner (BSH, Hamburg, Germany); Nicolas Kolodziejczyk (UBO, Brest, France); Karin Margretha H. Larsen (FAMRI, Tórshavn, Faroes); K. Latarius (BSH, Hamburg, Germany); C. Layton (DFO, Dartmouth, Nova Scotia, Canada); Taavi Liblik (TalTech, Tallinn, Estonia); Johanna Linders

(SMHI, Göteborg, Sweden); Peter Loewe (BSH, Hamburg, Germany); Kieran Lyons (Marine Institute, Galway, Ireland); Kjell-Arne Mork (IMR, Bergen, Norway); Sólveig R. Ólafsdóttir (MFRI, Reykjavik, Iceland); Hjalte Parner (ICES, Copenhagen, Denmark); Ricardo Sánchez-Leal (IEO, Cadiz, Spain); Tim Smyth (PML, Plymouth, UK); Alexander Trofimov (PINRO, Murmansk, Russian Federation); Victor Valencia (AZTI, San Sebastian, Spain); Pedro Vélez-Belchí (IEO, Tenerife, Spain); Tycjan Wodzinowski (MIR-PIB, Gdynia, Poland), and Svein Østerhus (NORCE, Bergen, Norway).

For a list of authors by section, including full affiliation and contact details, see Annex 1.

Technical assistance during the assembly of this report was provided by Eneko Aierbe and Rocío Graña (IEO, Gijón, Spain).



# 1 Introduction

The IROC combines decades of ocean observations across the North Atlantic ICES regions to describe the current status of sea temperature, salinity, and atmospheric conditions, as well as observed trends and recent variability. The IROC production focuses the main efforts from ICES Working Group on Oceanic Hydrography (WGOH; González-Pola *et al.*, 2019).

Long time-series of ocean properties are rare for the surface ocean and even more uncommon for the deep ocean. The North Atlantic region is unique in that it has a relatively large number of locations where oceanographic data have been collected repeatedly for multiple years or decades. The longest records extend back more than a century.

Section 1 synthesizes information from a selection of the longest available time-series into an overview of changes across the ICES Area. The main focus of this report is the observed variability in the upper ocean (upper 1000 m), and a summary of upper ocean conditions is provided in [Section 2](#). [Section 2.3](#) provides gridded fields constructed by optimal analysis of Argo float data, distributed by the Coriolis data centre in France. Finally, [Section 2.4](#) provides an estimate of the Subpolar Gyre Index. [Sections 4](#) and [5](#) contain short regional summaries on the variability of North Atlantic upper, and intermediate and deep waters, respectively. While the focus of the report is on temperature and salinity measurements, additional complementary datasets are included throughout, such as sea level pressure (SLP), air temperature, and ice cover.

The data presented here represent the cumulative knowledge collected by many individuals and institutions over decades of observations. Much of the data included in this report, and additional data, are available to download via a web tool<sup>1</sup>. A more detailed overview of particular regions and a full description of some of the datasets used to develop the time-series presented in this report can be found in the annual meeting reports of WGOH<sup>2</sup>.

WGOH met via video conference on 13–15 April 2021 to review oceanographic conditions in the North Atlantic in 2020. The following highlights emerged from the joint analysis of the available hydrographic time-series.

## Highlights for the North Atlantic 2020

- The fresh anomaly in the eastern North Atlantic persisted, with a slow-down or partial reversal of freshening evident in some areas. The strong freshening trend is evident downstream both towards the Arctic and the subtropics.
- While Subpolar Gyre surface waters were moderately cooler than the 2006–2015 climatology, a warming tendency has been confirmed since 2016.
- Arctic waters continue to freshen and warm, with salinity significantly lower than average in the Nordic Seas, Fram Strait, and the upper waters (200–400 m) of the Irminger Sea. A large drop in salinity was detected in the Denmark Strait Overflow Water (DSOW) and along the Greenland slopes below 2800 m.
- Lowest salinities within the upper 400 m in the last three decades were recorded in the Bay of Biscay. Notable freshening persists off the Iberian coast.

---

<sup>1</sup> <https://ocean.ices.dk/iroc>

<sup>2</sup> <https://www.ices.dk/community/groups/Pages/WGOH.aspx>

- Regarding deep waters, temperature and salinity remained stable and high in the Irminger Sea (above 2000 m), presented little change in the Iceland and Iberian basins, and showed warming and salinification in Rockall Trough. Moderately deep winter convection in the Labrador Sea did not exceed 1700 m in 2020 for the second consecutive year.
- Northwest Atlantic shelf waters remained warm. Warming was evident in surface and deep waters, with a > 100-year record high in the Gulf of St. Lawrence.
- North Sea surface water temperature remained high, while high temperatures were observed in the Baltic Sea throughout the entire water column. North Sea salinity increased, and central Baltic Sea surface salinity has been at a record high since the late 1980s.
- Sea ice coverage was low in most regions, with a record low sea-ice extent registered in the Baltic Sea since records began in the early 18th century.

### **Highlights for the North Atlantic atmosphere in winter 2019/2020**

- Winter 2019/2020 was the second consecutive winter with a strong positive North Atlantic Oscillation (NAO), and it was the seventh consecutive positive winter NAO.
- Air temperatures were relatively warm across Europe, northeast America, and the Nordic, Baltic, and Labrador seas.
- There were colder-than-average air temperatures over the central North Atlantic.
- Wind speeds across the region in winter 2019/2020 were generally higher than average, and areas from the west of Ireland and across the UK, North Sea, and Baltic Sea experienced particularly strong southwesterly winds throughout much of winter.

### **Initial outlook for 2021**

- The NAO index for December 2020–March 2021 is likely to be a strong negative, the first since 2013. The storm track from the USA east coast, across the Flemish Cap, and through to Norway and the Nordic Seas, will experience particularly weak winds throughout the season.
- Experimental seasonal forecasts predict that surface temperatures are likely to be warmer than average across the region in autumn 2021. However, waters to the northwest of Ireland and south of Cape Farewell are more likely to be near average than in other areas.

## 2 Summary of upper ocean conditions in 2020

This section summarizes conditions in the upper layers of the North Atlantic during 2020 using data from (i) a selected set of sustained observations, (ii) gridded sea surface temperature (SST) data, and (iii) gridded vertical profiles of temperature and salinity from Argo floats.

### 2.1 *In situ* stations and sections

Where *in situ* section and station data are presented in the summary tables and figures, normalized anomalies have been provided to allow better comparison of trends across regions (Figures 2.1, 2.2, and 2.3, and Table 2.1). The anomalies have been normalized by dividing the values by the standard deviation (s.d.) of the data during 1981–2010 (or the closest time-period available). A value of +2 thus represents temperature or salinity data measuring 2 s.d. higher than normal.

#### Information Box 2.1 - Definitions

**Sustained observations or time-series:** Regular measurements of ocean temperature and salinity made over 10–100 years. Most measurements are made one to four times a year, but some are made more frequently.

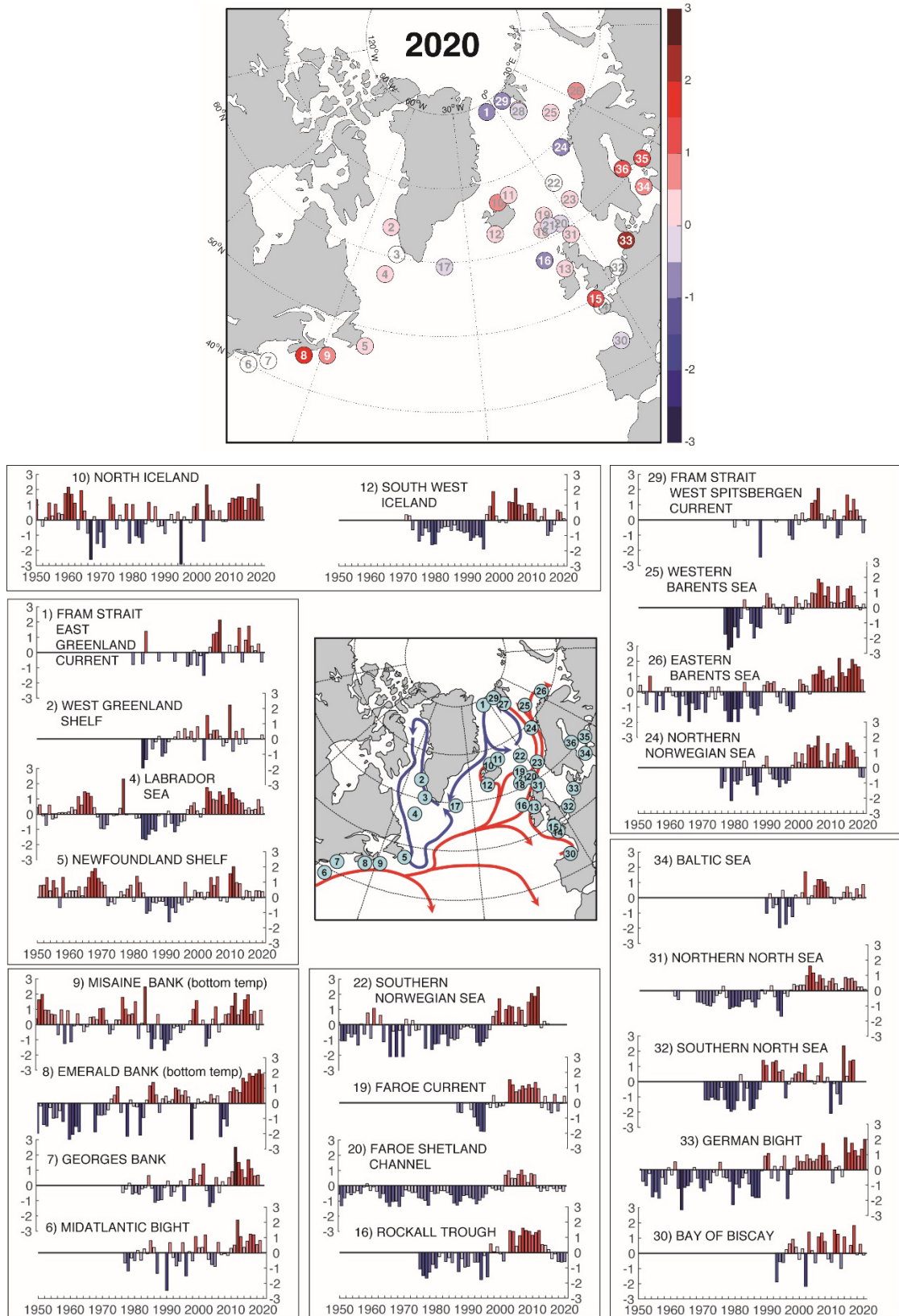
**Anomalies:** Mathematical differences between each individual measurement and the average value of temperature, salinity, or other variables at each location and time. Positive anomalies in temperature and salinity imply warm or saline conditions; negative anomalies imply cool or fresh conditions.

**Normalized anomalies:** anomalies that have been normalized by dividing the values for a given year by the standard deviation (s.d.) of the 1981–2010 data (or the closest time-period available). A value of +2 thus represents temperature or salinity data measuring 2 s.d. higher than normal.

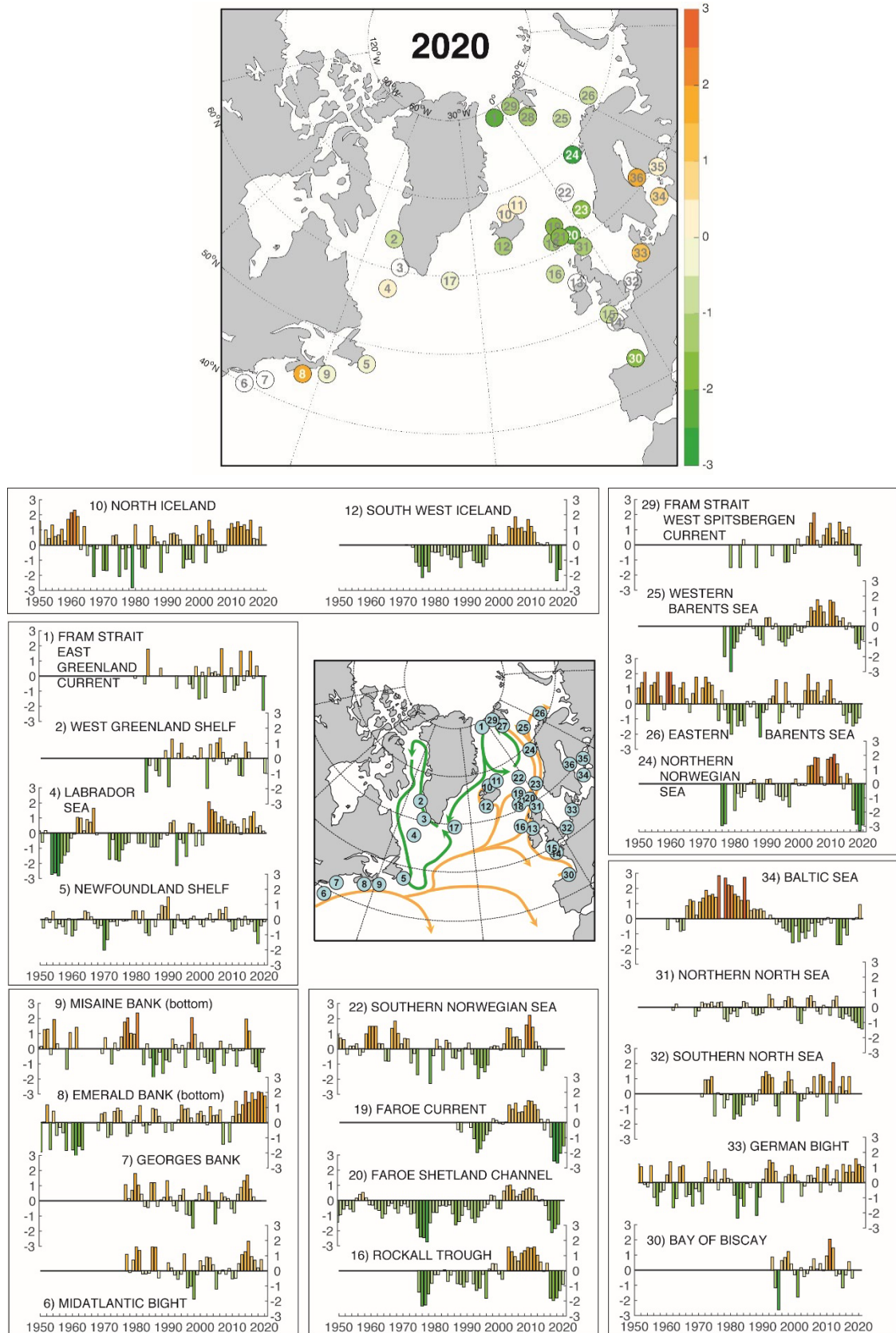
**Seasonal cycle:** The short-term changes at the surface of the ocean brought about by the passing of the seasons - the ocean surface is cold in winter and warms through spring and summer. Temperature and salinity changes caused by the seasonal cycle are usually much greater than the prolonged year-to-year changes we describe here.



Photo: Tomasz Szumski, Marine Institute, Galway, Ireland



**Figure 2.1.** Upper ocean temperature anomalies at selected locations across the North Atlantic. The anomalies are normalized with respect to the standard deviation (s.d.; e.g. a value of + 2 indicates 2 s.d. above normal). Upper panels: maps of conditions in 2020. Lower panels: time-series of normalized anomalies at each of the selected stations. Colour intervals: 0.5 s.d.; red: positive/warm; blue: negative/cool. More details can be found in [Section 4](#).



**Figure 2.2.** Upper ocean salinity anomalies at selected locations across the North Atlantic. The anomalies are calculated relative to a long-term mean and normalized with respect to the s.d. (e.g. a value of + 2 indicates 2 s.d. above normal). Upper panel: map of conditions in 2020. Lower panels: time-series of normalized anomalies at each of the selected stations. Colour intervals: 0.5 s.d.; orange: positive/saline; green: negative/fresh. More details can be found in Section 4.

Table 2.1. Changes in temperature (upper panel) and salinity (lower panel) at selected stations in the North Atlantic region during the past decade, 2011–2020. The index numbers on the left can be used to cross-reference each point with information in [Figures 2.1](#) and [2.2](#), and [Table 2.2](#). Unless specified, these are upper-layer anomalies. The anomalies are normalized with respect to the s.d. (e.g. a value of +2 indicates that the data observation of temperature or salinity for that year was 2 s.d. above normal). Blank boxes indicate that data were unavailable for a particular year at the time of publication. Note that no salinity data are available for station 13. Colour intervals: 0.5 s.d.; red: warm; blue: cold; orange: saline; green: fresh.

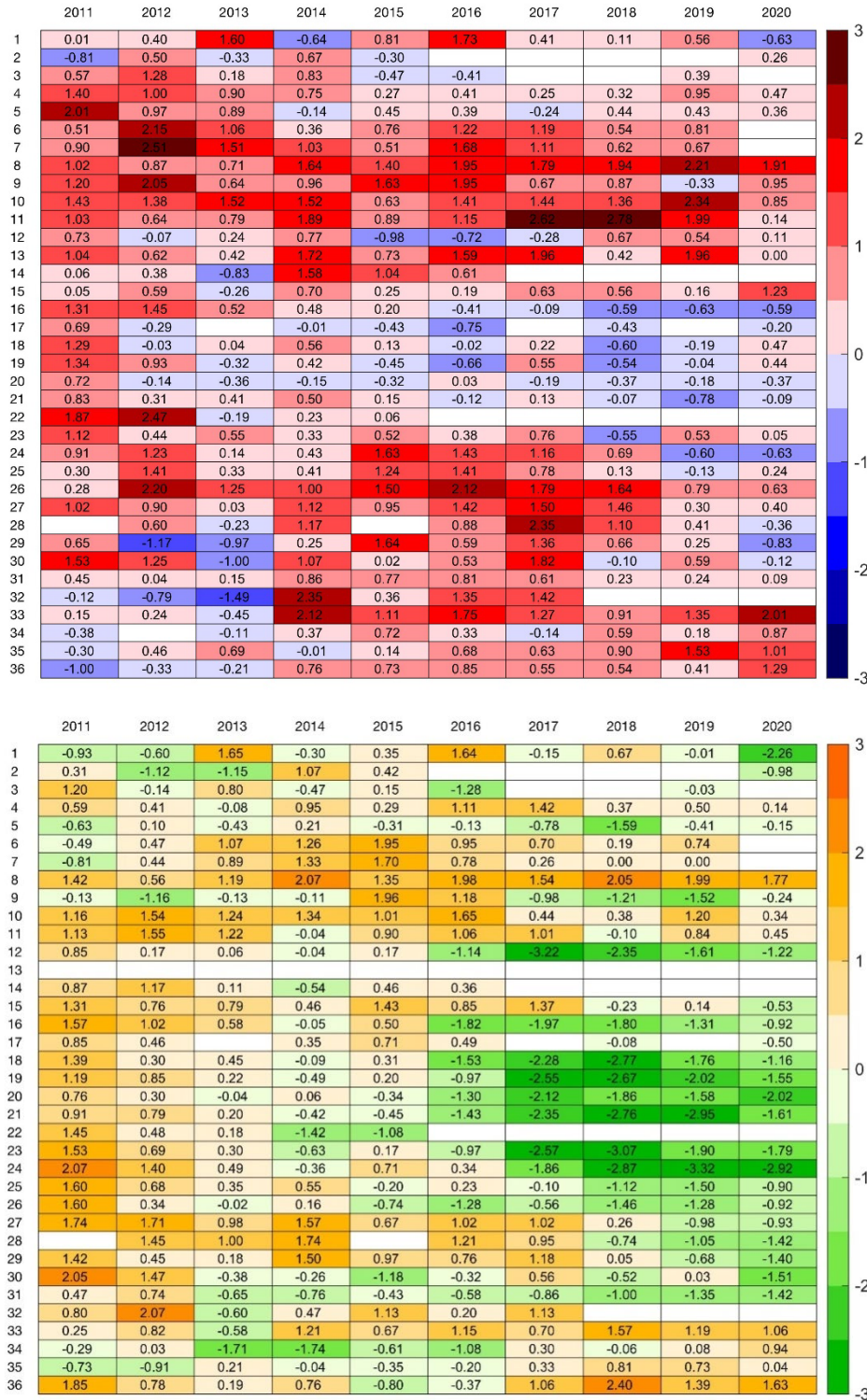


Table 2.2. Details of the datasets included in [Figures 2.1](#) and [2.2](#), and [Table 2.1](#). Blank boxes indicate that no information was available for the area at the time of publication. T: temperature, S: salinity. Some data are calculated from an average of more than one station; in such cases, the latitudes and longitudes presented here represent a nominal midpoint along that section.

Index	Description	Section	Measurement depth (m)	Reference period	Lat	Lon	Mean T	s.d.	Mean S	s.d.
1	Fram Strait East Greenland Current	4.21	50–500	1983–2010	78.83	–6.00	0.69	0.57	34.650	0.135
2	Fylla Section–Station 4–Greenland Shelf	4.1	0–50	1983–2010	63.88	–53.37	2.64	1.10	33.162	0.392
3	Cape Desolation Section–Station 3–Greenland Shelf	4.1	75–200	1983–2010	60.47	–50.00	5.72	0.66	34.923	0.062
4	Central Labrador Sea	4.2	15–50	1981–2010	57.07	–50.92	4.68	0.69	34.635	0.176
5	Station 27–Newfoundland Shelf T–Canada	4.3	0–175	1981–2010	47.55	–52.59	0.33	0.39	31.946	0.166
6	NE US continental shelf–Northern Middle Atlantic Bight	4.5	1–30	1981–2010	40.00	–71.00	11.36	0.94	32.710	0.430
7	NE US continental shelf–Northwest Georges Bank	4.5	1–30	1981–2010	41.50	–68.30	10.00	0.79	32.580	0.270
8	Emerald Basin–Central Scotian Shelf–Canada	4.4	250 (near bottom)	1981–2010	44.00	–63.00		0.83		0.151
9	Misaine Bank–Northeast Scotian Shelf–Canada	4.4	100 (near bottom)	1981–2010	45.00	–59.00		0.63		0.134
10	Siglunes Station 2–4 – North Iceland–North Icelandic Irminger Current–Spring	4.6	50–150	1981–2010	67.00	–18.00	3.41	0.98	34.859	0.108
11	Langanes Station 2–6 – Northeast Iceland–East Icelandic Current–Spring	4.6	0–50	1981–2010	67.50	–13.50	1.22	0.61	34.729	0.067
12	Selvogsbanki Station 5–Southwest Iceland–Irminger Current–Spring	4.6	0–200	1981–2010	63.00	–21.47	7.88	0.47	35.187	0.049
13	Point 33–Astan	4.10	5	1998–2010	48.78	–3.94	12.79	0.34	35.206	0.112
14	Western Channel Observatory (WCO)–E1–UK	4.10	0–40	1981–2010	50.03	–4.37	12.43	0.93	35.200	0.100
15	Malin Head Weather Station	4.11	Surface	1981–2010	55.37	–7.34	10.25	0.57		
16	Ellett Line–Rockall Trough–UK (Section Average)	4.12	30–800	1981–2010	56.75	–11.00	9.35	0.28	35.351	0.036
17	Central Irminger Sea Sub Polar Mode Water	4.15	200–400	1991–2010	59.40	–36.80	4.35	0.53	34.900	0.031
18	Faroe Bank Channel–West Faroe Islands	4.16	Upper layer high salinity core	1988–2010	61.40	–8.30	8.80	0.36	35.302	0.043
19	Faroe Current–North Faroe Islands (Modified North Atlantic Water)	4.16	Upper layer high salinity core	1987–2010	63.00	–6.00	8.11	0.39	35.249	0.043

**Table 2.2. (continued)**

Index	Description	Section	Measurement depth (m)	Reference period	Lat	Lon	Mean T	s.d.	Mean S	s.d.
20	Faroe Shetland Channel–Shetland Shelf (North Atlantic Water)	4.16	Upper layer high salinity core	1981–2010	61.00	–3.00	9.95	0.47	35.398	0.051
21	Faroe Shetland Channel–Faroe Shelf (Modified North Atlantic Water)	4.16	Upper layer high salinity core	1981–2010	61.50	–6.00	8.32	0.54	35.256	0.055
22	Ocean Weather Station Mike	4.19	50	1981–2010	66.00	2.00	7.71	0.44	35.176	0.036
23	Southern Norwegian Sea–Svinøy Section–Atlantic Water	4.19	50–200	1981–2010	63.00	3.00	8.04	0.39	35.234	0.039
24	Central Norwegian Sea–Gimsøy Section–Atlantic Water	4.19	50–200	1981–2010	69.00	12.00	6.89	0.34	35.154	0.031
25	Fugløya–Bear Island Section–Western Barents Sea–Atlantic Inflow	4.19	50–200	1981–2010	73.00	20.00	5.55	0.46	35.078	0.035
26	Kola Section–Eastern Barents Sea	4.20	0–200	1981–2010	71.50	33.50	4.22	0.52	34.771	0.056
27	Greenland Sea section – West of Spitsbergen 76.5N	4.19	200	1996–2010	76.50	10.50	3.19	0.61	35.058	0.043
28	Northern Norwegian Sea–Sorkapp Section–Atlantic Water	4.19	50–200	1981–2010	76.33	10.00	4.08	0.60	35.073	0.038
29	Fram Strait–West Spitsbergen Current	4.21	50–500	1983–2010	78.83	7.00	3.11	0.69	35.027	0.038
30	Santander Station 6 (Shelf Break)–Bay of Biscay–Spain	4.7	0–30	1993–2010	43.71		15.74	0.32	35.460	0.160
31	Fair Isle Current Water (waters entering North Sea from Atlantic)	4.17	0–100	1981–2010	59.00		9.93	0.61	34.874	0.132
32	Section Average–Felixstowe–Rotterdam–52 N	4.17	Surface	1981–2010	52.00	3.00		0.72		0.212
33	North Sea–Helgoland Roads	4.17	Surface	1981–2010	54.18	7.90	10.26	0.75	32.096	0.568
34	Baltic Proper–East of Gotland–Baltic Sea	4.18	Surface T Surface S	1990–2010 1987–2010	57.50	19.50	9.27	1.03	7.172	0.196
35	Baltic–LL7–Baltic Sea	4.18	70	1991–2010	59.51	24.50	3.97	0.73	7.961	0.666
36	Baltic–SR5–Baltic Sea	4.18	110	1991–2010	61.05	19.35	3.27	0.58	6.428	0.141

## 2.2 Sea surface temperature

Satellites have been measuring SST for approximately 40 years, which has enabled the creation of gridded datasets. [Figure 2.3](#) shows seasonal SST anomalies for 2020 extracted from the Optimum Interpolation SST dataset version 2 (OISST.v2) provided by the NOAA–CIRES Climate Diagnostics Center in the USA. The data may be less reliable at high latitudes, where *in situ* data are sparse and satellite data are hindered by cloud cover. Regions with > 50% ice cover over the averaging period appear blank.

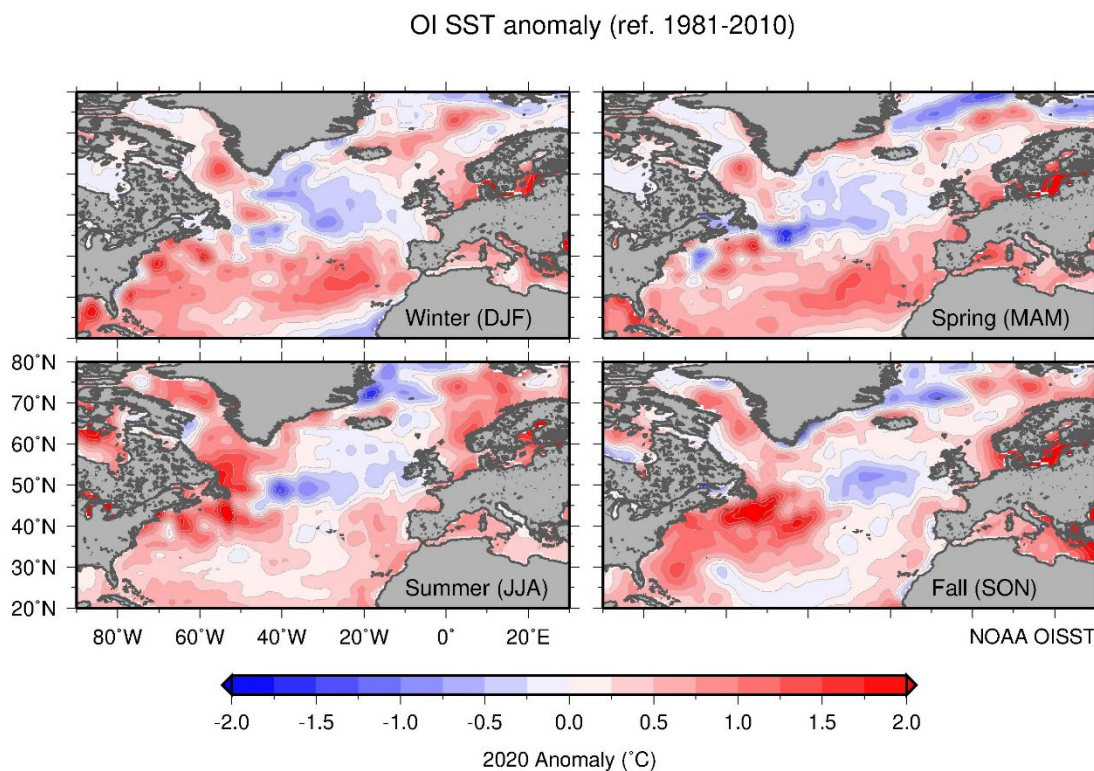


**Figure 2.3.** Maps of seasonal sea surface temperature anomalies (°C) over the North Atlantic for 2020 from the NOAA OISST.v2 dataset provided by the NOAA–CIRES Climate Diagnostics Center, USA. The data are produced on a 1° grid from a combination of satellite and *in situ* temperature data. The colour-coded temperature scale is the same in all panels, and the anomaly is calculated with respect to mean conditions for 1981–2010. Regions with ice cover for > 50% of the averaging period appear blank.



## 2.3 ARGO gridded temperature and salinity fields

*N. Kolodziejczyk and D. Desbruyères*

The ARGO network of profiling floats monitors large-scale global ocean hydrological variability (<http://www.argo.ucsd.edu>). Argo data are transmitted in real time and rapidly made available by the two Global Data Assembly Centres (Argo-GDAC). Delayed-mode data undergo expert calibration and are delivered later, on average with a delay between one and several years. In the North Atlantic, temperature and salinity conditions have been adequately described over the upper 2000 m since 2002, when the Argo network began to be implemented. The dataset is thus suitable for an overview of deep-sea oceanographic conditions in this basin, and provides the general context for the data collected at stations and sections, mostly located at the periphery of the basin.

### 2.3.1 ISAS: Gridded temperature and salinity fields

Temperature and salinity gridded fields are estimated on a regular  $0.5^\circ$  grid using the *In Situ* Analysis System (ISAS; Gaillard *et al.*, 2016). The dataset used for generating ISAS gridded fields is downloaded from the Coriolis Argo GDAC1. It should be noted that Coriolis assembles many types of data transmitted in real time, merging the Argo dataset with data collected by the Global Telecommunications System (GTS), such as data from moorings and CTDs, and data on marine animals. However, the Argo dataset remains the main contributor to the ISAS gridded fields in the open ocean. The ISAS optimal interpolation (OI) procedure is as follows: the *in-situ* temperature and salinity profiles are vertically interpolated on 152 standard levels between the surface and 2000 m depth. The horizontal mapping to produce gridded fields is performed at each standard level independently. The mapping method is based on an optimal estimation algorithm and includes a horizontal smoothing through specified covariance scales. The results presented here were produced with the last version of ISAS. The reference state used in the OI process was computed as the mean of a 2005–2012 analysis (using ISAS13; Gaillard *et al.*, 2016), and the *a priori* variances were computed from the same dataset. Two ISAS gridded temperature and salinity products are used:

- For the period 2002–2015, ISAS15 product is used (using ISASv7 tool; Kolodziejczyk *et al.*, 2017). For this period, Argo and *in situ* CTD from marine mammals and tropical mooring Array are used, extra quality control is applied to *in situ* profiles delayed mode and remaining real-time data before they are included in the analysis. ISAS15 product is the highest quality product in delayed mode.
- The last years of the analysed series, i.e. 2016–2020, use the Near Real Time (NRT) dataset prepared by Coriolis at the end of each month from real-time data. For this period, data are interpolated using ISASv6 tool including only real-time mode data (i.e. only from automatic QC processing). Because Argo salinity data require advanced quality checks and validation, NRT salinity fields have to be used with caution. Therefore, time-series of monthly salinity anomalies are not considered herein, and the focus is rather made on their seasonally and annually averaged patterns.

The ISAS interpolated fields are used to compute seasonal to interannual maps of temperature and salinity anomalies averaged within an upper layer (0–100 m depth) and intermediate and deep layers (700–1000 m; 1000–1500 m; 1500–2000 m depth). Note that the temperature and salinity anomalies throughout this section are computed using the climatological ISAS15 fields

(2006–2015). In order to compute temperature and salinity anomalies, the climatological monthly temperature and salinity fields are removed from each monthly ISAS field over the period 2002–2020. Note that the temperature and salinity fields are blanked in regions with water depths deeper than 1000 m, where the Argo coverage is either too sparse or unavailable. The seasonal time-windows are defined as winter (January–March; JFM), spring (April–June; AMJ), summer (July–September; JAS), and autumn (October–December; OND). The seasonal and interannual variability is monitored in selected areas ([Figure 2.4](#)), which are representative of the North Atlantic polar (Greenland Sea), subpolar (Labrador Sea and Irminger Basin), Eastern Atlantic), and subtropical variability (Gulf Stream, Azores). Within each selected area, the number of temperature and salinity profiles used in monthly objective analyses is shown in [Figure 2.5](#). This provides an assessment of the robustness of the temperature and salinity time-series in each area.

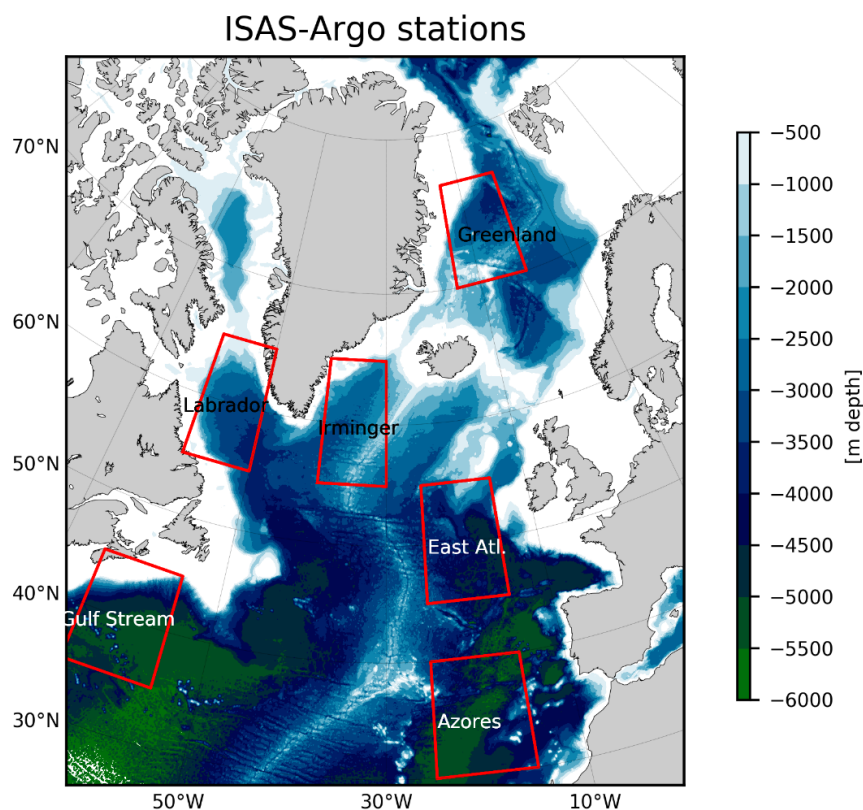


**Figure 2.4.** Location of the six areas in the North Atlantic: Azores region, Gulf Stream region, eastern Atlantic region (East Atl.; Iceland and Rockall basins), Irminger Sea, Labrador Sea, and Greenland Sea. These areas are used for computing averaged temperature and salinity profile time-series.

### 2.3.2 Highlights of 2020

- In 2020, the surface Subpolar Gyre was moderately colder than 2006–2015 climatology, but still maintained the warming tendency observed since 2016. The Subtropical Gyre remained warmer than average conditions (2006–2015; [Figures 2.6](#), [2.7](#), and [2.8](#)).
- In 2020, the intermediate layers of the Nordic Seas and subtropical basins continued to warm. In the Subpolar Gyre, the significant cooling trend of the intermediate layers observed since 2012 ended in the Labrador Sea and slowed in the Irminger Sea ([Figures 2.11](#) and [2.12](#)).

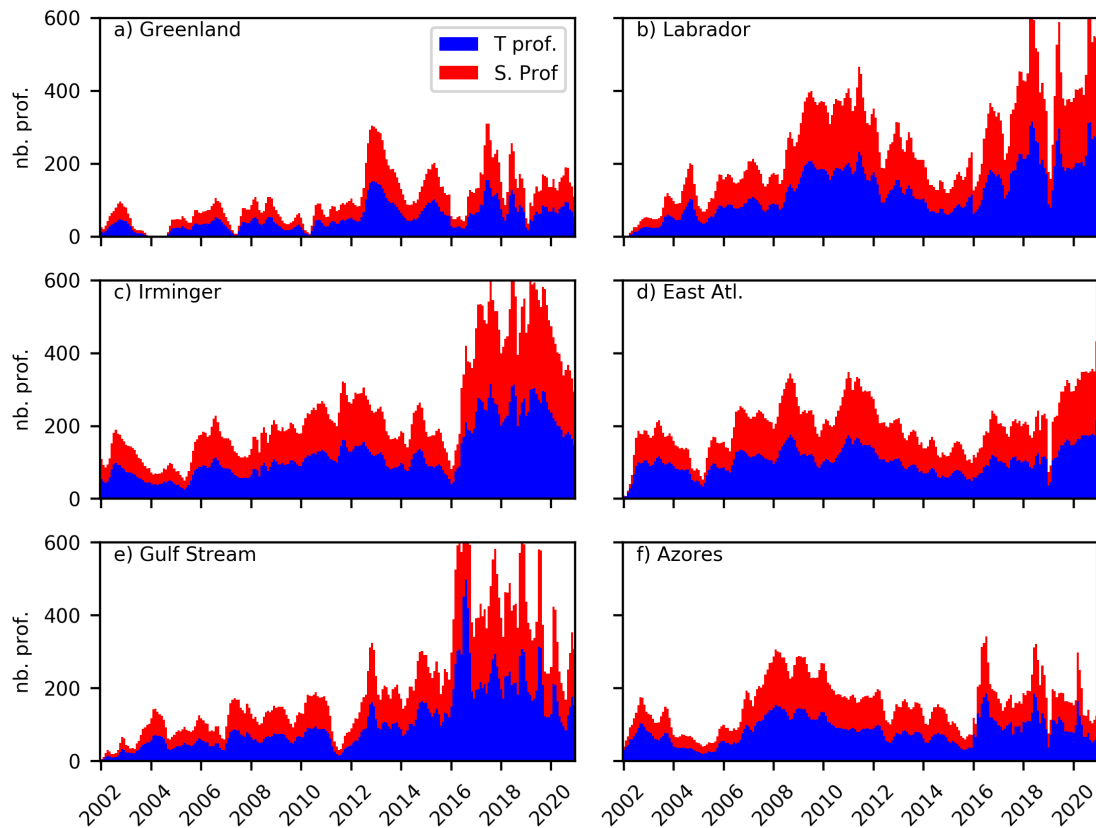


Figure 2.5. Number (nb.) of Argo temperature (blue) and salinity (red) profiles (prof.) used in monthly objective analyses in 2002–2020 in each selected area from [Figure 2.4](#). (a) Greenland Sea; (b) Labrador Sea; (c) Irminger Basin; (d) eastern Atlantic region (Iceland and Rockall basins); (e) Gulf Stream region; and (f) Azores region.

### 2.3.3 Surface layers

#### Seasonal patterns of T/S 2020 anomaly

The broad pattern of temperature and salinity anomalies in 2020 (with respect to the 2006–2015 climatological mean) showed a relatively warm and salty subtropical region, a relatively cold and fresh subpolar region, and contrasting conditions in the Nordic Seas ([Figure 2.6](#)). However, there were significant subregional and intra-annual changes in each of these regions. The warm subtropical anomalies appeared to spread over the width of the basin from east (in JFM) to west (in OND), while a cold and fresh anomaly could be observed off Newfoundland (45°N) in JFM before likely propagating northeast along the North Atlantic Current (NAC) up to 20°W in OND. In the subpolar region, negative temperature and salinity anomalies were observed in the Irminger Basin during JFM. This pattern has been sustained over the year 2020. In contrast, the Labrador Sea was warmer and saltier than usual around its northern (during JFM and AMJ) and eastern (JAS and OND) boundaries. The warm and salty anomaly was probably advected southward by the Labrador Current along the upper North American US continental slope. In the Nordic Seas, warm and salty anomalies primarily developed within the western portion of the domain (Iceland and Greenland seas), while cold anomalies developed along the eastern margin (Norwegian Sea). This asymmetric pattern is less evident in salinity, but still present (salty in the west and fresh in the east). Note that the situation in 2020 remains comparable to that in 2019.

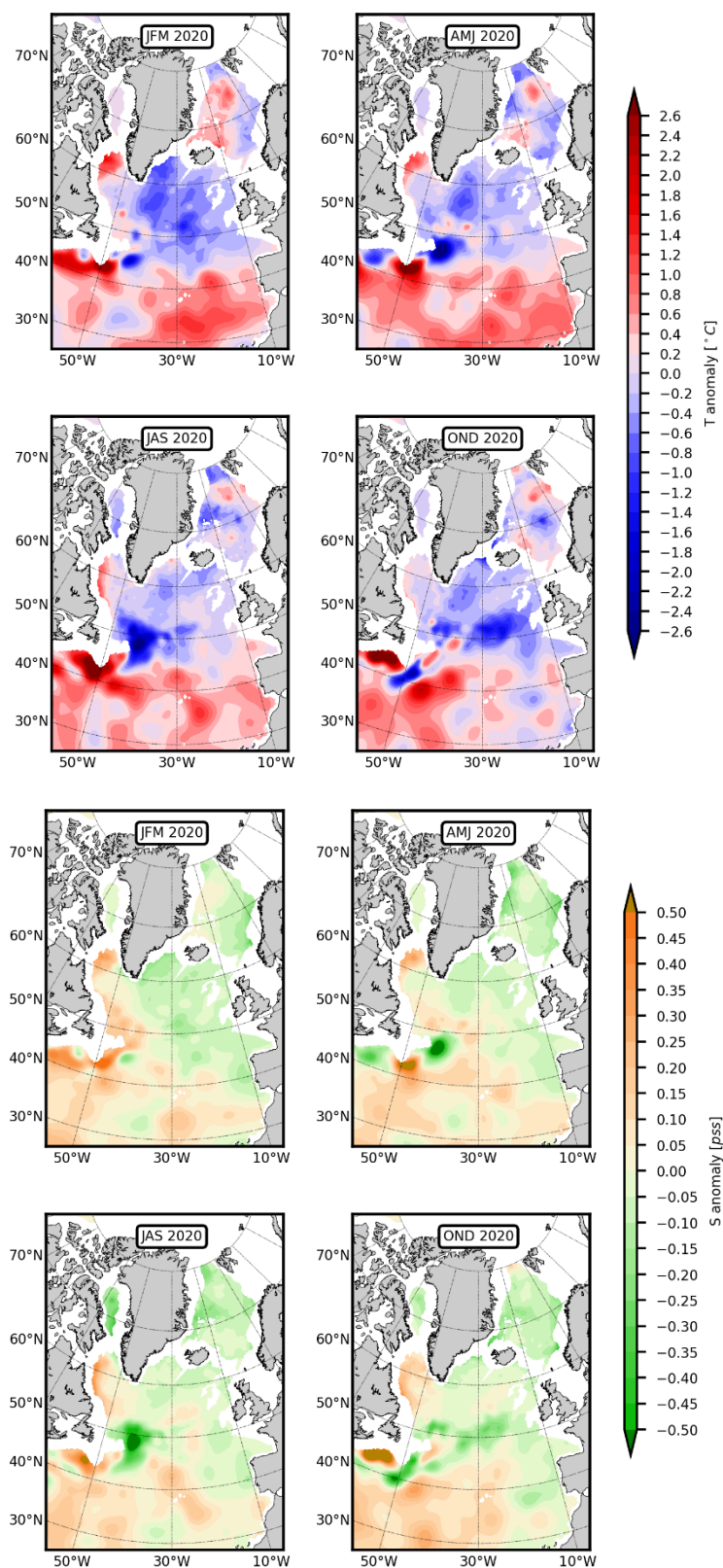


Figure 2.6. Near-surface temperature (upper panel) and salinity (lower panel) anomalies (0–100 m average) averaged over winter (JFM), spring (AMJ), summer (JAS), and autumn (OND) 2020. Anomalies are the differences between the ISAS monthly mean values and the reference climatology ISAS15 2006–2015. Data prepared from the Coriolis, ISAS monthly analysis of Argo data.

## Seasonal cycle and monthly anomalies

The 2020 seasonal cycles of temperature anomalies, averaged within the six areas representative of the main sub-basins of the North Atlantic domain (Figure 2.4), are depicted in Figure 2.7. The 2006–2015 climatology (solid) and the s.d. (dashed) over the period 2002–2020 are also shown in Figure 2.7.

- In 2020, the surface layer in the Greenland Sea (Figure 2.7, panel a) was warmer than the 2006–2015 reference period during the winter and early spring months (JFMA), remaining mostly colder than usual during the rest of the year (spring-summer-autumn).
- The surface layer of the Labrador Sea (Figure 2.7, panel b) was warmer than normal throughout the year.
- In the Irminger Sea (Figure 2.7, panel c), the surface layer was colder than normal throughout the year, especially during winter.
- In the eastern Atlantic (Figure 2.7, panel d), the 2020 surface layer exhibited colder temperatures than the 2006–2015 average, except during summer (JJA) when temperatures were not significantly higher than usual.
- The surface layer of the Gulf Stream and Azores regions, i.e. western and eastern Subtropical Gyre, respectively (Figure 2.7, panel e and f), were warmer than normal over the whole seasonal cycle.

In conclusion, the temperature seasonal cycle observed in 2020 in the main North Atlantic sub-basins was warmer than usual for the western subpolar basin (Labrador Sea) and colder than normal during most of the year in the eastern subpolar basins (Irminger, Iceland and Rockall basins). In contrast, the Greenland Basin was warmer only during the winter period. The Subtropical Gyre also showed a sustained warm anomaly throughout the entire year.

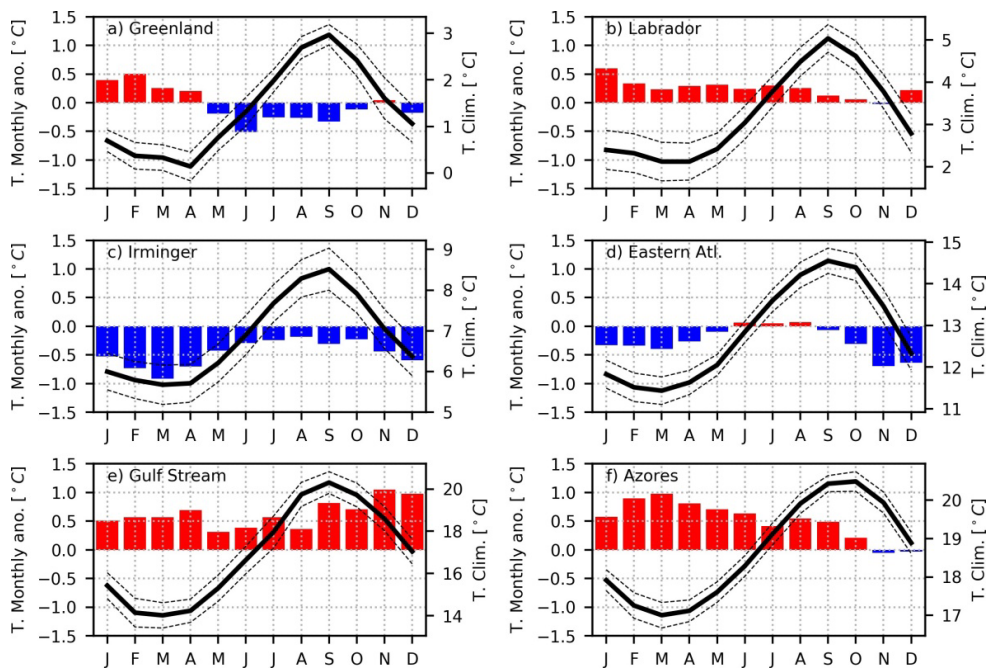
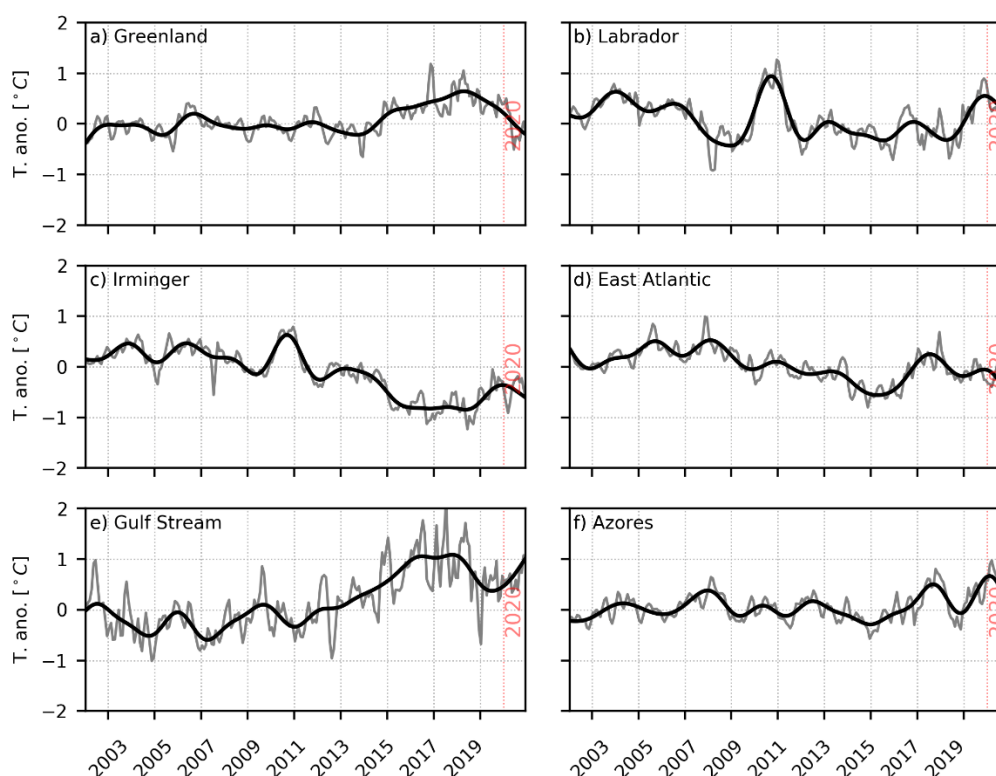


Figure 2.7. 2020 near-surface temperature (0–100 m average) monthly anomalies (bars) and climatological seasonal cycle (thick line) over the period 2006–2015, with its standard deviation (dashed lines) computed for the period 2002–2020. Anomalies are the differences between the ISAS monthly mean values and the reference climatology ISAS15 2006–2015. Data prepared from the Coriolis, ISAS monthly analysis of Argo data.

### Interannual variability and long-term tendency

[Figure 2.8](#) depicts the interannual variability of the upper layer (0–100 m) temperature anomaly (relative to 2006–2015) over the period 2002–2020 in the six North Atlantic areas. The Greenland Sea region, which has been warmer than average over the last five years, continued the cooling tendency observed since 2018, and reached average 2006–2015 surface temperature conditions in 2020 ([Figure 2.8](#), panel a). In 2020, the Labrador Basin ([Figure 2.8](#), panel b) remained warmer than usual, due to a warming trend seen since 2018 that is now mainly observed along the western boundary of the basin ([Figure 2.6](#)). The recent warming in the Labrador Basin has occurred after a decade (2008–2018) that was slightly colder than normal, except for the remarkable 2010 warm event. The Irminger Basin remained colder than usual in 2020 ([Figure 2.8](#), panel c) due to unabated cooling observed since 2008, despite the 2010 and 2019 warming events. The eastern Atlantic region (Iceland and Rockall basins; [Figure 2.8](#), panel d) shows a similar upper ocean temperature decrease, but 2020 remains within the 2006–2015 average.

When compared to the long-term 2006–2015 mean, the subtropical region was generally warmer in recent years, with warming being particularly significant over the Gulf Stream region ([Figure 2.8](#), panel e) since 2015. No long-term tendency has been observed since 2002 in the eastern Subtropical Gyre (Azores; [Figure 2.8](#), panel f), although 2019–2020 was warmer than usual, similar to 2017. Overall, surface temperatures were warmer in 2020 than at any other time in the record.



**Figure 2.8.** Upper ocean (0–100 m depth) temperature interannual anomalies (reference climatology: 2006–2015) over the 2002–2020 period (19 years) in the basin areas defined in [Figure 2.4](#). (a) Greenland Sea; (b) Labrador Sea; (c) Irminger Basin; (d) eastern Atlantic basin (Iceland and Rockall basins); (e) Gulf Stream region; and (f) Azores regions. Thin grey line: monthly interannual anomaly. Thick black curve: 24-month low-pass filtered (with a Butterworth filter) time-series.

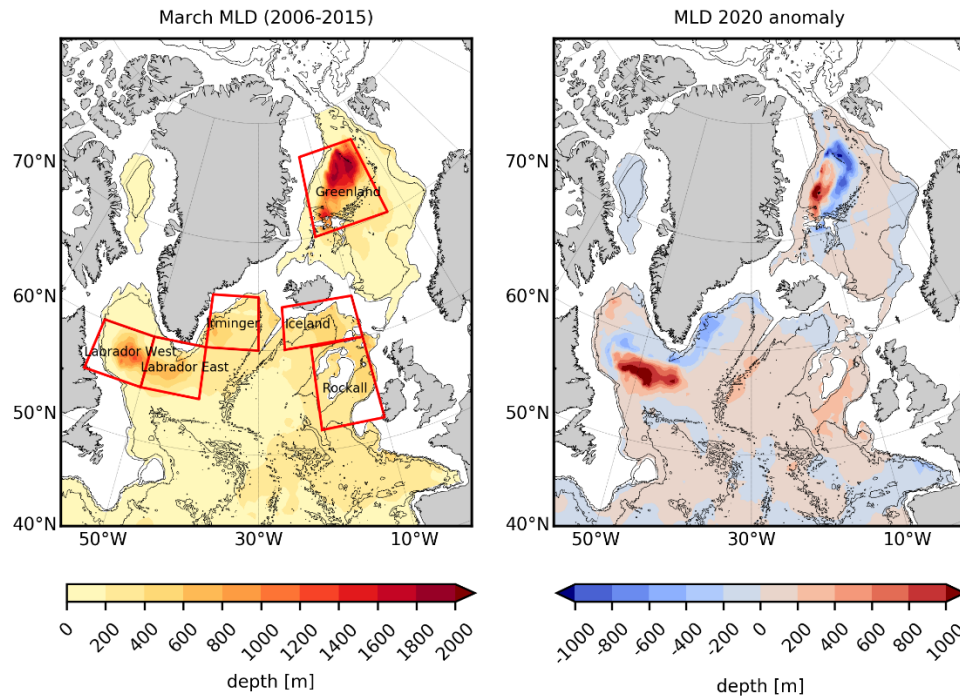


Figure 2.9. Left panel: climatological March Mixed Layer Depth (MLD) for winter 2006–2015. The selected areas to compute the yearly deepest MLD time-series in [Figure 2.10](#) are as follows: western and eastern Labrador Sea, and Irminger, Greenland, Iceland, and Rockall basins. Right panel: 2020 March MLD anomaly (in m). Isobath 1000-m, 2000-m, and 4000-m depth are plotted. Regions shallower than 1000-m depth are blanked.

### Mixed-layer depth

The mixed-layer depth (MLD) is an indicator of winter convection intensity in the North Atlantic and Nordic Seas. Winter heat and freshwater fluxes control the sea surface buoyancy loss (increase of density) of the ocean surface layers and trigger deep convection. In order to compare all areas throughout the decade, the MLD is defined here as the level at which density changes by more than  $0.03 \text{ kg m}^{-3}$  with respect to the 10-m depth value. This is a common criterion used for the global ocean (de Boyer Montégut *et al.*, 2004). Given the difference in stratification over the North Atlantic and Nordic Seas, it is probably not the optimal criterion for defining the MLD in this region. However, adopting this definition allows the comparison of the relative winter MLD across multiple years. To compute the 2006–2015 average and the 2020 anomaly of MLD ([Figure 2.9](#)), the month of March has been chosen as being the common period for maximum MLD, i.e. at the end of the winter season and before spring re-stratification. However, this is not always true, since the time-point when the deepest mixed layer occurs can vary from year to year at a single location and might not occur at the same time of year across the whole basin (generally between February and March in the North Atlantic; [Figure 2.10](#)). Therefore, in order to compute the interannual MLD time-series ([Figure 2.10](#)):

- i) This report focuses on several specific predefined winter convection areas in the North Atlantic, which were chosen based on the climatological March MLD over the period 2006–2015 ([Figure 2.9](#)). Note that the selected deep convection areas differ from the ones in [Figure 2.4](#). Six regions have been selected: Greenland convection zone in the Nordic Seas; western and eastern Labrador area; Irminger Basin convection zone; and Iceland and Rockall region in the eastern Subpolar Gyre ([Figure 2.9](#)).

- ii) For each year since 2002, the MLD is plotted corresponding to the month of the deepest MLD (colour code; [Figure 2.10](#)).

The 2020 winter ([Figure 2.9](#)) was characterized by a noticeable increase in MLD in both the Labrador and Greenland seas. However, in the Labrador Basin the centre of the deepest MLD anomaly shifted eastward, while the Irminger Basin presented a shallower MLD than usual ([Figure 2.9](#)). Interestingly, on the northern and western boundary of the Labrador Sea, deeper than usual MLD was observed. In the Greenland Sea, the deep convection area appeared smaller but deeper than usual and confined to the eastern part of Greenland Gyre. In 2020, in the Irminger and North Iceland basins, the March MLD was shallower than usual, while in the Southern Iceland and Rockall basins, it appeared deeper than usual.

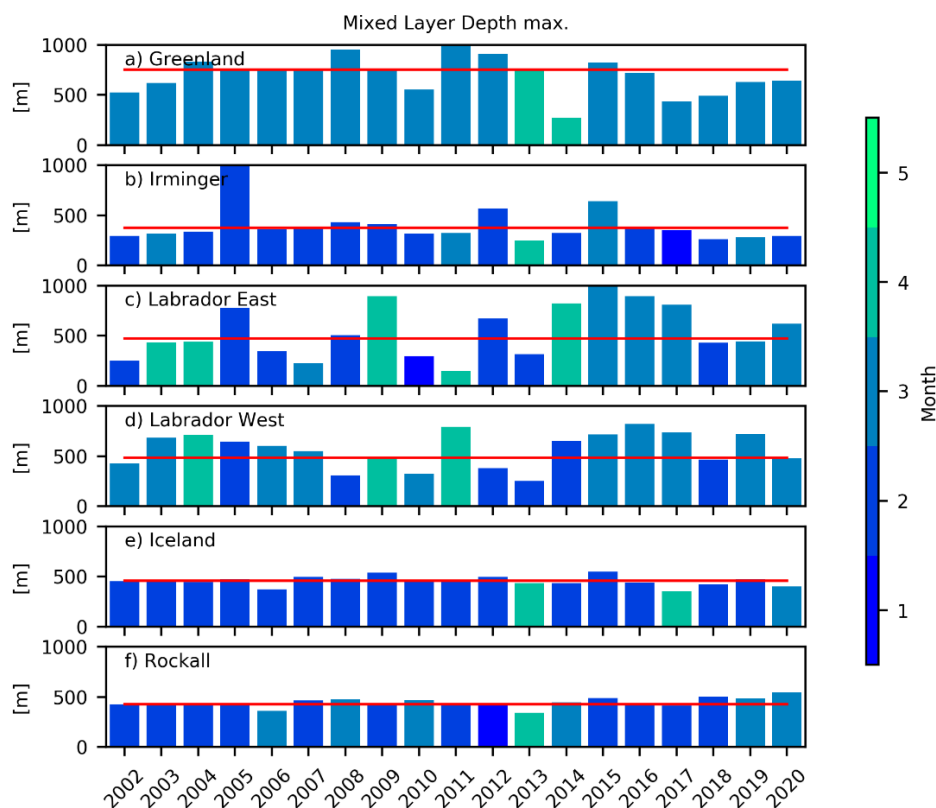


**Figure 2.10.** Yearly deepest MLD over the period 2002–2020 averaged in the selected area from [Figure 2.9](#): (a) Greenland Sea; (b) Irminger Basin; (c) eastern and (d) western Labrador Sea; (e) Iceland Basin; (f) Rockall Basin. Colourbar: winter month of the year when the deepest MLD occurs (between January and April).

[Figure 2.10](#) shows the deepest MLD averaged in the different regions depicted in [Figure 2.9](#) for the period 2002–2020. In the Greenland Sea, the deepest MLD generally occurs during March ([Figure 2.10](#), panel a). In 2020, the MLD remained below average, although it has been increasing since the last minimum event in 2017. In the Irminger Basin ([Figure 2.10](#), panel b), the maximum MLD has remained shallower than normal since its 2015 maximum. In 2020, the MLD was deeper than normal in the eastern Labrador region ([Figure 2.10](#), panel c) and near normal in the western Labrador region ([Figure 2.10](#), panel d). This is explained by the spatial distribution of the deep convection, which was slightly shifted toward the eastern part of the Labrador basin ([Figure 2.9](#)). In contrast, in 2019, the deepest convection was mainly located in the western Labrador basin ([Figure 2.10](#), panel d). In 2020, deep convection in Labrador Sea returned to levels slightly larger than average, but was still lower than the levels associated with

the deepest events observed during the period 2014–2017 (Figure 2.10, panels c and d). Interestingly, it was more common to observe anomalously shallow MLDs in the eastern Labrador Basin before 2014 (only one third of the years registered positive anomalies). Since 2016, including 2020, MLDs in the Iceland Basin have been shallower. In contrast, the Rockall region presented deeper MLD than usual.

### 2.3.4 Intermediate and deep layers

A map of 2020 interannual anomalies of temperature and salinity in the intermediate layer (700–1500 m) of the North Atlantic is shown in Figure 2.11. Figure 2.12 shows time-series of temperature anomalies in the intermediate and deep layers averaged in each area (Figure 2.4) for the period 2002–2020. In 2020, the overall spatial pattern was one of a relatively warm subtropical region, a relatively cold subpolar region, and relatively warm Nordic Seas (when compared to the 2006–2015 climatological period; Figure 2.11, panel a). This tripole pattern characterizing the intermediate layer was already observed the preceding year, and appears to have persisted in 2020. The strongest centres of action were located in the western Subtropical Gyre, where the Gulf Stream (NAC) area is found, and in the Irminger, Labrador, and Greenland seas. The North Atlantic intermediate salinity anomalies show a similar pattern with a saltier anomaly in the Subtropical Gyre and Nordic Seas, and a fresher Subpolar Gyre (Figure 2.11, panel b). Note that the cold anomaly pattern observed at 40°N, off the Iberic Peninsula, is associated with a similar pattern of fresh anomaly (Figure 2.11, panels a and b). This is probably due to the southward shift of the warm and salty Mediterranean water panache at intermediate depth.

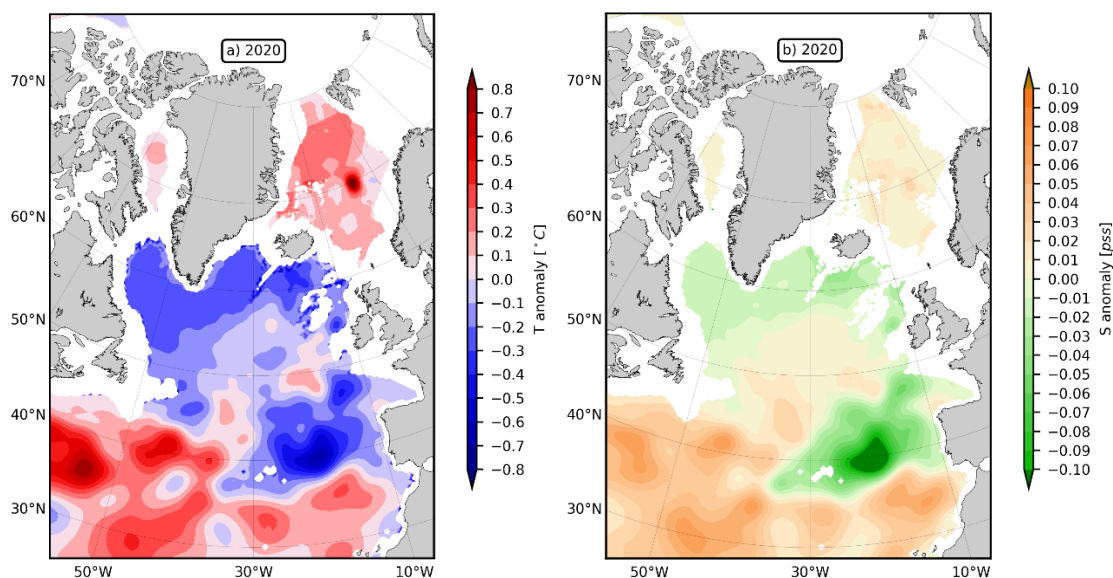


Figure 2.11. 2020 maps of annual (a) temperature and (b) salinity anomalies averaged within 700–1500 m in the North Atlantic. Anomalies are the differences between the ISAS monthly mean values and the reference climatology ISAS15 2006–2015. Data prepared from the Coriolis ISAS monthly analysis of Argo data.

The contrasting interannual behaviour of temperature in those regions is striking (Figure 2.12). Since 2012, the Gulf Stream area has warmed nearly 0.05°C in deep layers (in 1500–2000 m), and 0.1°C (in 1000–1500 m) and 0.5°C (in 700–1000 m) in intermediate layers (Figure 2.12, panel e). The Subpolar area (Labrador and Irminger seas) has cooled around 0.3°C in intermediate layers (700–1500 m depth; Figure 2.12, panels b and c). In the Labrador Sea, even the deepest layers (1500–2000 m depth) have cooled by nearly 0.1°C during the same period. Interestingly, since

2016, the intermediate layer cooling trend seems to be halted in the Labrador Sea (Figure 2.12, panel b), and since 2019 in the Irminger Sea (Figure 2.12, panel c). In contrast to those latter two regions, temperatures in the intermediate and deep layers of the Greenland Sea (Figure 2.12, panel a) have been characterized by an unabated positive trend (increase between 0.1°C and 0.3°C since 2002 for deep and intermediate layer, respectively). In the eastern Subtropical Gyre (Figure 2.12, panel d), in addition to significant interannual variability, intermediate layers (700–1500 m depth) appear to have cooled slightly since 2012. In contrast, the deep layer shows a warming trend (0.15°C) for 2002–2017, with subsequent relatively stable conditions.

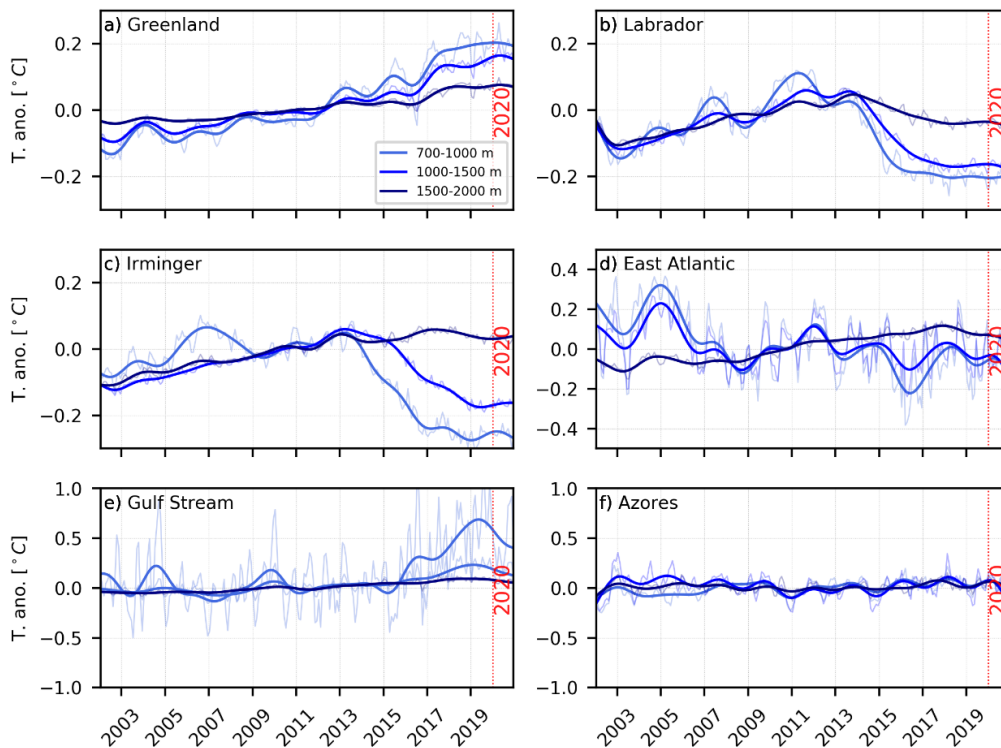


Figure 2.12. Time-series of temperature anomalies (using 2006–2015 as reference) averaged over the 700–1000 m (light blue), 1000–1500 m (blue), and 1500–2000 m (dark blue) layers in (a) eastern Atlantic, (b) Irminger Sea, (c) Labrador Sea, (d) Greenland Sea, (e) Gulf Stream region, and (f) Azores region over the period 2002–2020. The thin lines are monthly anomalies, and the 24-month low pass filtered (with Butterworth filter) time-series of monthly anomalies is plotted in thick lines.

## 2.4 Subpolar Gyre Index

*L. Chafik*

The surface circulation of the North Atlantic Ocean is dominated by two gyres, one that circulates warmer water in a clockwise direction, known as the Subtropical Gyre, and another that circulates cooler waters in the opposite direction, known as the Subpolar Gyre. The Subpolar Gyre encompasses a host of currents, of which the main ones are: the North Atlantic, East Greenland, and Labrador currents. Both the Subtropical and Subpolar gyres are driven by a combination of processes, the most important for the

Subpolar Gyre being the strength and direction of surface winds, the exchange of heat between atmosphere and ocean, and the large-scale circulation known as the overturning circulation (Buckley and Marshall, 2016).

The principal dynamics of the North Atlantic Subpolar Gyre are revealed through sea surface height variability over the Subpolar and Subtropical gyres. Satellite altimetry measurements are available since 1993 (Taburet *et al.*, 2019). An updated version of the gyre index has been produced by applying the method of Häkkinen and Rhines (2004) to this 27-year dataset (1993–2019). The Subpolar Gyre index now appears as the second principal component and not as the first principal component as previously reported (Hátún and Chafik, 2018). The new Subpolar Gyre index does not include the trend associated with the first mode, but it is still adept in capturing the main dynamics and intensity of the cyclonic Subpolar Gyre circulation and is recognized to have significant implications for a wide range of climatic (Hátún *et al.*, 2005; Buckley and Marshall, 2016; Moffa-Sánchez and Hall, 2017) as well as ecological (Hátún *et al.*, 2009, 2016, 2017) aspects in the North Atlantic.

The Subpolar Gyre is strongly affected by the atmospheric circulation of the North Atlantic, as often proxied by the NAO index (Delworth *et al.*, 2016). However, the advantage of using the gyre index for ocean research, over the NAO index, is that it integrates the oceanic imprint of atmospheric forcing, and thus has more direct implications for the marine climate and ecosystems in the subpolar North Atlantic.

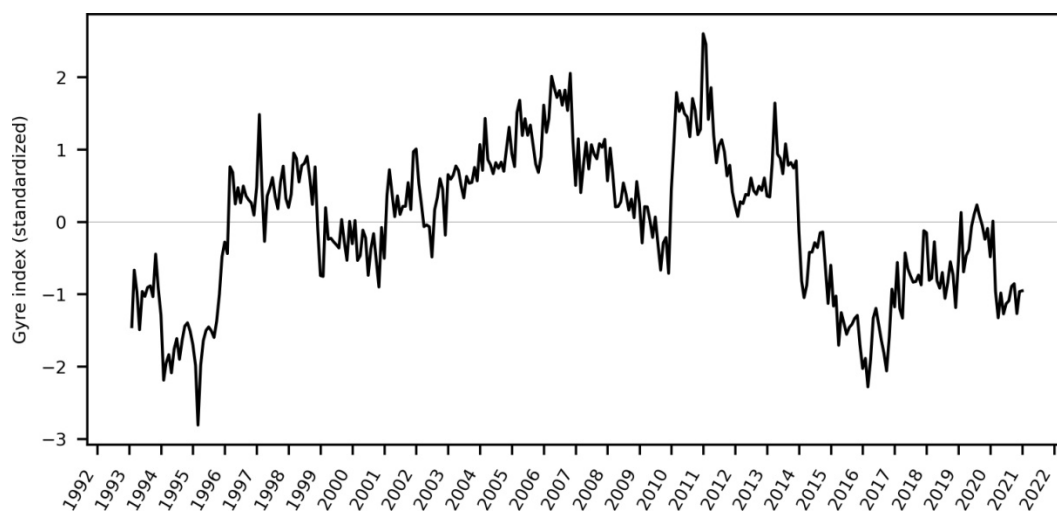


**Figure 2.13.** The monthly gyre index (second principal component) from January 1993 until December 2021. Data source: altimetry data were obtained through the Copernicus Marine Environment Monitoring Service (<http://marine.copernicus.eu>). Index source: Léon Chafik, National Oceanography Centre, Southampton, UK.

In the late 1980s–early 1990s, the atmospheric circulation, as represented by the NAO index, intensified. This led to a strengthened Subpolar Gyre circulation, as reflected by negative Subpolar Gyre index values during this period before 1996 (Figure 2.13). However, since 1996, a large volume of warm and saline, and hence nutrient-poor, subtropical waters accessed the Subpolar Gyre, as a delayed response to the prolonged positive NAO phase (Robson *et al.*, 2012). This change in the water masses led to a transition of the gyre index to a positive phase (Figure 2.13).

Since 2011, strong atmospheric forcing and winter convection, associated with a positive NAO index (e.g. Yashayaev and Loder, 2017), has resulted in a strengthened Subpolar Gyre state, similar to the early 1990s. This is clearly illustrated by negative gyre index values in past years ([Figure 2.13](#)). The Subpolar Gyre index has remained negative in 2020, but less so than during the recent cold anomaly (Josey *et al.*, 2018) in the 2015–2017 period.



CTD. Photo: Tomasz Szumski, Marine Institute, Galway, Ireland

## 3 The North Atlantic atmosphere

*S.R. Dye*

The North Atlantic Oscillation (NAO) is a pattern of atmospheric variability that has a significant impact on oceanic conditions. It affects windspeed, precipitation, evaporation, and the exchange of heat between ocean and atmosphere, and its effects are most strongly felt in winter. The NAO index is a simple device used to describe the state of the NAO. It is a measure of the strength of the sea level air pressure gradient between Iceland and Lisbon, Portugal. When the NAO index is positive, there is a strengthening of the Icelandic low-pressure system and the Azores high-pressure system. This produces stronger mid-latitude westerly winds, with colder and drier conditions over the western North Atlantic and warmer and wetter conditions in the eastern North Atlantic. When the NAO index is negative, there is a reduced pressure gradient, and the effects tend to be reversed.

There are several slightly different versions of the NAO index calculated by climate scientists. The Hurrell winter (December/January/February/March or DJFM) NAO index (Hurrell *et al.*, 2003) is most commonly used and is particularly relevant to the eastern North Atlantic. Note that although we may think of winter as coming at the end of the year, here the 'winter season' spans an annual boundary and precedes the year of interest, so winter of December 2019 to March 2020 sets up conditions for summer of 2020.

The NAO is the dominant pattern of atmospheric pressure variability in the North Atlantic. However, when the NAO itself is weak (i.e. the dominant atmospheric pattern is not a NAO type pattern), this may be because a different pattern is occurring. Two other dominant atmospheric regimes have been identified as useful descriptors: (i) the Atlantic Ridge mode, when a strong anticyclonic ridge develops off western Europe (similar to the East Atlantic pattern); and (ii) the Blocking regime, when the anticyclonic ridge develops over Scandinavia. The four regimes (positive NAO, negative NAO, Atlantic Ridge, and Blocking) have all been occurring at around the same frequency (20–30% of all winter days) since 1950 (Hurrell and Deser, 2010). For this reason, we also include maps of sea level pressure, windspeed, and air temperature as this offers a more detailed understanding of the North Atlantic atmospheric variability than the NAO Index alone.

### 3.1 The North Atlantic Oscillation NAO index

Following a long period of increase, from an extreme and persistent negative phase in the 1960s to a most extreme and persistent positive phase during the late 1980s and early 1990s, the Hurrell NAO index underwent a large and rapid decrease during winter 1995/1996. In many of the years between 1996 and 2009, the Hurrell winter NAO index was both fairly weak and a less useful descriptor of atmospheric conditions, mainly because the sea-level pressure patterns were not typical of the NAO. In winter 2009/2010, the index was strongly negative ([Figure 3.1](#)), and its anomaly pattern exerted a dominant influence on atmospheric conditions. This was the strongest negative anomaly since 1969, and the second strongest negative value for the Hurrell winter NAO index on record (starting in 1864). Winter 2014/2015 saw the strongest NAO index since 1995, and the fourth most positive NAO index in the last 110 years (Hurrell and National Center for Atmospheric Research Staff (Eds.), 2017). In winter 2019/2020, the NAO index was

strong and positive for a second successive year, concluding a decade of winters (2011-2020) dominated by strong NAO positive conditions (7 out of the 10 years).

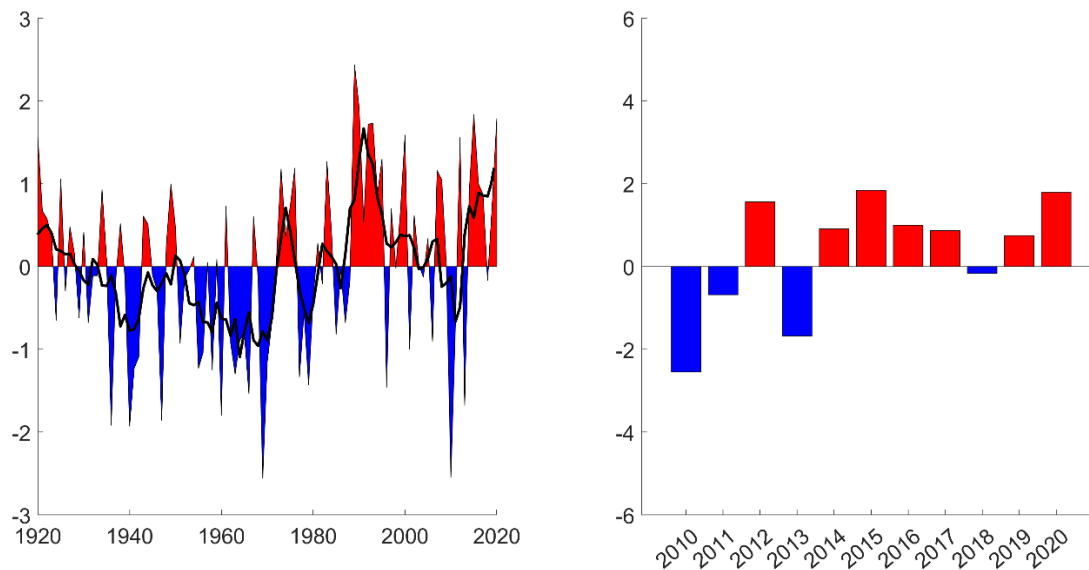


**Figure 3.1.** The Hurrell winter (DJFM) NAO index for the past 100 years, with a two-year running mean applied (left panel), and for the current decade (right panel). Data source: NAO Index Data provided by the Climate Analysis Section, NCAR, Boulder, USA, (National Center for Atmospheric Research Staff (Eds.), 2021).

## 3.2 Sea level pressure and wind speed

The spatial pattern of atmospheric conditions indicated by a particular value NAO index are more understandable when the anomaly fields are mapped. Impacts on ocean properties are particularly dominated by winter conditions; hence, the inclusion of sea level pressure (SLP) and wind-speed maps for the winter period ([figures 3.2](#) and [3.3](#)).

The top panel of [Figure 3.2](#) shows winter SLP averaged over 30 years (1981–2010). The dominant features (action centres) are the Iceland Low, situated southwest of Iceland, and the Azores High, west of Gibraltar. The middle panel of [Figure 3.2](#) shows the mean SLP for winter 2019/2020 (December 2019 through March 2020), and the bottom panel shows the 2019/2020 winter SLP anomaly (i.e. the difference between the top and middle panels).

The pattern of SLP is closely related to patterns of wind. The geostrophic (or gradient) wind blows parallel to the isobars, with lower pressure to the left in the northern hemisphere; the closer the isobars, the stronger the wind. The strength of the winter-mean surface-wind averaged over the 30-year period (1981–2010) is shown in the upper panel of [Figure 3.3](#), while the middle panel shows the mean surface-wind for winter 2019/2020, and the lower panel the anomaly in winter 2019/2020.

The SLP anomaly for winter 2019/2020 ([Figure 3.2](#)) was a typical positive NAO pattern, as expected given the strong positive NAO that extended further west than usual. A high-pressure (anticyclonic) anomaly was present across western Europe and extended across the Azores to the western North Atlantic. A strong cyclonic anomaly extended across the Norwegian and Barents seas.

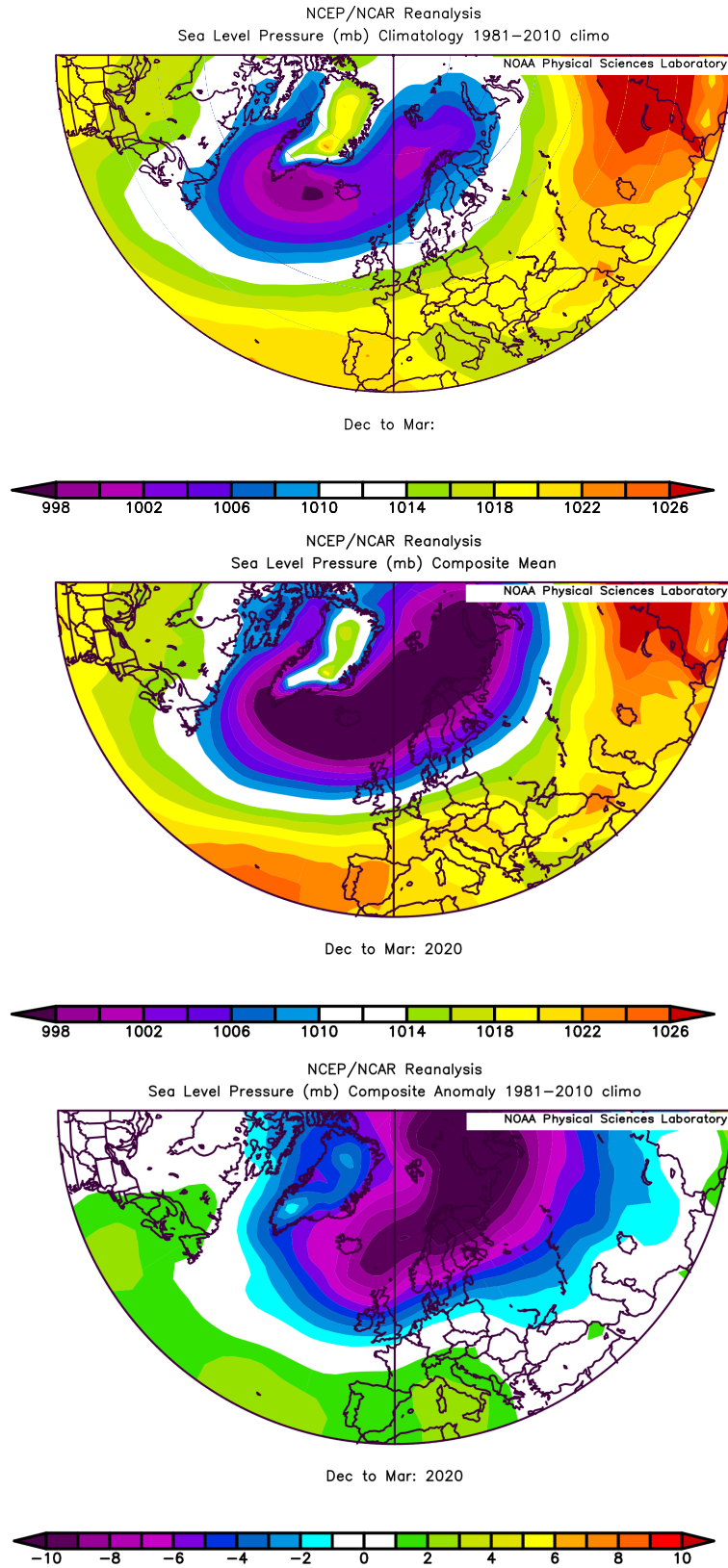


Figure 3.2. Winter (DJFM) sea-level (SLP) pressure fields. Top panel: SLP averaged over 30 years (1981–2010). Middle panel: SLP in winter 2019/2020. Bottom panel: winter 2019/2020 SLP anomaly, calculated as the difference between the top and middle panels. Images provided by the NOAA/ESRL Physical Sciences Division, Boulder, CO.

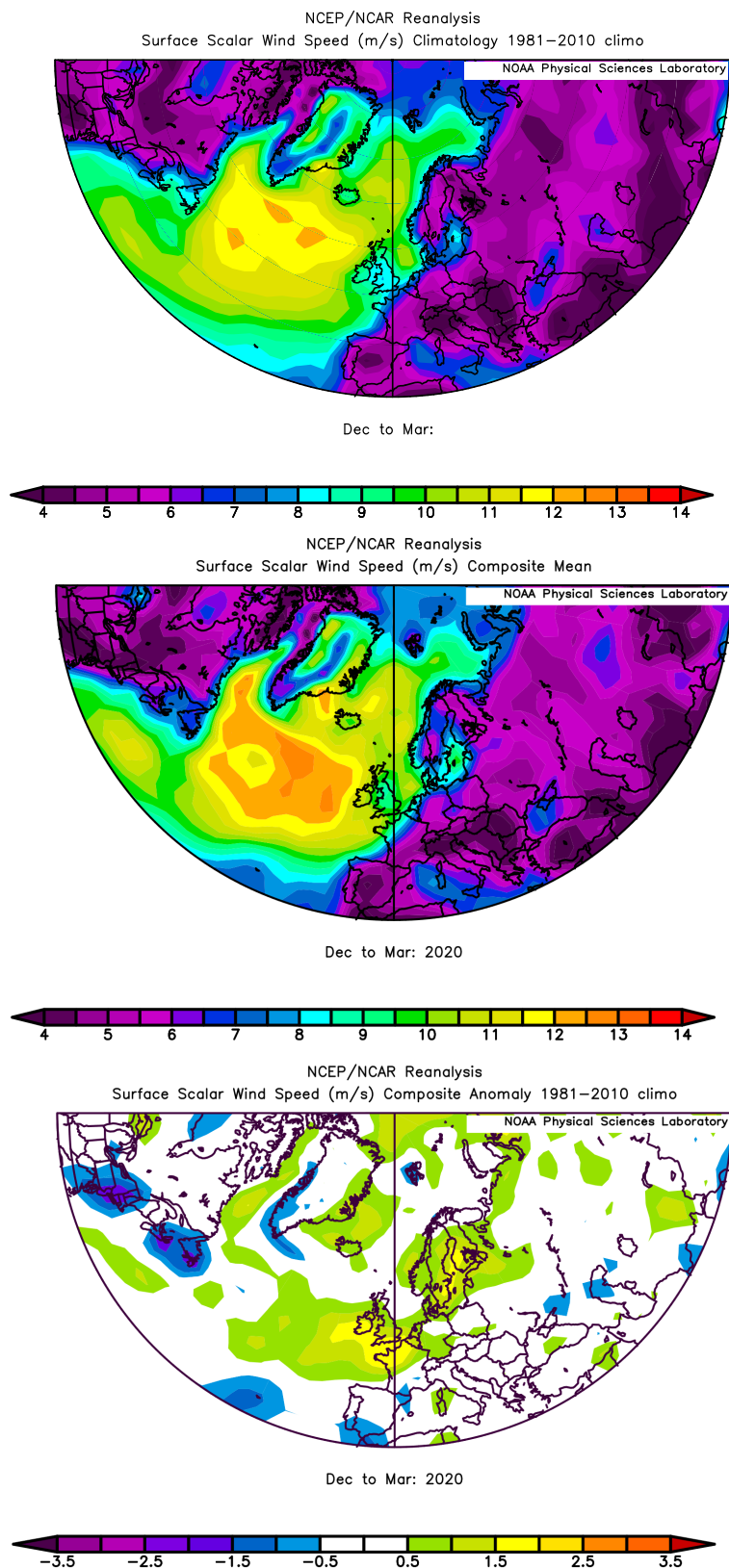


Figure 3.3. Winter (DJFM) wind speed fields. Top panel: scalar wind speed averaged over 30 years (1981–2010). Middle panel: scalar wind speed in winter 2019/2020. Bottom panel: winter 2019/2020 scalar wind speed anomaly, calculated as the difference between the top and middle panels. Images provided by the NOAA/ESRL Physical Sciences Division, Boulder, CO.

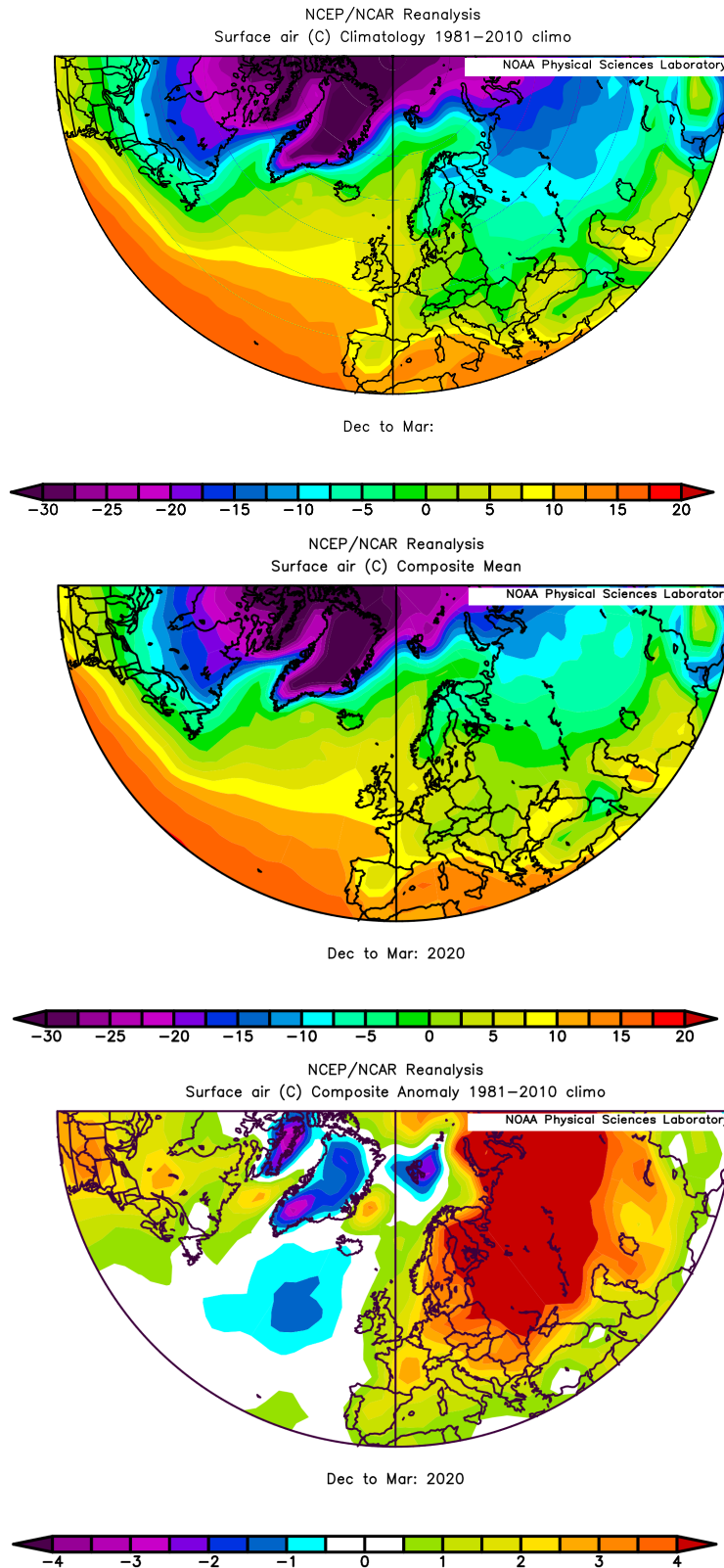


Figure 3.4. Winter (DJFM) surface air temperature fields. Top panel: surface air temperature averaged over 30 years (1981–2010). Middle panel: surface air temperatures in winter 2019/2020. Bottom panel: winter 2019/2020 surface air temperature anomaly, calculated as the difference between the top and middle panels. Images provided by the NOAA/ESRL Physical Sciences Division, Boulder, CO (available online at <http://www.cdc.noaa.gov>).

The influence of this typical SLP anomaly during a strong positive NAO index can be seen in windspeeds ([Figure 3.3](#)), which showed a strengthening of the prevailing southwesterlies in the east of the region. Windspeeds across the region in winter 2019/2020 were generally higher than average. The area from the west of Ireland across the UK, North Sea, and Baltic Sea experienced particularly strong southwesterly winds through much of winter.

### 3.3 Surface air temperature

North Atlantic winter mean surface air temperatures are shown in [Figure 3.4](#) (Kalnay *et al.*, 1996). The 1981–2010 mean conditions ([Figure 3.4](#), top panel) show warm temperatures penetrating far to the north on the eastern side of the North Atlantic and the Nordic Seas, caused by the northward movement of warm oceanic water. The middle panel of [Figure 3.4](#) shows the conditions in winter 2019/2020, and the bottom panel shows the difference between the two.

Over most of the main body of the North Atlantic Ocean, away from the shelves and marginal seas, air temperature was near average. Winter air temperatures were warmer than average (1981–2010) over Europe, northeast America, and the Nordic, Baltic, and Labrador seas. Over the central North Atlantic, air temperatures were cooler than average (1981–2010) where average windspeeds are greatest, and the western extension of the Azores high pressure system drew cool air from northeast Canada into the northwest of the region.

### 3.4 Outlook beyond 2020

An initial assessment of the North Atlantic atmosphere at the end of the IROC year is included. Atmospheric conditions during winter are a determining factor of oceanic conditions for the following year; therefore, this outlook offers some predictive capability for spring–autumn 2021.

The SLP pattern for December 2020–March 2021 suggests a strong negative NAO index winter, the first since 2013. The storm track from the USA east coast, across Flemish Cap, and through to Norway and the Nordic Seas will experience particularly weak winds through the season. A region from the west of Spain and across the Azores experienced strong westerly winds through much of winter. Air temperatures were relatively warm across Europe, northeast America, the Nordic Seas, and Labrador Sea, with colder than normal air temperatures over a region of the eastern North Atlantic, and further south than the cool anomaly in 2020.

Recent advances in understanding the predictability of the NAO are showing significant skill in seasonal predictions of the European winter through predictability of the winter NAO (Scaife *et al.*, 2014), Arctic Oscillation (AO), and Sudden Stratospheric Warming (SSW) events (Scaife *et al.*, 2015). Results published by the Met Office suggest that there is even significant skill in predicting the winter NAO index one year ahead (Dunstone *et al.*, 2016) with a correlation coefficient ( $r$ ) between observed NAO and predicted of about 0.4 for the second winter, comparing well with that of about 0.6 for the first winter as described in Scaife *et al.* (2014).

Experimental forecasts from the US over seasonal periods<sup>3</sup> predicted that summer 2020 surface temperatures were likely to be warmer than average across the region, but that the Subpolar Gyre to the west of Ireland and Iceland, and southeast of Cape Farewell, were more likely to be

---

<sup>3</sup> [www.cpc.ncep.noaa.gov/products/NMME/](http://www.cpc.ncep.noaa.gov/products/NMME/) Last accessed 4 July 2022

near average than other areas. Forecasts over the next five years from the UK Met Office Decadal forecast January 2021<sup>4</sup> suggest a warmer outlook for the Subpolar Gyre region than has been seen in the last few cold anomaly years. As experimental forecasts are at an early stage, these are noted here so that we can track their performance and gauge their utility as they develop. The Met Office assessment of the earlier predictions for most recently completed 5-year period (2015–2020) suggests that the forecast did not predict the observed conditions (outside the 5–95% confidence interval) over the North Atlantic Subpolar Gyre.



Photo: Tomasz Szumski, Marine Institute, Galway, Ireland

---

<sup>4</sup> [www.metoffice.gov.uk/research/climate/seasonal-to-decadal/long-range/decadal-fc/index](https://www.metoffice.gov.uk/research/climate/seasonal-to-decadal/long-range/decadal-fc/index) Last accessed 4 July 2022

## 4 Detailed area descriptions, part I: The upper ocean

### Introduction

This section presents time-series from sustained observations in each of the ICES areas shown in [Figure 4.1](#). The general pattern of oceanic circulation in the upper layers of the North Atlantic in relation to the areas described here is shown in [Figure 4.2](#). In addition to temperature and salinity, other indices are presented where available, such as air temperature and sea-ice extent. The regional context of the sections and stations are summarized, noting any significant changes.

Most standard sections or stations are sampled annually or more frequently. Many of the time-series presented here have been extracted from larger datasets, and have been chosen as indicators of the conditions in a particular area. Where appropriate, data are presented as anomalies to demonstrate how the values compare with the average, or normal, conditions, usually considered as the long-term mean of each parameter during 1981–2010. For datasets that do not extend as far back as 1981, the average conditions have been calculated from the start of the dataset through to 2010.

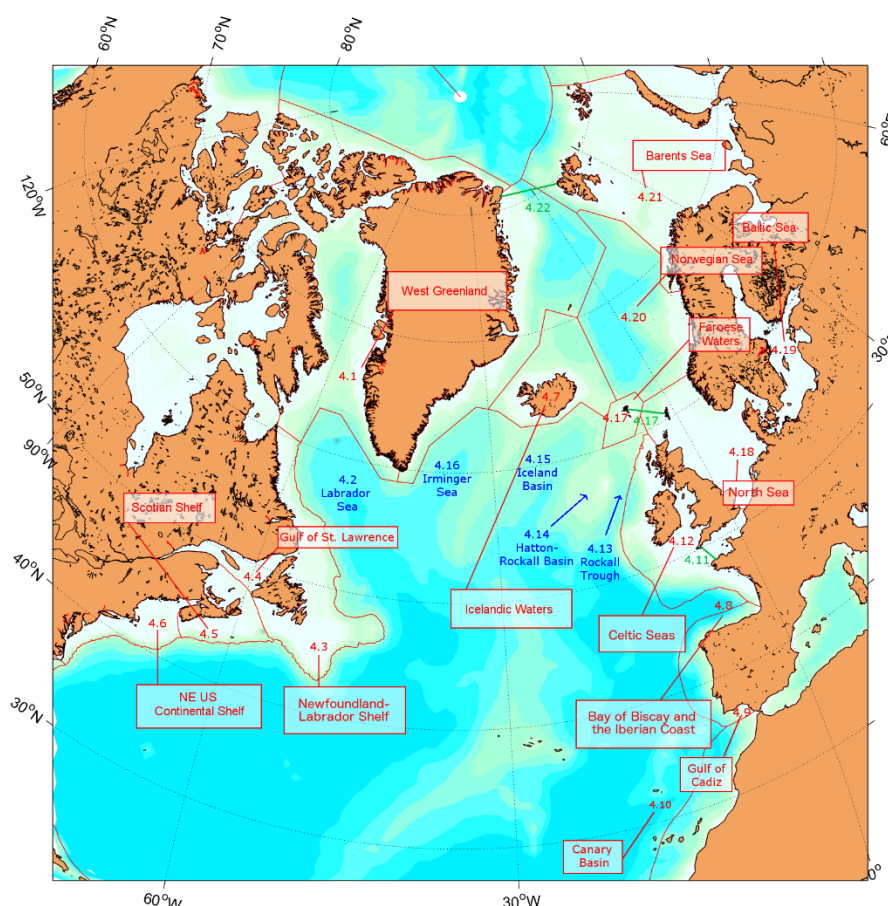
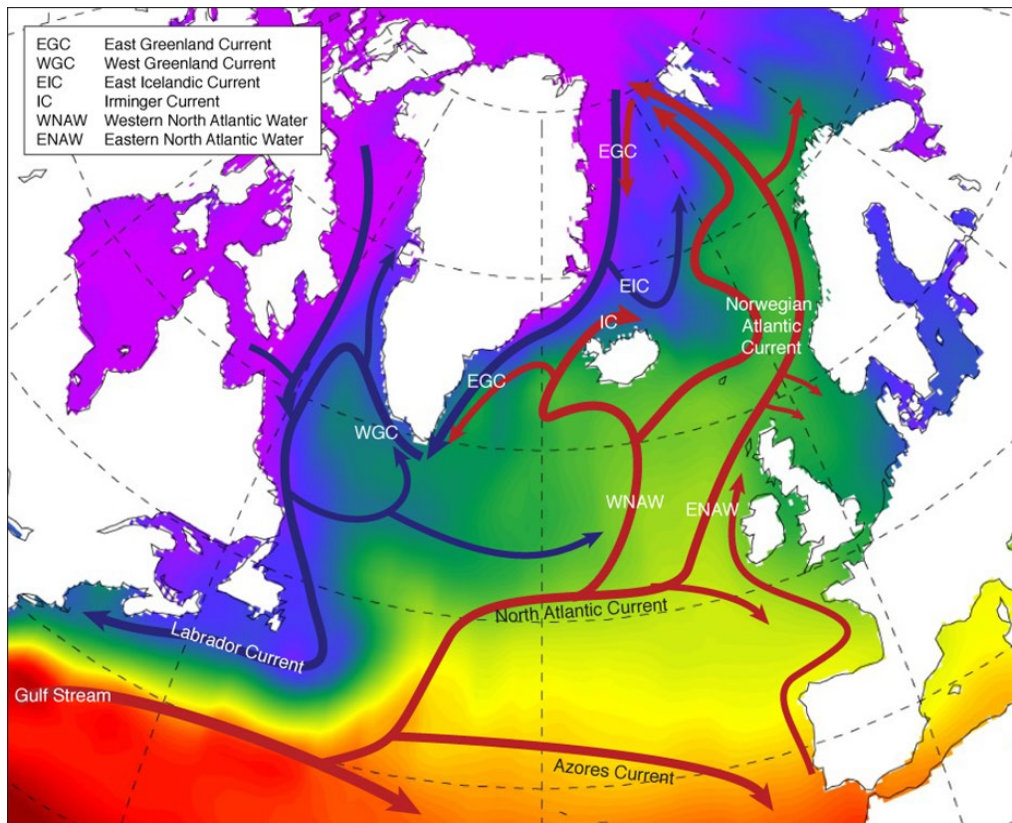


Figure 4.1. Schematic of marine areas used to organize data presented in this Section. Numbers refer to the Subsection in this report where the marine area is described. Regions are labelled in red. Ocean basins are labelled in blue. Straits are labelled in green. NOAA Large Marine Ecosystems boundaries (<https://www.lmehub.net>) are shown as background reference, but hydrographic regions are loosely defined so they do not perfectly overlap.



**Figure 4.2.** Schematic of the general circulation of the upper ocean (0–1000 m) in the North Atlantic. Blue arrows: movement of cooler waters of the Subpolar Gyre; red arrows: movement of warmer waters of the Subtropical Gyre.

In places, the seasonal cycle has been removed from a dataset either by calculating the average seasonal cycle during 1981–2010, or by drawing on other sources, such as regional climatology datasets. Smoothed versions of most time-series are included using a Loess smoother, a locally weighted regression with a two- or five-year window (chosen depending on which was the most appropriate to each time-series).

In some areas, data are sampled regularly enough to allow a good description of the seasonal cycle. Where possible, monthly data from 2020 are presented and compared with the average seasonal conditions and statistics.

Although there are no real boundaries in the ocean, it is intended that the data presented represent conditions in particular areas. This section groups datasets into areas based on existing definitions. The NOAA Large Marine Ecosystems (LMEs)<sup>5</sup> serve as an overall reference as they cover all regions. However, ICES Marine Ecoregions<sup>6</sup>, the bathymetry of ocean basins<sup>7</sup>, and the general pattern of ocean circulation are also considered (Figure 4.2). While the data presented here offer the best available indicative time-series within a region, it should be noted that, in large areas with complex circulation patterns, consideration should be given to how representative these data are of the whole ecoregion.

<sup>5</sup> <https://www.lmehub.net> Last accessed 4 July 2022.

<sup>6</sup> <https://www.ices.dk/advice/ICES%20ecoregions%20and%20advisory%20areas/Pages/ICES-ecosystems-and-advisory-areas.aspx> Last accessed 4 July 2022.

<sup>7</sup> [https://www.gebco.net/data\\_and\\_products/undersea\\_feature\\_names/](https://www.gebco.net/data_and_products/undersea_feature_names/) Last accessed 4 July 2022.

## 4.1 West Greenland

*B. Cisewski*

The NOAA LME project identifies the ecosystem of the Canadian Eastern Arctic–Western Greenland as a single LME. Here, only conditions in the Western Greenland portion of the region are examined. The hydrographic conditions presented are monitored at two oceanographic sections across the continental slope of West Greenland in the southwestern part of the ecoregion, at a position that is influenced by the West Greenland Current (WGC; [Figure 4.3](#)). The WGC carries water northward along the west coast of Greenland and consists of two components: a cold, fresh inshore component, which is a mixture of Polar Water and melt water, and a warmer, saltier offshore component, which is called Irminger Sea Water. Being part of the cyclonic Subpolar Gyre, the WGC is subject to hydrographic variations on time-scales associated with variability in the gyre.

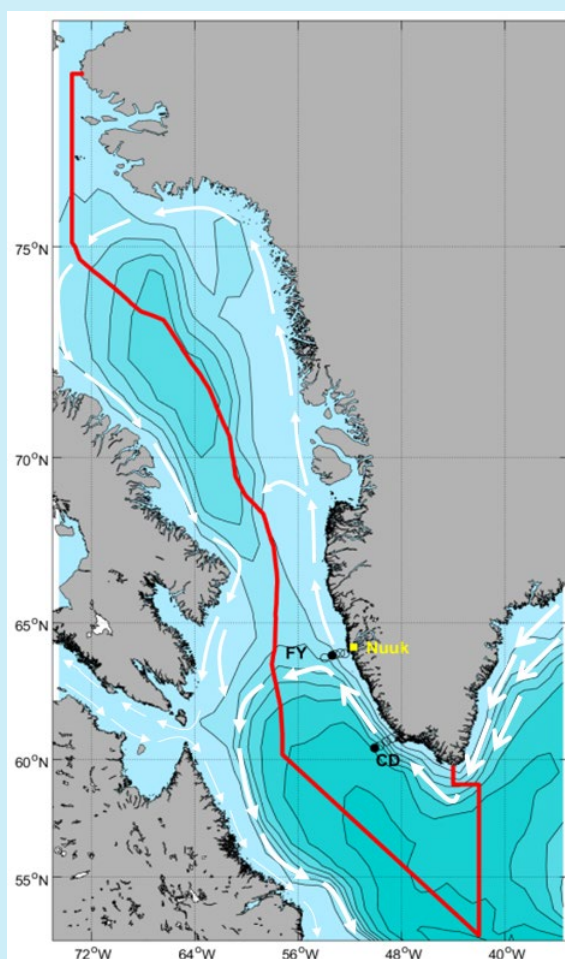


**Figure 4.3.** Circulation schematic for the Labrador Sea and Davis Strait. The location of Nuuk is marked in yellow. White arrows show the path of the surface circulation. The thick arrows are the West Greenland current (WGC). The red lines show the extent of NAFO Area 1a, Western Greenland. Circles labelled 'FY' are the stations of the Fyllas Bank hydrographic section, with station 4 marked as a black circle. Circles labelled 'CD' are the stations of the Cape Desolation hydrographic section, with station 3 marked as a black circle.

In winter 2019/2020, the NAO index was positive for the seventh consecutive winter. The annual mean air temperature at Nuuk Weather Station in West Greenland was  $-0.8^{\circ}\text{C}$  in 2020, which was  $0.6^{\circ}\text{C}$  above the long-term mean (1981–2010).

The hydrographic conditions are monitored at two oceanographic NAFO/ICES sections, which span across the western shelf and continental slope of Greenland near Cape Desolation and Fyllas Bank. Two offshore stations at each section have been chosen to document changes in hydrographic conditions off West Greenland (Figure 4.3). However, in autumn 2019, the Cape Desolation section had to be abandoned due to time constraints. In November 2020, water temperature in the 0–50 m layer at Fyllas Bank Station 4 was  $2.92^{\circ}\text{C}$  and salinity was 32.78, i.e.  $0.28^{\circ}\text{C}$  above and 0.38 below the long-term means, respectively.

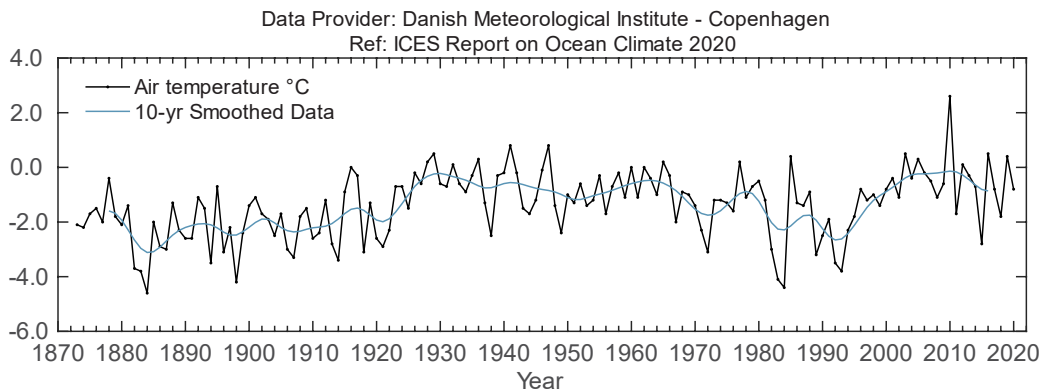


Figure 4.4. West Greenland. Annual mean air temperature at Nuuk station ( $64.16^{\circ}\text{N}$   $51.75^{\circ}\text{W}$ ). Data source: Cappelen (2021).

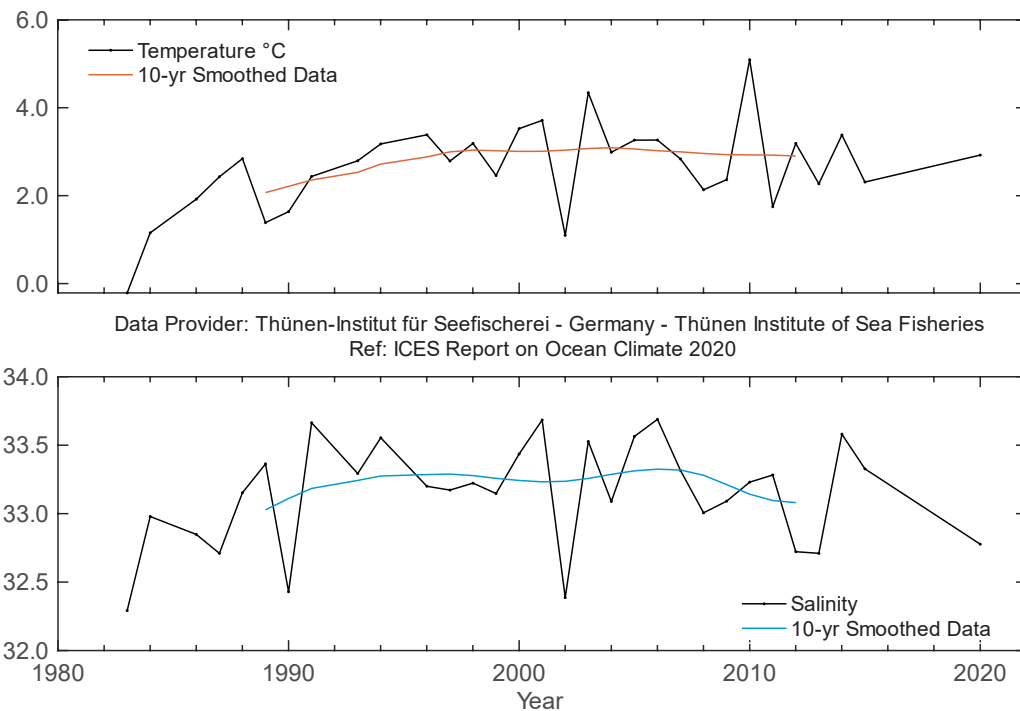


Figure 4.5. West Greenland. Mean temperature (upper panel) and salinity (lower panel) in the 0–50 m water layer at Fyllas Bank Station 4 ( $63.88^{\circ}\text{N}$   $53.37^{\circ}\text{W}$ ).

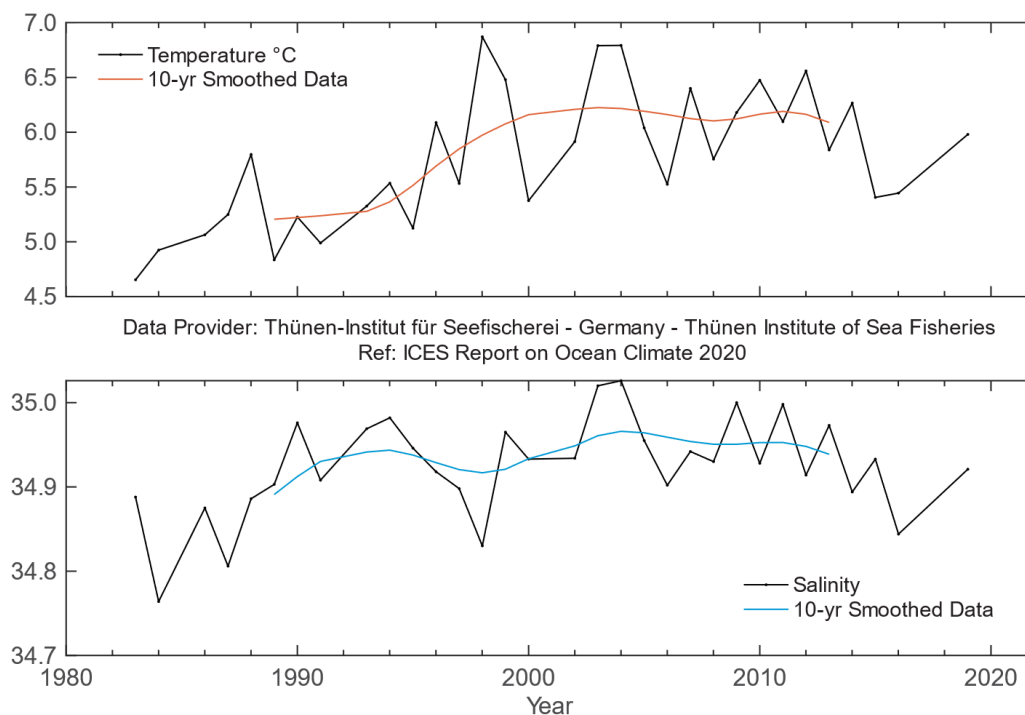


Figure 4.6. West Greenland. Temperature (upper panel) and salinity (lower panel) in 75–200 m water layer at Cape Desolation Station 3 (60.47°N 50°W). Data until 2019.

## 4.2 Labrador Sea

### *I. Yashayaev*

---

**SECOND CONSECUTIVE YEAR WHEN WINTER CONVECTION AND INTERMEDIATE WATER MASS PRODUCTION DID NOT REACH THE 2015-2018 MAGNITUDE, DESPITE BEING MODERATELY STRONG.**

---

The Labrador Sea is located between Greenland and the Labrador coast of eastern Canada. It is a deep, semi-enclosed basin bounded by the West Greenland and Newfoundland–Labrador shelves. Cold, low-salinity waters of polar origin circle the Labrador Sea in a counterclockwise current system that includes both the north-flowing WGC on the eastern side and the south-flowing Labrador Current on the western side. Patches of warmer and saltier AW, typically found under the offshore extension of the WGC, can be traced to their origin in the low latitudes of the North Atlantic by following the NAC and Gulf Stream. The AW mixes with other water masses and progressively becomes colder and fresher as it flows north into the Labrador Sea, following its eastern boundary, and eventually circuits the sea’s northern and western peripheries.

Interannual changes in the hydrographic conditions of the Labrador Sea are controlled by a number of factors, including annual heat loss to the atmosphere, heat and salt gain from the AW, and freshwater gains from the Arctic outflow, sea-ice melt, precipitation, and

interannual changes in the hydrographic conditions of the Labrador Sea are controlled by a number of factors, including annual heat loss to the atmosphere, heat and salt gain from the AW, and freshwater gains from the Arctic outflow, sea-ice melt, precipitation, and continental run-off. In addition, instantaneous conditions and process development depend on the cumulative effect of past heat, salt, and freshwater gains, and their respective temperature, salinity, and density changes, also termed ocean preconditioning (Yashayaev and Loder, 2017). The Labrador Sea has a significant role in the subpolar region and climate system as a whole. Its extreme winter surface heat losses result in the formation of cold and dense intermediate-depth waters which can reach a depth of 2500 m. This process makes the Labrador Sea the primary location in the northern hemisphere for the atmospheric ventilation of the intermediate and deep layers of the Atlantic Ocean. Through winter cooling of surface and subsurface waters and their subsequent mixing and sinking to depths of 500–2500 m (depending on winter severity), a relatively dense and deep intermediate water mass is formed, known as Labrador Sea Water (LSW). This water spreads over the Atlantic Ocean ventilating its deep layers and feeding and driving the global ocean's overturning circulation or ocean conveyor belt.

### Oceanographic monitoring of the Labrador Sea

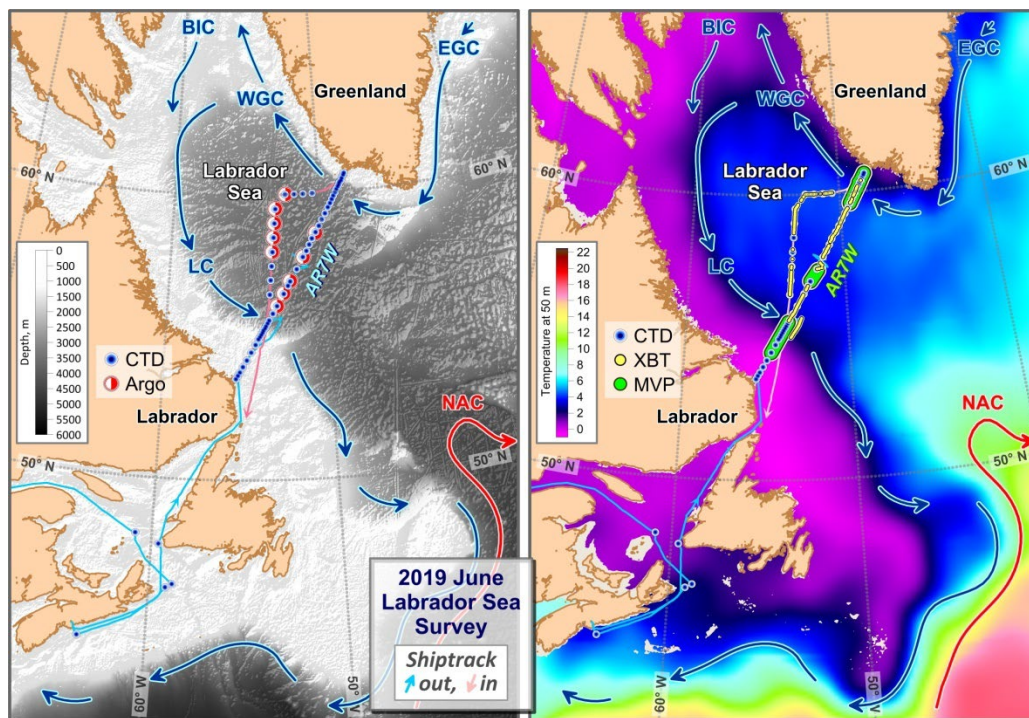


Figure 4.7. Labrador Sea. Topography, surface currents, and temperature at 50 m. CTD, water sampling, eXpendable BathyThermograph (XBT) and Moving Vessel Profiler (MVP) casts, and Argo float deployments conducted in the Labrador Sea in June 2019 by the Bedford Institute of Oceanography (Fisheries and Oceans Canada).

In summer 2020, the Bedford Institute of Oceanography (Fisheries and Oceans Canada) repeated its annual survey of the Atlantic Repeat 7-West (AR7W) repeat hydrography line in the Labrador Sea. This key Atlantic transect has been occupied and sampled at least yearly since

1990, except for 2017, resulting in a 31-year record (1990–2020) of deep-sea observations. [Figure 4.7](#) shows an example of the AR7W surveys, comprising CTD, water sampling, expendable BathyThermograph (XBT) and Moving Vessel Profiler (MVP) casts, and Argo float deployments.

The international Argo program has provided the oceanographic community with unprecedented year-round monitoring of key oceanographic variables from the sea surface to 2000 m. The central Labrador Sea ship survey and Argo float observations have been used to construct time-series of temperature, salinity, and density absolute values and anomalies averaged annually, which reveal interannual-to-multidecadal changes in regional conditions over nearly eight decades. Examples of these series for the upper (50–200 m) and deep intermediate (1000–1800 m) water layers are presented in [Figures 4.8](#) and [5.11](#) (see [Section 5.2.5](#)), respectively. Key factors causing these properties to change are (i) advection of freshwater from the Arctic, continental run-off and precipitation, and heat and salt from other Atlantic basins; and (ii) local atmospheric forcing, mainly, but not exclusively, projected onto the deep Labrador Sea through winter convection. In order to better understand the appearance and causes of interannual-to-multidecadal changes in the region, the progressive developments of deep convection alternated with periods of ocean relaxation over the past thirty years are described in more detail.

### **Deep convection, water ventilation, and hydrographic trends**

A sequence of severe winters in the early 1990s led to deep convection, with the maximum depth reached in 1994. This process filled the upper 2500 m of the water column with cold, fresh, and dense water. Conditions have generally become milder since the mid-1990s. During 1995–2011, the upper and deep layers of the Labrador Sea became warmer and more saline as net annual surface heat loss decreased, while the influence of the Atlantic Waters (AW) on these layers increased ([Figures 4.8](#) and [5.11](#); [Section 5.2.5](#)). This tendency inversed in 2011, and the upper and intermediate layers cooled and freshened during 2011–2018. The cooling and freshening trend stopped in 2019, and salinity and temperature seem to have stabilized the last two years.

A closer examination of temperature and salinity records shows that these warming and cooling trends were not always uniform. A short spike in cooling and freshening in the deep intermediate series ([Figure 5.11](#); [Section 5.2.5](#)) was associated with the deep convection event of 2008 (Yashayaev and Loder, 2009). The 2010 and 2011 winter-heat losses were low in magnitude and were matched by record-weak convection, with the MLD typically not exceeding 800 m. The situation changed abruptly the following year, starting a new and important trend in LSW production and regional hydrographic properties. In winter 2012, convection reached, and possibly exceeded, 1400 m in depth, evident from both Argo float and ship survey temperature and salinity profile data. Interestingly, 2012 salinity in the top 50 m was the lowest since 2003, possibly influencing the strength of convection in winter 2013, which was not as deep as in the previous year. The situation reversed once again in 2014, when a strong winter cooling triggered convective mixing in the Labrador Sea, reaching deeper than 1600 m. Convection continued to deepen over the following four winters reaching, and probably exceeding, 2000 m depth at the end of the period. The mixed part of the water column became colder and denser with each cooling cycle. Finally, as mentioned in the previous paragraph, the deepening of convection and water column cooling and densification stopped in 2019, although convection still remained fairly strong, reaching at least 1500 m in 2019 and 1600 m in 2020.

The observed multiyear development in convection is the result of recurring, relatively strong, surface winter cooling (often, but not always, coinciding with high NAO index values), which

causes deep mixing, and results in the preconditioning of the water column. This may, in turn, facilitate a deeper convection the next year under a weaker winter cooling. The water column preconditioning can also be viewed as the ocean's own "memory" or ability to carry forward some information from past winter cooling events. This suggests that certain properties imposed on the water column by a stronger-than-usual convective mixing in previous years, such as low temperature, weak vertical stability, and weak overall stratification, may result in the kind of preconditioning that facilitated the strengthening and deepening of convection observed in winter 2018. The effect of preconditioning weakened in the following two years.

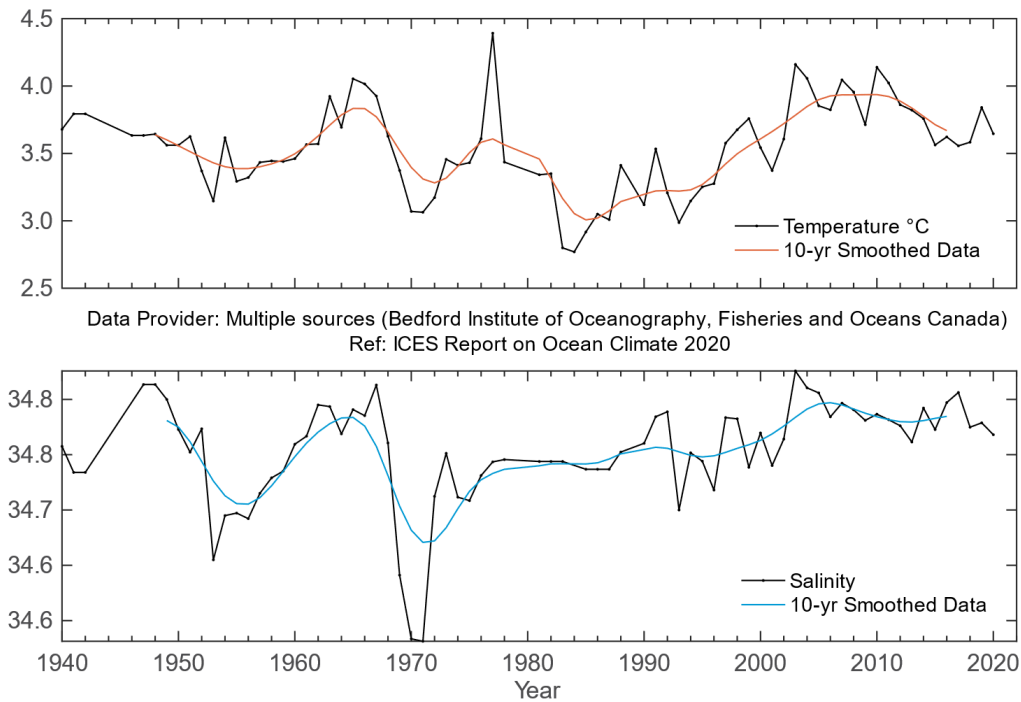


**Figure 4.8. Labrador Sea. Temperature (upper panel) and salinity (lower panel) anomalies at 50–200 m, from CTD and Argo data in the west-central Labrador Sea (centred at 56.7°N 52.5°W). Estimates of seasonal cycle (derived from all data in the time-series) have been removed from the observations.**

In winter 2018, as in the previous two winters (Yashayaev and Loder, 2017), the mid-high latitude North Atlantic experienced a more moderate cumulative loss of oceanic heat to the atmosphere than the two-decade record-high observed in winter 2015. 2018 winter heat losses in the Labrador Sea were the lowest since winter 2014. However, despite the reduction in cumulative winter heat losses, the depth of winter convection has been steadily increasing since 2015, gradually forming the most significant class of LSW since 1994, in terms of volume, depth, and density. Temperature and salinity profiles obtained by the ship survey and Argo floats show that the winter mixed layer, and hence convection in the central Labrador Sea, reached and exceeded 2000 m in 2018 (the deepest since the beginning of the century) ending the 7-year trend of winter mixed-layer deepening. A reservoir filled with this well-ventilated, record deep, cold and fairly fresh LSW is evident in seawater property sections (not shown). LSW formed in 2018 is characterized by low temperature ( $< 3.3^{\circ}\text{C}$ ) and salinity ( $< 34.86$ ) between 1000 and 2000 m. The winter convection during 2015–2018, especially winter 2018, is arguably the deepest since the record-deep cooling down to 2400 m in 1994. It produced one of the largest LSW year classes ever observed outside the early 1990s. This long-term persistence in LSW development is largely the result of water column preconditioning at intermediate depths, allowing

convection to deepen without increasing net heat surface heat loss in consecutive winters. However, the two following winters, 2019 and 2020, demonstrated that the effect of such preconditioning is not limitless – the maximum depth of convections for these winters was several hundred metres shallower than in 2018. The winter NAO index was slightly positive in 2019, but exceptionally high (the highest since 2015, and third highest since 1995) in 2020. The latter presents an exemplary case of the net surface heat loss over central Labrador Sea uncorrelated with the respective winter NAO index. The reason for this disparity is the character of the atmosphere in winter 2020. The higher-than-normal NAO index was associated with stronger winds, but from the north rather than from the west, and with the zone of most intense winds shifted to the east. This atmospheric situation did not favour high surface heat losses in the convection zone.

### Hydrographic changes in the Labrador Sea over the past 80 years

The long-term changes observed in the Labrador Sea until 2016 have been extensively discussed in a series of publications (Yashayaev *et al.*, 2007; Yashayaev and Loder, 2009, 2016, 2017). Here, the series is updated ([Figures 4.8](#) and [5.11](#); [Section 5.2.5](#)) allowing the earlier statement concerning the long-term variability in temperature and salinity to be revisited.

The deep intense winter mixing during winters 2014–2018, and the associated progressive cooling of the top 2000 m, have interrupted the general warming and stratification-building trend that has persisted in the intermediate waters of the Labrador Sea since the mid-1990s. Despite the reduction in net surface heat loss after 2015, the water column cooling continued until 2018, aided by multiyear convective preconditioning. In response to winter cooling enhanced by convective preconditioning, both the upper (50–200 m) and deeper (1000–1800 m) layers cooled between 2011 and 2018 ([Figures 4.8](#) and [5.11](#); [Section 5.2.5](#)). However, the situation changed in 2019 and 2020, with temperature increasing in the upper layer to near-normal, and stabilizing in the deeper layer.

Events of moderate freshening of the upper layer spread across of the central basin in 2013, 2015, and 2018–2020 ([Figure 4.8](#)).

With respect to multidecadal changes in the subpolar North Atlantic, the progressively deepening convective mixing that reoccurred in the Labrador Sea during the period 2012–2018 has reversed the general warming trend observed in the intermediate waters during 1994–2011. The situation changed again in 2019 and 2020, leading to a weakening in convection and ending the cooling trend. As a result of the sustained recurrence of stronger-than-normal convection and production of LSW, the annual average temperature and density in the region's upper 2000 m have predominantly varied on a bi-decadal time-scale, rather than having a long-term trend, as might be expected from anthropogenic climate change.

The above-average regional winter cooling during 2012–2020, enhanced by convective preconditioning, has increased the rate of removal of gas-saturated waters from the top 200 m. The moderately strong winter convection (down to 1600 m) in winter 2020 further added to increased gas uptakes (dissolved oxygen, anthropogenic gases, and carbon dioxide) and consequently increased gas concentrations in the lower half of the Labrador Sea 0–2000 m layer.

### Conclusion

Winter convection in the Labrador Sea is one of the main factors controlling interannual-to-multidecadal variability in the intermediate layer throughout the North Atlantic and is a key process driving or strongly influencing the Atlantic Meridional Overturning Circulation. This makes the Labrador Sea one of the few locations globally where surface waters are exchanged

with those residing at much greater depths. In addition, this process also has an important role in biogeochemical cycling in the Labrador Sea, since strong convection enhances the entrainment of gases, such as oxygen and carbon dioxide, into the deep water from the atmosphere and upper-layer freshwater.

Interannual variability in Labrador Sea ocean heat content and cumulative surface heat loss during the cooling season indicate that anomalously strong winter atmospheric cooling, associated with the NAO, is continuing to drive the recurrent convection. In turn, recurrent deep convection is contributing to decadal-scale variability in deep-water properties and in the transport across and from the subpolar North Atlantic (by the ocean's western boundary and interior pathways) and potentially the Atlantic Meridional Overturning Circulation.

### 4.3 Newfoundland-Labrador Shelf

*F. Cyr and P. Galbraith*

---

**THE REGIONAL CLIMATE IN NEWFOUNDLAND AND LABRADOR WAS GENERALLY WARMER THAN NORMAL IN 2020, CONTRASTING TO THE COLDER-THAN-AVERAGE CONDITIONS THAT MOSTLY PREVAILED DURING 2014–2017.**

---

The Newfoundland-Labrador Shelf region is located on the western side of the Labrador Sea, stretching from the Hudson Strait to the tail of the Grand Banks. The bathymetry on the shelf consists of shallow banks separated by deeper channels or saddles. The ocean circulation is dominated by the southward flowing Labrador Current system, which brings cold and fresh Arctic-origin waters, sea ice, and icebergs on the shelf down the Grand Banks, as well as warmer and saltier LSW along the continental slope.

Hydrographic conditions are determined in part by the strength of the winter atmospheric circulation over the northwest Atlantic (e.g. winter NAO index), advection by the Labrador Current, freshwater runoff, cross-shelf exchange with warmer continental slope water, etc. Superimposed are large seasonal and interannual variations in solar-heat input, sea-ice cover, and storm-forced mixing. The resulting water mass on the shelf exhibits large annual cycles with strong horizontal and vertical temperature and salinity gradients.

The winter NAO index, a key indicator of the direction and intensity of the winter wind field patterns over the Northwest Atlantic, was positive for a seventh consecutive year. Despite this, the regional climate in Newfoundland and Labrador was mostly warmer than normal in 2020, contrasting to the colder-than-average conditions that mostly prevailed during 2014–2017.

Annual air temperatures on the west side of the Atlantic were warmer than normal, especially on the island of Newfoundland where temperatures were 1 s.d. above normal in St. John's and Bonavista. In Iqaluit, on Baffin Island, the temperature was 0.7 s.d. above normal. A similar anomaly (+0.7 s.d.) was also observed at Cartwright in southern Labrador ([Figure 4.10](#)).

The seasonal (DJFMAMJ) mean sea-ice volume in three regions of the Newfoundland-Labrador Shelf, northern Labrador, southern Labrador, and Newfoundland, had been generally

decreasing since the early 1990s. After a recent rebound to near-normal conditions between 2014 and 2017, the sea-ice volumes have been back to normal conditions since 2018, reaching  $-1.1$ ,  $-1.3$ , and  $-1.0$  s.d. below normal, respectively (Figure 4.9). Averaged over these three regions, the 2020 mean sea ice volume ( $-1.1$  s.d.) was at its lowest value since the record-low of 2011 ( $-1.7$  s.d.).

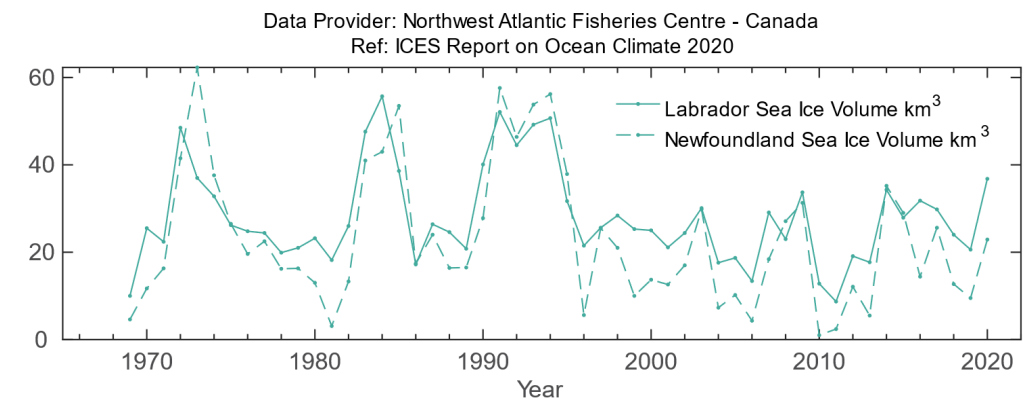


**Figure 4.9. Northwest Atlantic: Newfoundland–Labrador Shelf. Winter and spring sea-ice areas off Newfoundland–Labrador between 45°N and 55°N.**

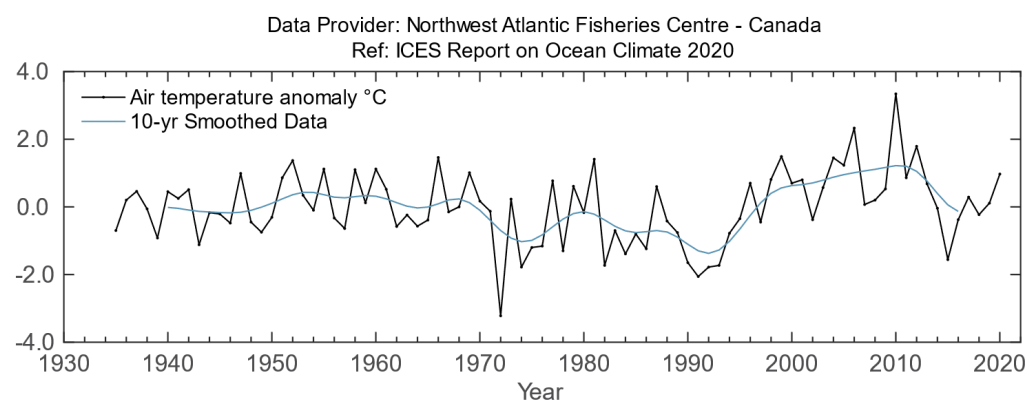


**Figure 4.10. Northwest Atlantic: Newfoundland–Labrador Shelf. Annual air temperature anomalies at Cartwright on the Labrador Coast.**

At the standard monitoring site off eastern Newfoundland (Station 27), the depth-averaged annual water temperature has progressively cooled down since the 2011 record high temperatures of  $+1.4^{\circ}\text{C}$  (2.0 s.d.) above normal (Figure 4.11). This warmer-than-average period generally coincided with fresher-than-average conditions that culminated in 2018, at  $-1.6$  s.d., the freshest anomaly year since 1970. In 2019 and 2020, however, both temperature and salinity were normal.

A robust index of ocean climate conditions in eastern Canadian waters is the areal extent of the cold intermediate layer (CIL) defined as the continental shelf waters  $< 0^{\circ}\text{C}$  along standard hydrographic sections (Figure 4.12). After its formation during winter, the CIL remains isolated between the seasonally heated upper layer and the warmer shelf-slope water throughout summer and early autumn. During the 1960s, when the winter NAO was at its most negative phase of the 20th century, the volume of CIL water was at a minimum (warmer-than-normal

conditions), and during the positive winter NAO years of the early 1990s, the CIL volume reached near-record high values (colder-than-normal conditions).

From the late 1990s to about 2011, the area of CIL water gradually reduced as a consequence of increased ocean temperatures. However, the CIL area then expanded and reached 2.3 s.d. above normal in 2015, the second largest anomaly since the beginning of the time-series, after 1984 (+ 2.35 s.d.). This recent cooling phase lasted approximately between 2014 and 2017, and was driven by the beginning of the ongoing positive winter NAO phase. Since 2018, the CIL area has been shrinking, reaching -2.5 s.d. and -1.3 s.d. on the southern Labrador and Newfoundland shelves, respectively. For the Newfoundland Shelf, this is the most negative anomaly since 2011.

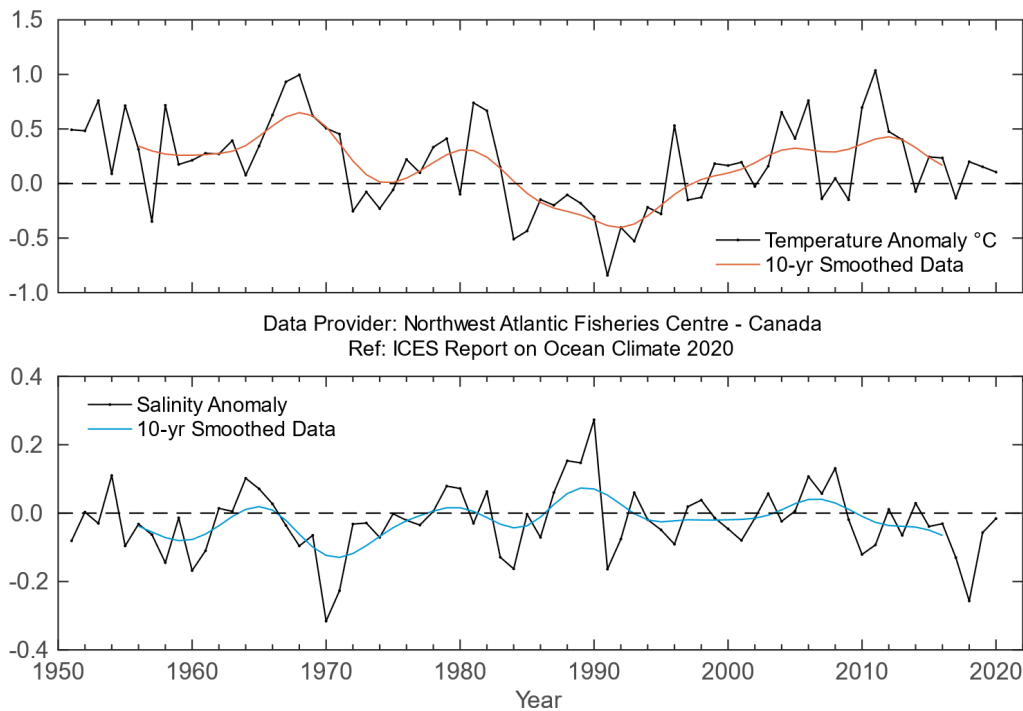


**Figure 4.11. Northwest Atlantic: Newfoundland–Labrador Shelf. Annual depth-averaged Newfoundland Shelf temperature (top panel) and salinity (middle panel) anomalies at Station 27 (47.55°N 52.59°W).**

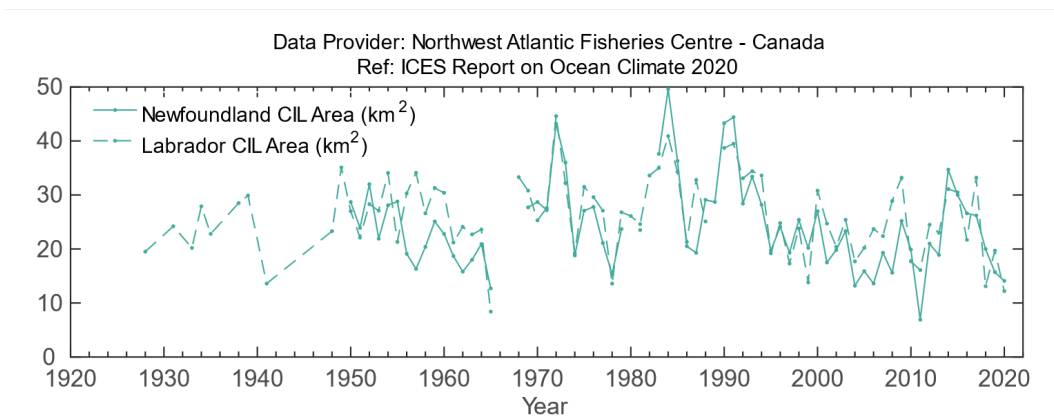


**Figure 4.12. Spatial extent of cold intermediate layer (CIL).**

## 4.4 Gulf of St. Lawrence

*P. Galbraith*

---

**DEEP-WATER TEMPERATURE (300 M) IN THE GULF OF ST. LAWRENCE AT A 100+ YEAR RECORD HIGH. THE LAST SIX YEARS WERE THE WARMEST ON RECORD.**

---

The Gulf of St. Lawrence is a semi-enclosed Canadian sea, covering an area of about 235 000 km<sup>2</sup> and containing 35 000 km<sup>3</sup> of water, which opens to the Atlantic Ocean through Cabot Strait (104 km wide and 480 m at its deepest) and the Strait of Belle Isle (17 km wide and 60 m at its sill). In winter, it can become completely covered by sea ice, and nearly half of its volume of water usually gets cooled to temperatures below 0°C within the winter mixed layer. This creates a CIL that persists until late autumn and determines the bottom-temperature habitat on the Magdalen Shallows.

Waters deeper than roughly 150–200 m are entrained inwards from the continental slope by estuarine circulation, taking several years to reach the heads of the Gulf deep channels, while mixing and diffusion occurs. This layer has been warming since 2009, above 7°C in places in recent years.

The maximum sea-ice volume reached during winter was below normal at 38 km<sup>3</sup> (– 1.0 s.d. against the 1981–2010 climatology; [Figure 4.13](#)). In the 11-year span since 2011, 8 of the 13 lowest maximum ice volumes of the time series have occurred.

In winter, a near-freezing mixed layer is formed in the Gulf of St. Lawrence that averages 75 m in thickness. The layer has been sampled every March since 1996 using a unique helicopter-based survey, which now samples around 100 stations to 200 m depth from stationary flight. In March 2020, the volume of the mixed layer colder than – 1°C was near normal at 13 100 km<sup>3</sup> ([Figure 4.14](#)).

The volume of CIL (defined here as water masses with a temperature below 1°C) present in August and September is estimated from temperature profiles taken mostly during multispecies surveys conducted since the mid-1980s ([Figure 4.15](#)). The volume in 2020, of 5900 km<sup>3</sup>, was well below normal (– 2.0 s.d.; i.e. warmer-than-normal conditions). The last above-normal conditions occurred in 2008.

Sea surface temperatures (SST) were greatly affected by the passage of a tropical storm in late August, and the warmest July of the satellite record for the St. Lawrence Estuary turned into the coolest September on record. However, the ocean didn't lose any heat. A Viking oceanographic buoy (PMZA-VAS, Shediac Valley) located in the Gulf recorded temperature-salinity profiles that show evidence of mixing down to a depth of 55 m with near-surface cooling and deeper warming, but nearly identical 0–55 m depth-averaged temperature. The SST May–November average was normal at + 0.1 s.d., hiding this monthly variability ([Figure 4.16](#)).

Deep-water temperatures have been increasing overall in the Gulf since 2009, with inward advection from Cabot Strait ([Figure 4.17](#)). The gulf-wide average temperature at 300 m has been at a new 100+ year record high every year since 2015, standing at 6.8°C in 2020 (+ 1.3°C, + 8.2 s.d.).

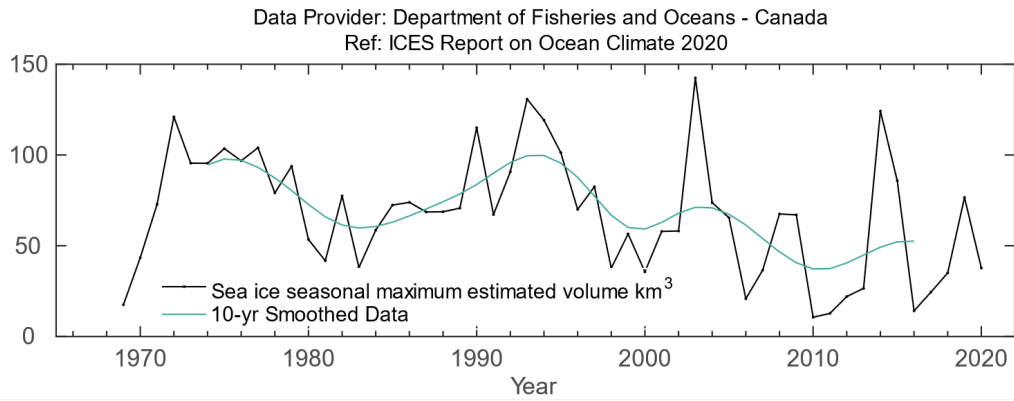


Figure 4.13. Northwest Atlantic: Gulf of St. Lawrence. Seasonal maximum sea-ice volume in the Gulf of St. Lawrence estimated from weekly ice charts.

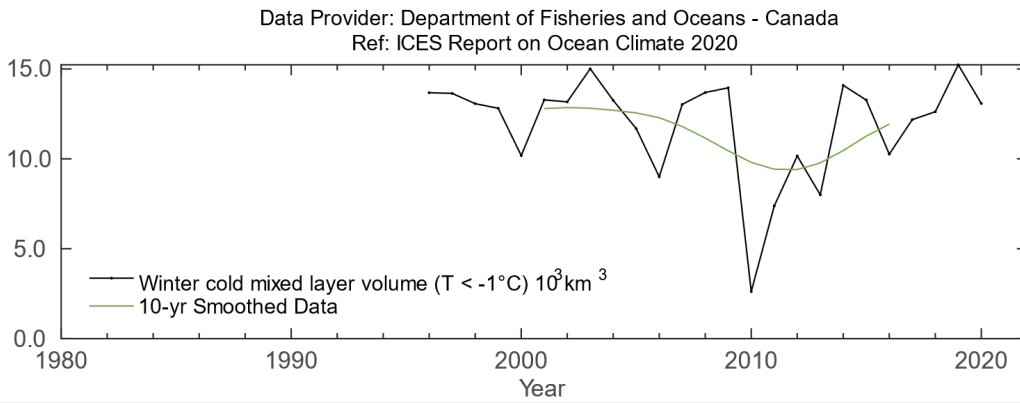


Figure 4.14. Northwest Atlantic: Gulf of St. Lawrence. Winter mixed layer ( $T < -1^\circ\text{C}$ ) volume in the Gulf of St. Lawrence.

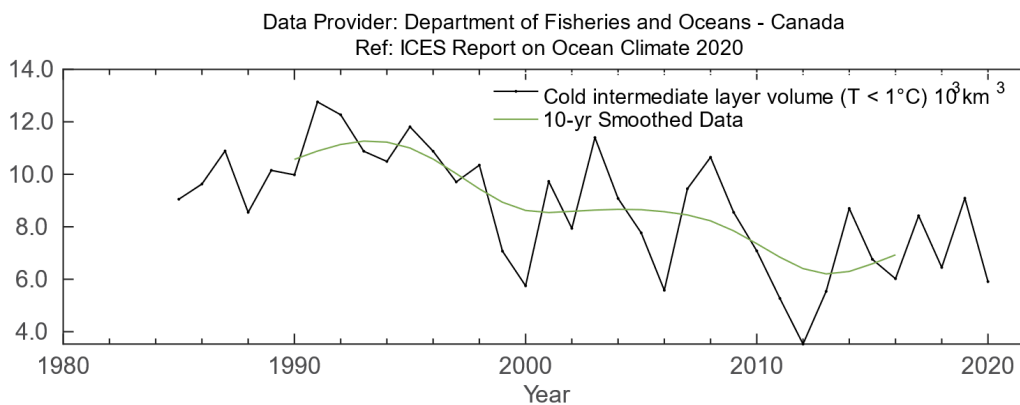


Figure 4.15. Northwest Atlantic: Gulf of St. Lawrence. Cold Intermediate Layer volume ( $T < 1^\circ\text{C}$ ) present in August and September in the Gulf of St. Lawrence.

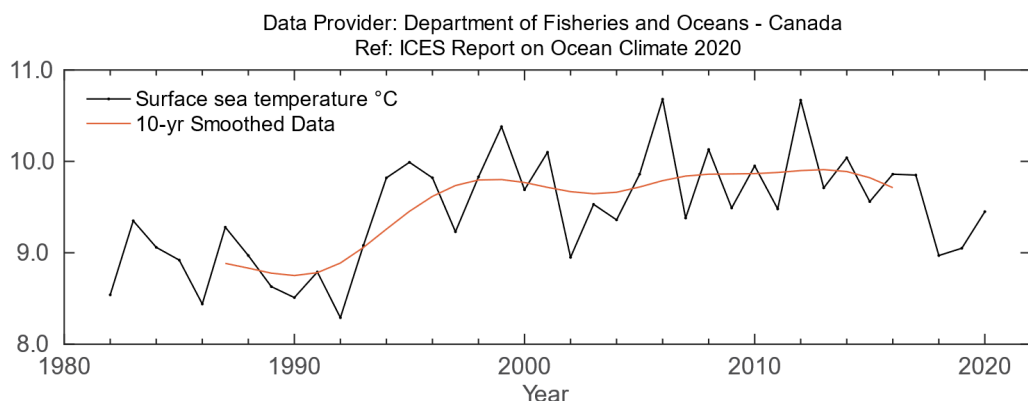


Figure 4.16. Northwest Atlantic: Gulf of St. Lawrence. Seasonally averaged sea surface temperature (May–November) in the Gulf of St. Lawrence.

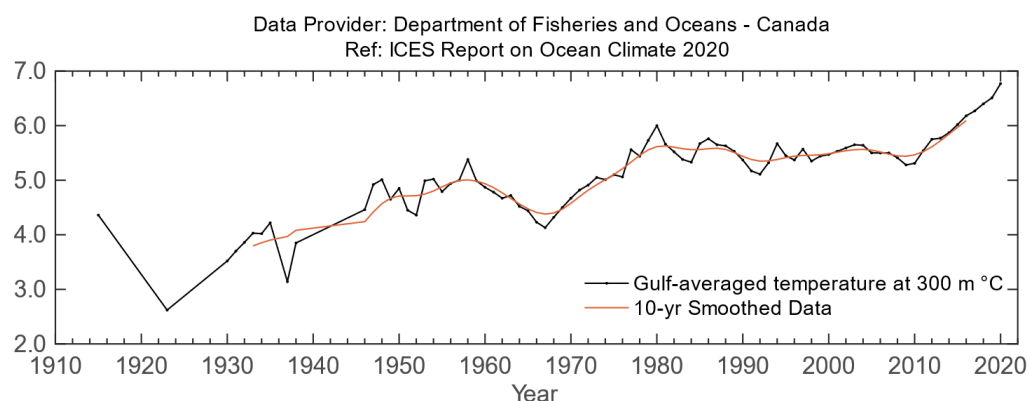


Figure 4.17. Northwest Atlantic: Gulf of St. Lawrence. Averaged temperature at 300 m.

## 4.5 Scotian Shelf

*D. Hebert, C. Layton, and P. S. Galbraith*

The Scotian shelf is the continental shelf off the coast of Nova Scotia and is identified as a NOAA LME. It is characterized by a complex topography, consisting of many offshore shallow banks and deep mid-shelf basins. It is separated from the Newfoundland Shelf in the northeast by the Laurentian Channel, and borders the Gulf of Maine to the southwest. Surface circulation is dominated by a general flow towards the southwest, interrupted by clockwise movement around the banks and anticlockwise movement around the basins, the strengths of which vary seasonally.

Hydrographic conditions on the Scotian Shelf are determined by heat transfer between the ocean and atmosphere, inflow from the Gulf of St Lawrence and the Newfoundland Shelf, and exchange with offshore slope waters. Water properties have large seasonal cycles and are modified by freshwater run-off, precipitation, and melting of sea ice. Temperature and salinity exhibit strong horizontal and vertical gradients that are modified by diffusion, mixing, currents, and shelf topography.

In 2020, annual mean air temperature over the Scotian Shelf (represented by Sable Island observations; [Figure 4.18](#)) was +1.1°C (+1.6 s.d.) above the long-term mean (1981–2010). The linear trend from 1900 to 2020 is +1.4°C (95% confidence limits: +1.0°C, +1.7°C). The January–April 2020 seasonal sea-ice average on the Scotian Shelf, measured seaward of Cabot Strait between Nova Scotia and Newfoundland, was 2100 km<sup>2</sup>, well below the 1981–2010 long-term mean of 6700 km<sup>2</sup>. The maximum weekly area of 8200 km<sup>2</sup> was well below the 20 900 km<sup>2</sup> long-term mean ([Figure 4.19](#)). Other than in 2019, sea-ice conditions have been below average since 2015.

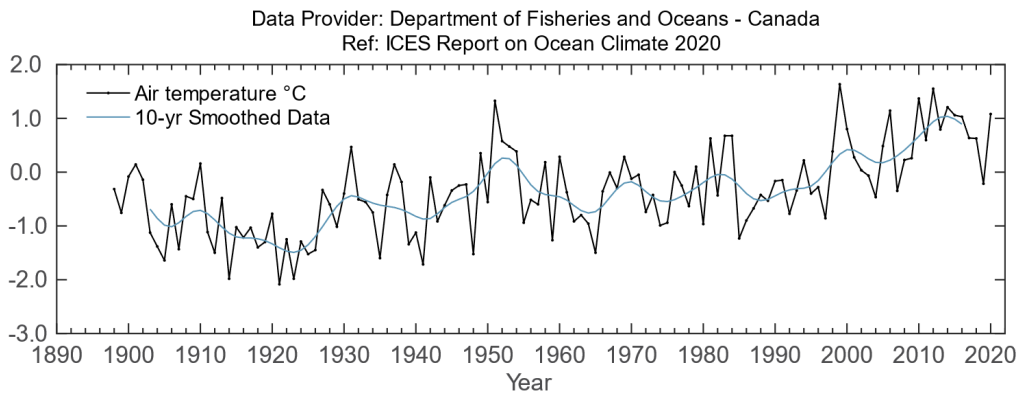


**Figure 4.18. Northwest Atlantic: Scotian Shelf. Air temperature anomalies at Sable Island on the Scotian Shelf.**

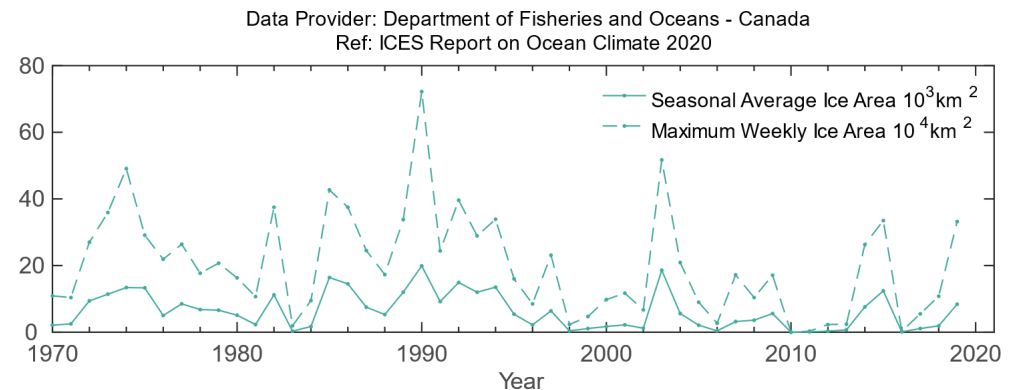


**Figure 4.19. Northwest Atlantic: Scotian Shelf. Monthly means of ice area seaward of Cabot Strait. Data until 2019.**

Topography separates the northeastern Scotian Shelf from the rest of the shelf. In the northeast, the bottom tends to be covered by relatively cold water (2–5°C), whereas the basins in the central and southwestern regions typically have bottom temperatures of 6–10°C. The origin of the latter is the offshore slope waters, whereas water in the northeast comes principally from the Gulf of St. Lawrence. The interannual variability of the two water masses differs.

Measurements of temperatures at 100 m at the Misaine Bank Station capture the changes in the northeast Scotian Shelf ([Figure 4.20](#)). They revealed above-average annual temperature in 2020, +0.6°C (+0.9 s.d.), and near normal for salinity, –0.03 (–0.2 s.d.). The deep Emerald Basin anomalies represent the slope water intrusions onto the shelf that are subsequently trapped in the inner basins. In 2020, the 250 m annual temperature was near a record high +1.6°C (+1.9 s.d.), making the last seven years the warmest on record. Similarly, the salinity anomaly was well above normal, +0.3°C (+1.9 s.d.). The last eight years were the saltiest on record

(Figure 4.21). Model simulations of the region showed a large flux of warm salty water from the slope region. Ocean temperatures and salinity in the deep basins of the Scotian Shelf were far above normal in 2020, near record highs, reflective of warm salty conditions in the slope region offshore.

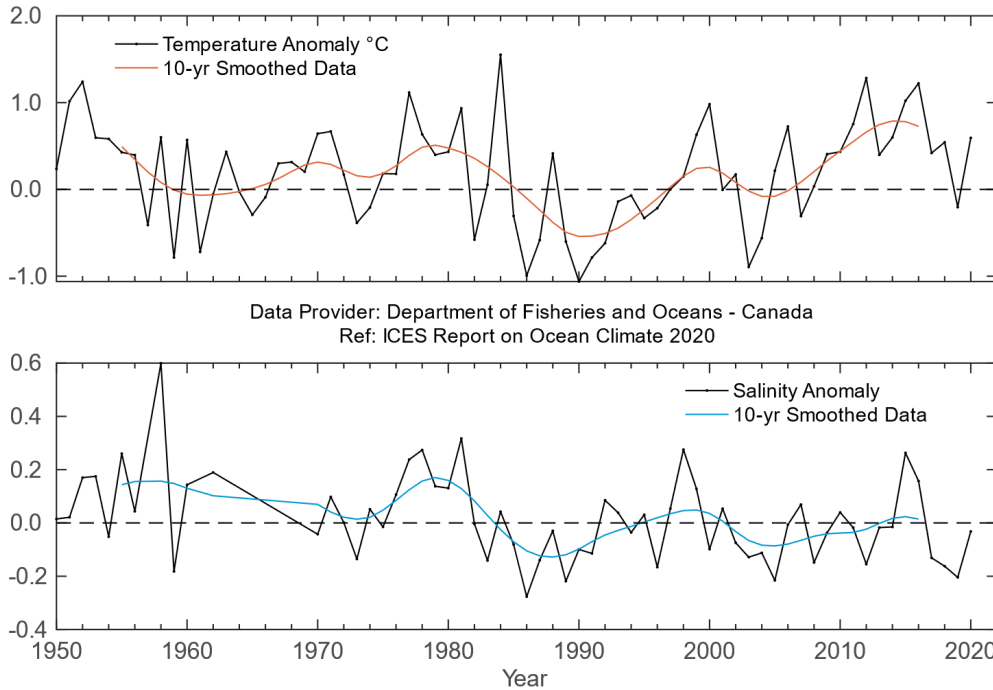


Figure 4.20. Northwest Atlantic: Scotian Shelf. Near-bottom temperature (upper panel) and salinity (lower panel) anomalies at Misaine Bank (100 m).

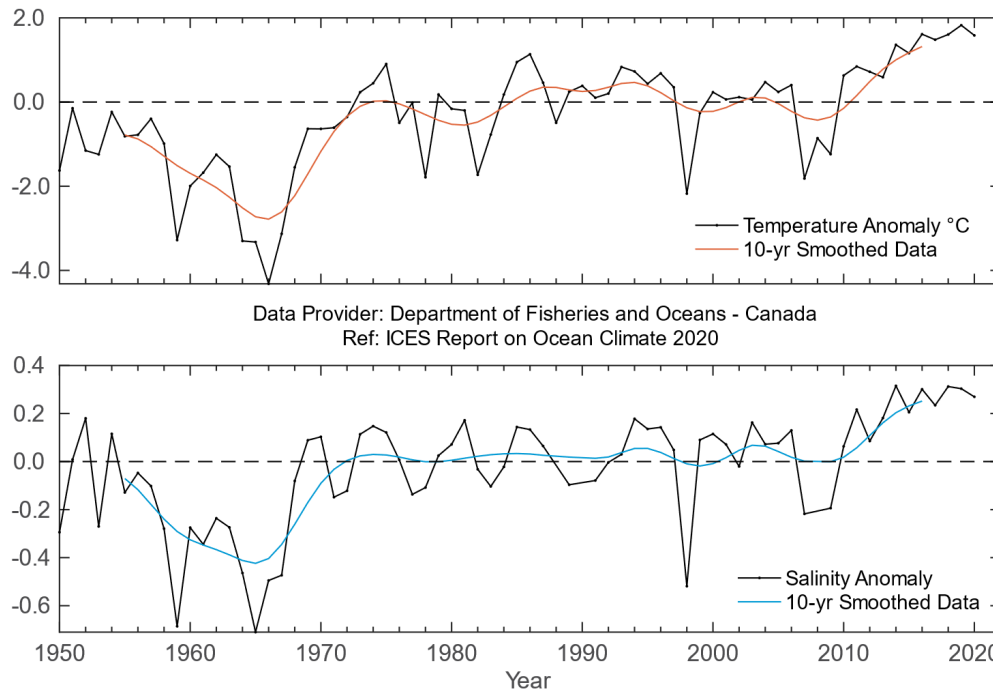


Figure 4.21. Northwest Atlantic: Scotian Shelf. Near-bottom temperature (upper panel) and salinity (lower panel) anomalies in the central Scotian Shelf (Emerald Basin, 250 m).

## 4.6 Northeast US continental shelf

*P. Fratantoni*

---

**THERE IS NO 2020 UPDATE FOR THE NORTHEAST US CONTINENTAL SHELF.**

---

The northeast US continental shelf extends from the southern tip of Nova Scotia, Canada, southwest through the Gulf of Maine and the Middle Atlantic Bight, to Cape Hatteras, North Carolina ([Figure 4.22](#)). Contrasting water masses from the Subtropical and Subpolar gyres influence the hydrography in this region. Located at the downstream end of an extensive interconnected coastal boundary current system, the northeast US continental shelf is the direct recipient of cold/fresh Arctic-origin water, accumulated coastal discharge, and ice melt that has been advected thousands of kilometers around the boundary of the subpolar North Atlantic. Likewise, subtropical water masses, advected by the Gulf Stream, slope currents, and associated eddies also influence the composition of water masses within this shelf region. The western boundary currents of the Subpolar and Subtropical gyres respond to variations in basin-scale forcing through changes in position, volume transport, and/or water mass composition. It is partly through these changes that basin-scale climate variability is communicated to the local northeast US continental shelf. Shelf-wide, hydrographic conditions have been monitored annually in this region since 1977 as part of quarterly ecosystem monitoring and twice-yearly bottom-trawl surveys conducted by the US National Marine Fisheries Service, Northeast Fisheries Science Center.

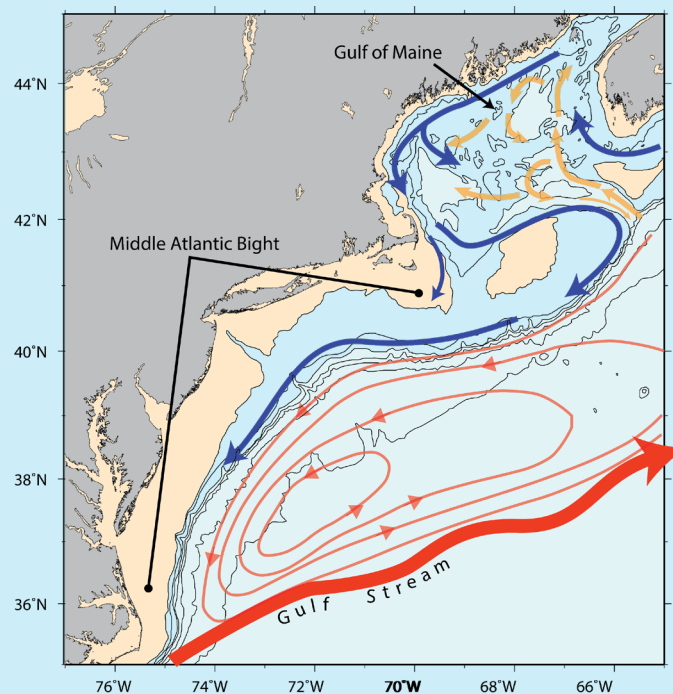


**Figure 4.22.** Circulation schematic for the northeast US shelf region. Blue arrows: shelf water circulation. Orange arrows: deeper slope water circulation pathways. Water depths deeper than 200 m are shaded blue. Water depths shallower than 50 m are shaded tan.

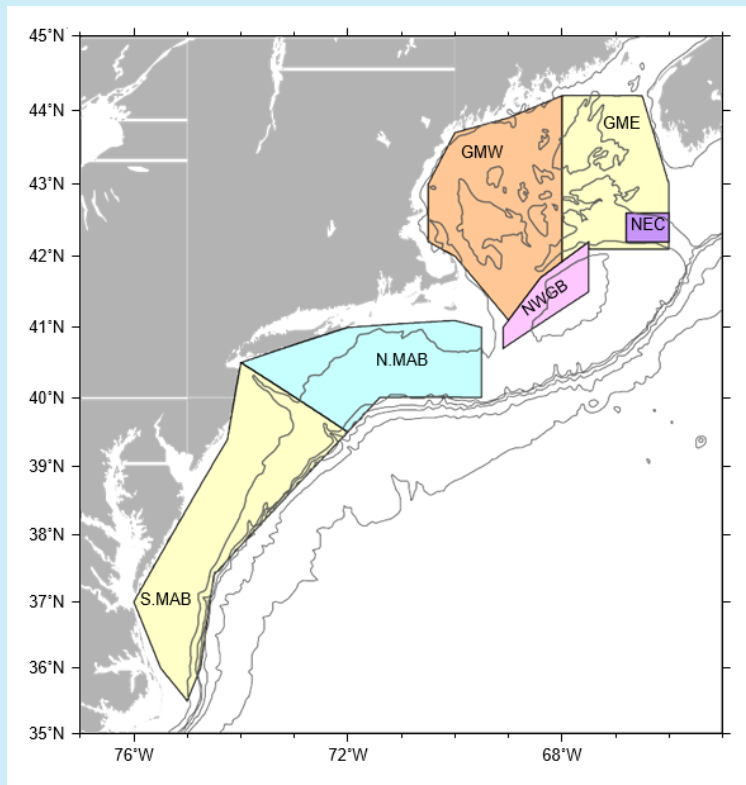


**Figure 4.23.** The six regions within which CTD observations are used to compute regional average time series - eastern and western Gulf of Maine: GME and GMW; northern and southern Middle Atlantic Bight: N.MAB and S.MAB; northeast Channel: NEC; and northwest Georges Bank: NWGB. The 50-, 200-, 500-, 1000-, 2000-, and 3000-m isobaths are shown.

Typically, US National Oceanic and Atmospheric Administration’s Northeast Fisheries Science Center conducts multiple shelf-wide surveys every year in support of its mission to monitor the northeast US shelf ecosystem. Monitoring efforts have been ongoing since 1977. However, operations were suspended in 2020 in response to the global COVID-19 pandemic. For this reason, no update on hydrographic conditions in this region is available for 2020. For the most recent regional overview, please see Section 4.6 in the IROC 2019 (González-Pola *et al.*, 2020).



MIOC Cruise. Photo: Tomasz Szumski, Marine Institute, Galway, Ireland

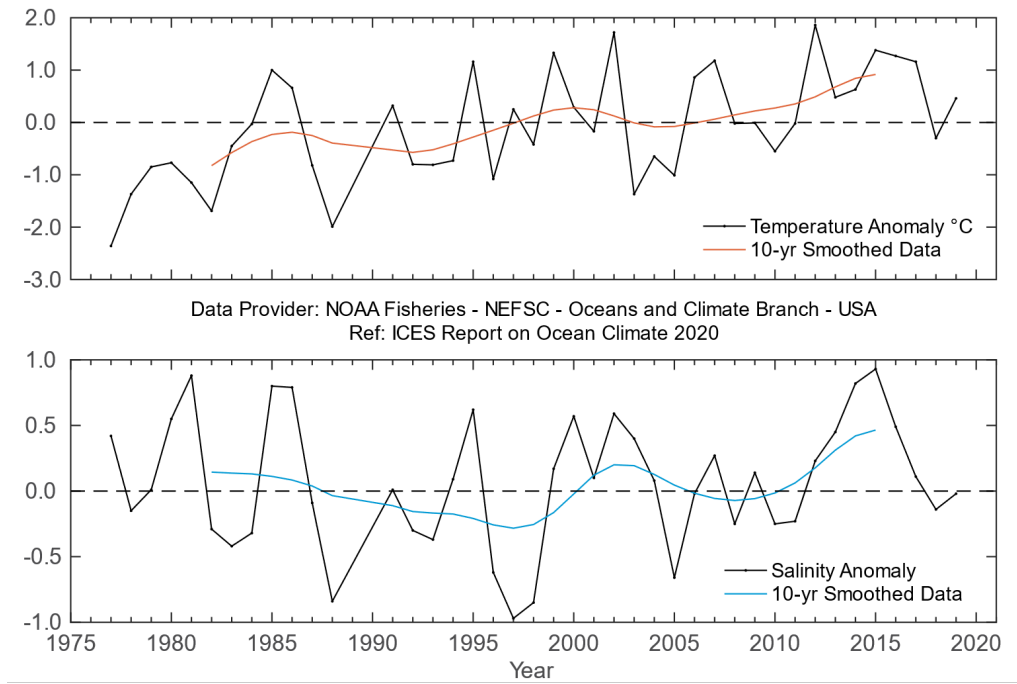


**Figure 4.24.** Northeast US continental shelf. Time-series plots of 0–30 m averaged temperature anomaly (upper panel) and salinity anomaly (lower panel) in the region between Cape Hatteras, North Carolina, and Hudson Canyon. Anomalies are calculated relative to the period 1981–2010 using hydrographic data from shelf-wide surveys. Data until 2019.

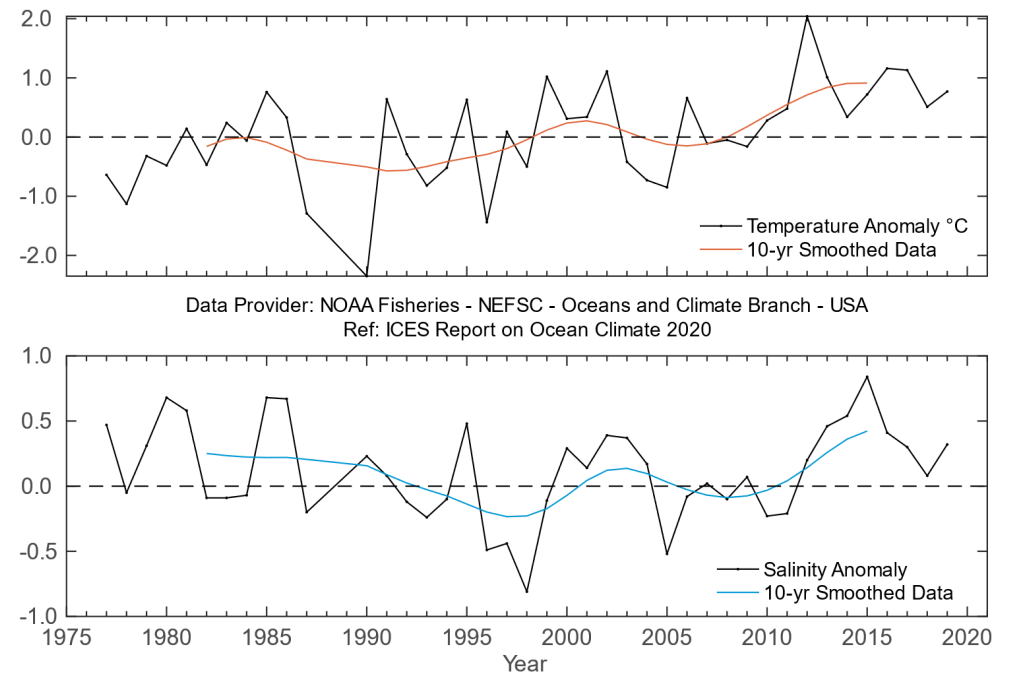


**Figure 4.25.** Northeast US continental shelf. Time-series plots of 0–30 m averaged temperature anomaly (upper panel) and salinity anomaly (lower panel) in the region between Hudson Canyon and Cape Cod, Massachusetts. Anomalies are calculated relative to the period 1981–2010 using hydrographic data from shelf-wide surveys. Data until 2019.

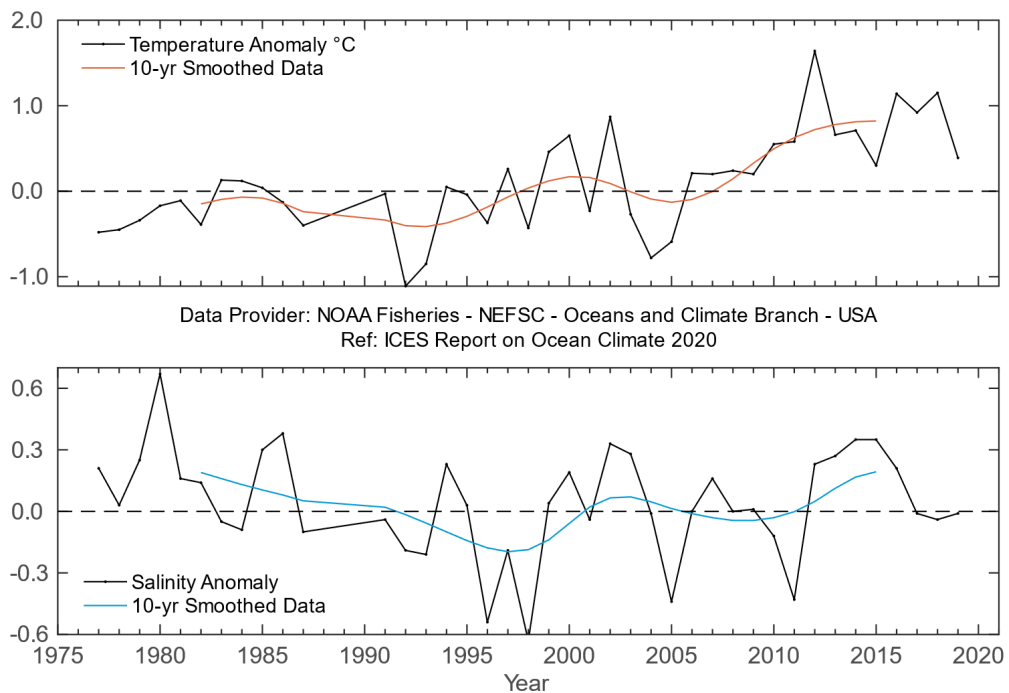


**Figure 4.26.** Northeast US continental shelf. Time-series plots of 0–30 m averaged temperature anomaly (upper panel) and salinity anomaly (lower panel) in the western Gulf of Maine. Anomalies are calculated relative to the period 1981–2010 using hydrographic data from shelf-wide surveys. Data until 2019.

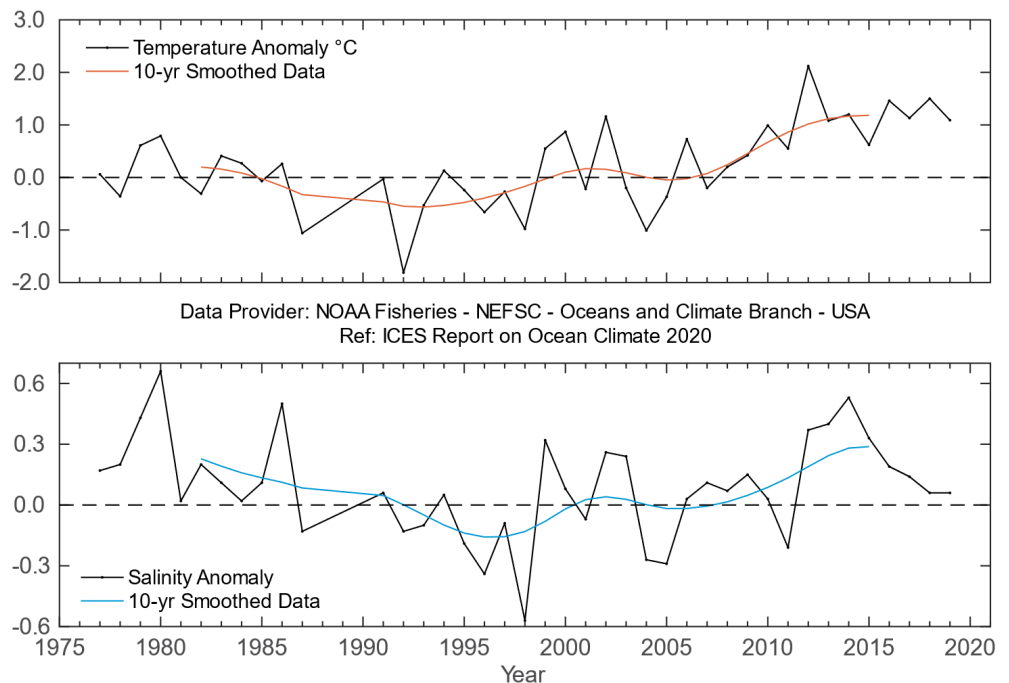


**Figure 4.27.** Northeast US continental shelf. Time-series plots of 0–30 m averaged temperature anomaly (upper panel) and salinity anomaly (lower panel) in the eastern Gulf of Maine. Anomalies are calculated relative to the period 1981–2010 using hydrographic data from shelf-wide surveys. Data until 2019.

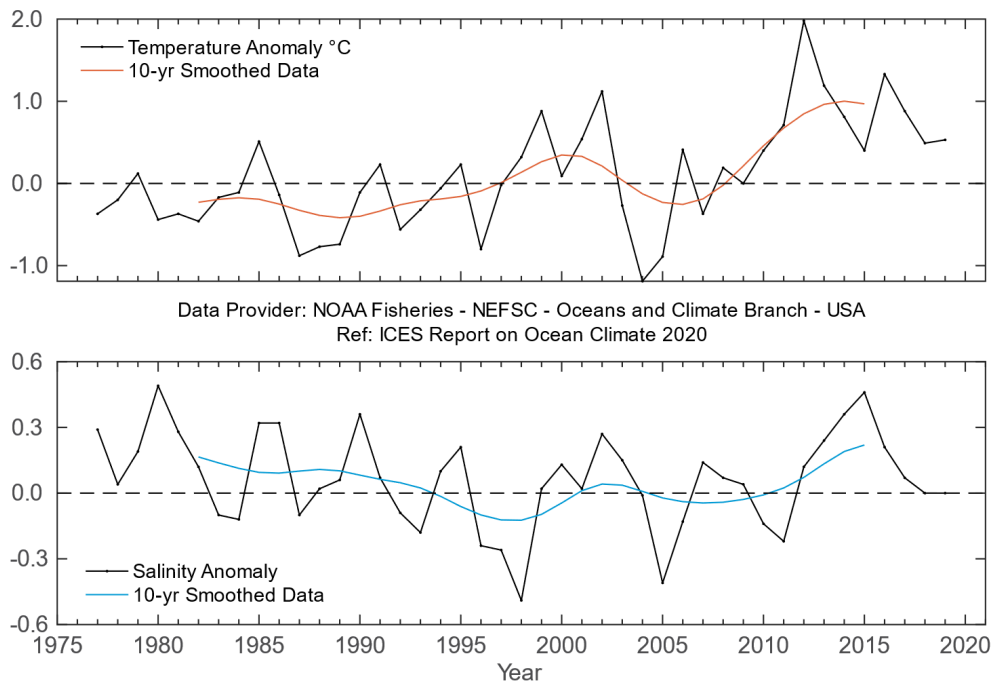


Figure 4.28. Northeast US continental shelf. Time-series plots of 0–30 m averaged temperature anomaly (upper panel) and salinity anomaly (lower panel) on George Bank. Anomalies are calculated relative to the period 1981–2010 using hydrographic data from shelf-wide surveys. Data until 2019.

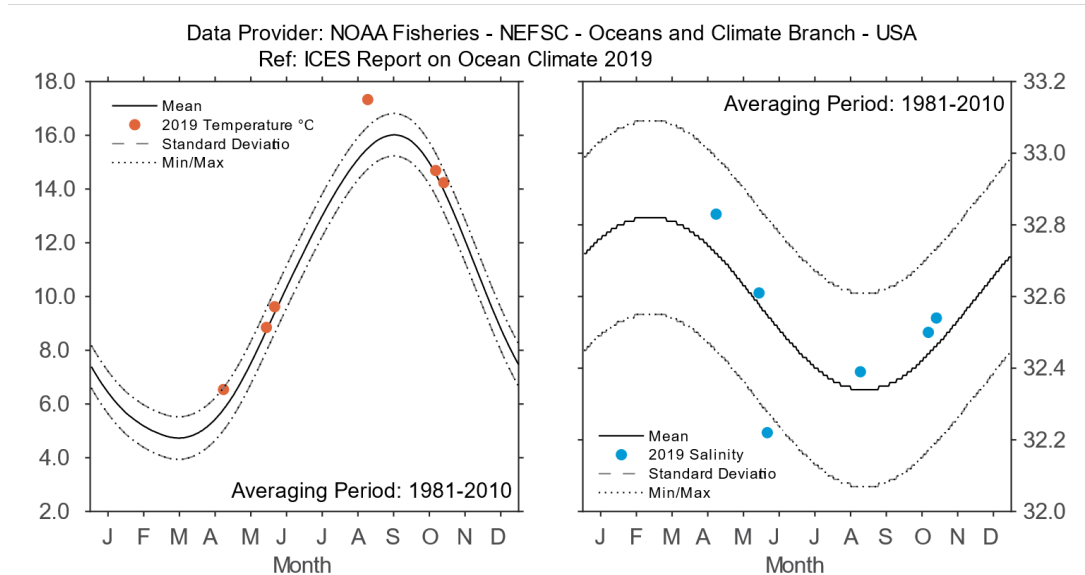


Figure 4.29. Northeast US continental shelf. 2019 temperature (left) and salinity (right) averaged over 0–30 m at northwest Georges Bank, relative to the annual cycle calculated 1981–2010. The envelope corresponding to the monthly range and 1 s.d. are shown. Data from 2019.

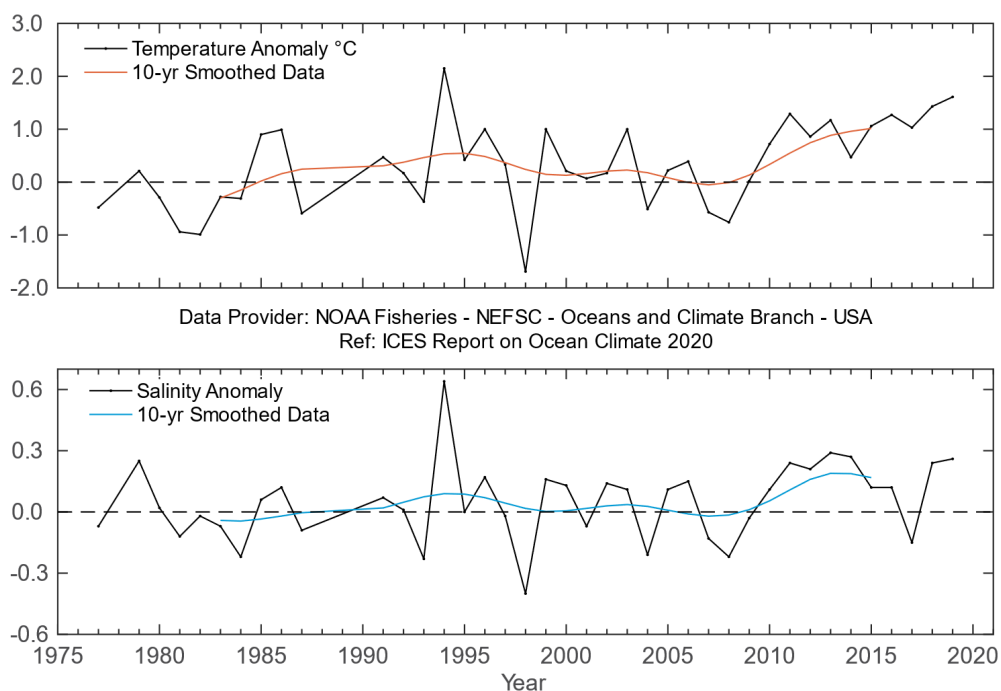


Figure 4.30. Northeast US continental shelf. Time-series plots of 150–200 m averaged temperature anomaly (upper panel) and salinity anomaly (lower panel) in the Northeast Channel. Anomalies are calculated relative to the period 1981–2010 using hydrographic data from shelf-wide surveys. Data until 2019.



## 4.7 Icelandic waters

*S. R. Ólafsdóttir and M. Danielsen*

The Iceland shelf and seas are identified as a NOAA LME and an ICES ecoregion. In Icelandic waters, mixing of different water masses occurs. These converge in an area of submarine ridges (Greenland-Scotland Ridge, Reykjanes Ridge, and Kolbeinsey Ridge) that form natural barriers to the main ocean currents ([Figure 4.31](#)). The warm Irminger Current (6–8°C), a branch of the NAC, flows from the south, and the cold East Greenland and East Icelandic currents (–1°C to 2°C) flow from the north. Deep and bottom currents in the seas around Iceland are principally the overflow of cold water from the Nordic Seas and the Arctic Ocean over the submarine ridges into the North Atlantic.

Hydrographic conditions in Icelandic waters are generally closely related to atmospheric or climatic conditions in and over the country and the surrounding seas, mainly through the Icelandic low-pressure and Greenland high-pressure systems. These conditions in the atmosphere and the surrounding seas affect biological conditions, expressed through the food chain in the waters, including recruitment and abundance of commercially important fish stocks.

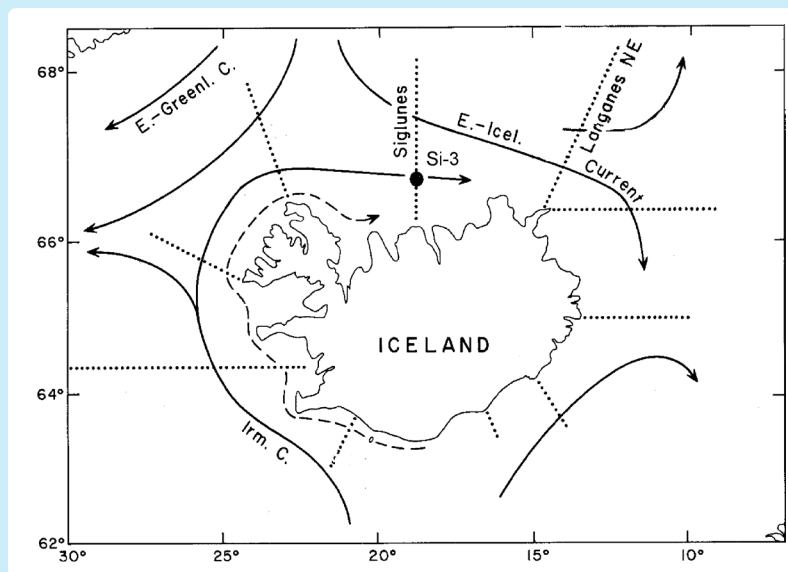


**Figure 4.31.** Main currents and location of standard sections in Icelandic waters.

Mean annual air temperature in 2020 was slightly above average in southern Iceland (Reykjavik) and continued to be above average in northern Iceland (Akureyri; [Figure 4.32](#)). The temperature in the AW south of Iceland in spring ([Figure 4.34](#)) was close to the long-term average, but 0.3°C lower than the previous year. The salinity increased by 0.02 between 2019 and 2020, but was still below average, as it has been since 2016. In north Icelandic waters, temperature and salinity decreased in spring by 1.5°C and 0.09, respectively, but both continued to be above the long-term average ([Figure 4.33](#)). In the surface layer northeast of Iceland, in the East Icelandic Current, temperature decreased by 1.1°C, falling below the long-term average, while salinity decreased by 0.03, but stayed above average ([Figure 4.35](#)).

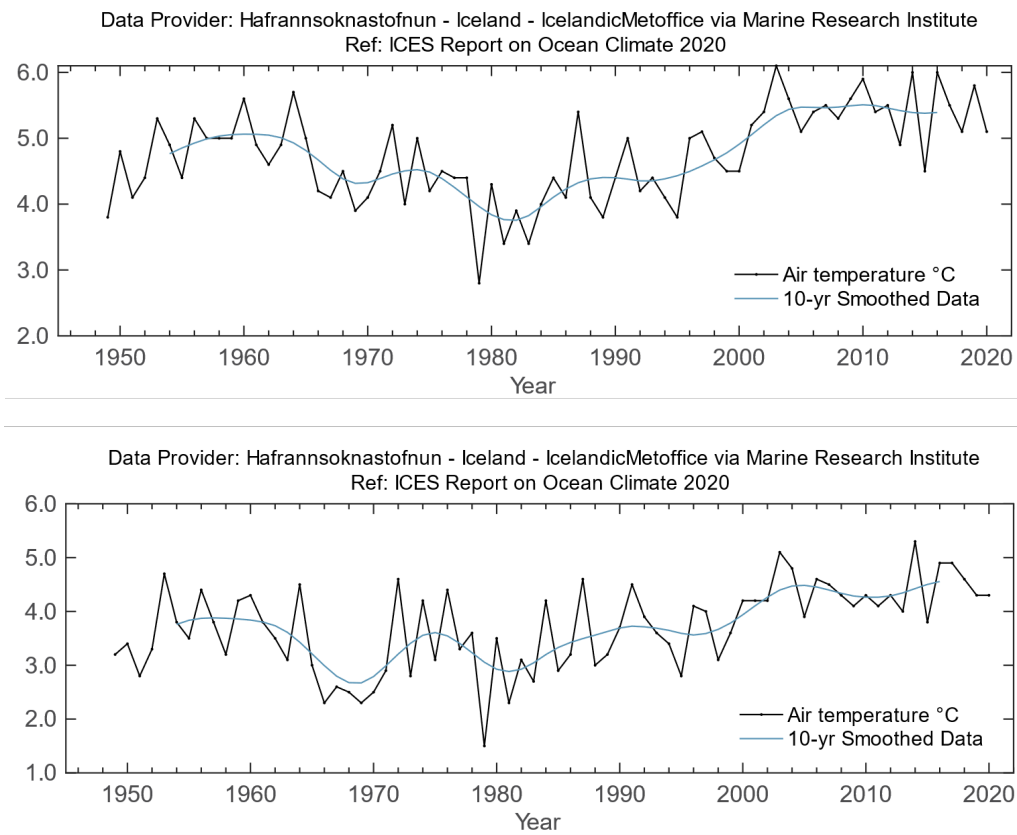


Figure 4.32. Icelandic waters. Mean annual air temperature at Reykjavik (upper panel) and Akureyri (lower panel).

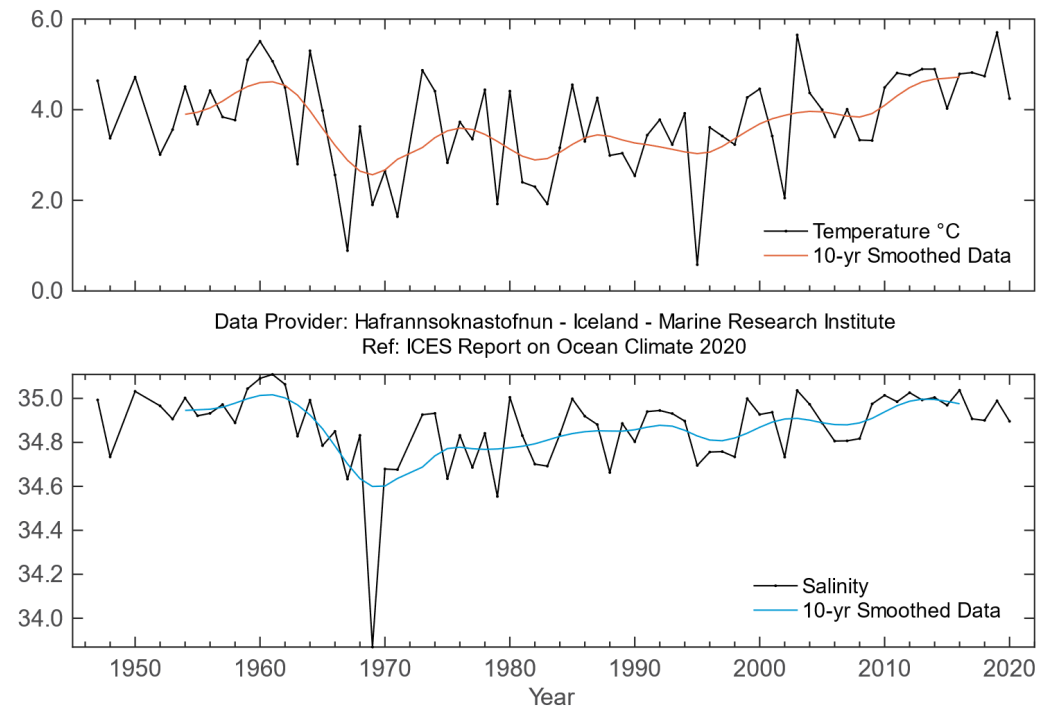


Figure 4.33. Icelandic waters. Temperature (upper panel) and salinity (lower panel) at 50–150 m at Siglunes Stations 2–4 in North Icelandic waters.

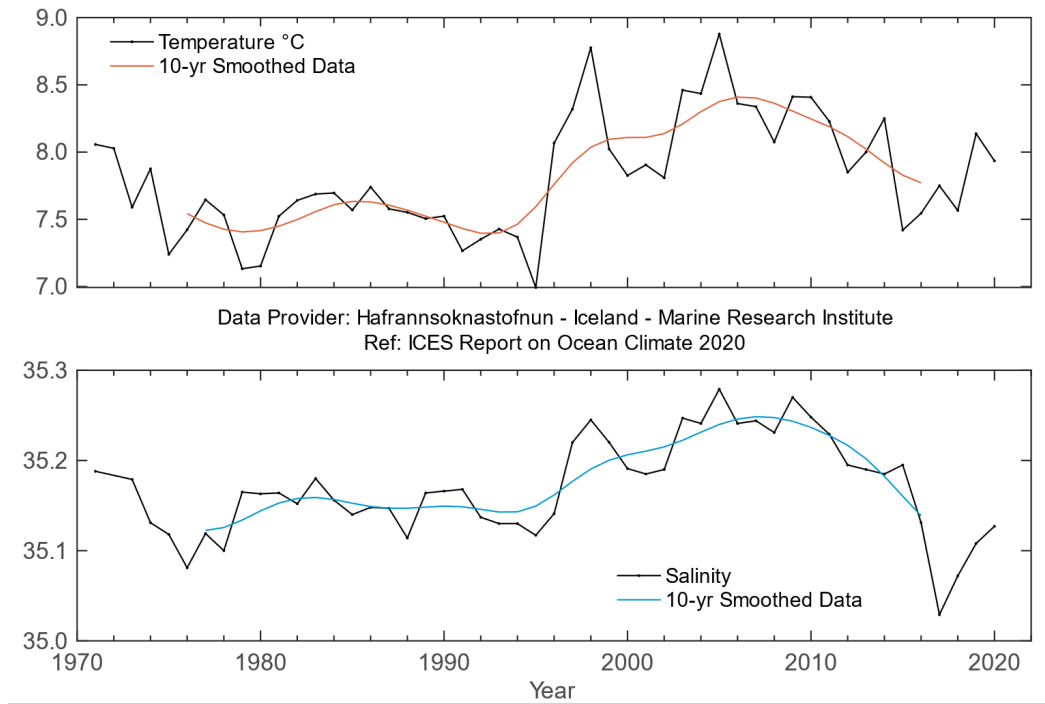


Figure 4.34. Icelandic waters. Temperature (upper panel) and salinity (lower panel) at 0–200 m at Selvogsbanki Station 5 in South Icelandic waters.

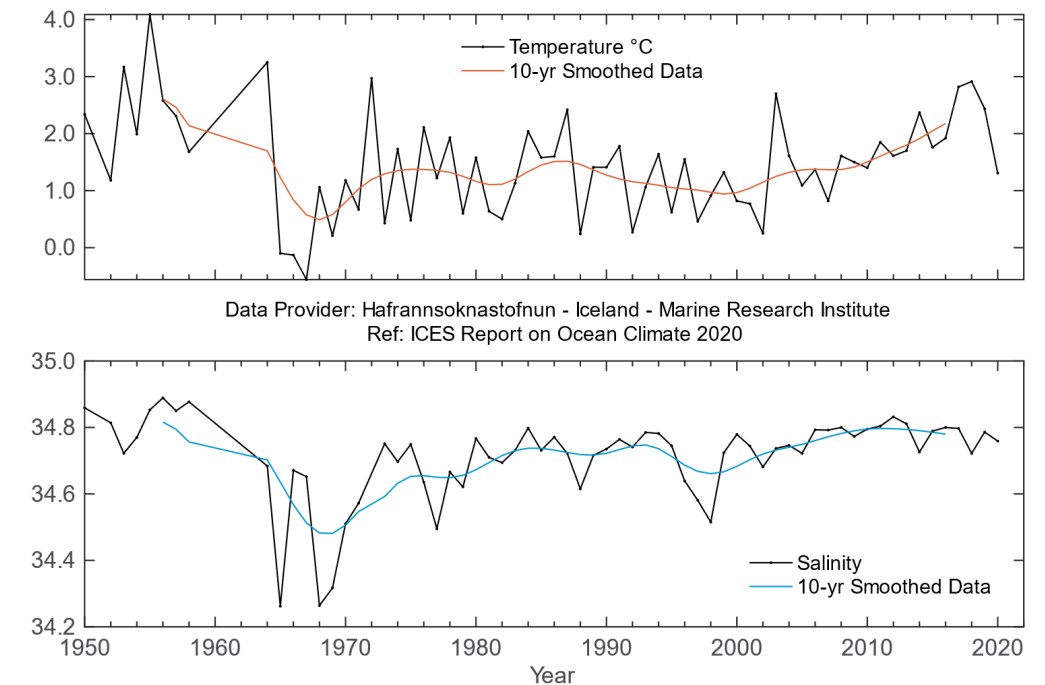


Figure 4.35. Icelandic waters. Temperature (upper panel) and salinity (lower panel) at 0–50 m in the East Icelandic Current (Langanes Stations 2–6).

## 4.8 Bay of Biscay and the Iberian Coast

*A. Fontán, C. González-Pola, and V. Valencia*

### LOWEST RECORDED UPPER-WATER SALINITY IN THE LAST THREE DECADES, CONCURRENT WITH ABOVE-AVERAGE TEMPERATURES.

The western Iberian coast is located at the northeastern edge of the subtropical anti-cyclonic gyre, sometimes referred to as the intergyre region. It is characterized by a weak upper ocean circulation, with a mean southward flow of a few  $\text{cm s}^{-1}$  (e.g. Paillet and Mercier, 1997). The Bay of Biscay is considered an adjacent sea with weak anticyclonic circulation (Pingree, 1993; van Aken, 2002). The area also encompasses the northern tip of the northwest Africa upwelling system. Coastal upwelling events dominate in spring/summer, and a geostrophically balanced poleward flow, known as the Iberian Poleward Current, develops in autumn and winter (Pingree and Le Cann, 1990). Regional modal waters making up the upper permanent thermocline are known as Eastern North Atlantic Central Waters (ENACW). Below them, Mediterranean Water (MW) spreads northwards from its source in the Gulf of Cadiz, mostly as a slope current. Below the MW, the Labrador Sea Water (LSW) can be identified at approximately 1800 m. Finally, the deep ocean is occupied by a mixture of cold polar waters known as North Atlantic Deep Water (NADW).

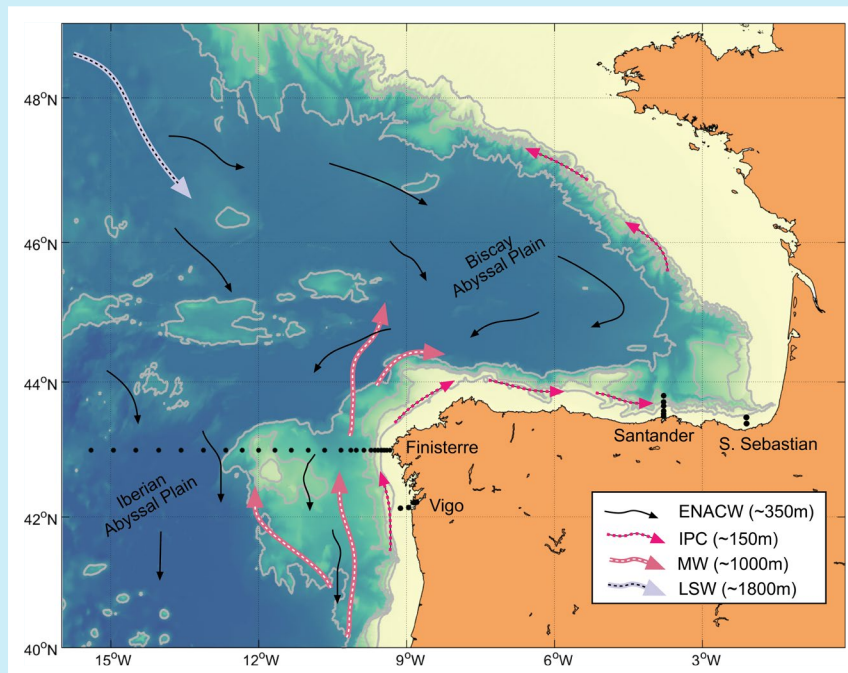


**Figure 4.36.** Circulation schematic for northwest Iberia and the Bay of Biscay. Black thin arrows show the dominant southward flow in the upper ocean carrying mainly ENACW. The Iberian Poleward Current and the MW pathways are also shown. Black dots show the repeated hydrographic stations, which are either occupied monthly, Vigo, Santander, and San Sebastian, or 1–2 times per year, Finisterre section.

The year 2020 was, all year-round, warm to extremely warm for the Iberian Peninsula, and the Balearic and the Canary islands. Annual atmospheric temperature was the highest observed since the late 1920s in the southern Bay of Biscay (Figure 4.37), exceeding 1.2°C and 2 s.d. above the long-term average. In terms of precipitation, 2020 can be considered very wet for the southern Bay of Biscay, but precipitation was irregularly distributed, with March, October, and December peaks. The annual continental run-off was around the long-term average (1981–2010), resulting from below-average river flow most of 2020, excluding March, May, October, and December.

The sea surface temperature (SST) was consistent with air temperature in 2020, being 1 s.d. or more above the long-term average across the entire Bay of Biscay region during most of the year. The annual SST in 2020 was the third highest value since the late 1940s, almost 1.3°C (+ 3 s.d.) above the long-term average, (Figure 4.38). Subsurface waters were very fresh, but still warmer than normal, influenced by the development of winter mixed layers down to 300 m. Freshening, first observed in 2014, was enhanced in 2020, reaching the lowest values that have been observed in at least the last three decades. Altogether, ocean conditions in 2020 were influenced by a combination of warmer- and wetter-than-normal atmospheric conditions, a weak signature of southern origin waters, and the influence of fresher waters spreading across the eastern North Atlantic. The status of deeper waters in the region is described in Section 5.2.6.

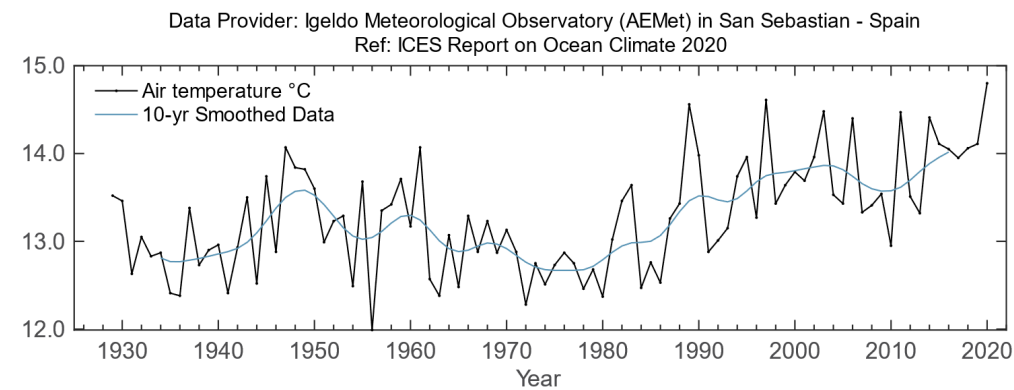


Figure 4.37. Bay of Biscay and eastern Atlantic. Air temperature at San Sebastian (43°18.50' N 002°02.37' W).

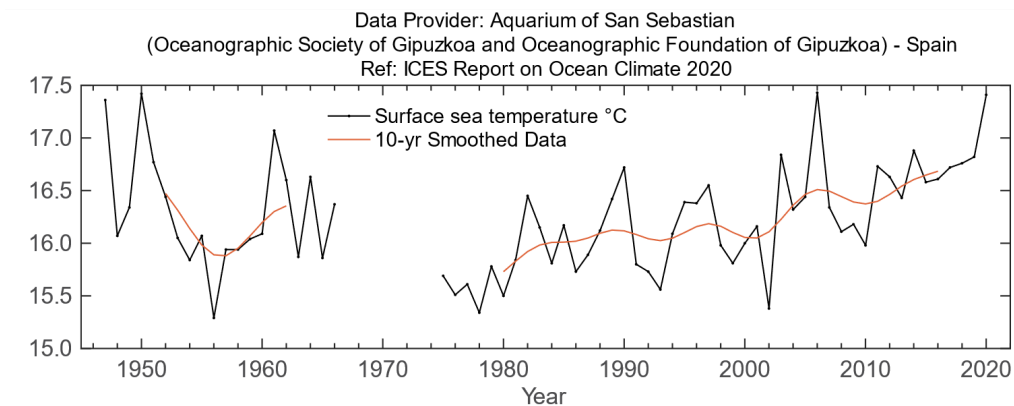
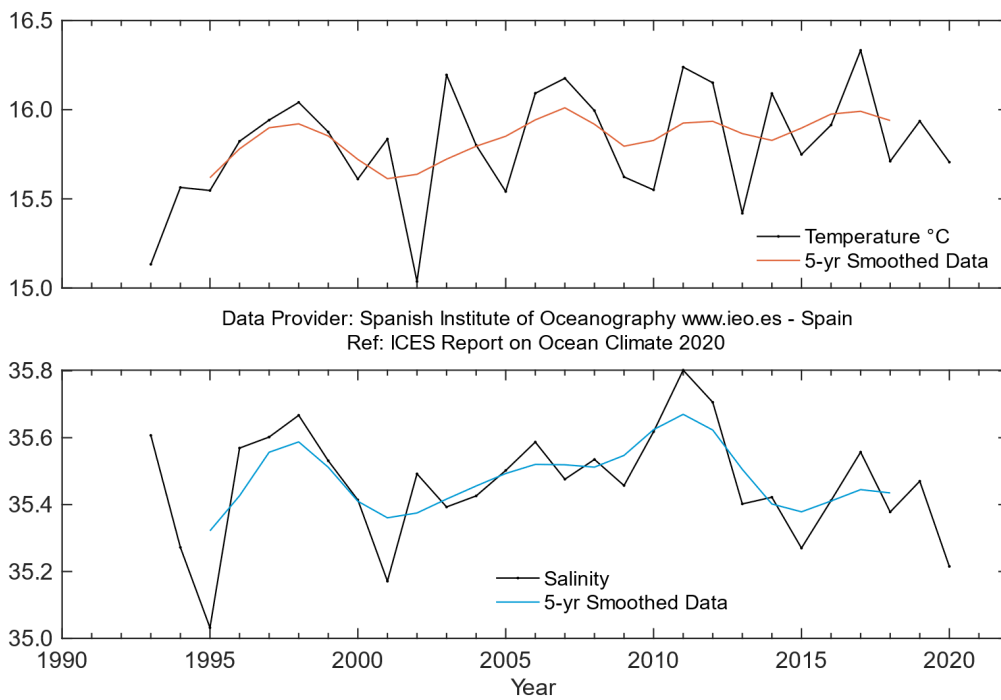
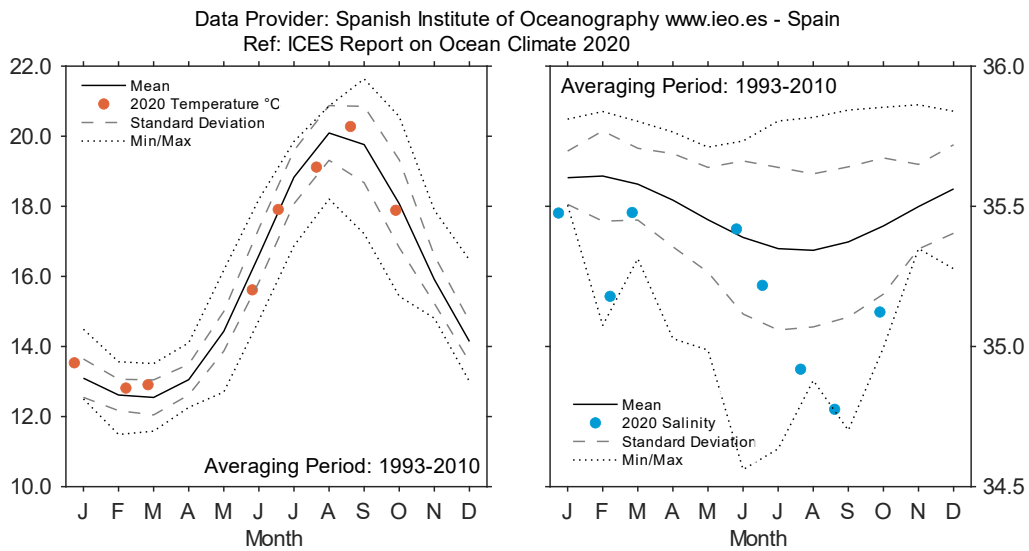


Figure 4.38. Bay of Biscay and eastern Atlantic. Sea surface temperature at San Sebastian (43°18.50' N 002°02.37' W).



**Figure 4.39.** Bay of Biscay and eastern Atlantic. Temperature (upper panel) and salinity (lower panel) at Santander Station 6, 0–3 0m (43°42.50'N 3°47.00'W).



**Figure 4.40.** Bay of Biscay and eastern North Atlantic. 2020 monthly temperature (left panel) and salinity (right panel) at Santander Station 6, 0–30 m (43°42.50'N 3°47.00'W).

## 4.9 Gulf of Cadiz

*R. Sánchez-Leal*

**STEADY FRESHENING BETWEEN 100–350 M AND SALINIFICATION BETWEEN 350–550 M SUSTAINED THE 2009–2020 INCREASE IN STRATIFICATION BETWEEN ATLANTIC AND MEDITERRANEAN OUTFLOW WATERS. 2020 SET THE HISTORIC MAXIMUM.**

The Gulf of Cadiz is located off the southwestern Iberian Peninsula. The circulation dynamics are largely governed by water exchange through the Strait of Gibraltar, the ocean gateway between the Atlantic Ocean and the Mediterranean Sea. The two-layered inverse estuarine circulation features MW flowing into the Gulf of Cadiz under AW flowing into the Mediterranean Sea. Dominant features include: (i) the baroclinic Gulf of Cadiz Current that advects relatively fresh and cool waters from the Portuguese Coastal Transition Zone (CTZ) to feed the Atlantic Inflow (AI) in the Mediterranean basin; (ii) the meridional branch of the Azores Current, a largely barotropic flow that brings warmer more saline AW to supplement the AI into the Mediterranean; (iii) an inshore current system linked with coastal runoff; and (iv) a cyclonic upwelling hotspot generated by tidal stirring over the Trafalgar Banks. The subsurface circulation is given by the Mediterranean Overflow, a branched, warm, saline, and dense gravity current attached to the seabed that follows the intricate bottom topography ([Figure 4.41](#)).

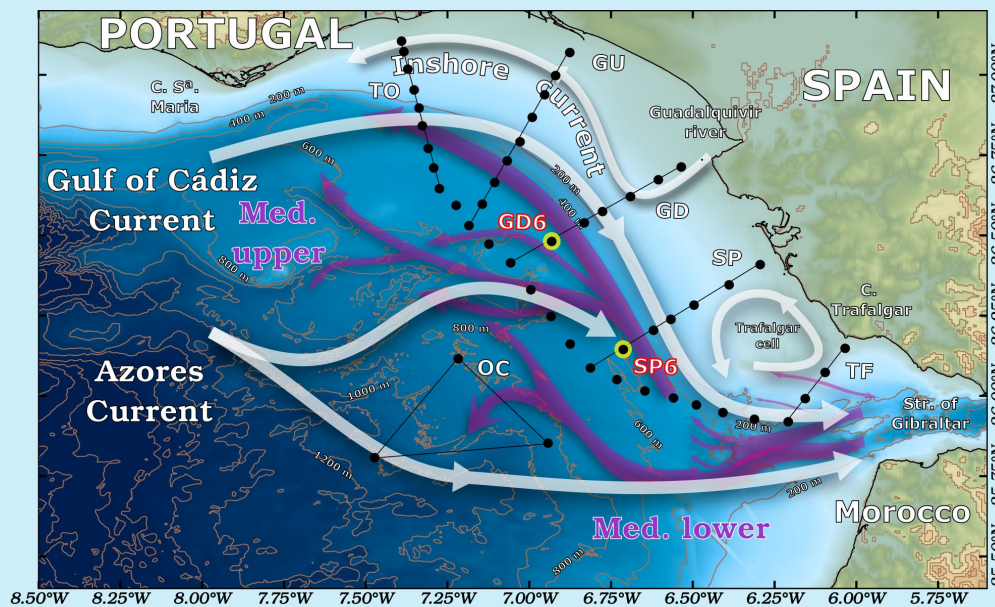


**Figure 4.41.** Sketch of the main currents in the Gulf of Cadiz. White arrows: surface circulation. Purple arrows: subsurface circulation. The STOCA project standard sections are included (black lines) and the fixed oceanographic station under the responsibility of the Spanish Institute of Oceanography, Cadiz, whose data are presented in this report (GD6 and SP6). Puertos del Estado provides data from a weather buoy located at GD6.

The instrumental record in the Gulf of Cadiz suggests a statistically significant warming trend ( $0.21^{\circ}\text{C decade}^{-1}$ ) of air temperature and ocean SST over the last two decades. The smoothed time-series indicate interannual variability, with colder-than-average SST in 2009, 2013, and 2018/2019. Warmer SST occurred in 2010/2011, 2016/2017, and 2020. In 2020, SST anomalies returned to positive after the historical minimum ( $0.6^{\circ}\text{C}$  cooler-than-average) recorded in 2019.

The monthly time-series for the surface layer (0-20 m) shows the seasonal cycle of temperature and salinity (Figure 4.43) computed from observations collected at SP6 during 2009–2020. Mean and 95% confidence intervals are reconstructed from the harmonic fit of all available observations from that period. The time-series illustrate that seasonal variability dominates at all depth levels of the water column (Figure 4.42). Temperature and salinity were above the seasonal average almost the entire year, except in late summer. August was anomalously cold and fresh, with temperature about  $1.5^{\circ}\text{C}$  and salinity 0.2 below the seasonal average.

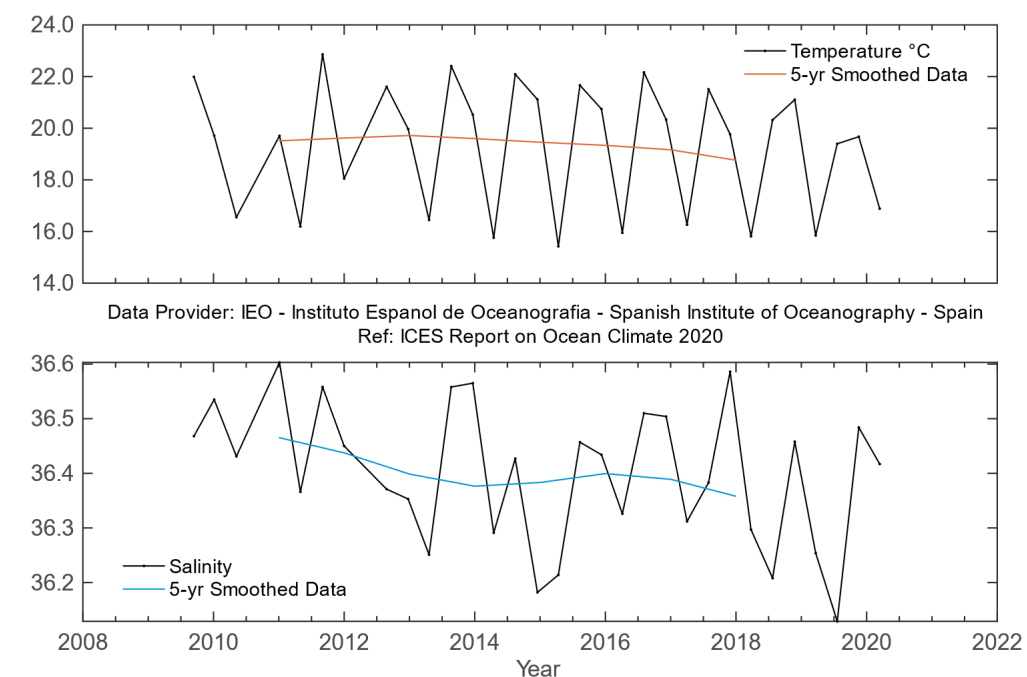


**Figure 4.42. Gulf of Cadiz. Potential temperature (upper panel) and salinity (lower panel) for the 0–20 m water column at the station SP6 ( $36^{\circ}08.68'N$   $006^{\circ}42.76'W$ ) of the STOCA programme.**



Photo: Tomasz Szumski, Marine Institute, Galway, Ireland

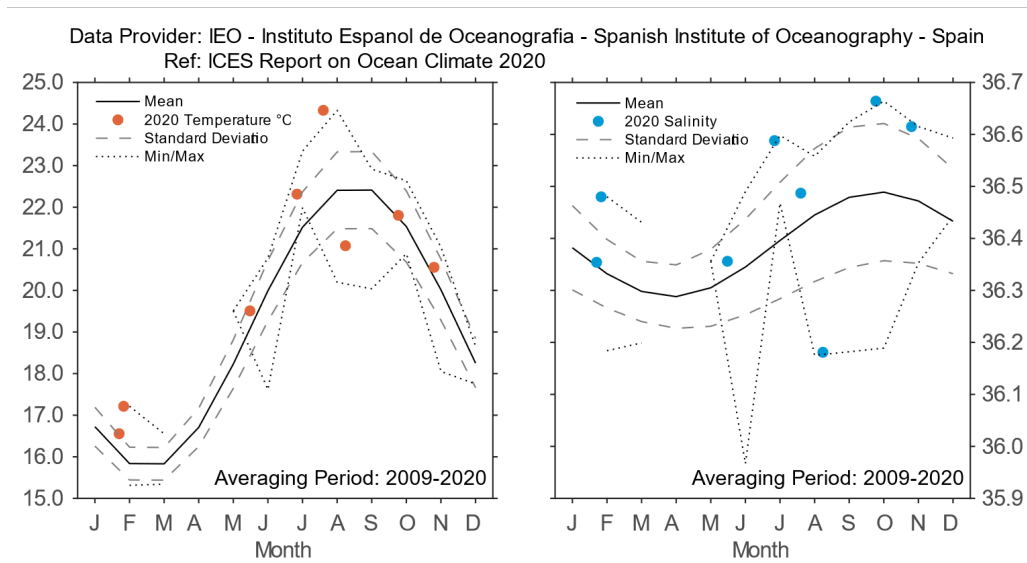


Figure 4.43. Gulf of Cadiz. 2020 monthly temperature (left panel) and salinity (right panel) at STOCA SP6 station, 10 m (36°08.68' N 006°42.76' W).

## 4.10 Canary Basin

*P. Vélez-Belchí*

**2020 CONFIRMS THE END OF THE COOLING AND FRESHENING CYCLE THAT BEGAN IN 2014 FOR THE NORTH ATLANTIC CENTRAL WATERS (NACW). THE COOLING AND FRESHENING TREND CONTINUES FOR THE INTERMEDIATE WATERS (800–1400 DBAR) AFTER THE 2014 MAXIMUM.**

The Canary Basin sits at the boundary between the oceanic waters of the subtropical Atlantic gyre and the upwelling waters from the Canary Current LME (CCLME) off the coast of northwest Africa. Since the early 2000s, the Canary Islands archipelago region has been monitored by the Spanish Institute of Oceanography (Tel *et al.*, 2016); specifically the oceanic waters west of Lanzarote (stations 11–23, [Figure 4.44](#)) and the CTZ of the CCLME upwelling region (stations 1–10, [Figure 4.44](#)).

In the upper water levels, the area is under the influence of the southward-flowing Canary Current and the Canary Upwelling Current, associated with the upwelling front ([Figure 4.44](#)). At intermediate levels, it is under the influence of the tongue of slowly propagating Mediterranean Waters (MW) and the slope current known as the Canary Intermediate Poleward Current (Hernández-Guerra *et al.*, 2017; Vélez-Belchí *et al.*, 2017).

The waters above the seasonal thermocline, are characterized on the  $\theta/S$  diagram by scattered temperature and salinity values due to seasonal heating and evaporation. These waters occupy the upper 300 m in the oceanic region, and the upper 100 m in the stations under the effect of the coastal upwelling which are considered the surface waters. Below

the seasonal thermocline and through the permanent thermocline are the NACW, roughly between 300 m and 700 m depth. These waters are characterized on the  $\theta/S$  diagram by an approximately straight-line relationship between potential temperature ( $11.4^\circ\text{C} < \theta < 14.9^\circ\text{C}$ ) and salinity ( $35.6 < S < 36.1$ ). At intermediate levels, roughly between 700 m and 1200 m, two distinct water masses are found in the Canary Islands region, the fresher ( $S < 35.3$ ) and slightly lighter Antarctic Intermediate Waters (AAIW), and the saltier ( $S > 35.4$ ) and heavier MW.

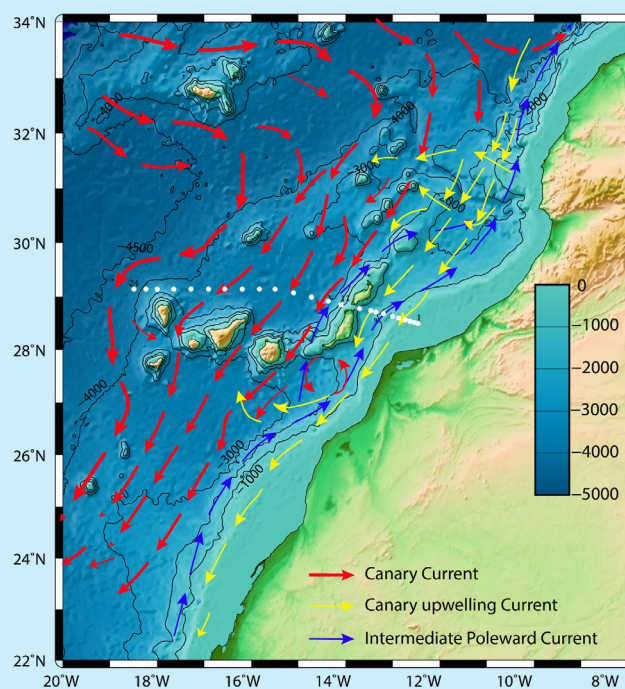


**Figure 4.44.** Circulation schematic for the Canary Basin. Red arrows: southward Canary Current consisting mainly of NACW and intermediate waters. Yellow arrows: Canary Upwelling current that flows in the thermocline waters. White dots: distribution of the 24 hydrographic stations sampled in the Canary Islands archipelago region since 1997. Changes in the CTZ and in oceanic waters are monitored at stations 5–10, and stations west of Lanzarote (11–24), respectively.

In the oceanic surface waters, the overall warming trend observed ( $0.07 \pm 1.34^\circ\text{C decade}^{-1}$ ) was smaller than the trend observed with SST observations from satellite, although it should be noted that the time-series do not resolve properly the seasonal cycle.

In the depth stratum that characterizes the NACW waters (200–800 dbar), there is an overall, non-statistically significant, warming of  $0.06 \pm 0.06^\circ\text{C decade}^{-1}$ , and an increase in salinity of  $0.005 \pm 0.011^\circ\text{C decade}^{-1}$  (Figure 4.45). Between the 1990s and the early 2000s, there was a decrease in the temperature and salinity of all upper-layer waters. This trend was followed in the mid-2000s by a marked increase in both temperature and salinity, which peaked in 2014 in the hottest and saltiest year in the record. Between 2014 and 2018, both temperature and salinity decreased. The year 2020 has confirmed to be the end of this cycle, but the increase in temperature and salinity during 2019/2020 is still low, and mean temperature and salinity was lower than that observed in the late 1990s (Vélez-Belchí *et al.*, 2015). The overall increase in temperature and salinity were almost compensated by density, confirming that the observed trends are due to deepening of the isoneutral surfaces, rather than changes along the isoneutral surfaces. For the same depth stratum, this overall increase in salinity and temperature for the

NACW waters was also observed in the CTZ, although with slightly smaller values ( $0.05 \pm 0.13^\circ\text{C decade}^{-1}$ ,  $0.001 \pm 0.022^\circ\text{C decade}^{-1}$ ), due to the influence of upwelling. The variability in the CTZ is higher due to the proximity of the upwelling region and the frequent intrusions of upwelling filaments. For the same reason, the uncertainty is higher in the trend estimates.

The surface waters (25–150 dbar) in the CTZ show a non-statistically significant cooling of  $-0.20 \pm 0.42^\circ\text{C decade}^{-1}$ , and a non-statistically significant decrease in salinity of  $-0.051 \pm 0.054 \text{ decade}^{-1}$ , both consistent with an increase in the upwelling in the CCLME. The upwelling of the CCLME continues to strengthen, with 2015 as the coolest and freshest year on record for the upwelling-influenced surface waters. SST satellite observations corroborate changes in the upwelling regime inferred from the *in situ* observations, with different areas showing increases in upwelling. However, the magnitude of the observed trend in the satellite SST is different, due to the thin layer of ocean that the satellite observes.

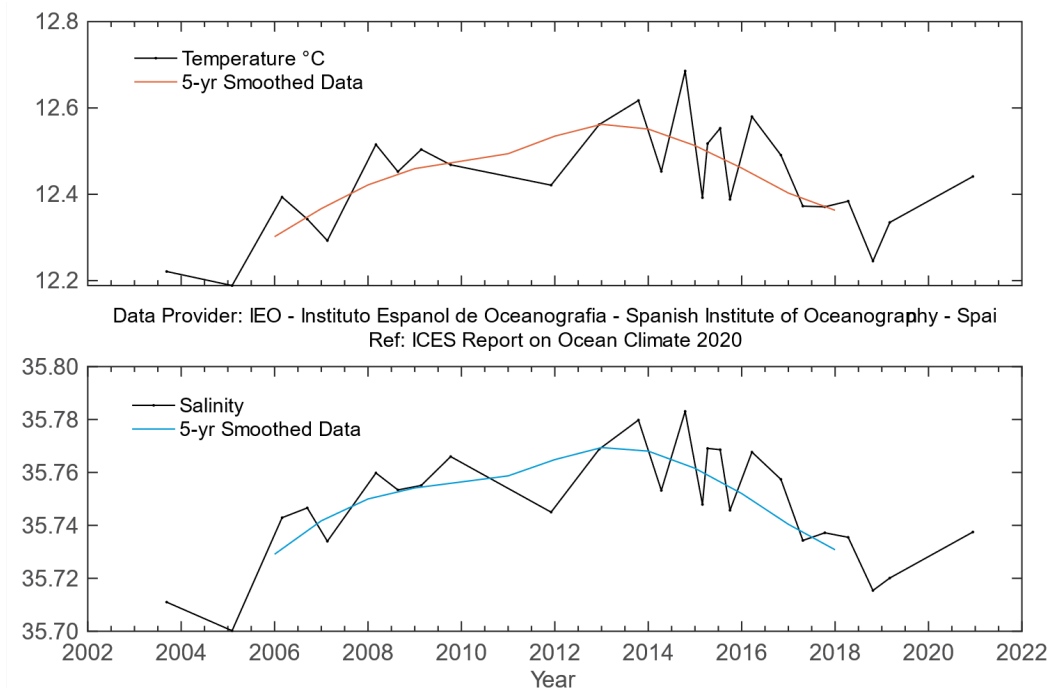


Figure 4.45. Potential temperature (upper panel) and salinity (lower panel) for the 200–800 m layer in the oceanic waters of the Canary basin.

## 4.11 Southwest Approaches

*T. Smyth*

The datasets presented here are from the western end of the English Channel and the boundary of the Celtic Sea and the Bay of Biscay ecoregions. The area is commonly referred to as the Southwest Approaches, which relates to the passage of shipping through the English Channel. As these data come from a boundary between the different ecoregions, this term has also been adopted here, as it relates to the region forming a pathway for AW to enter the southern North Sea.

Station E1 (50.03°N 4.37°W) is situated on the southern UK coast in the western English Channel. The water depth is 75 m, and the station is tidally influenced by a 1.1-knot maximum surface stream at mean spring tide. The seabed is mainly sand, resulting in a low bottom stress (1–2 ergs cm<sup>-2</sup> s<sup>-1</sup>). The station may be described as oceanic with the development of a seasonal thermocline. Stratification typically starts in early April, persists throughout summer, and is eroded by the end of October. The typical depth of summer thermocline is around 20 m. The station is greatly affected by ambient weather.

Measurements have been taken at station E1 since the end of the 19th century, with data currently available since 1903 (Figure 4.46). The series is unbroken, apart from gaps for the two world wars and a hiatus in funding between 1985 and 2002. The data take the form of vertical profiles of temperature and salinity. Early measurements were obtained with reversing mercury-in-glass thermometers and discrete salinity bottles. More recently, electronic equipment (Seabird CTD) has been utilized. The time-series demonstrates considerable interannual variability in temperature.

E1 was sampled on 16 occasions during 2020 (Figure 4.46), approximately every fortnight in summer and monthly in winter. At the surface, E1 started 2020 slightly above average and only reached a minimum temperature of just below 10°C. Spring and early summer temperatures were around the long-term mean (at the surface), but some heat during late summer manifested as temperatures in excess of 19°C during August. At 50 m, temperatures were above the series mean for the first half of the year and around average for summer until the breakdown in stratification vented warmer temperatures throughout the water column. Autumn and early winter temperatures were slightly above the long-term mean. For almost all of 2020, salinity was below the long-term mean throughout the water column, with the exception of early summer at the surface (Figure 4.47).

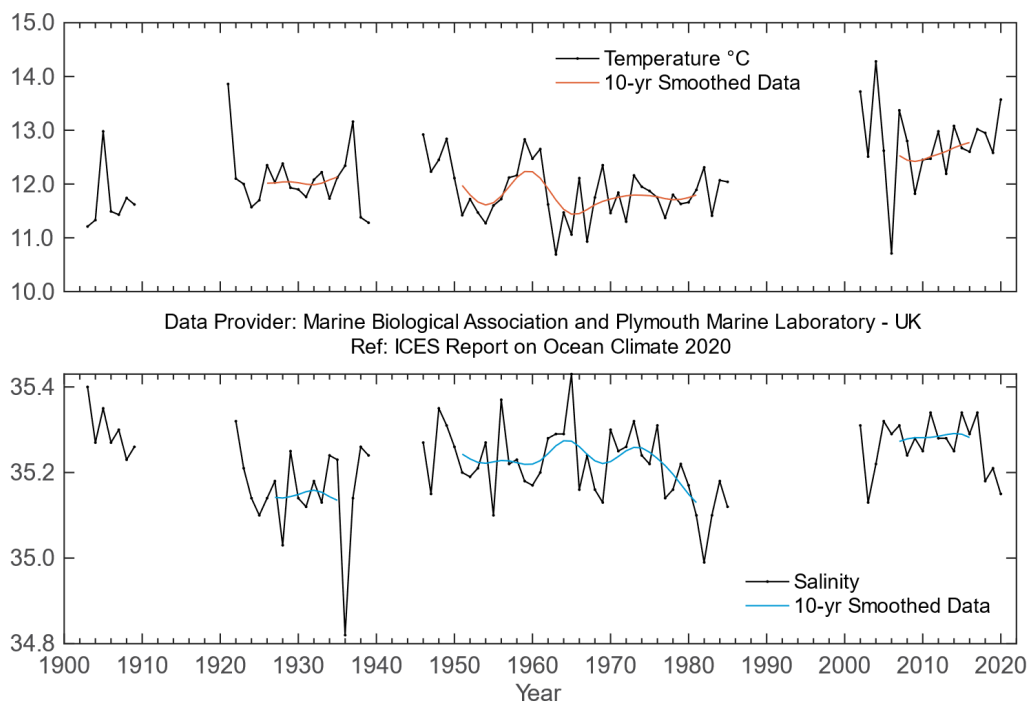


Figure 4.46. Southwest Approaches. Temperature (upper panel) and salinity (lower panel) anomalies of surface water (0–40 m) at Station E1 in the western English Channel (50.03°N 4.37°W).

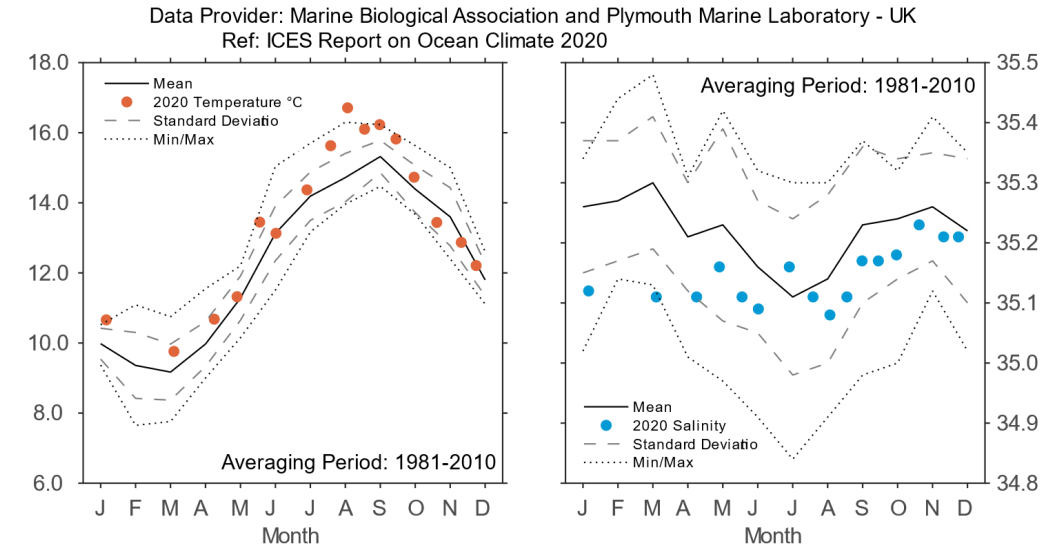


Figure 4.47. Southwest Approaches. Monthly average seasonal cycle with 2020 temperature (left panel) and salinity (right panel) observations of surface water (0–40 m) at Station E1 in the western English Channel (50.03°N 4.37°W).

## 4.12 Celtic Seas

*K. Lyons and C. Cusack*

**IN 2020, FOR THE 6TH CONSECUTIVE YEAR, THE AVERAGE SURFACE TEMPERATURE OFF SOUTHWEST IRELAND REMAINED BELOW NORMAL.**

The Celtic Seas is defined as an ICES ecoregion, and is included in NOAA LME 24 (Celtic-Biscay Shelf). The Celtic Seas region contains the shelf seas of northwestern Europe and part of the Rockall Trough. The shelf seas are mainly relatively shallow (< 100 m). The structure of the water column on the shelf is primarily driven by (i) vertical mixing due to tides and wind, and (ii) the seasonal variation in solar heating, leading to seasonal (summer) density-driven currents (e.g. Irish Coastal Current). In addition to the influence of coastal waters on the shelf, the area is strongly influenced by the poleward transport of AW, as well as the continental slope current that brings waters northward from the Bay of Biscay region

Due to Covid-19 government travel restrictions, the collection of 2020 sea surface temperature data at Malin Head was delayed and will be reported in the next edition of the IROC (IROC 2021). For the most recent overview of this station, please see Section 4.12 in the IROC 2019 (González-Pola *et al.*, 2019).

For the short M3 buoy SST time-series, cool conditions continued, and the mean temperature in 2020 was 0.36°C below the 2003–2010 mean. Monthly mean SST values were near or below normal throughout the year.

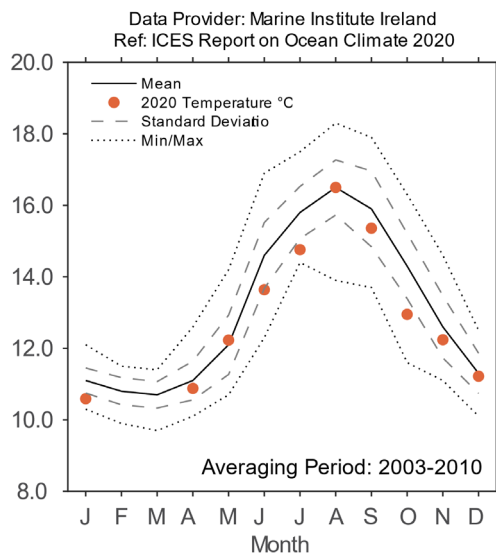
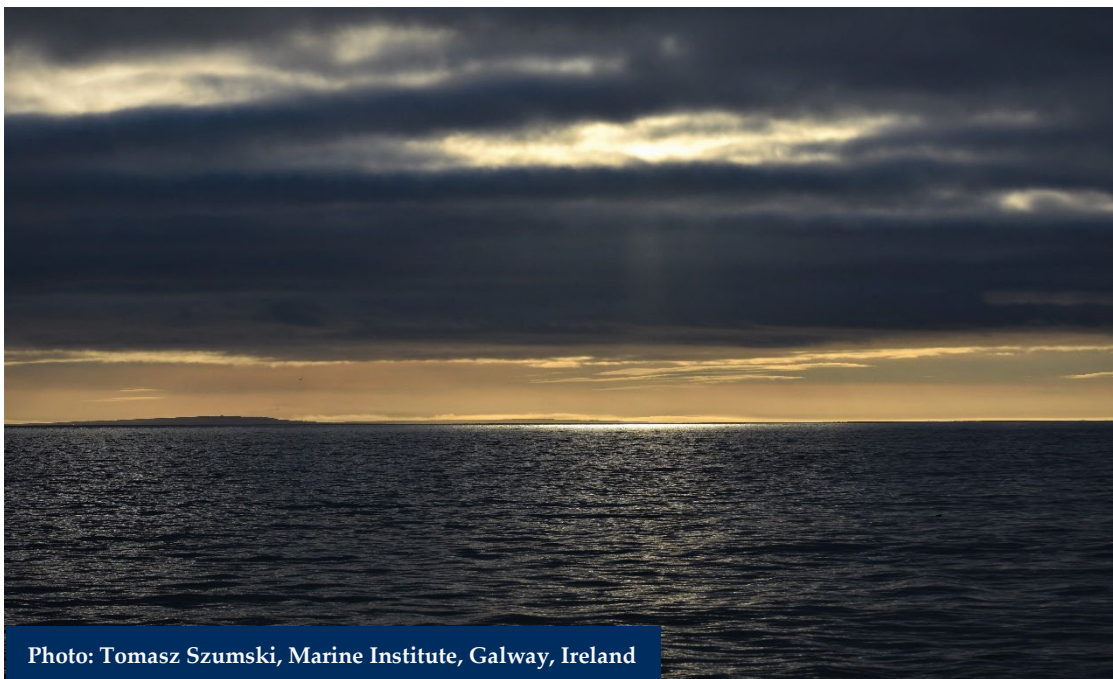


Figure 4.48. Celtic Seas. Monthly average seasonal cycle with 2020 monthly temperature at the M3 Weather Buoy southwest of Ireland (51.22°N 10.55°W).



### 4.13 Rockall Trough

*S. Jones and N. P. Holliday*

---

FRESH AND NEAR-AVERAGE TEMPERATURE CONDITIONS IN THE ROCKALL TROUGH UPPER OCEAN IN 2020, BUT WITH SIGNS OF INCREASING SALINITY.

---

Rockall Trough is a deep ocean basin situated west of UK and Ireland, within the Celtic Seas and oceanic Northeast Atlantic ecoregions. It has significantly different oceanographic characteristics than the shallower shelf-sea areas. Rockall Trough is separated from the Iceland Basin by Hatton and Rockall banks, and from the Norwegian Sea by the shallow (500 m) Wyville–Thomson Ridge. It is a route for warm North Atlantic upper water to reach the Norwegian Sea, where it is converted into cold, dense overflow water as part of the thermohaline overturning in the North Atlantic. The upper water column is characterized by poleward-moving eastern North Atlantic Water (NAW), which is warmer and more saline than the Iceland Basin waters that also contribute to the Norwegian Sea inflow (Figure 4.49).

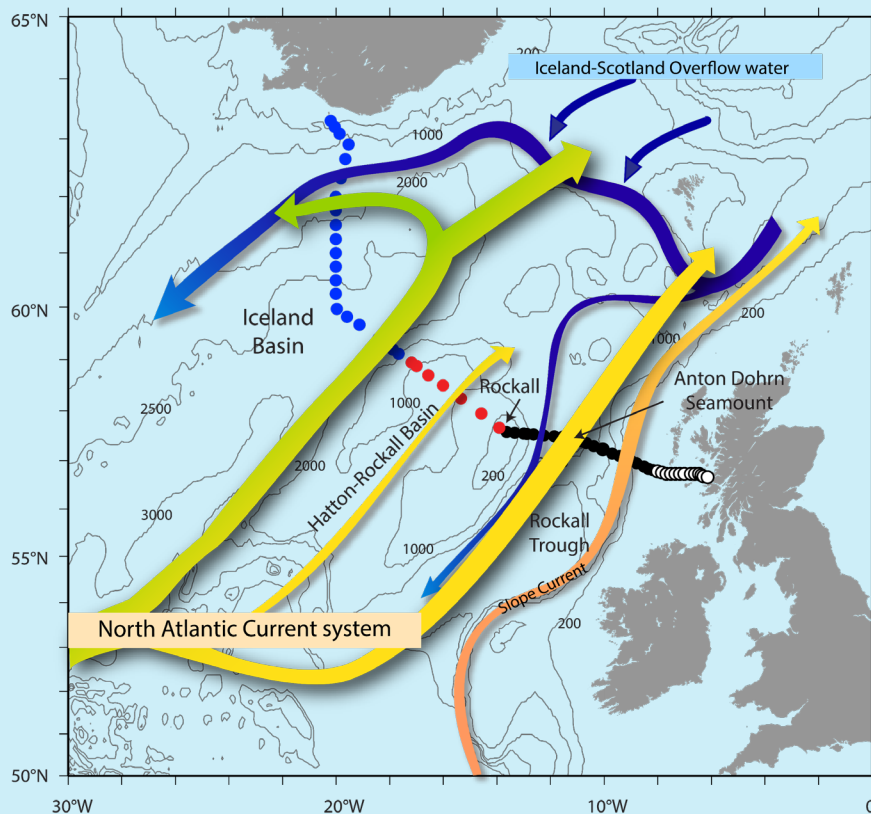


**Figure 4.49.** Circulation schematic for the Rockall Trough, Hatton–Rockall Basin, and Iceland Basin. Green, yellow, and orange colours indicate the upper waters of the North Atlantic Current and the slope current. Dark blue arrows show the approximate locations of the main overflow currents.

The temperature of the upper 800 m remained close to the 1981–2010 mean in 2020. The upper ocean had been cooling since a peak of 9.8°C in 2007, but this trend appears to have halted or slightly reversed in 2019 and 2020 (Figure 4.50). The salinity of the upper 800 m has been decreasing since the end of the 2000s, with sharp freshening to a near-record minimum in 2017. Upper-ocean salinity increased slightly from this deep minimum in 2019 and 2020. The Ellett Line CTD transect was not occupied in 2019 and 2020, but equivalent data points in the time-series were generated using Argo profiles from within the basin, supported by moorings deployed by the OSNAP project for that year.

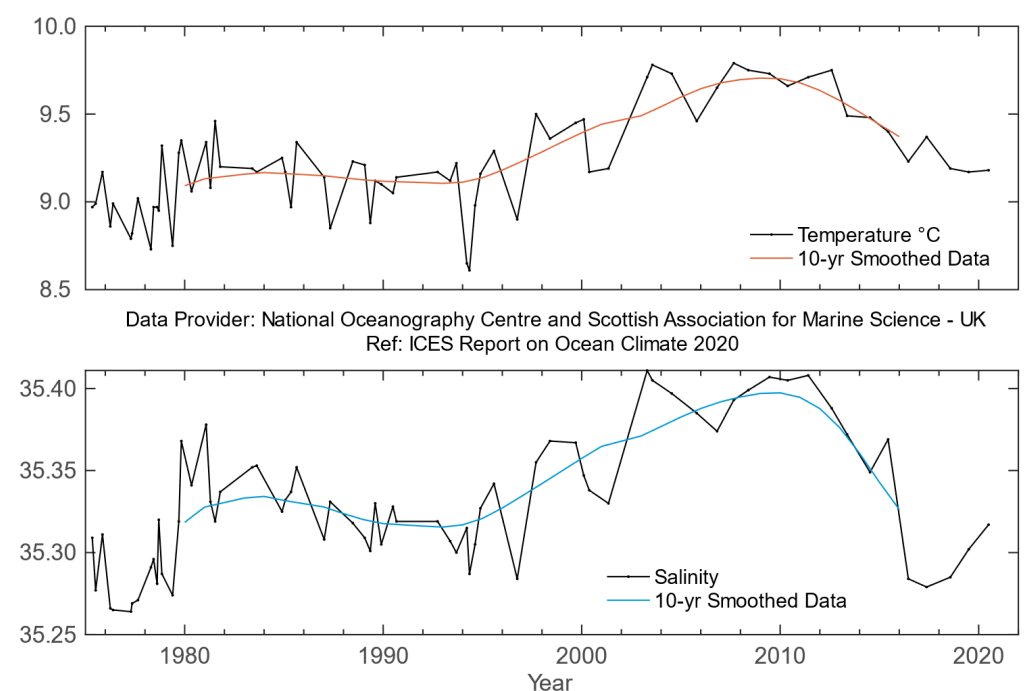


Figure 4.50. Rockall Trough. Temperature (upper panel) and salinity (lower panel) for the upper ocean (potential density 27.2–27.50 kg m<sup>-3</sup>, representing the top 800 m, but excluding the seasonally warmed surface layer).

#### 4.14 Hatton-Rockall Basin

*S. Jones and N. P. Holliday*

The shallow Hatton–Rockall Basin (1000 m) lies between the Iceland Basin to the west and Rockall Trough to the east and is bounded by the Hatton and Rockall banks. The basin is filled with well-mixed subpolar-mode water moving northward as part of the NAC complex. Winter mixing reaches 800–1000 m here. Temperature and salinity vary considerably depending on the type of NAC water that enters the basin. The region is in the transition zone between cold, fresh, central Subpolar Water and warm, saline, eastern Subpolar Water.

The range in basin mean temperature and salinity in the upper 1000 m is more than 1°C and 0.1 higher than those in Iceland Basin to the west and Rockall Trough to the east. This high variability may be due to seasonal to decadal changes in the structure and location of the NAC system as it crosses the Hatton-Rockall Basin (Houpert *et al.*, 2020). The lowest temperature and salinity values were seen at the start of the time-series in 1996, followed by a steady rise to maximum values in the late 2000s (Figure 4.51). After 2010, there was a decrease in temperature and salinity in line with neighbouring basins. Since 2018, salinity has increased by 0.06, but remains lower than the 1996–2010 average. The temperature has risen since 2016 to a value close to the long-term mean.

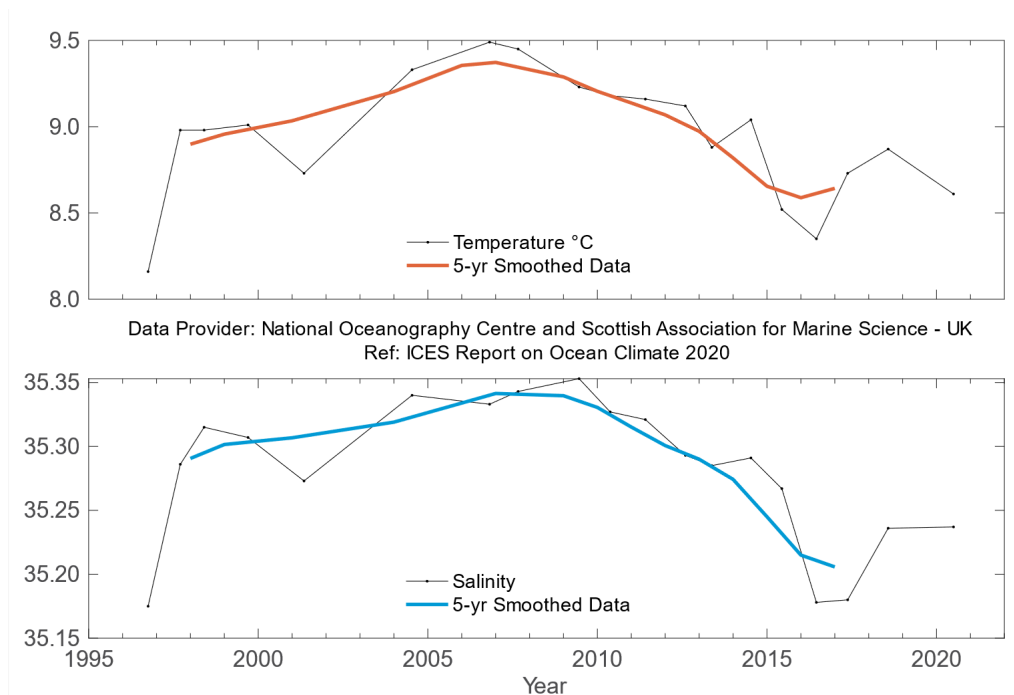


**Figure 4.51. Hatton-Rockall Basin. Temperature (upper panel) and salinity (lower panel) for the upper ocean (potential density 27.20–27.50 kg m<sup>-3</sup>, representing the top 600 m and excluding the seasonally warmed surface layer.**

## 4.15 Iceland Basin

*S. Jones and N. P. Holliday*

A major part of the NAC flows into the Iceland Basin, adjacent to the shallow Hatton Bank on the southeast side of the basin (Figure 4.49). The NAC typically consists of one or two fronts between warmer, more saline water in the east, and colder, fresher water to the north and west. The region is rich in eddy activity, and the water properties are quite variable over time and space. Most of the water entering the Iceland Basin from the south flows through into the Norwegian Sea over the Iceland–Scotland Ridge. A smaller fraction of the NAC water recirculates south of Iceland in the boundary currents of the main anticlockwise circulation of the Subpolar Gyre.

Upper-ocean (ca. upper 500–600 m) temperature and salinity vary from year to year, but also exhibit multiyear changes. From 1996 to the late 2000s, both temperature and salinity were increasing, but have since exhibited a sharp decrease (Figure 4.52). By 2017, temperature and salinity values were the lowest recorded since 1996. The freshening after 2010 implies that the basin is receiving more water originating in the west and central subpolar region and less warm, saline water from the eastern intergyre regions. Superimposed on that multiyear trend is rapid cooling observed between 2014 and 2015, caused by a high flux of heat from the ocean to the atmosphere (Duchez *et al.*, 2016) and rapid freshening in 2015–2017 (Holliday *et al.*, 2020). These deep minima have recovered somewhat from 2017 onwards, but both temperature and salinity are still below the long-term mean. The Ellett Line transect was not occupied from 2018

onwards, but equivalent data points in the time-series were generated using Argo profiles from within the basin for that year.

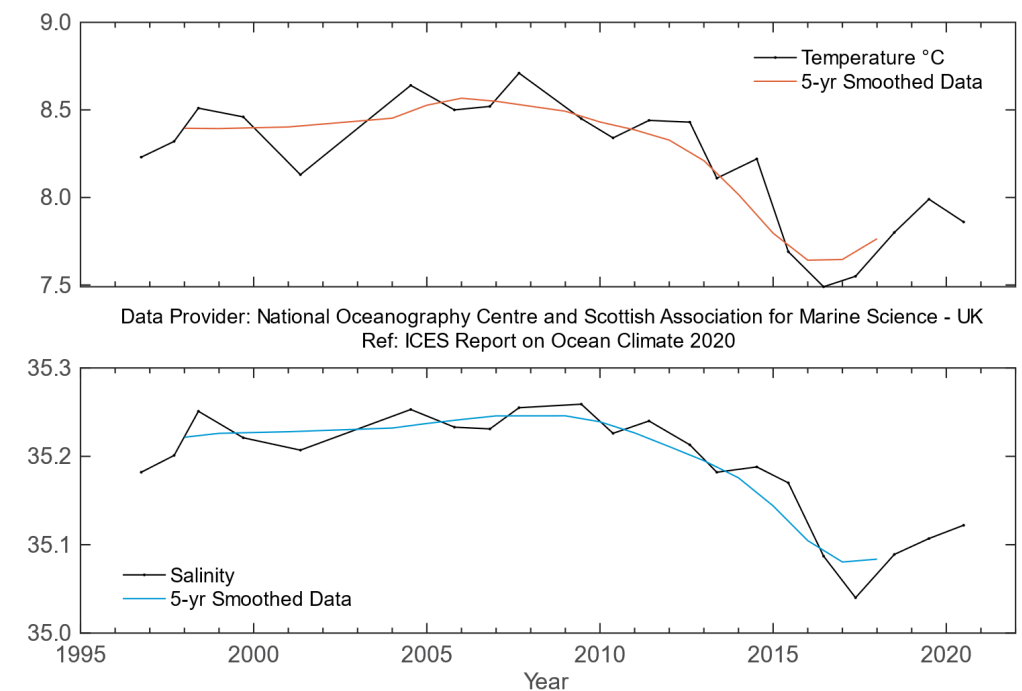


Figure 4.52. Iceland Basin. Temperature (upper panel) and salinity (lower panel) for the upper ocean (potential density 27.20–27.50 kg m<sup>-3</sup>, representing the top 500 m and excluding the seasonally warmed surface layer).

## 4.16 Irminger Sea

*M. F. de Jong*

The Irminger Sea is the ocean basin between South Greenland, the Reykjanes Ridge, and Iceland. This area forms part of the North Atlantic Subpolar cyclonic Gyre. Due to this gyre, the exchange of water between the Irminger and the Labrador seas proceeds relatively fast. In the bottom layers of the Irminger Sea, cold water originating in the (sub)Arctic seas flows from the Denmark Strait and to the south over the continental slope of Greenland.

The subpolar mode water (SPMW) in the centre of the Irminger Sea, in the pressure interval 200–400 dbar, showed a minimum in temperature and salinity in 1995/6 and reached its highest temperature and salinity in 2004 (Figure 4.53). Both temperature and salinity have gradually decreased since then. The temperature of the SPMW in the central Irminger Sea reached a minimum in 2016, about 0.4°C below the long-term mean, and has since warmed slightly to 0.1°C below the long-term mean in 2020. Salinity, which in 2018 showed the first small (–0.002) negative salinity anomaly since 2003, has now further decreased to –0.015 due to the North Atlantic freshwater anomaly (Figure 4.53). This fresh anomaly has clearly affected convection, which remained shallow in 2020.

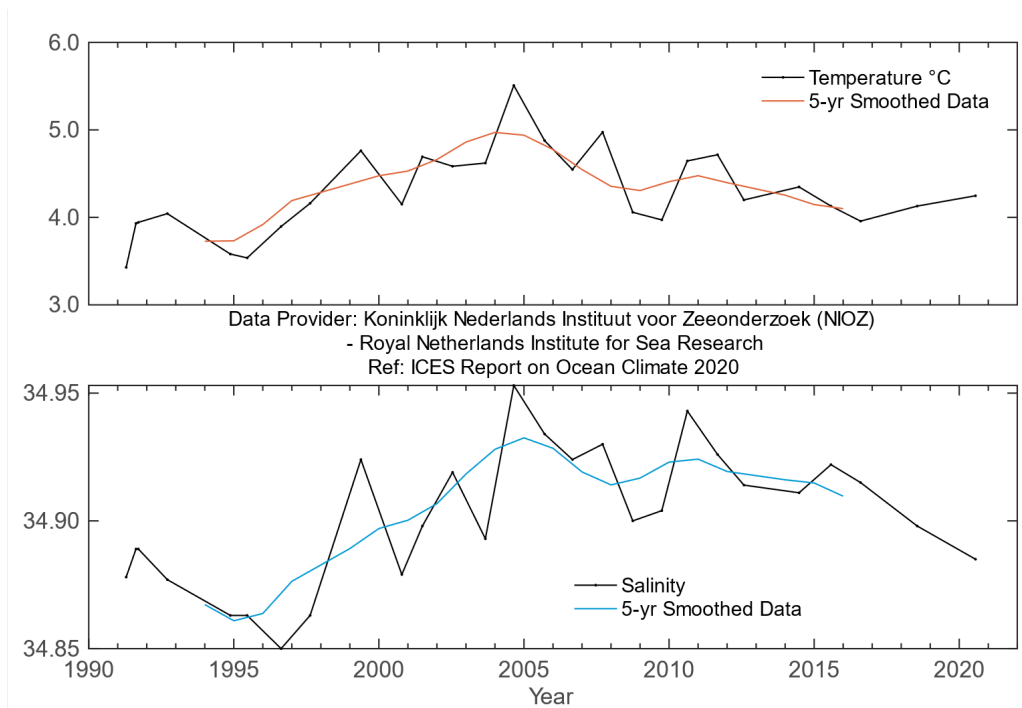


**Figure 4.53.** Irminger Sea. Temperature (upper panel) and salinity (lower panel) of Subpolar Mode Water in the central Irminger Sea (averaged over 200–400 m).

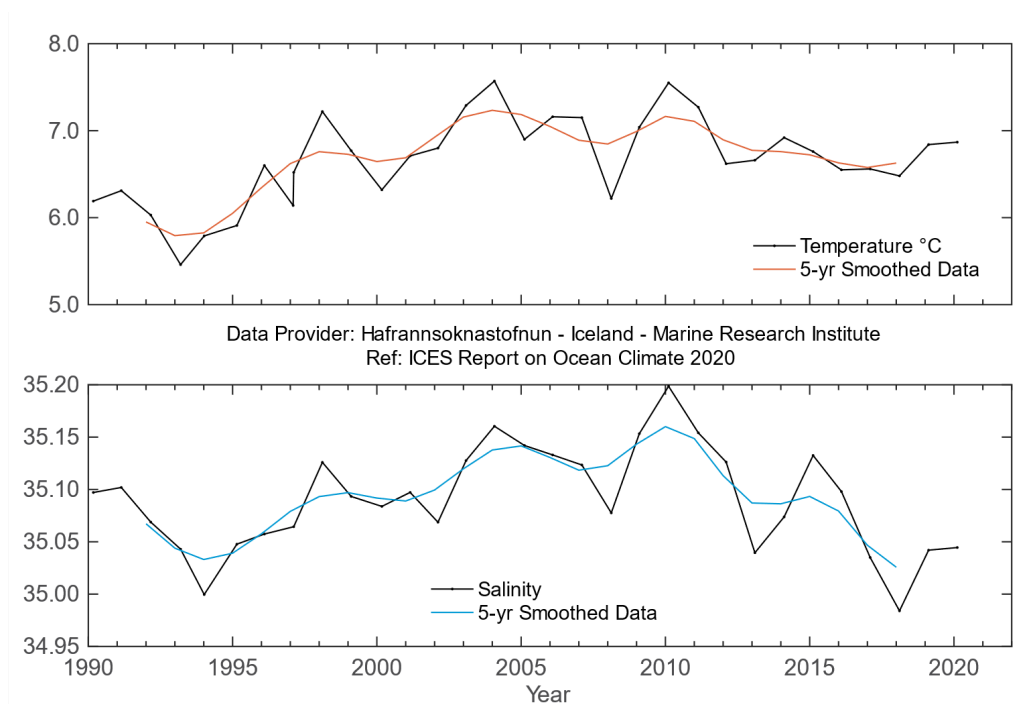


**Figure 4.54.** Irminger Sea. Temperature (upper panel) and salinity (lower panel) of Subpolar Mode Water in the northern Irminger Sea (Station FX9, 64.33°N 28°W), from winter observations averaged over 200–500 m).

## 4.17 Faroese waters and the Faroe Shetland Channel

*K. M. Larsen, B. Berx, and J. Hindson*

---

LOW NAW AND MNAW SALINITIES STILL OBSERVED, THOUGH THERE ARE INDICATIONS OF INCREASING SALINITY. TEMPERATURES CLOSE TO THE LONG-TERM MEAN, EXCEPT IN THE FAROE REGION, WHERE THEY ARE INCREASING AND MAINLY ABOVE THE LONG-TERM MEAN.

---

Data from the Faroese Waters ecoregion are grouped together here with data from the Faroe–Shetland Channel. This small region sits at the boundary between the Celtic, North, and Norwegian seas ecoregions, and at the boundary between the North Atlantic Ocean and Nordic Seas.

One of the NAC branches crosses the Greenland–Scotland Ridge ([Figure 4.56](#)) on either side of the Faroes. Its properties are sampled in the Faroe Bank Channel before it crosses the ridge, and in the Faroe Current after it crosses the ridge. Some of this water recirculates and is sampled within the Faroe–Shetland channel as Modified North Atlantic Water (MNAW).

Further east, the continental slope current flows along the edge of the northwest European continental shelf. Originating in the southern Rockall Trough, the continental slope current flows carries warm, saline AW into the Faroe–Shetland Channel. A proportion of this AW crosses onto the shelf itself and enters the North Sea, where it is diluted with coastal water and eventually leaves in the Norwegian Coastal Current. The remainder enters the Norwegian Sea and joins the water coming from north of the Faroes to become the Norwegian Atlantic Water.

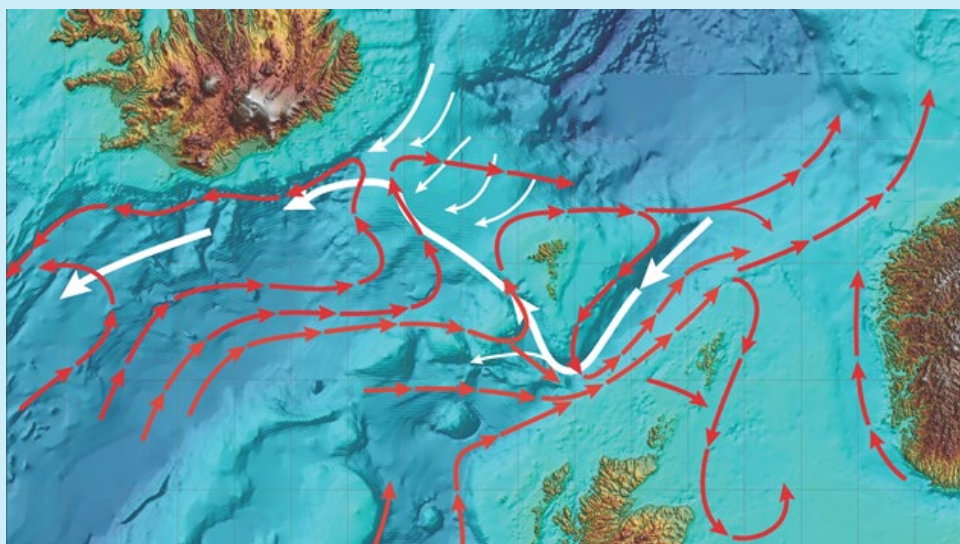


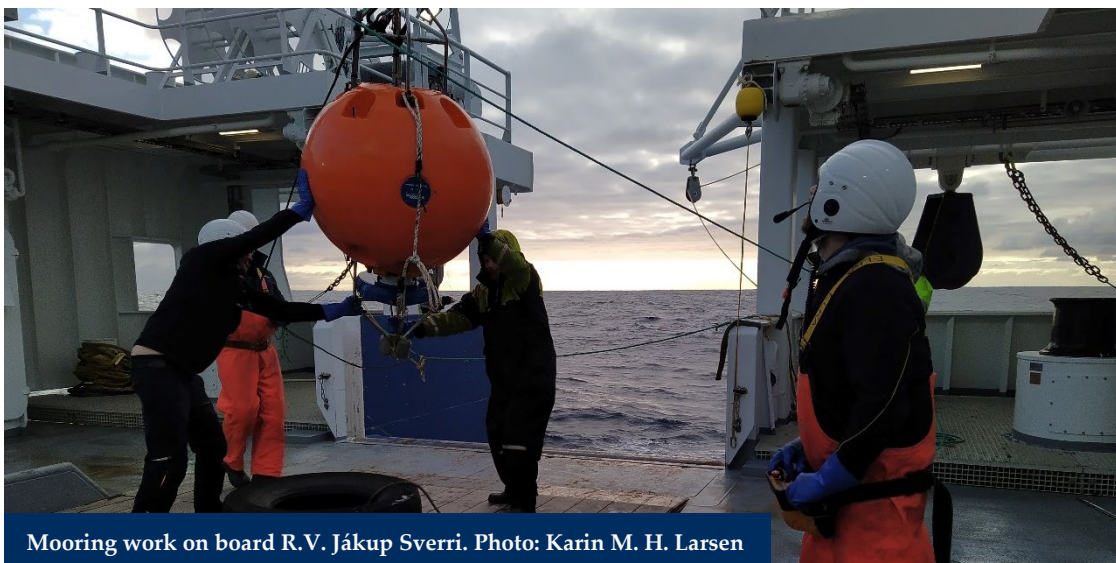
Figure 4.55. Circulation schematic for Faroese Waters and the Faroe–Shetland Channel. Red lines: poleward movement of AW. Thick white lines: return circulation (at depth) of waters from the Nordic Seas.

In general, both temperature and salinity in all upper-layer waters around the Faroes and in the Faroe-Shetland Channel increased markedly during the 1990s and 2000s. During the first half of the 2010s, both temperature and salinity decreased, with record low values of salinity observed in the second half of the 2010s.

After the record-high salinities observed in the Faroe Bank Channel ([Figure 4.56](#)) and the Faroe Current ([Figure 4.57](#)) in November 2009, salinities decreased at both locations. In autumn and winter 2016/2017, salinity decreased abruptly and continued to decrease in 2017 and 2018, though at a slower rate. In 2019 and 2020, salinities recovered somewhat, but were still below the long-term average. Temperatures in the Faroe Bank Channel and the Faroe Current were relatively high and stable during most of the 2000s. In 2012, they decreased, and were close to the long-term mean until 2017, not accompanying the decrease in salinity. Since 2018, temperatures have increased and were just above the long-term mean in 2020.

On the Faroe shelf, the annual average temperature has been relatively high since the early 2000s, but in 2015, the annual averaged temperature was the lowest observed since 2000. Since 2015, temperatures have been slightly higher and above the long-term mean (not shown). The 2020 monthly mean temperatures were very close to the long-term mean, except for in November and December, which were warmer than average ([Figure 4.58](#); left panel). The long-term trend in salinity on the Faroe shelf follows the trend observed for off-shelf waters. Salinity increased from the start of the observations in 1995 to record-high values in 2010. Since 2010, salinity has been decreasing. Record-low values were observed in the Faroe Bank Channel in autumn 2016, which were already evident in the Faroe shelf salinity in late summer 2016. Similar to observations off-shelf, the freshening continued on-shelf over the following years, particularly during the winter months, with record-low salinities observed even in January 2020. Despite this, annual mean salinity in 2018–2020 were higher than the 2017 annual mean record low ([Figure 4.58](#); right panel).

In the early 1990s, surface water temperature and salinity for the Faroe-Shetland Channel were warmer and more saline than the long-term mean. Driven by basin-scale processes, the salinity of both AW types distinguished in the Faroe–Shetland Channel (NAW and MNAW) showed significant freshening in 2017 and 2018 ([Figures 4.59](#) and [4.60](#)). The salinity of both these water masses was still significantly below the long-term mean in 2020. While the temperatures of the AW on both sides of the Faroe–Shetland Channel have decreased significantly since the record high temperatures of 2010, these remain close to the long-term mean.



Mooring work on board R.V. Jákup Sverri. Photo: Karin M. H. Larsen

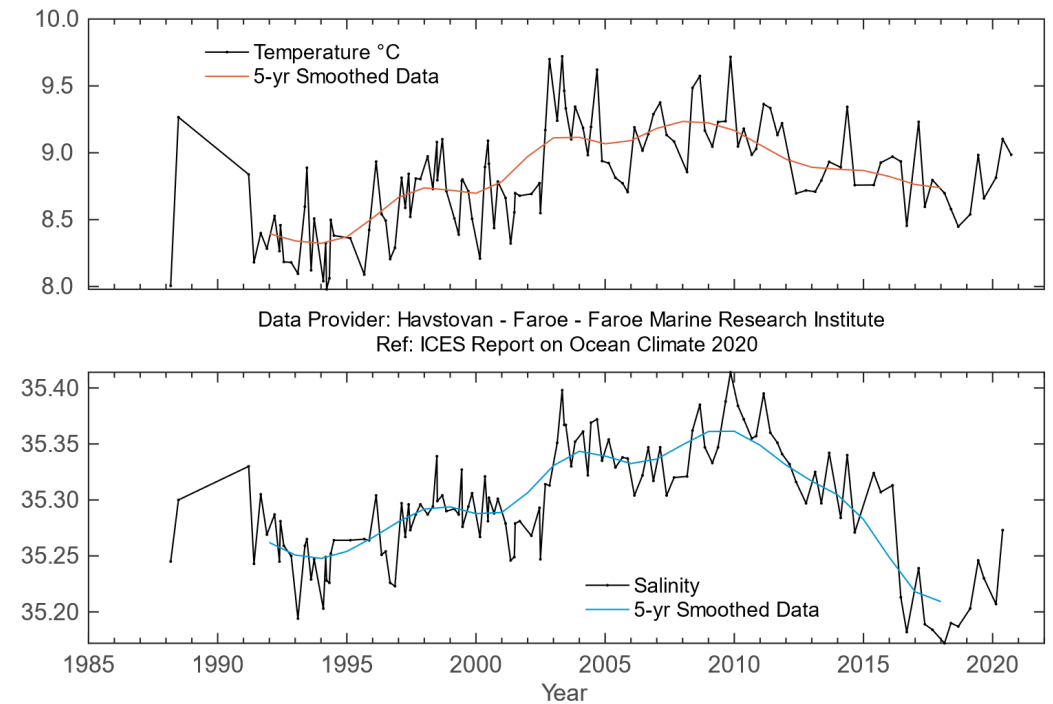


**Figure 4.56. Faroese waters. Temperature (upper panel) and salinity (lower panel) in the high salinity core of Atlantic Water over the Faroe Bank Channel (maximum salinity averaged over a 50-m deep layer).**

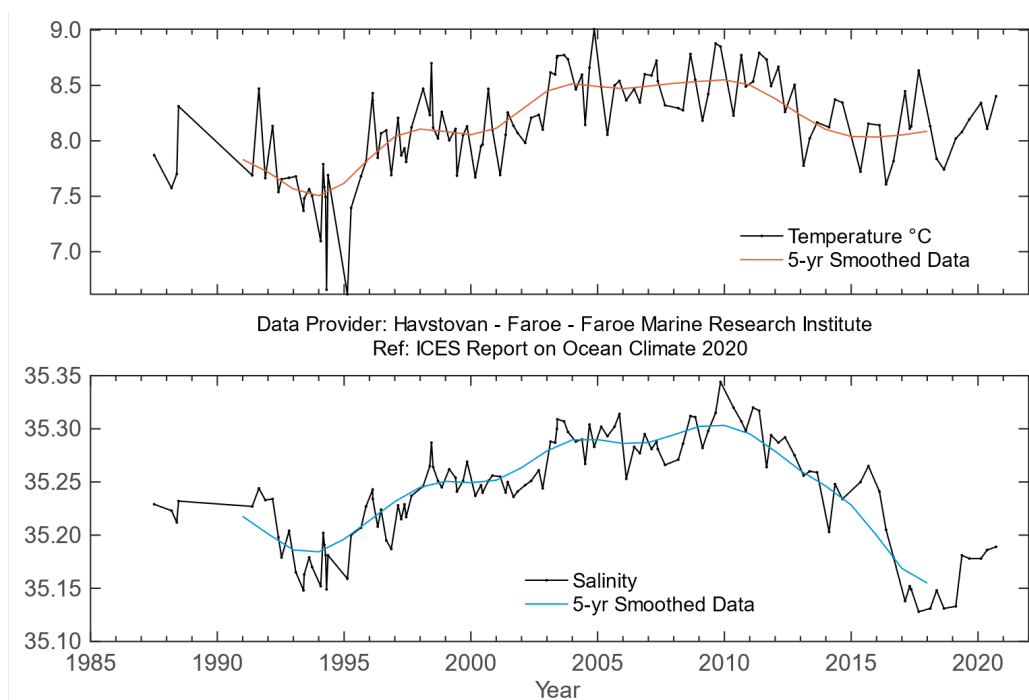


**Figure 4.57. Faroese waters. Temperature (upper panel) and salinity (lower panel) in the high salinity core of the Faroe Current north of the Faroes (maximum salinity averaged over a 50-m deep layer).**

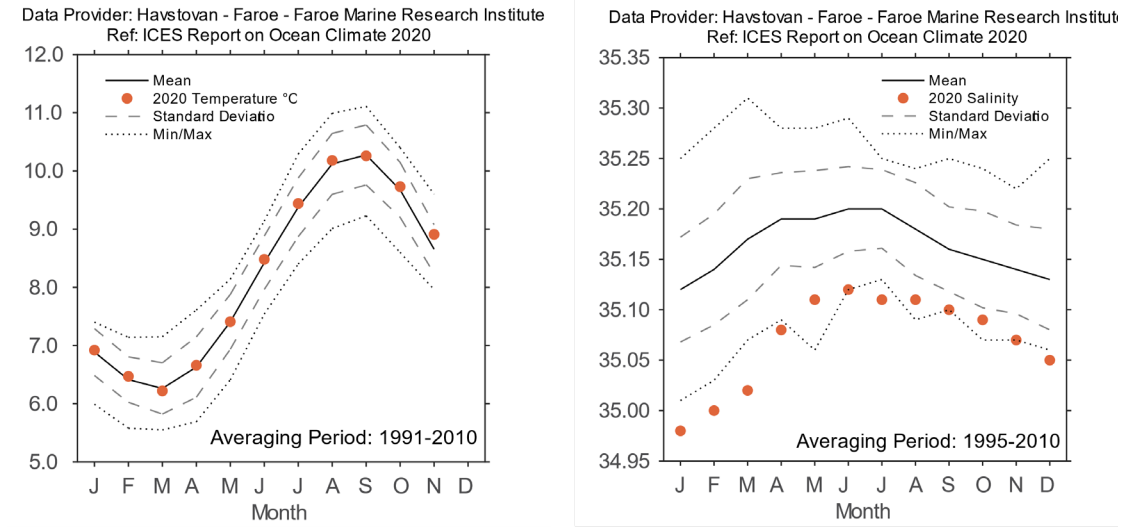


**Figure 4.58. Faroe waters. 2020 monthly temperature (left) from the Faroe coastal station at Oyrargjogv (62.12°N 7.17°W) and monthly salinity (right) from the Faroe coastal station at Skopun (61.91°N 6.88°W). Note the different averaging periods.**

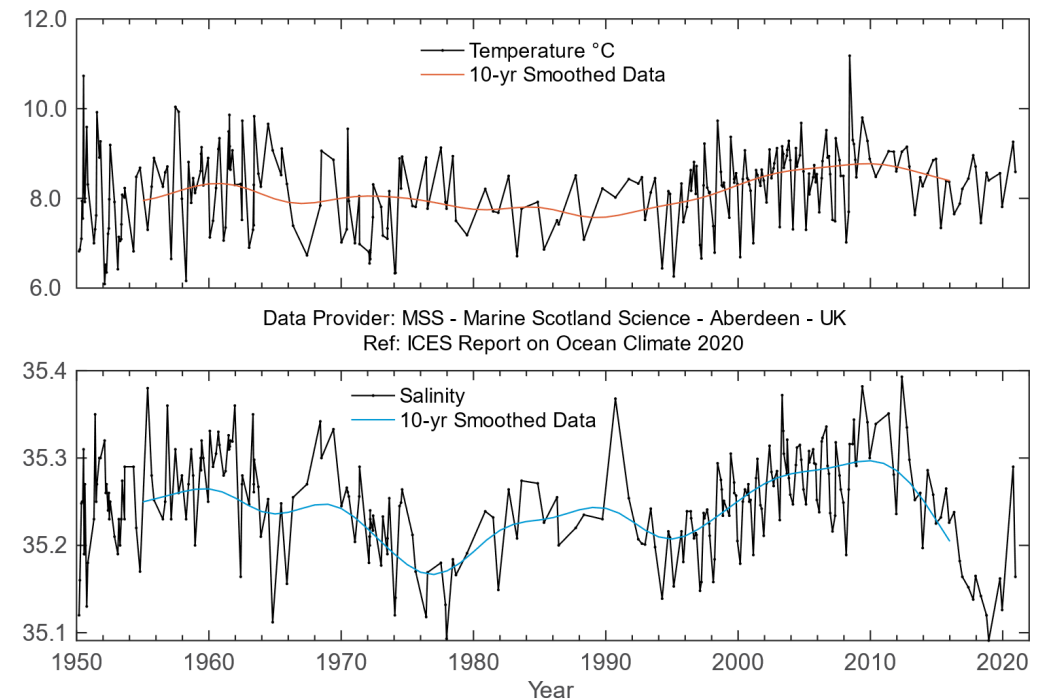


**Figure 4.59. Faroe–Shetland Channel. Temperature anomaly (upper panel) and salinity anomaly (lower panel) in the modified Atlantic water entering the Faroe–Shetland Channel from the north after circulating around the Faroes.**

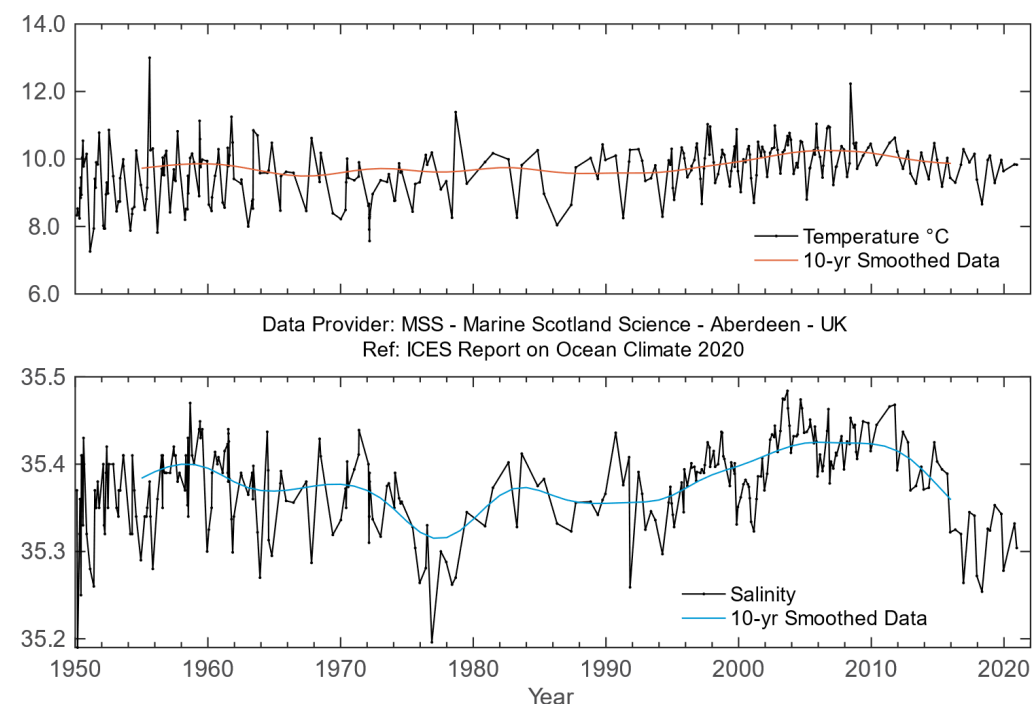


**Figure 4.60. Faroe–Shetland Channel. Temperature anomaly (upper panel) and salinity anomaly (lower panel) in the Atlantic water in the slope current.**



## 4.18 North Sea

*H. Klein, P. Loewe, M. Latarius, M. Köllner, K. A. Mork, and J. Albretsen*

---

**THE ANNUAL AREA AVERAGED NORTH SEA SST AND TOTAL SUMMER HEAT CONTENT ARE STILL ABOVE THE CLIMATOLOGICAL MEAN. AFTER A PERIOD OF FRESHENING, THE TOTAL SUMMER SALT CONTENT IS INCREASING, BUT SLIGHTLY BELOW THE LONG-TERM MEAN.**

---

North Sea oceanographic conditions are determined by the inflow of saline AW (Figure 4.61) and the ocean–atmosphere heat exchange. Inflow through the northern entrances (and, to a lesser degree, through the English Channel) can be strongly influenced by the NAO. Numerical model simulations also demonstrate strong differences in the North Sea circulation depending on the state of the NAO. The AW mixes with river runoff and lower-salinity Baltic Sea outflow along the Norwegian coast. A balance of tidal mixing and local heating forces the development of a seasonal stratification from April/May to September in most parts of the North Sea.

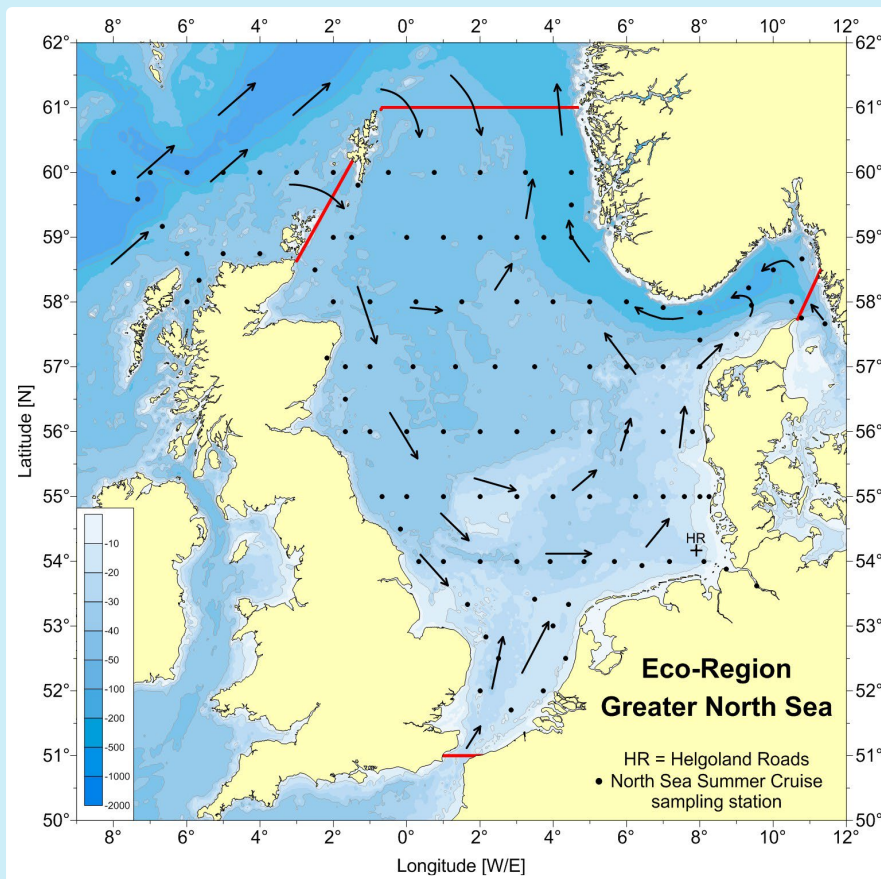


Figure 4.61. Schematic representation of North Sea circulation. Red lines: extent of the North Sea region; the sampling station at Helgolands Roads is marked with a HR+. Black arrows: mean residual circulation patterns. Black dots: summer sampling undertaken in the North Sea by Bundesamt für Seeschifffahrt und Hydrographie (BSH; German Federal Maritime and Hydrographic Agency).

### Annual conditions

In 2020, the anomalies of the area-averaged monthly North Sea SST varied between +1.1°C in June and, after a steep drop, 0.0°C in July. The anomalies of the two first months and of the last months were  $\geq +1^\circ\text{C}$  (Figure 4.62). The same pattern occurred locally at Helgolands Roads in the southern North Sea (Figure 4.63).

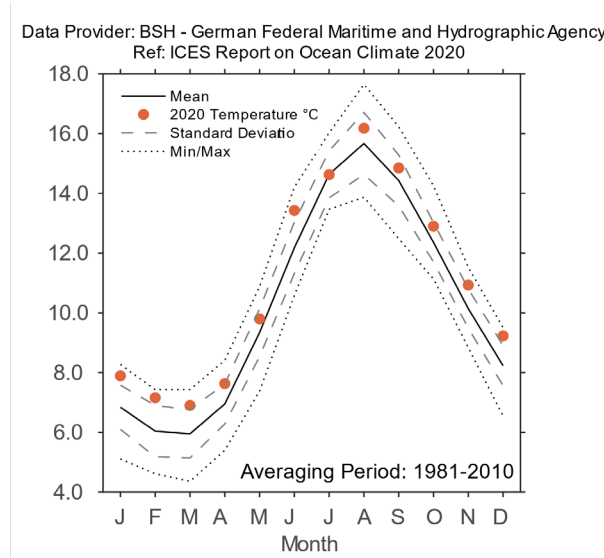


Figure 4.62. North Sea. Monthly means of area averaged North Sea SST.

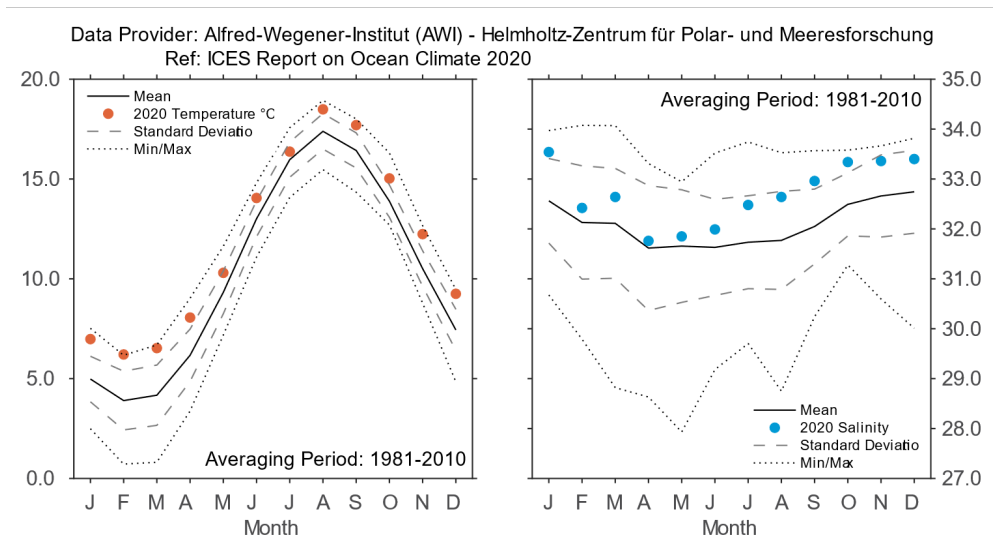


Figure 4.63. Southern North Sea. Monthly surface temperature (left panel) and salinity (right panel) at Station Helgoland Roads.

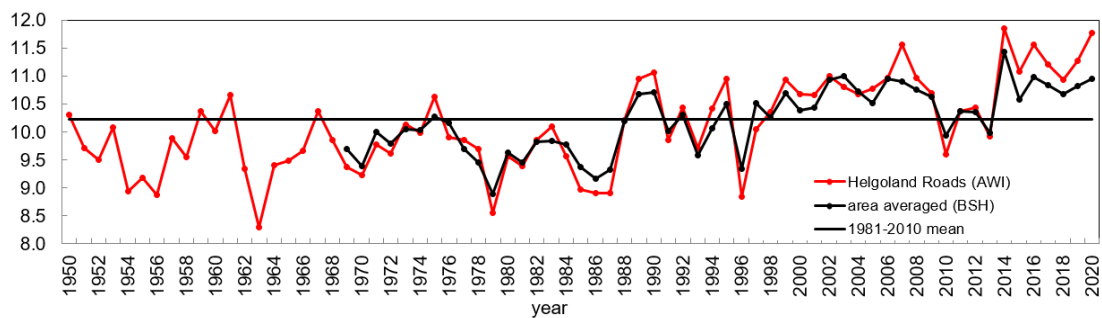
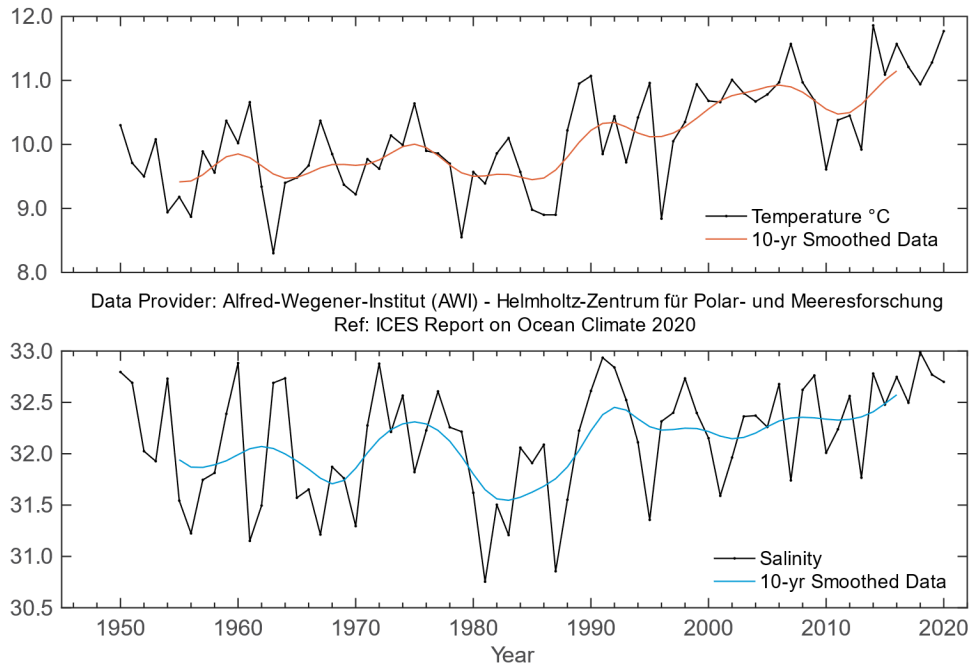


Figure 4.64. North Sea. Annual average of the area averaged North Sea SSTs.

The annual mean area-averaged North Sea SST was 11.0°C (+ 0.7°C; [Figure 4.64](#)). The annual local average at Helgoland Roads in the southern North Sea was 11.8°C (+ 1.5°C). Both time-series show the same trend over time, but there is a broader temperature range at Helgoland Roads due to the shallower water depths in the German Bight. Aside from the inflow of warmer AW at the northern boundary and occasionally through the English Channel, much of North Sea SST variability is due to local ocean–atmosphere heat flux.

Due to low Elbe River run-offs into the German Bight since 2014, the mean annual sea surface salinity (SSS) is still above the long-term mean at Helgoland Roads ([Figure 4.65](#)).



**Figure 4.65. Southern North Sea. Annual mean surface temperature anomaly (upper panel) and salinity anomaly (lower panel) at Station Helgoland Roads.**

### Summer conditions

Compared to the 2000–2010 average, there were only negative temperature anomalies in the surface layer over the entire area, increasing from the coasts toward the centre of the North Sea, where the anomaly peaked at 2.5°C. Distinct differences occurred in the bottom layer, which showed negative anomalies of up to 1°C in the western North Sea, but positive anomalies in the central and eastern North Sea, reaching up to +3°C above Dogger Bank and +2.5°C south of Norway and west of Jutland. The differences between surface and bottom-water temperatures in the central North Sea was about 6°C, and up to 8°C south of Norway.

The area-averaged summer SST (JAS) in 2020 was 14.2°C, about 0.3°C below the 1981–2010 mean. Between 55°N and 60°N, there was a sharp thermocline at depths between about 15 and 40 m. The vertical gradients within the thermocline reached values of 1.9°C m<sup>-1</sup>. Compared to 2019, the total heat content decreased slightly to 1.645 × 10<sup>21</sup> J, which is close to the 2000–2020 mean of 1.652 × 10<sup>21</sup> J.

During summer 2020, the surface inflow of AW (S > 35) over the east Shetland Shelf and the Fair Isle Channel advanced southward in a small tip to about 58°N. In the bottom layer, there was a broad inflow across the entire North Sea reaching southward to 57°N. There was no inflow of

AW through the English Channel. The surface salinity distribution showed only a small deviation from the 2000–2010 mean in the western North Sea. In the eastern North Sea, anomalies were positive, locally up to +1.5. In the bottom-water layer, there were only minor deviations from the long-term salinity mean of about  $\pm 0.5$ . Compared to 2019, the total salt content increased slightly to  $1.119 \times 10^{12}$  t, approaching the 2000–2020 mean of  $1.123 \times 10^{12}$  t.

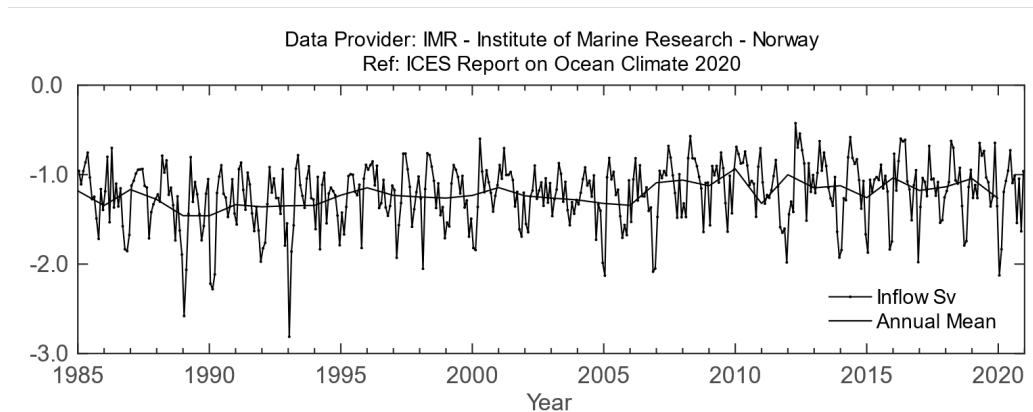


**Figure 4.66. Northern North Sea. Modelled annual mean (bold) and monthly mean volume transport of Atlantic Water into the northern and central North Sea southwards between the Orkney Islands and Utsire, Norway.**

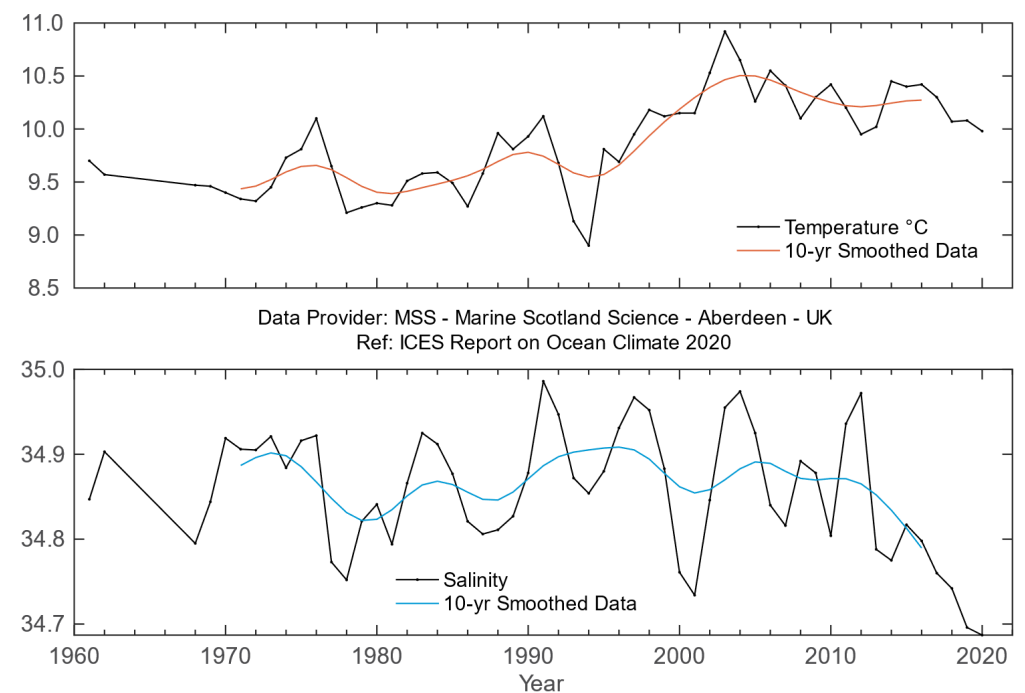


**Figure 4.67. Northern North Sea. Temperature anomaly (upper panel) and salinity anomaly (lower panel) in the Fair Isle Current entering the North Sea from the North Atlantic.**

**AW inflow**

The ocean circulation model NORWECOM is used to calculate transports of inflowing AW through a transect between Utsira, Norway, and the Orkneys. The model results for 2020

indicate that the annual AW inflow was close to the 1985–2010 average. The inflow during the first quarter in 2020 was relatively high (the fourth highest of all January–March-periods since 1985), but was low the rest of the year. The overall contribution of AW to the North Sea and the Skagerrak thus remains stably low, maintaining the trend observed during the last decade ([Figure 4.66](#)). Salinity of the Fair Isle inflow into the North Sea was still low, but had not decreased further ([Figure 4.67](#)).

#### 4.19 Skagerrak, Kattegat, and the Baltic Sea

*J. Linders, T. Wodzinowski, and T. Liblik*

The seas in the Baltic Sea ecoregion are characterized by large salinity variations. In the Skagerrak, water masses from different parts of the North Sea are present. The Kattegat is a transition area between the Baltic Sea and the Skagerrak. The water in the Baltic Sea is strongly stratified with a permanent halocline. The deep water in the Baltic Sea proper enters through the Belts and the Sound and can be stagnant for long periods. In the relatively shallow area in the southern Baltic Sea, smaller inflows pass relatively quickly, and conditions in the deep waters are very variable. Surface salinity is very low in the northern, central, and eastern Baltic Sea. The Gulf of Bothnia and the Gulf of Finland are at least partly ice covered during winter.

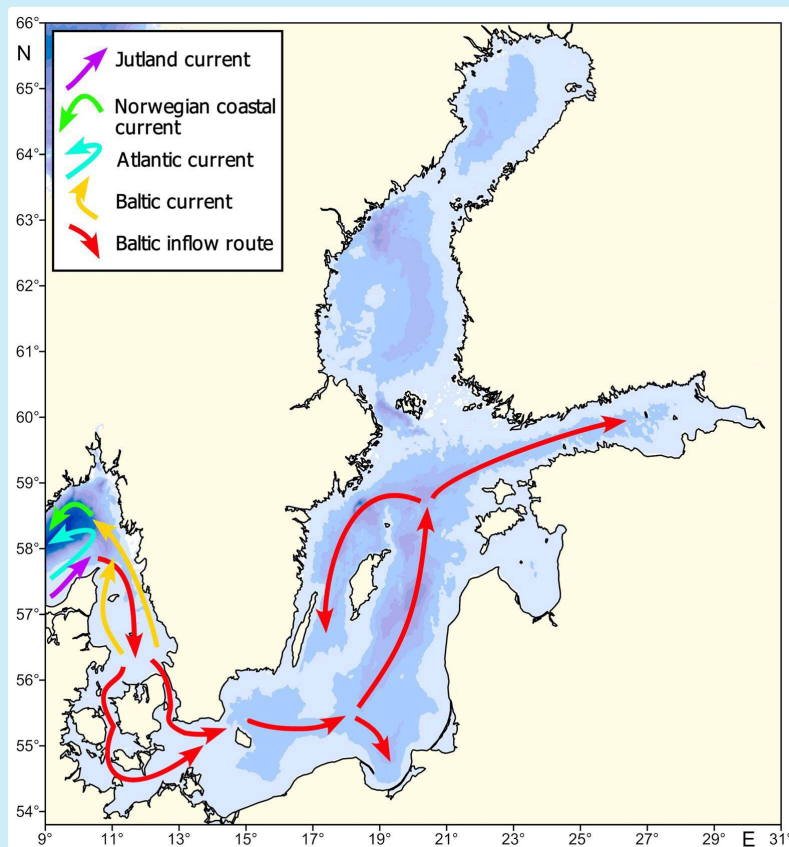
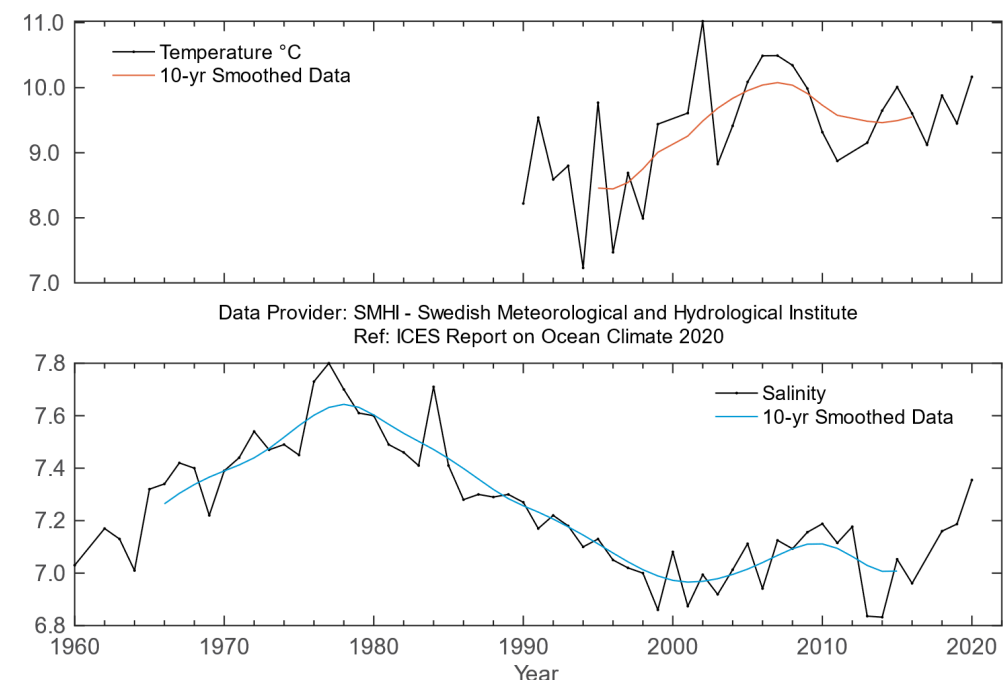


Figure 4.68. Skagerrak, Kattegat, and the Baltic Sea. Water masses circulation map.

Owing to its central location relative to the Skagerrak, Kattegat, and the Baltic Sea, the weather in Sweden can be taken as representative for the area. The mean air temperature in Sweden was at a record high in 2020, about 0.5°C higher than in 2014, the previous warmest year on record. Most meteorological stations broke their temperature records, including Stockholm, Lund, and Uppsala, which have a time-series of recorded temperatures extending back to the mid-18th century. Especially January, June, and November were warmer than normal. The mean precipitation was also higher than normal in large parts of Sweden during 2020, and the number of hours of sun.



**Figure 4.69. Skagerrak, Kattegat, and the Baltic Sea. Surface temperature, yearly mean (upper panel) and surface salinity, yearly mean (lower panel) at Station BY15 (east of Gotland) in the Baltic Sea proper.**

In spring and winter 2020, the Skagerrak and Kattegat areas had surface temperatures above normal. In the Baltic Sea, the annual mean SST was significantly higher than the long-term average, and exceeded the standard deviation of the annual means in the Baltic Sea proper. A similar situation occurred in the eastern part of the reservoir during autumn. In addition, surface salinity was mostly above normal in the Baltic Sea proper, a tendency that could be seen already in 2019. The high salinity and temperature levels were not limited to the surface, but were present at most depths, together with a more distinct halocline around 50–60 m.

The severe oxygen-depleted conditions in the deep-water in the Baltic Sea proper continued in 2020. Areal calculations are presented in relation to the area of the Baltic Sea proper (which includes the Arkona Basin, the Bornholm Basin, the Gulf of Gdansk, and the eastern, western, and northern Gotland Basin), the Gulf of Riga, and the Gulf of Finland. Around 18% ( $45 \times 10^3 \text{ km}^2$ ) of the bottoms were affected by anoxic ( $< 0 \text{ ml l}^{-1}$ ) conditions and 31% ( $79 \times 10^3 \text{ km}^2$ ) by a combination of both hypoxic and anoxic ( $< 2 \text{ ml l}^{-1}$ ) conditions. Overall, a smaller bottom area was affected by anoxic conditions than in 2018/2019, while the hypoxic area largely remained unchanged.

A major Baltic inflow can significantly refresh the deep water along its route into the Baltic Sea proper, but no major Baltic Sea inflow was detected in 2020. The last inflow events occurred in 2014–2016.

The ice season 2019/2020 started in late October and ended in late May. The season was very mild, and the ice extent reached the seasonal maximum of 37 000 km<sup>2</sup> on 5 March. This was the lowest recorded maximum ice extent since the beginning of the 18th century.

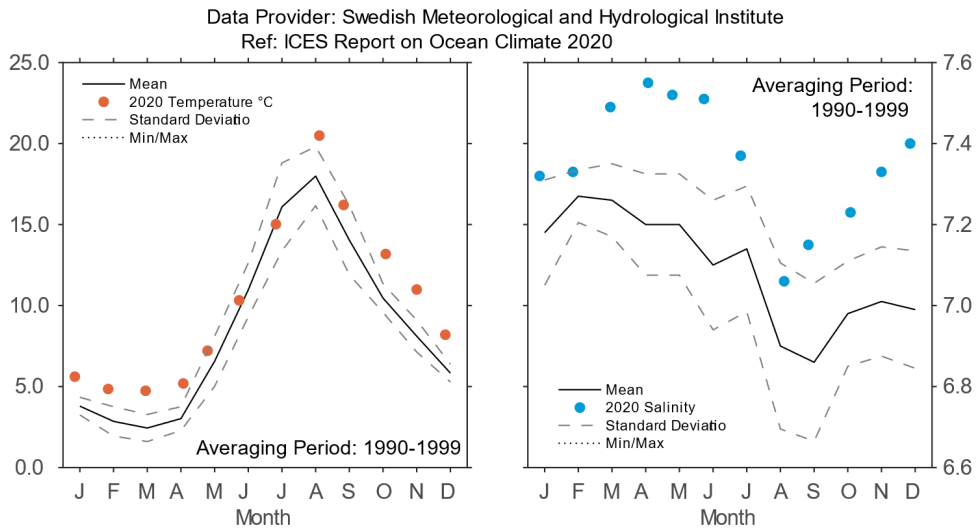


Figure 4.70. Skagerrak, Kattegat, and the Baltic Sea. Monthly surface temperature (left panel) and salinity (right panel) at Station BY15 (east of Gotland) in the Baltic Sea proper.

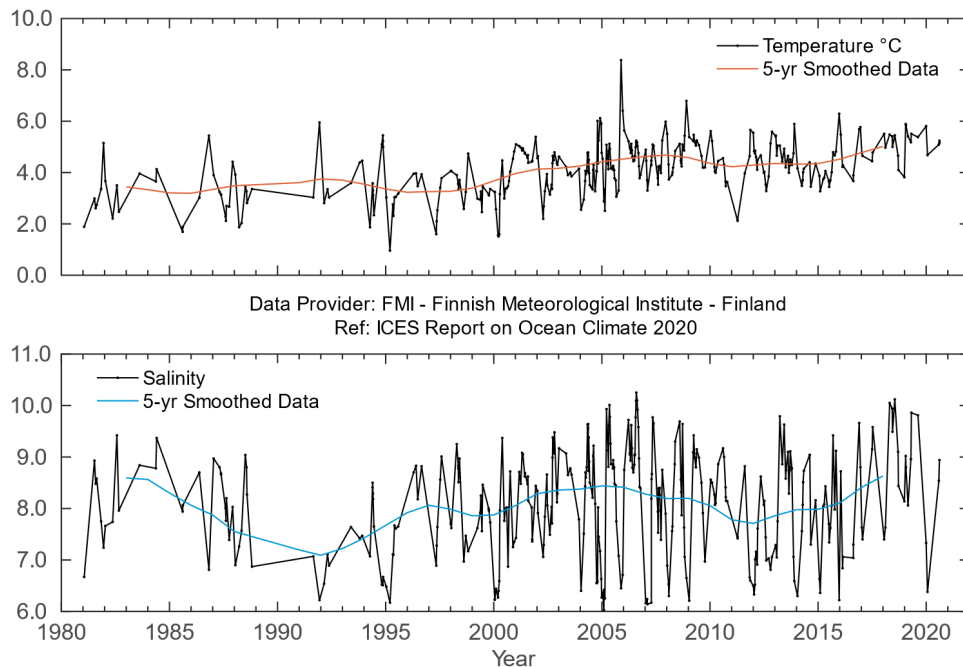


Figure 4.71. Skagerrak, Kattegat, and the Baltic Sea. Temperature (upper panel) and salinity (lower panel) at Station LL7 in the Gulf of Finland.

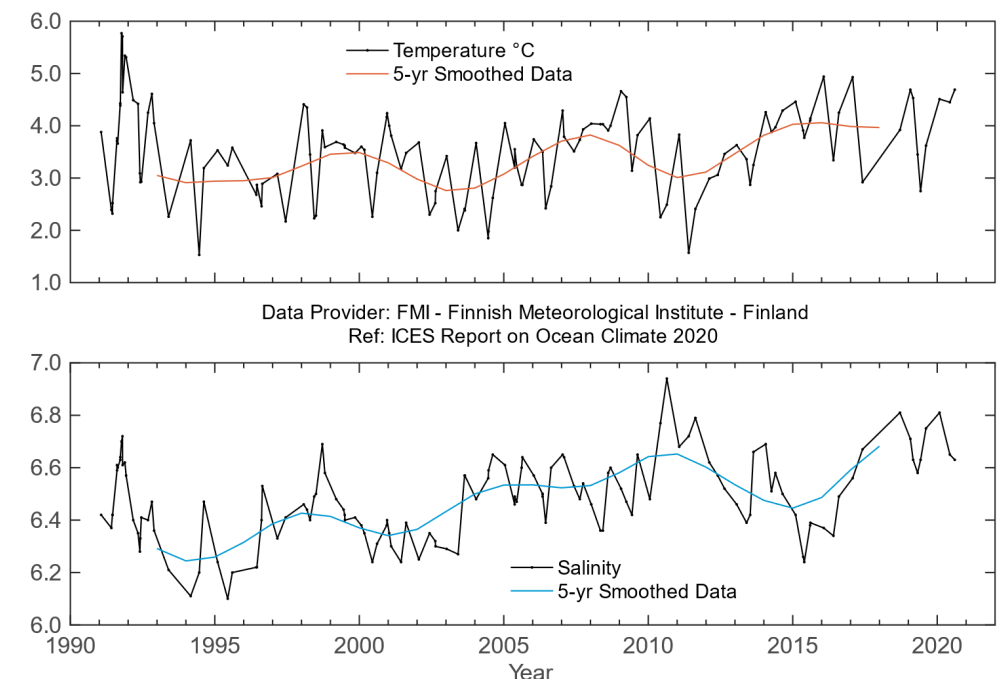


Figure 4.72. Skagerrak, Kattegat, and the Baltic Sea. Temperature (upper panel) and salinity (lower panel) at Station SR5 in the Bothnian Sea.

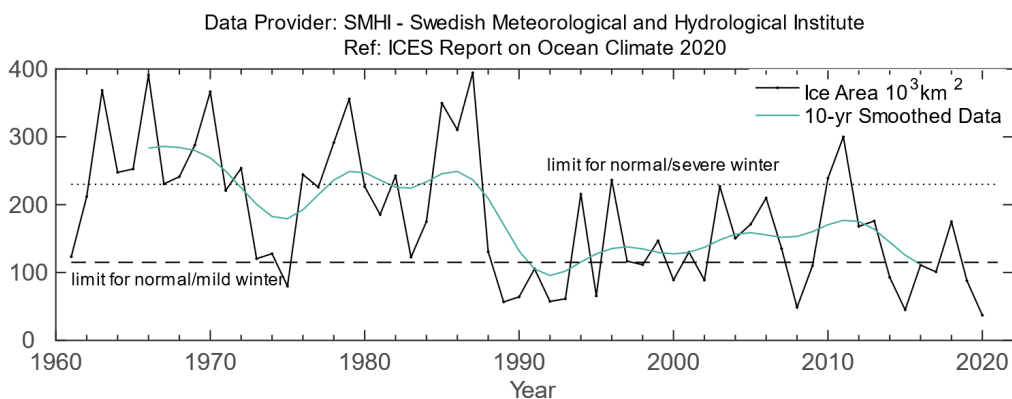


Figure 4.73. Skagerrak, Kattegat, and the Baltic Sea. The maximum ice extent in the Baltic starting from 1960.



## 4.20 Norwegian Sea

*Mork, K.A.*

### FRESHENING AND HIGH, BUT DECLINED HEAT CONTENT IN THE NORWEGIAN SEA

The Norwegian Sea is characterized by warm AW on the eastern side and cold Arctic water on the western side, separated by the Arctic front (Figure 4.74). AW enters the Norwegian Sea through the Faroe–Shetland Channel and between the Faroes and Iceland via the Faroe Front. A smaller branch, the North Icelandic Irminger Current, enters the Nordic Seas on the western side of Iceland. AW flows north as the Norwegian Atlantic Current, which splits when it reaches northern Norway; some enters the Barents Sea, whereas the rest continues north into the Arctic Ocean as the West Spitsbergen Current.

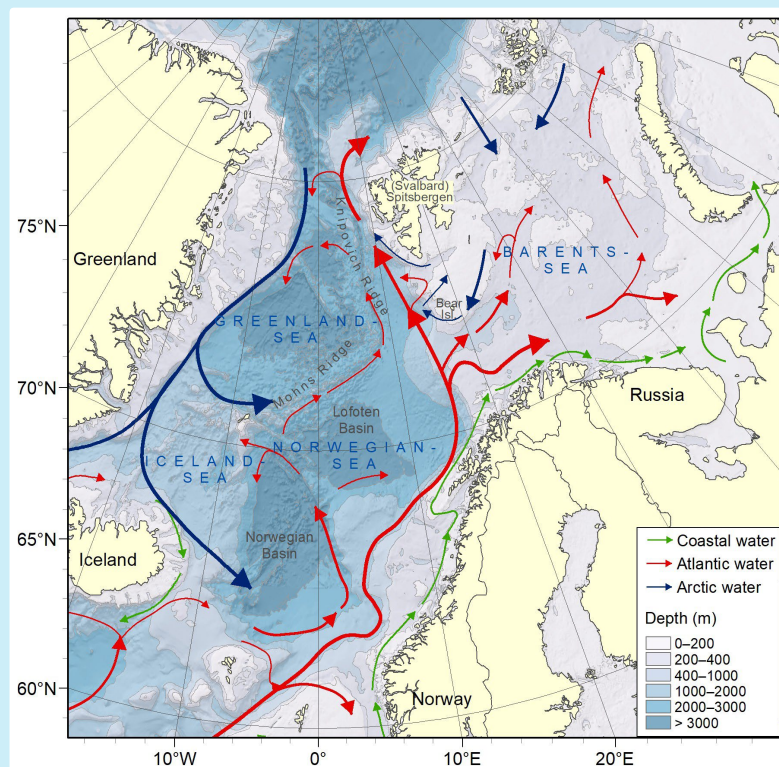
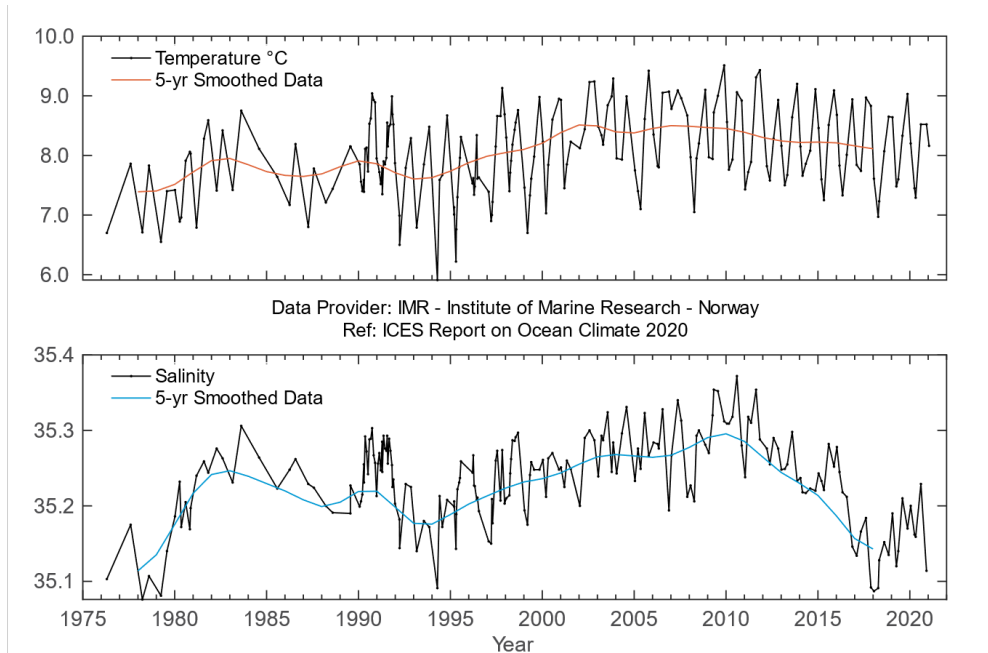
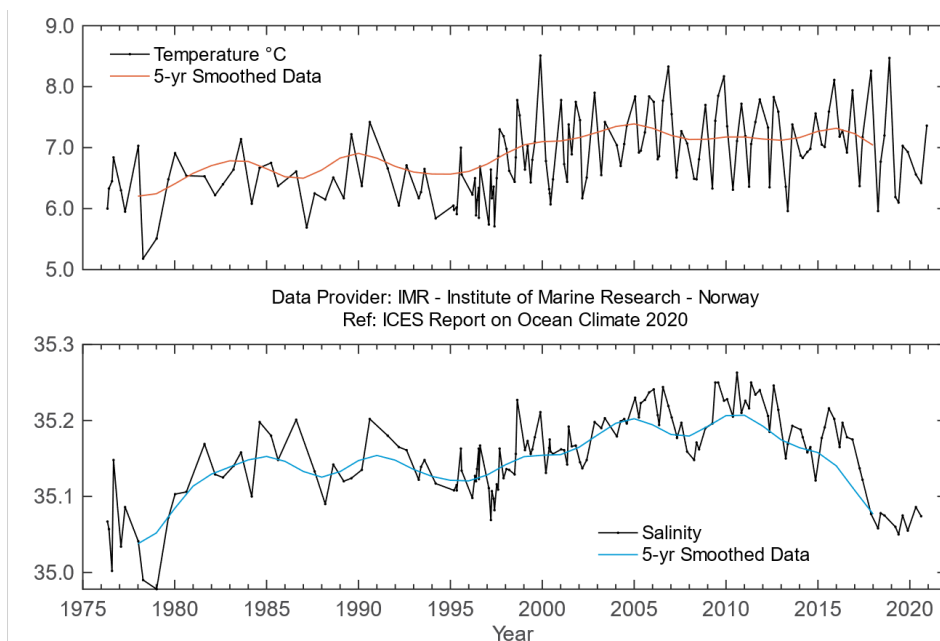


Figure 4.74. Circulation schematic for the Norwegian and Barents seas. Red lines: poleward movement of AW. Blue lines: circulation of Arctic Water. Green lines: circulation of coastal waters.

Three sections, distributed from south to north in the eastern Norwegian Sea, demonstrate the development of temperature and salinity in the core of the AW: Svinøy-NW (northwest; Figure 4.75), Gimsøy-NW (Figure 4.76), and Sørkapp-W (west; Figure 4.77). In general, there has been an increase in temperature in all three sections from the mid-1990s until recent years, followed by a decline in temperature. Annual temperature averages in 2020 were close to the long-term means at both the Svinøy-NW and Sørkapp-W sections, and 0.3°C below the long-term mean at the Gimsøy-NW section.



**Figure 4.75. Norwegian Sea. Temperature (upper panel) and salinity (lower panel) above the slope at Svinøy-NW Section (63°N).**



**Figure 4.76. Norwegian Sea. Temperature (upper panel) and salinity (lower panel) above the slope at Gimsøy-NW Section (69°N).**

Salinity increased until around 2010 and then decreased in recent years at all three sections. In both the Svinøy-NW and Gimsøy-NW sections, salinity during 2019 and 2020 showed the lowest values since the end of the 1970s. Salinity increased somewhat in 2020 at Svinøy-NW, but was still considerably lower than the long-term mean. Annual salinity averages in 2020 were 0.07, 0.10, and 0.05 below the long-term means at the Svinøy-NW, Gimsøy-NW, and Sørkapp-W sections, respectively.

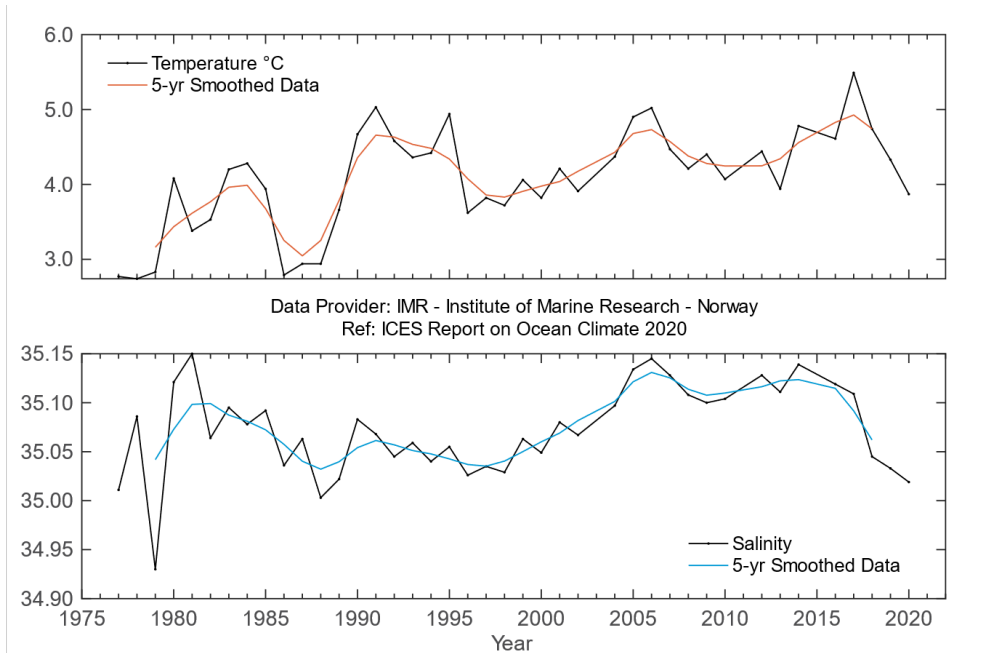


**Figure 4.77. Norwegian Sea. Temperature (upper panel) and salinity (lower panel) above the slope at Sørkapp-W Section (76°N).**

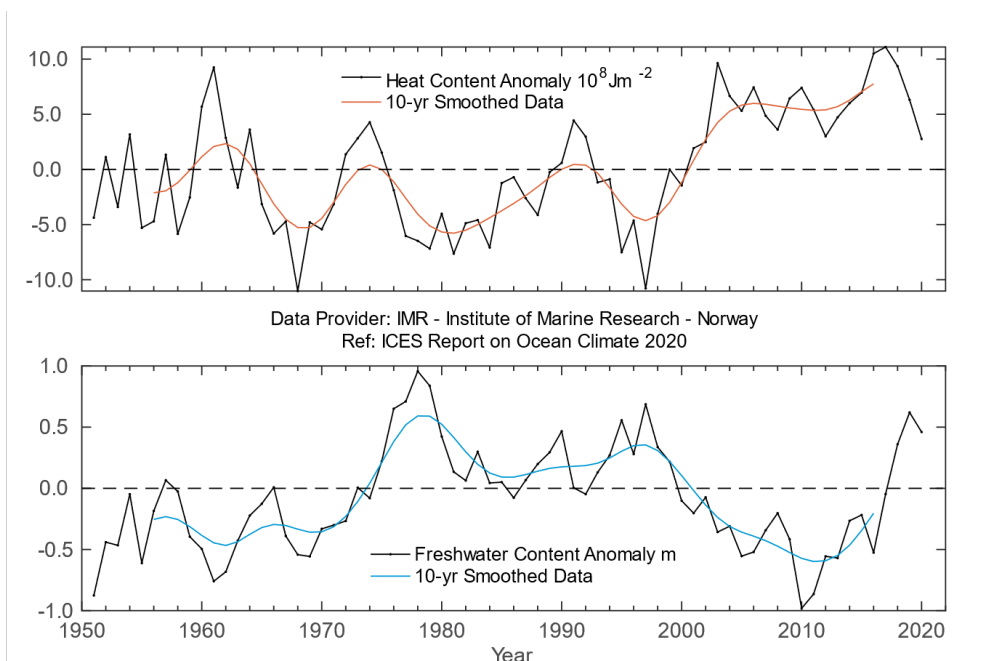


**Figure 4.78. Norwegian Sea. Heat (upper panel) and freshwater (lower panel) contents of Atlantic Water in the Norwegian Sea.**

The ocean heat and freshwater content of AW, observed since 1951 using spring hydrographic data, describe the climate variability in the Norwegian Sea (Figure 4.78). The heat content in the Norwegian Sea has been above the long-term mean since 2000, reaching a record-high in 2017. The freshwater content has increased since 2010. In 2020, both heat and freshwater content were above the long-term mean.

## 4.21 Barents Sea

*A. Trofimov and R. Ingvaldsen*

---

### WARM AND LOW-ICE CONDITIONS CONTINUE IN THE BARENTS SEA IN 2020.

---

The Barents Sea is a shelf sea that receives an inflow of warm AW from the west ([Figure 4.74](#)). The inflow exhibits considerable seasonal and interannual fluctuations in volume and water mass properties causing high variability in heat content and ice coverage of the region.

In 1996 and 1997, after a period with high temperatures in the first half of the 1990s, temperatures in the Barents Sea dropped to slightly below the long-term average. From March 1998, temperature in the western Barents Sea increased to just above average, but remained below average in the eastern part during 1998. From the beginning of 1999, there was a rapid temperature increase in the western Barents Sea that spread to the eastern part. Since then, temperature has remained above average.

The Fugløy-Bear Island Section covers the inflow of AW and coastal water masses from the Norwegian Sea into the Barents Sea, while the Kola Section covers the same waters in the central Barents Sea. During 2016–2019, AW temperature in the western Barents Sea (Fugløy-Bear Island Section) decreased by 0.7°C ([Figure 4.79](#)). The decrease in temperature was linked to lower temperatures upstream in the Norwegian Sea. However, in 2020, the temperatures increased slightly (to 0.1°C above the 1981–2010 average) as compared to 2019, seemingly linked to higher inflow during winter. AW salinity in the Fugløy-Bear Island Section has been decreasing since 2011 and was at the same level in 2019 as during a very fresh and cold period in the late 1970s ([Figure 4.79](#)). The salinity increased slightly in 2020 from 2019, which again can be linked to stronger inflow during winter.

In the central Barents Sea (Kola Section), air and water temperatures in 2020 were still above the 1981–2010 average, as typical for warm years. In January–September, the observation period in the Kola Section (0–200 m) in 2020, positive temperature anomalies in AW varied insignificantly; anomalies averaged over the period January–September were +0.3°C and +0.4°C in the central (Murman Current) and outer (Central branch of the North Cape Current) parts of the section, respectively. Temperature anomalies in coastal waters (inner part of the section) were higher and increased from +0.7°C in August to +1.1°C in November. The 2020 annual mean AW temperature in the central Kola Section (0–200 m) was typical of warm years and exceeded the 1981–2010 average by 0.3°C. However, it was 0.1°C lower than in 2019 and the second lowest value, after 2011, observed since 2004 ([Figure 4.80](#)).

Throughout the observation period in 2020, coastal and AW salinity in the Kola Section (0–200 m) was lower than the 1981–2010 average. Negative salinity anomalies in AW varied insignificantly; anomalies averaged over the period January–September were –0.04 and –0.08 in the central and outer parts of the section, respectively. Salinity anomalies in coastal waters varied from –0.01 in August to –0.17 in November. The 2020 annual mean AW salinity in the central Kola Section (0–200 m) was 0.05 lower than average, but 0.02 higher than in 2019 ([Figure 4.80](#)).

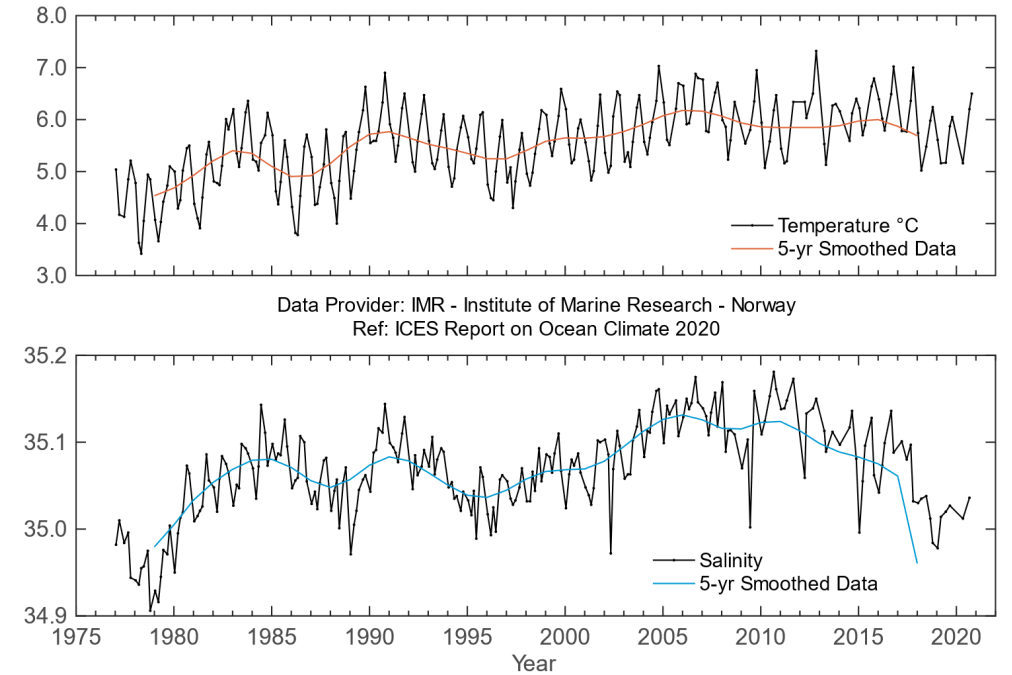


**Figure 4.79. Barents Sea. Temperature (upper panel) and salinity (lower panel) in the Fugløya–Bear Island Section.**

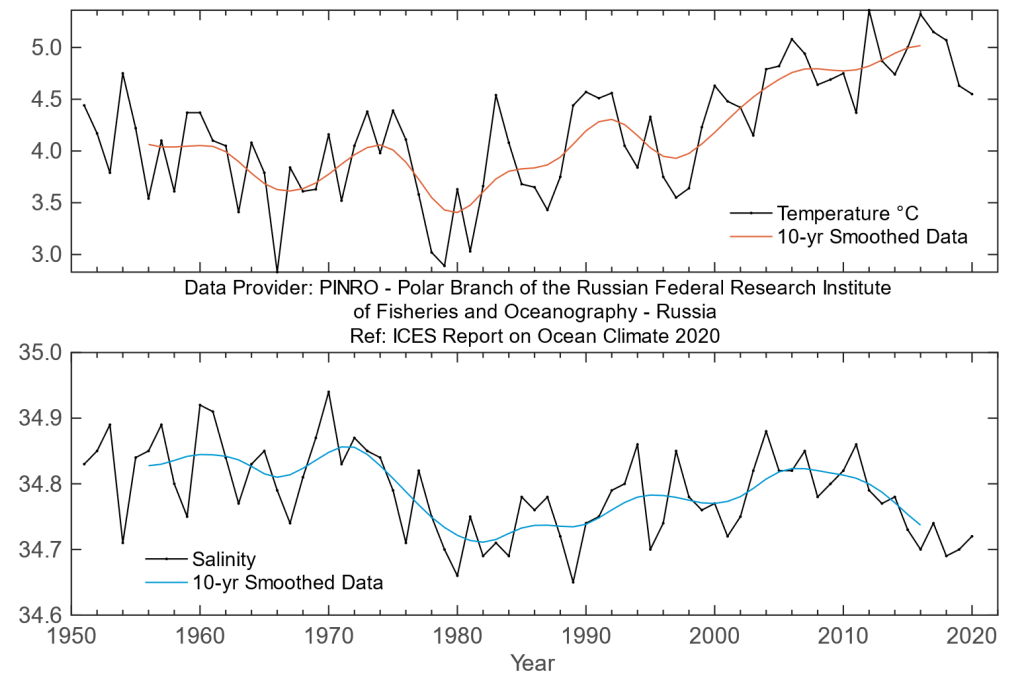


**Figure 4.80. Barents Sea. Temperature (upper panel) and salinity (lower panel) in the Kola Section (0–200 m).**

According to data from the Barents Sea Ecosystem Survey carried out in August–October 2020, surface, deeper, and bottom waters were still warmer than the 1981–2010 average (by 1.4, 0.5, and 0.7°C on average, respectively) in most of the Barents Sea (from 95% of the covered area at the surface to 66% near the bottom). The largest positive anomalies were observed at the surface and in the southeast. Negative anomalies were mainly found in deeper and bottom waters in the north. Compared to 2019, surface waters were much warmer (by 1.4°C on average) in most

of the Barents Sea (82% of the surveyed area). Deeper and bottom waters were generally 0.5°C colder than in 2019 in the central and eastern parts of the sea, and about 0.5°C warmer in the western and northern parts. Surface waters were also fresher than the 1981–2010 average and comparable to 2019 mainly in the western and central parts of the sea. Negative anomalies and differences in salinity between 2020 and 2019 were generally observed in the north and southeast. Bottom salinity was slightly lower than both the long-term average and 2019 values in 82 and 75% of the surveyed area, respectively. Positive anomalies and differences were mostly found in the southeastern part of the sea. In autumn 2020, the areas of AW (> 3°C) and Arctic waters (< 0°C) were close to those in 2019. AW still occupied a rather large area, while the area of Arctic waters remained small. The area of cold bottom waters has been increasing for the past four years since a record-low value in 2016, and in 2020 reached the largest extent since 2011.

In 2020, the Barents Sea ice extent was still below the 1981–2010 average. There was almost no ice in the sea from July to November. Due to much warmer-than-normal air temperatures in summer and autumn 2020, ice formation started later than usual. As a result, ice coverage did not exceed 1% in October and was a record low 3% in November. In November and December, the ice coverage was much lower than the 1981–2010 average (by 26 and 20%, respectively) and 2019 values (by 16 and 11%). The 2020 annual mean ice coverage of the Barents Sea was 11% below average, and 2% less than in 2019.

Volume fluxes split into quarterly periods show that volume flux decreased in winter (January–March) and spring (April–June) during 2015–2019, but increased in summer (July–September) and autumn (October–December). This pattern shifted in 2020, possibly due to strong winds and stormy conditions, and the first quarter of 2020 had very high inflow. The inflow in spring 2020 was also relatively high, and higher than in 2019, but these values might change when the time-series (which currently stops in May 2020) is updated.

## 4.22 Fram Strait

*A. Beszczynska-Möller and W. J. von Appen*

---

**IN 2020 TEMPERATURE OF AW CARRIED TOWARDS THE ARCTIC OCEAN ALONG THE EASTERN RIM OF THE GREENLAND SEA AND FRAM STRAIT WAS CLOSE TO ITS LONG-TERM MEAN, WHILE SALINITY WAS SIGNIFICANTLY BELOW. IN THE DEEP WATERS OF THE GREENLAND SEA, TEMPERATURE AND SALINITY CONTINUE TO INCREASE.**

---

The Fram Strait ([Figure 4.74](#)) is the northern border of the Nordic Seas. It is the only deep passage connecting the Arctic to the rest of the world oceans and is one of the main routes whereby AW enters the Arctic (the other is the Barents Sea). The AW flows along the eastern rim of the Greenland Sea, and in Fram Strait it is carried north by the West Spitsbergen Current. AW temperature, salinity, volume, and heat fluxes exhibit strong seasonal and interannual variations. A significant part of the AW also recirculates within, and shortly north of, Fram Strait, and joins the flow to the south as the Return Atlantic Water (RAW). Polar Water from the Arctic Ocean flows south in the East Greenland Current (EGC) and affects water masses in the Nordic Seas.

The AW at the eastern rim of the Greenland Sea (along the 75°N section, between 10° and 13°E) reached its highest temperature value in 2005–2007, with a peak in 2006 (Figure 4.81). After this period, AW temperature decreased significantly in 2008–2009 and remained below its long-term mean value until 2011. In 2012, the temperature of AW in the eastern Greenland Sea increased and remained relatively stable until 2018, with small variations (up to 0.5 s.d.) and values exceeding its long-term mean by 0.25–0.55°C. In 2018 and 2019, the AW temperature decreased when compared to 2015–2017, reaching 4.37°C in 2019 (0.2°C below the long-term average). In 2020, the AW temperature returned to its long-term mean value of 4.5°C. A significant increase in the salinity of AW in the eastern Greenland Sea was observed in 2005–2006 (Figure 4.81), with the maximum of 35.16 in 2006 (exceeding the long-term average by 0.07). This peak was followed by a sharp decrease in 2007, and further slow descent until 2009 when AW salinity returned to its long-term average. In 2010, salinity started to rise again and reached its second peak in 2012 (0.06 above its long-term mean). It remained relatively steady until 2014 (with a slight decrease in 2013). Since 2015, a notable decrease in salinity has been observed, and in 2018 it ceased to be above the long-term average for the first time in 14 years (2004–2017). In 2020, it reached the lowest value in the entire record (35.02, i.e. 0.07 or 1.8 s.d. below its long-term average).

No measurements have been conducted in the western and central part of the Greenland Sea section at 75°N since 2010 (Figure 4.81). The RAW temperature at the western rim of the Greenland Sea reached its maximum in 2006 (2.9°C) and slowly decreased to slightly lower than its long-term average at the end of the observation period (2010). The temperature maximum in 2006 was accompanied by a very strong peak in RAW salinity (0.13 above the long-term mean, and > 3 s.d.). In 2007, RAW salinity dropped, remained slightly higher than its long-term average until 2008, and then decreased to close to the average in 2009 and 2010. Temperature and salinity in the upper layer of the central Greenland Basin, within the Greenland Gyre, were modified by the advection of AW and winter convection.

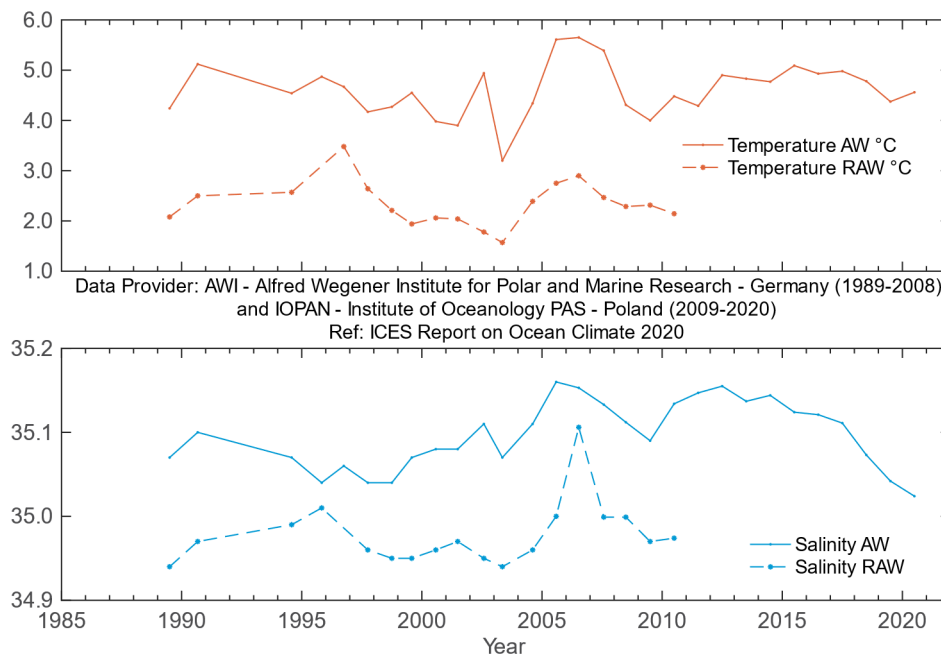


**Figure 4.81.** Greenland Sea and Fram Strait. Temperature (upper panel) and salinity (lower panel) of Atlantic Water (AW) and Return Atlantic Water (RAW) in the Greenland Sea Section at 75°N. AW properties are 50–150 m averages at 10–13°E. The RAW is characterized by temperature and salinity maxima below 50 m averaged over three stations west of 11.5°W. RAW has not been measured since 2010.

In the southern Fram Strait, at the standard section along 76.50°N (at the level of 200 dbar, spatially averaged between 9° and 12°E), a record-high summer temperature for AW was observed in 2006 (maximum of 4.5°C, exceeding the long-term average by 1.3°C), accompanied by the highest AW salinity (35.13) in the observation period (Figure 4.82). After that peak, temperature and salinity decreased rapidly in 2007 and 2008 before increasing again in summers 2009–2012. In 2011–2015, the temperature of AW in the southern Fram Strait remained relatively constant (3.7–3.8°C, exceeding the long-term average by approx. 0.6°C) except in summer 2013 when it dropped to 3.22°C and levelled out with the long-term mean value. Since 2015, a moderate increase was observed, and in 2017, AW temperature reached its decadal maximum of 4.1°C, the second largest value after the 2006 maximum of 4.5°C. In 2019, AW temperature dropped significantly to 3.36°C (only 0.2°C above its long-term average) and remained close to those values in 2020. AW salinity in the southern Fram Strait was the same in 2011, 2012, and 2014 (35.13) as during the 2006 maximum, exceeding its long-term mean by 0.07 (Figure 4.82). In 2015, salinity experienced a drop and thereafter recovered and remained the same in 2016 and 2017 (~ 1 s.d., i.e. 0.04, above its long-term mean of 35.06). Since 2018, salinity has been notably decreasing, and in 2019 reached a minimum of 35.02 (the lowest value observed in the last 20 years, 1 s.d. below its long-term average). In 2020, AW salinity was very close to the 2019 value (Figure 4.82).

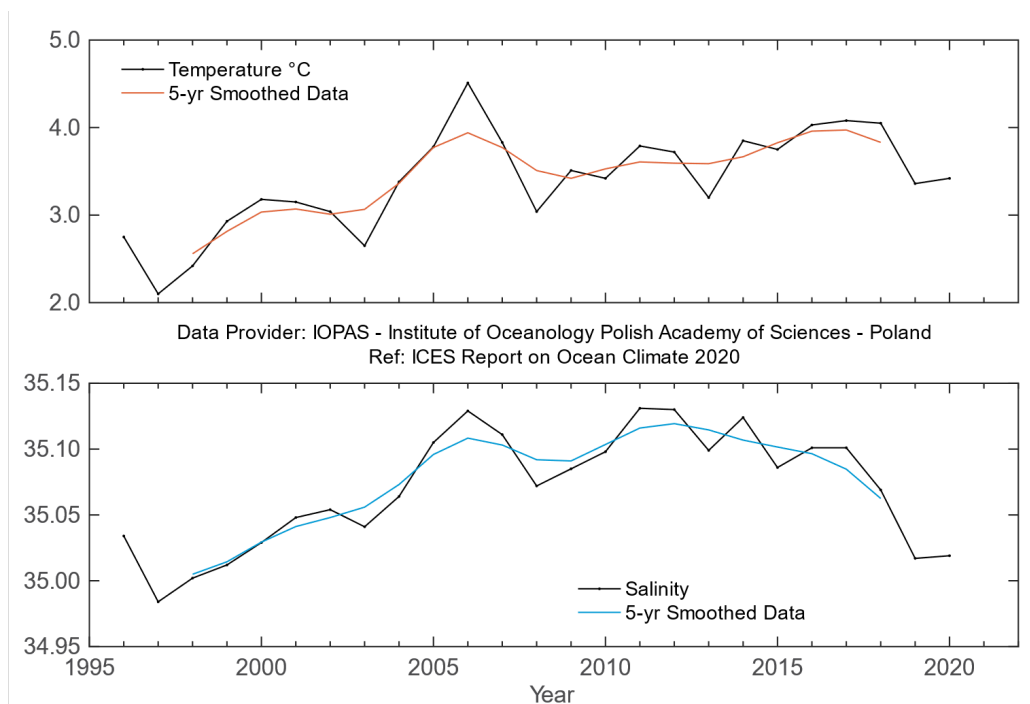


**Figure 4.82. Greenland Sea and Fram Strait. Temperature (upper panel) and salinity (lower panel) at 200 dbar in the southern Spitsbergen Section (76.50°N).**

In the northern Fram Strait at the standard section along 78.83°N, three characteristic areas can be distinguished in relation to the main flows: the West Spitsbergen Current (WSC) between the shelf edge and 5°E, the Return Atlantic Current (RAC) between 3°W and 5°E, and the Polar Water in the EGC between 3°W and the Greenland Shelf (Figure 4.83).

The spatially averaged mean temperature of the upper 500 m layer in the WSC reached its peak in 2006 (4.54°C) and decreased afterwards, varying in 2007-2011 ± 0.4°C with respect to the long-term average, and reaching 0.7–0.8°C below the long-term mean in 2012/2013. In 2014,

temperature increased again and reached the second highest value in the observation period (4.24°C, exceeding the long-term mean by 1.13°C) in 2015. Temperature in the WSC remained high (> 1 s.d.) until 2017, after which it decreased, reaching 2.54°C in 2020 (0.6°C below the long-term average). The highest salinity in the upper 500 m in the WSC was observed in 2006 (35.11), followed by a decrease to the long-term average in 2007–2008. On from 2009, WSC salinity increased again until reaching 0.5 above the long-term mean in 2011. After a slight decrease in 2012/2013, salinity in the WSC reached its second maximum (35.09) in 2014, followed by slightly lower values in 2015 and 2016. In 2017, AW salinity in the WSC increased again to 35.07, remaining below the 2014 maximum, but still 0.05 above the long-term average. In 2018, WSC salinity dropped slightly below its long-term average and has been significantly decreasing since, reaching, in 2020, the lowest salinity in over 30 years (34.97; 1.4 s.d. below the long-term average).

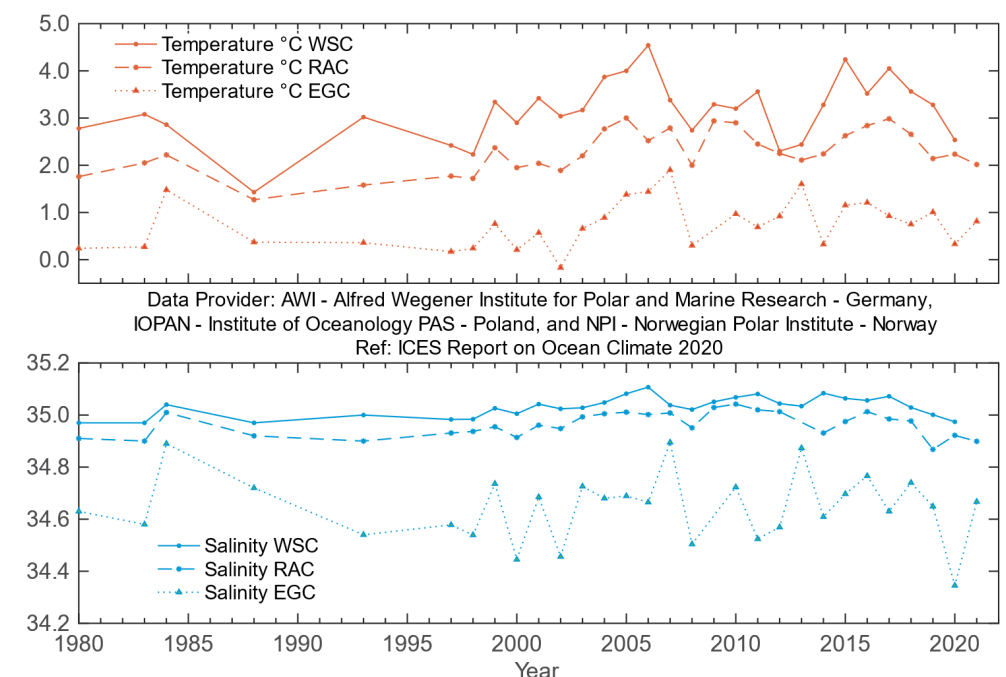


**Figure 4.83. Greenland Sea and Fram Strait. Temperature (upper panel) and salinity (lower panel) in Fram Strait (78.83°N) at 50–500 m: in the Atlantic Water (AW) in the West Spitsbergen Current (WSC; between the shelf edge and 5°E), in the Return Atlantic Current (RAC; between 3°W and 5°E), and in the Polar Water in the East Greenland Current (EGC; between 3°W and the Greenland Shelf).**

At the standard section along 78.83°N, the location of the AW in the WSC core located over the upper-shelf slope reached down to about 700–800 m in 2017 and 2018 (with the AW lower boundary represented by the isotherm of 2°C), while in 2019, it was found slightly shallower at the depth of about 300–600 m. In 2020, the AW layer was even shallower than in the previous year, reaching down only to 300–400 m. The offshore branch of the WSC, located over the lower shelf slope, was less pronounced and slightly shallower in 2020 than in previous years (with the isotherm of 2°C found at the depth of about 300 m). It was also occupied by colder and significantly less saline water than in the previous years. The low salinity surface layer over the WSC core, which covered the upper 20–30 m in 2017, was absent in 2018–2020. The low salinity surface layer in the offshore WSC branch was found west of 6°E in 2020, reaching down to a

depth of 50 m, and the frontal zone between Arctic and Atlantic origin waters in the northern Fram Strait was located at about 1–1.5°E.

The highest temperature in the RAC was observed in 2005 (3°C) and in 2009–2010 (slightly above 2.9°C). On from 2011, it decreased slowly until it reached 2.1°C in 2013 ([Figure 4.83](#)), and then increased slowly to 2.2°C in 2014. The RAC temperature in 2016 remained close to that in 2014/2015, while the temperature difference between the AW in the WSC and the AW recirculating in the RAC was only half of the 2015 value (0.7°C in 2016 compared to 1.5°C). In 2017, the RAC temperature rose to the second highest value in the observation period (2.99°C), close to the 2005 maximum. Since 2018, it has been gradually decreasing and reached 2.2°C in 2020. The maximum salinity in the RAC was observed in 2010 and in subsequent years (2011, 2012, and 2014) exceeded its long-term mean by about 0.05. It levelled out in 2015 and increased again in 2016. In 2017–2018, the RAC salinity slightly decreased, and in 2019 dropped strongly and reached its minimum in the entire observation period (34.87). In 2020, salinity in the RAC was higher than in 2019, but still significantly below its long-term average.

In the EGC domain, temperature reached its peak in 2007 (1.9°C), decreased significantly to 0.3°C in 2008, and since has remained relatively stable (within 0.3°C of its long-term mean), with a slight decrease to 0.33°C in 2014 before returning to 1.0°C in 2015 ([Figure 4.83](#)). In 2020, the EGC temperature dropped to its decadal minimum (0.33°C), the same as observed in 2014. Salinity in the EGC was highest in 2007 (34.90), close to the earlier maximum of 34.89 in 1984. After 2007, the EGC salinity dropped below its long-term average except for an intermediate peak (34.87) in 2013. The EGC salinity reached the second lowest minimum value on record of 34.45 in 2000 and 2002 and was close to this value in 2008. In 2020, salinity in the EGC decreased significantly and reached the lowest value on record for the entire observation period (34.35; 2.3 s.d. below the long-term average).

## 5 Detailed area descriptions, part II: The intermediate and deep ocean

### Introduction

This section focuses on the deeper waters of the Nordic Seas and the North Atlantic, typically below 1000 m. The general circulation scheme and dominant water masses are given in [Figure 5.1](#).



**Figure 5.1.** Schematic circulation of the intermediate-to-deep waters in the Nordic Seas and North Atlantic.

At the northern boundary of the region of interest, the cold and dense outflow from the Arctic Ocean enters Fram Strait along its western side and reaches the Greenland Sea. The outflow is a mixture of Eurasian Basin and Canadian Basin deep waters and Upper Polar Deep Water (UPDW). The Eurasian Deep Water feeds the densest water of all Nordic Seas, the Greenland Sea Bottom Water. The Canadian Basin Deep Water and UPDW supply the Arctic Intermediate Water (AIW) in the Greenland Sea, and the UPDW also includes winter convection products. The deep southward outflow from the North Atlantic in the deep western boundary current is fed by the cold and dense overflow waters. The deepest and densest is the DSO. This water mass originates in the AIW produced in the Greenland and Iceland seas by winter convection

and mixing with surrounding water masses. The DSOW sinks to the bottom as it passes over the Denmark Strait sill, vigorously entraining ambient water. Downstream, it is overlain by LSW, an intermediate water mass formed by deep winter convection in the Labrador Sea. The middle layer of the deep, cold-water export in the deep western boundary current is supplied by the Iceland-Scotland Overflow Water (ISOW) that originates in water masses formed in the Norwegian Sea (AIW and Norwegian Sea Deep Water). Passing through the Iceland Basin, ISOW also entrains upper ocean water and LSW. The deep Antarctic Bottom Water enters the North Atlantic on the western side, but its signature is also present in eastern Atlantic abyssal basins. At intermediate levels, MW originates from vigorous mixing of Atlantic central waters and MOW at the Gulf of Cádiz. This water mass spreads at about 1000 m depth in all directions, with a main vein progressing northwards along the European margin. Around the Canaries, MW encounters the northern limit of AAIW.

## 5.1 Nordic Seas

The deep waters of the Greenland, Iceland, and Norwegian seas are all warming. The source of the warming is the deep outflow from the Arctic Ocean, a south-flowing current of the Eurasian and Canadian Basin Deep Waters and the UPDW found on the western side of Fram Strait at ca. 2000 m depth. The Greenland Sea Deep Water (GSDW) is warming fastest owing to its direct contact with this Arctic outflow, whereas the Iceland and Norwegian seas are warming more slowly because they are products of the mixing of their own ambient waters with GSDW and Arctic outflow water.

### 5.1.1 Greenland Sea

*A. Beszczynska-Möller, A.*

Continuous warming has been observed in the Greenland Sea deep layer at 3000 m, both in the Greenland Sea Gyre (not measured since 2011) and in the eastern part of the deep basin (at 005°E measured since 2001, [Figure 5.2](#)). GSDW temperature is similar at both locations, with a relatively steady increase of temperature from  $-1.18^{\circ}\text{C}$  to  $-0.876^{\circ}\text{C}$  observed between 1993 and 2020. In 2020, deep-water temperature exceeded its long-term average by  $0.142^{\circ}\text{C}$  (3.55 s.d.). The strongest temperature increase, of  $0.03^{\circ}\text{C}$ , was recorded between 2010 and 2011, while recent year-to-year temperature changes have been lower (between 0 and  $0.02^{\circ}\text{C}$ ). Between 2019 and 2020, the deep water in the eastern Greenland Sea warmed by  $0.008^{\circ}\text{C}$ . For the entire observation period (1993–2020), the average warming rate in the deep Greenland Sea can be estimated at  $0.11^{\circ}\text{C decade}^{-1}$ .

The warming of deep waters in the Greenland Sea has been accompanied by an increase in salinity, albeit its interannual variability differs between the central Greenland Sea Gyre (1993–2010 observation period) and the eastern Greenland Sea (measured since 2001). A relatively steady increase in salinity from 34.901 in 1993 to 34.916 in 2010 was observed in the Greenland Sea Gyre. In the eastern part of the deep Greenland Sea, the year-to-year changes are much stronger than in the central gyre, but the overall trend observed for 2001–2020 is positive and similar to that in the central basin. The salinity increase is of the order of  $0.01 \text{ decade}^{-1}$ . The maximum salinity of 34.920 was reached in 2020, while the second highest salinity (34.919) was recorded in the eastern Greenland Sea in 2015, 2017, and 2019. In the last decade, salinity in the deep layers of the eastern Greenland Sea remained above its long-term average (exceeding its long-term average by 1.83 s.d. in 2020).

After a period of cessation of deep convection, the doming structure in the Greenland Sea Gyre is being replaced by a two-layered water mass arrangement. During the measurement period 1993–2010, the winter convection depth varied between 700 and 1600 m and was only significantly deeper in small-scale convective eddies. In winter 2007/2008, the maximum convection depth was estimated to be 1700 m, deeper than the previous year (1200 m) and similar to the maxima observed during 2001/2002 and 2002/2003. Since then, the import of warm and saline AW to the Greenland Sea is not balanced by an import of cool and fresh Polar Water from the north. The GSDW formerly included a small admixture of surface freshwater through the convective process and, therefore, had a lower salinity than the Arctic outflow waters. The observed increase in GSDW salinity may be the result of an adjustment to the Arctic outflow in the continued absence of deep convection and an increased presence of AW in the upper layer.

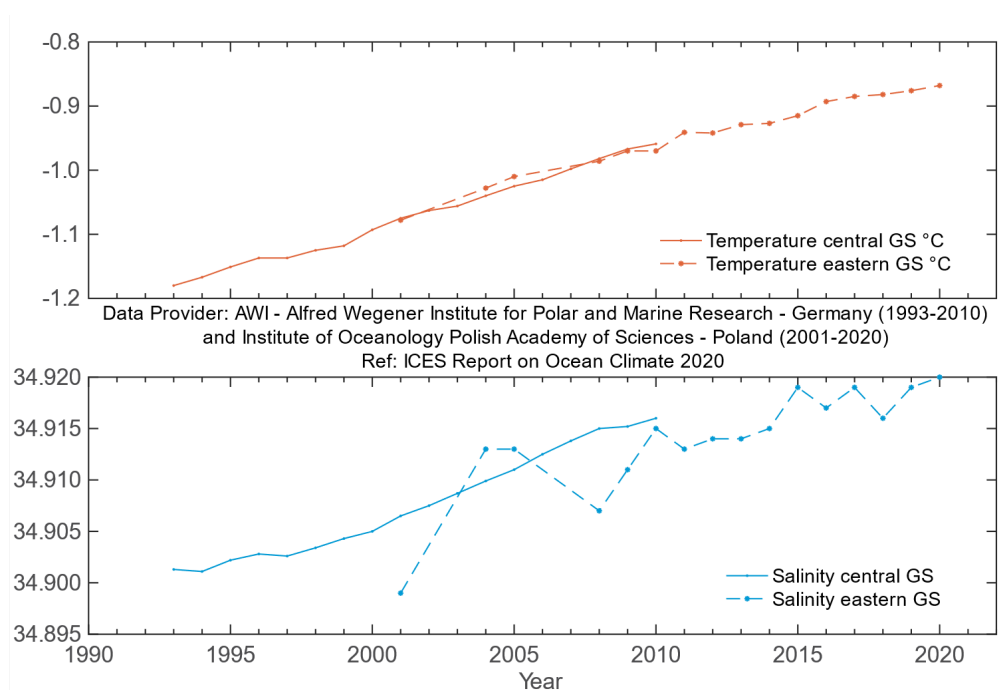


Figure 5.2. Greenland Sea and Fram Strait. Temperature (upper panel) and salinity (lower panel) at 3000 m in the Greenland Sea Section at 75°N. Solid line: central Greenland Sea Gyre; dashed line: eastern Greenland Sea at 005°E.

### 5.1.2 Norwegian Sea

#### *S. Østerhus*

The longest time-series in the Nordic Seas is from the Ocean Weather Ship station M in the Norwegian Sea. It reveals persistent warming since the mid-1980s (Figure 5.3). The warming trend for the period 1981–2010 was 0.06°C, while the trend in the last decade (2010–2020) has been slightly lower.

The weather ship station M was permanently occupied by weatherships from 1948 to 2009. During this period, temperature and salinity were measured weekly in the Norwegian Sea Deep Water (NSDW) by means of Nansen bottles equipped with reversing thermometers. Water samples were analysed for oxygen content onboard and for salinity concentration ashore after each cruise (cruise duration was normally one month). Since 2009, station M has been occupied

three to eight times per year, and temperature and salinity profiles have been measured by a CTD. The increased variation in temperature during the last decade is probably due to the smaller number of observations.

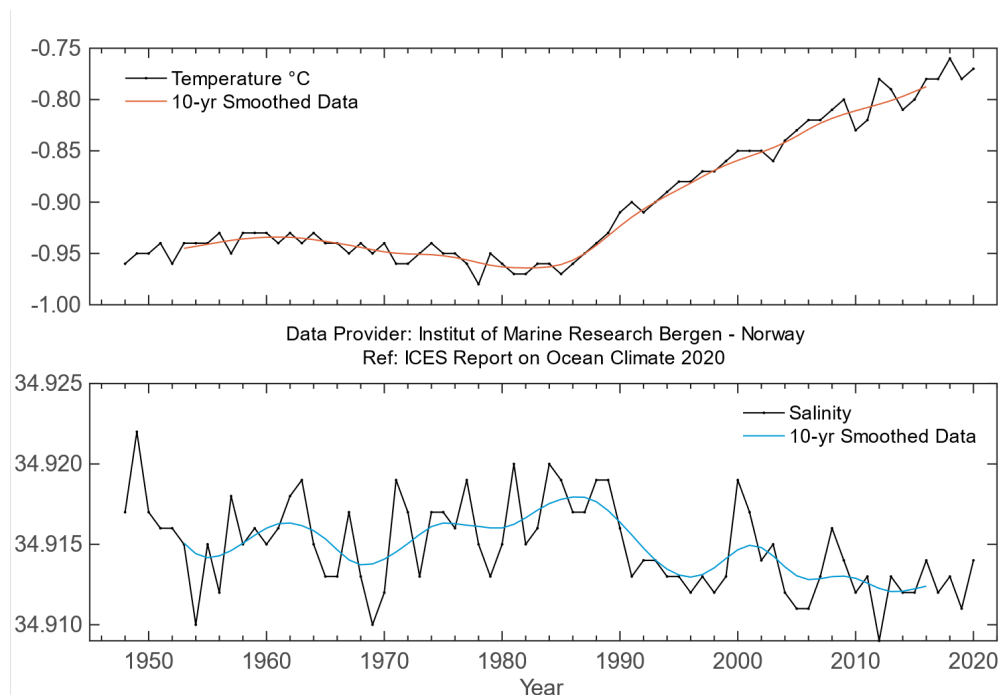
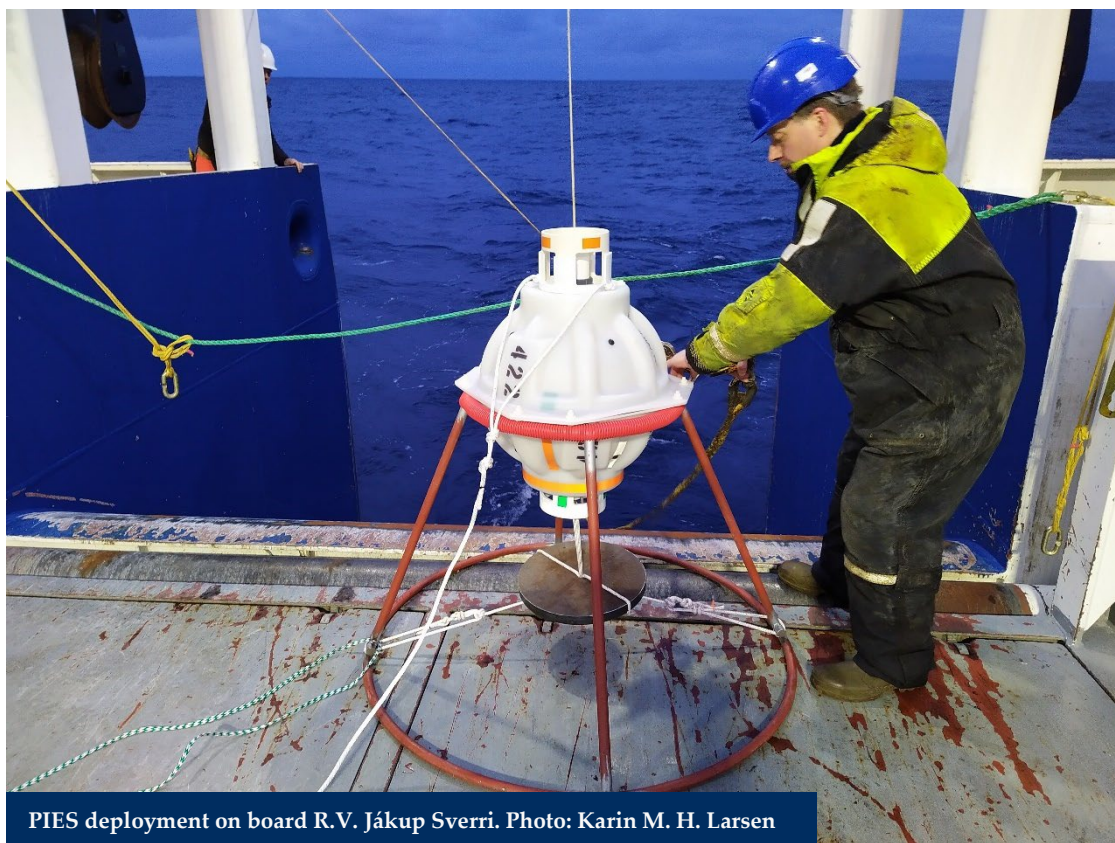


Figure 5.3. Norwegian Sea. Temperature (upper panel) and salinity (lower panel) at 2000 m at Ocean Weather station M (66°N 002°E).



### 5.1.3 Iceland Sea

*S. R. Ólafsdóttir and M. Danielsen*

In the Iceland Sea, an increase in temperature in the depth range 1500–1800 m has been observed almost continuously since the beginning of the time-series in the early 1990s and was still observed at the end of 2020 (Figure 5.4). Deep water in the eastern part of the Iceland Sea has warmed 0.2°C in 30 years, but a similar trend has not been observed for salinity.

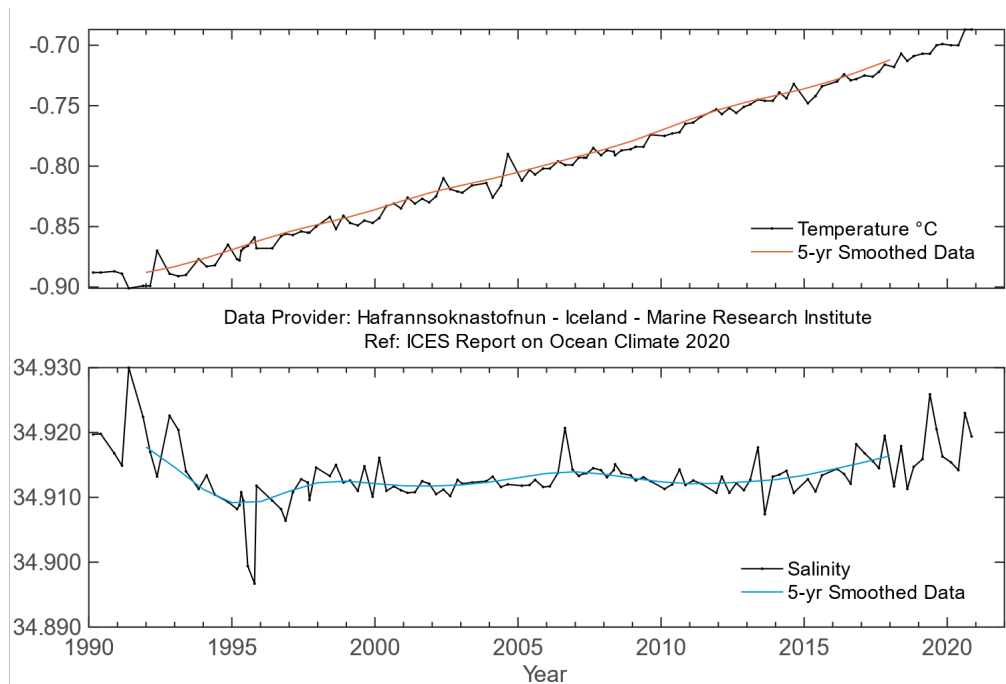


Figure 5.4. Icelandic waters. Temperature (upper panel) and salinity (lower panel) at 1500–1800 m in the Iceland Sea (68.00°N 012.67°W).

## 5.2 North Atlantic

### 5.2.1 Iceland-Scotland Ridge overflow waters

*B. Berx and J. Hindson*

In the deep layers of the Faroe-Shetland Channel, the properties at 800 m are the same as those of Norwegian Sea Deep Water as it passes through the Channel back into the North Atlantic.

Due to measurement record being defined by depth coordinates, rather than following the properties of a specific water mass, the time-series does show some variability. In general, the temperature of the deep water decreased from the 1950s to the 1990s (Figure 5.5), followed by a period of fluctuations, with both increasing and decreasing temperatures, until about 2000. Since then, there has been a warming trend, which continues in 2020, and temperatures are now close to the highest temperatures observed in the early 1980s. Salinity was relatively stable in the first period of measurements (1950 to mid-1970s), followed by a slow decline until reaching the lowest annual mean salinity on record in 1997. Since then, there has been a slow but gradual increase in salinity (Figure 5.5), which continued in 2020.

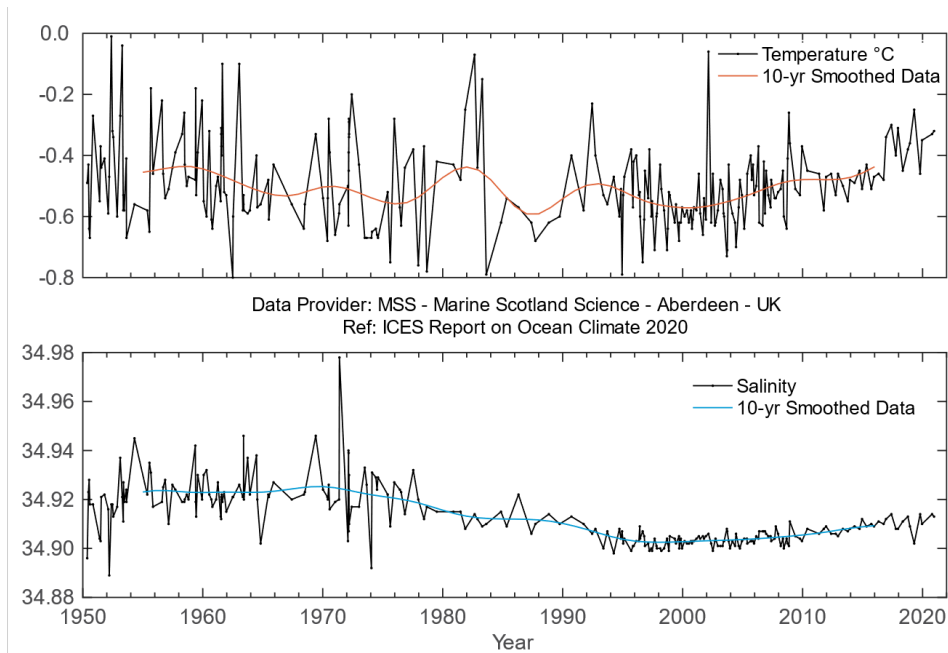


Figure 5.5. Faroe-Shetland Channel. Temperature (upper panel) and salinity (lower panel) at 800 m.



### 5.2.2 Iceland Basin

*S. Jones and N. P. Holliday*

In the Iceland Basin, LSW is the dominant water mass below about 1000 m, evident as a large recirculating body of relatively fresh and low stratified water with a core that lies between 1700 and 2000 m (Holliday *et al.*, 2015). After the Norwegian Sea Deep Water flows through the Faroe-Shetland Channel and Faroe Bank Channel and into the Iceland Basin, it becomes known as ISOW (Figure 5.1). The dense water, supplemented by a small amount of additional flow over the sill between Iceland and the Faroes, mixes rapidly with the upper ocean and intermediate water of the Iceland Basin, entraining the lighter water and increasing the volume of the overflow plume. Therefore, the properties of the ISOW measured at 20°W in the Iceland Basin are a product of the properties of the dense water at the sill and the entrained ambient water.

ISOW temperature and salinity vary closely with the LSW and upper ocean water in the Iceland Basin. Temperature and salinity increased between 1996 and 2011 and then gradually decreased

between 2011 and 2017. The Ellett Line transect has not been occupied since 2017, and Argo floats do not adequately sample the deepest waters in Iceland Basin, so no observations were possible for the deep-water time-series in 2020 (Figure 5.7). For the intermediate water time-series, however, observations from Argo floats show that temperature and salinity have remained near average for the past five years, with no evidence of the deep freshening or the partial recovery observed in the upper waters (Figure 5.6).

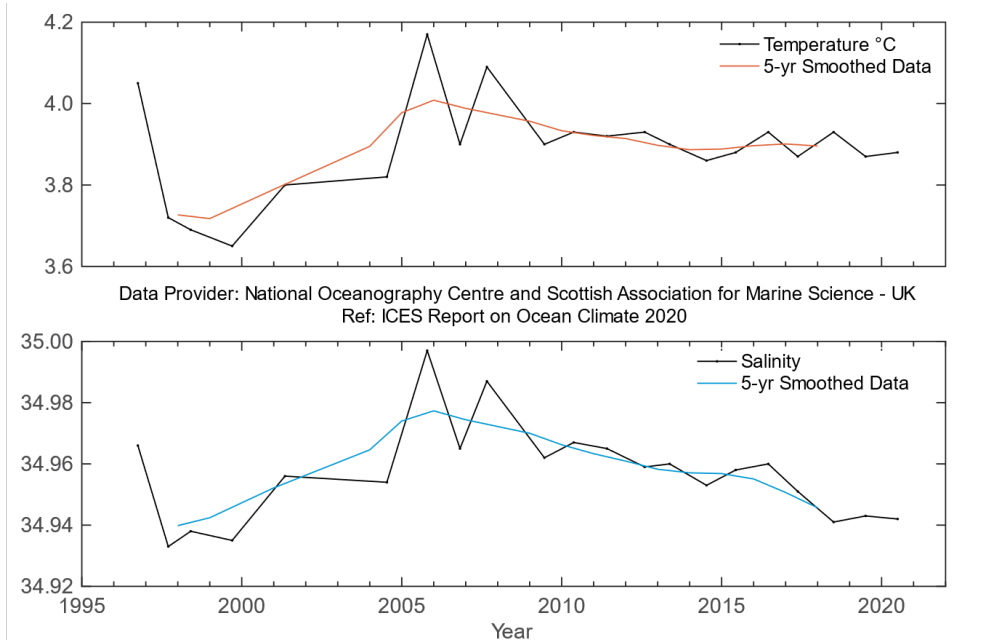


Figure 5.6. Iceland Basin. Temperature (upper panel) and salinity (lower panel) of Labrador Sea Water ( $27.70 \leq \sigma_{\theta} \leq 27.85 \text{ kg m}^{-3}$ , approx. 1200–2000 m).

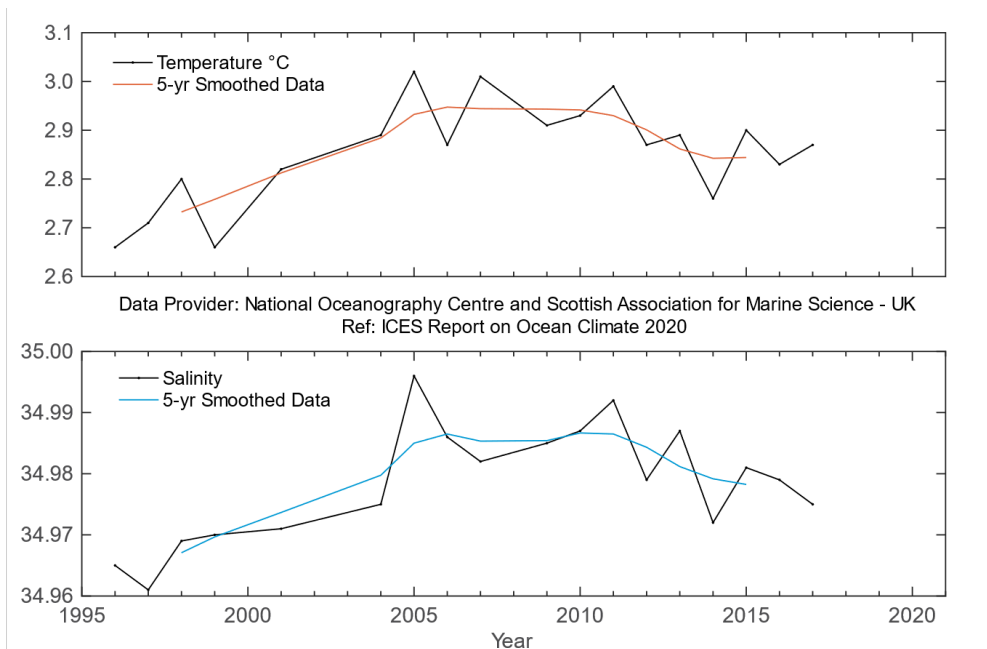
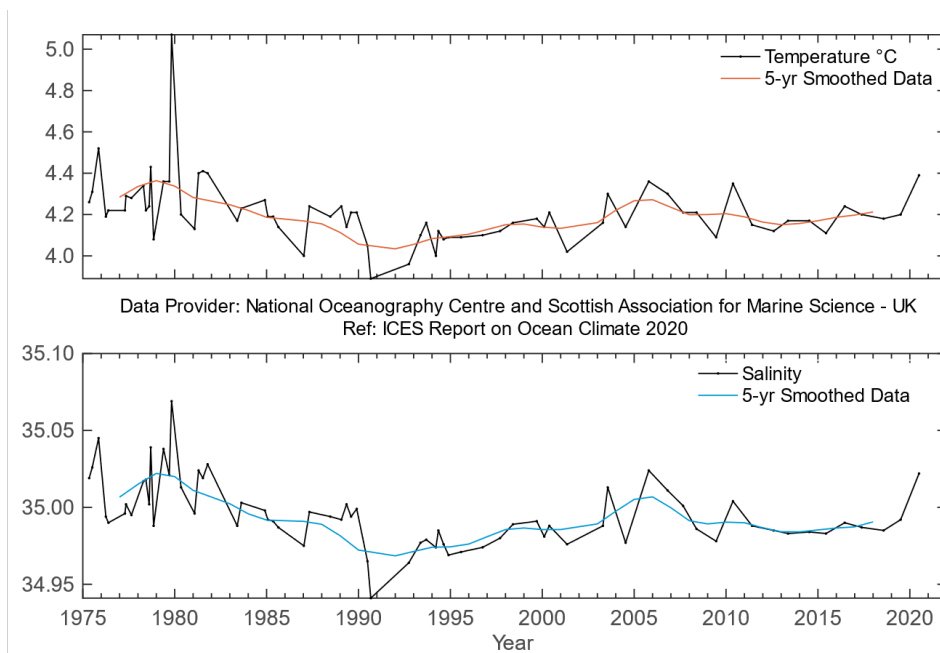


Figure 5.7. Iceland Basin. Temperature (upper panel) and salinity (lower panel) of Iceland-Scotland Overflow Water ( $\sigma_{\theta} > 27.85 \text{ kg m}^{-3}$ , approx. 2000–2600 m). Data until 2017.

### 5.2.3 Rockall Trough

*S. Jones and N. P. Holliday*

In Rockall Trough, LSW is the dominant water mass below about 1500 m and usually has its maximum concentration between 1700 and 2000 m. East of the Anton Dohrn seamount, this peak tends to be characterized by a minimum in salinity and potential vorticity, although its patchy temporal distribution (possibly due to aliasing of mesoscale eddies) results in a noisy year-on-year signal. Over the time-series, there are no significant trends in temperature and salinity (Figure 5.8). From 1975 to the mid-1990s, there was a cooling and freshening trend, which was followed by gradual warming and increasing salinity. In 2020, an increase was observed in the LSW potential temperature and salinity derived from Argo observations, but the OSNAP mooring time-series did not register any significant change.



**Figure 5.8. Rockall Trough. Temperature (upper panel) and salinity (lower panel) of Labrador Sea Water ( $27.70 \leq \sigma_{\theta} \leq 27.85 \text{ kg m}^{-3}$ , approx. 1500–2000 m).**

### 5.2.4 Irminger Basin

*M. F. de Jong*

A cold and low-salinity core was observed between 1600 and 2000 m in the central Irminger Sea during the early 1990s. This was the result of the presence of deep LSW formed in the Labrador Sea in the period 1988–1995 combined with local deep convection. Since summer 1996, this LSW core has generally been increasing in temperature and salinity as it mixes with surrounding water masses. Within the overall increasing temperature trend, there were slight temperature drops, after winters with deep convection in Irminger Sea, in 2009, 2013, and 2014. The maximum temperature on record was observed in 2018 (nearly  $0.33^{\circ}\text{C}$  above the long-term mean), and it remained high in 2020 ( $0.29^{\circ}\text{C}$  above the long-term mean). Salinity, reached a maximum in 2014 after which it levelled off. This remained the case in 2020, with salinity values  $0.038$  above the long-term mean (Figure 5.9).

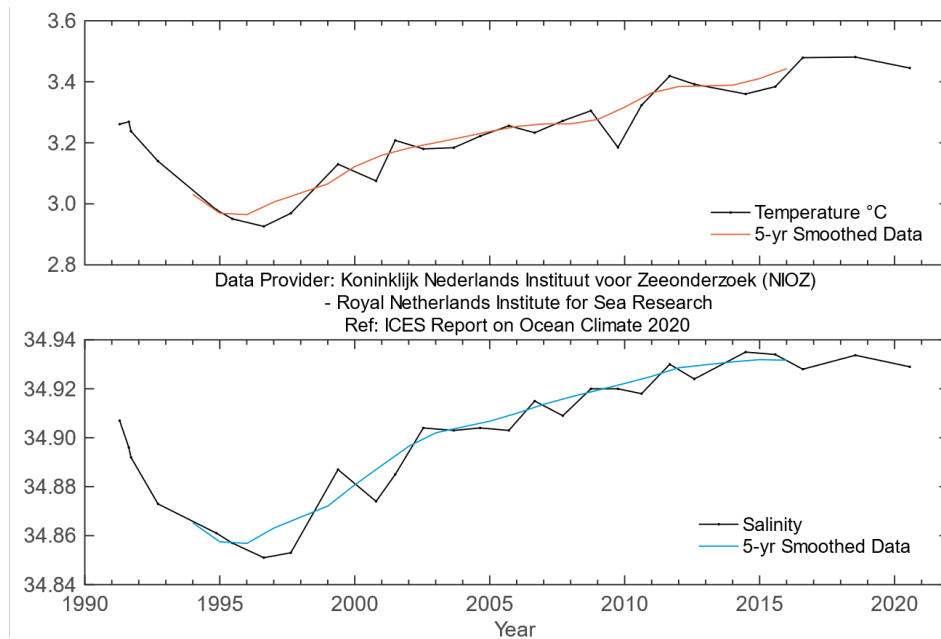


Figure 5.9. Irminger Sea. Temperature (upper panel) and salinity (lower panel) of Labrador Sea water (averaged over 1600–2000 m).



## 5.2.5 Labrador Basin

*I. Yashayaev and B. Cisewski*

In the Labrador Sea, the 1000–1800 m depth layer average temperature and salinity decreased between the beginning of the 1970s and the early 1990s by about 0.9°C and 0.09, respectively. In 2011, less than two decades after reaching its record minimum, temperature was as high as in 1970, when its previous maximum was observed, and salinity was the highest since 1971. These trends were interrupted in winter 2012 by strong convection, resulting in cooling of the deep intermediate layer (1000–1800 m). The deep intermediate layer temperature continued to decrease during five subsequent years, 2013–2017, and has stabilized over the past three years, 2018–2020. A freshening trend accompanied the recent cooling of the deep intermediate layer, but ended a year earlier than the latter, in 2016. The 1000–1800 m depth layer average salinity then slightly increased between 2016 and 2017/2018 and over the past two years, 2019/2020, decreased again (Figure 5.10).

The properties of the North Atlantic Deep Waters (NADW) in the deep boundary current west of Greenland are monitored at 2000 m depth at Cape Desolation station 3 (Figure 5.11). Since

the beginning of the 1990s, both temperature and salinity initially showed a decreasing trend, until they reached minimum values in 1998 and 1997, respectively. After that, NADW temperature showed a positive trend until 2019, whereas salinity remained constant between 2007 and 2019. In autumn 2020, measurements at the Cape Desolation section could not be conducted due to time constraints.

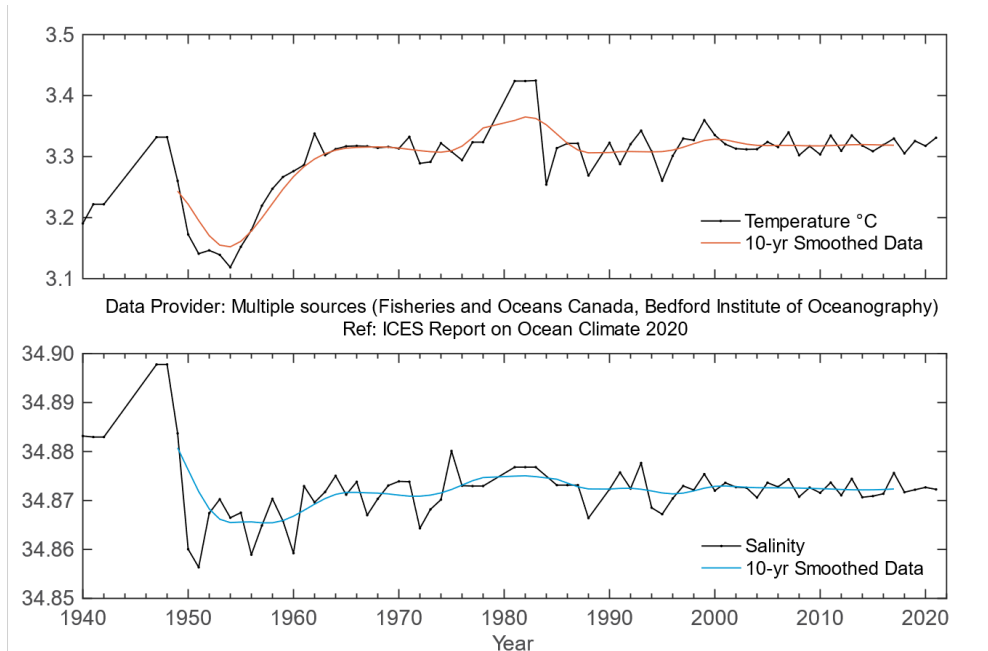


**Figure 5.10. Labrador Sea. Temperature (upper panel) and salinity (lower panel) anomalies in the deep intermediate layer of the Labrador Sea. Vertical profile data were averaged over 1000–1800 m and then over calendar years.**

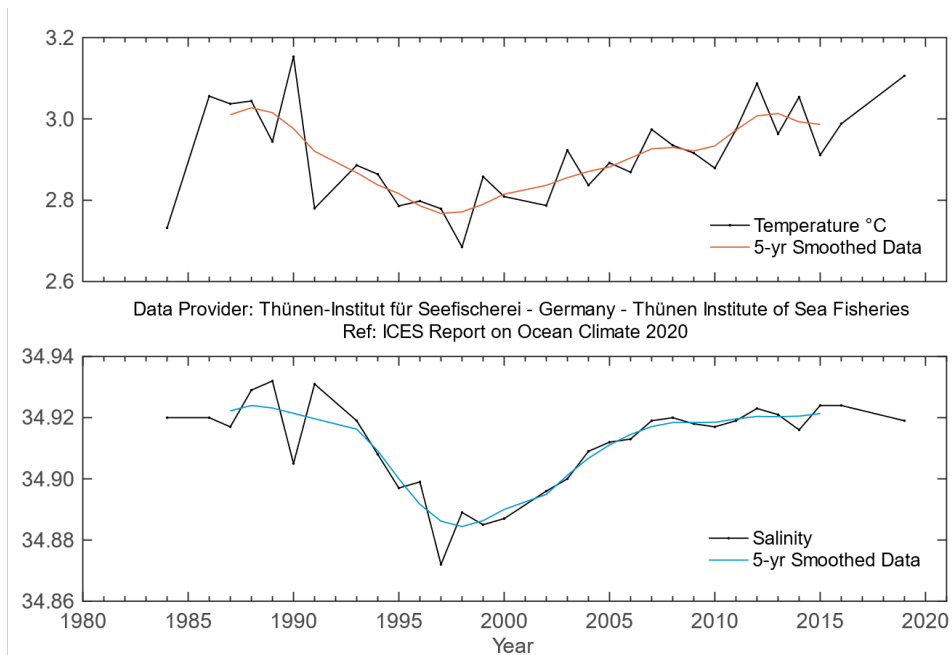


**Figure 5.11. West Greenland. Temperature (upper panel) and salinity (lower panel) at 2000 m water depth at Cape Desolation station 3 (60.47°N 050.00°W). Data until 2019.**

## 5.2.6 West Iberian margin

C. González-Pola

The entire water column down to 1000 m (core MW) has been sampled at the outer slope stations in Santander (Figure 4.36) on a monthly basis since the early 1990s (González-Pola *et al.*, 2005). Warming during two decades until the mid-2010s is evident at most layers, corresponding to the ENACW (300–600 m (Figure 5.12) and upper MW (600–1000 m; Figure 5.13).

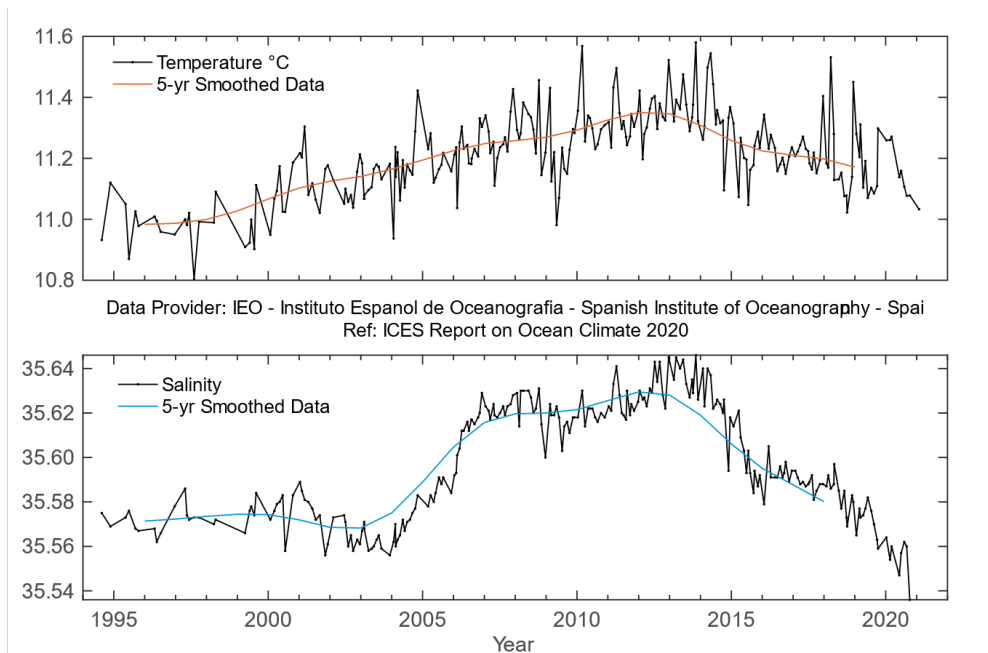


**Figure 5.12. Bay of Biscay. Potential temperature (upper panel) and salinity (lower panel) for the 300–600 m layer at Santander station 7.**

The evolution of the water masses has been strongly influenced by a significant shift in the salinity of the lower ENACW (ca. 400 m) in 2005, after the occurrence of very strong winter mixing (Somavilla *et al.*, 2009). In 2014, the upper central waters showed freshening and cooling for the first time in about a decade. The initial large drop was followed by a two-year stabilization (2016/2017) before continuing dropping from 2018 onwards. In 2020, salinity above 400 m was below the overall long-term record, while temperature returned to early 2000s values. Deeper water masses (at the level of the MW, ca. 1000 m) followed the weak freshening trend observed since the salinity maximum reached in 2007–2009.

Since 2003, a programme designed to supplement the monthly monitoring of the upper ocean in the area has monitored waters deeper than 1000 m and the full water column (> 5500 m) at the western Iberian margin deep (Prieto *et al.*, 2015). Cruises were carried out semi-annually during 2003–2010 and annually after that. The Finisterre section, measuring roughly 400 km in length, starts west of the Iberian Peninsula (43.0°N 9.3°W) and reaches the centre of the Iberian Abyssal Plain (43.0°N 15.5°W).

The Finisterre section provides information about upper, intermediate, and deep waters. The limit of the intermediate waters is considered to be near 2000 m depth, where the core of LSW and the base of the permanent thermocline are typically centred. From the MW core to the LSW

core, there is a strong gradient and some coherence in variability, indicating the influence of large-scale atmospheric patterns. After nearly two decades of measurements, a striking 3–4-year see-saw pattern is becoming evident both in temperature and salinity, imposed over a background decreasing trend (Figure 5.14).

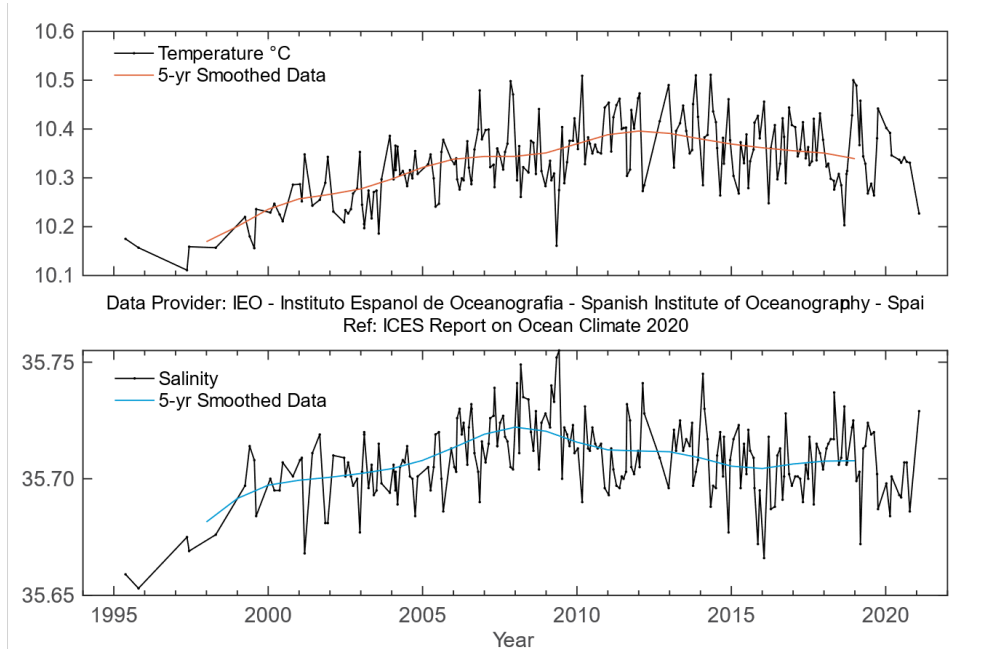


Figure 5.13. Bay of Biscay. Potential temperature (upper panel) and salinity (lower panel) for the 600–1000 m layer at Santander station 7.

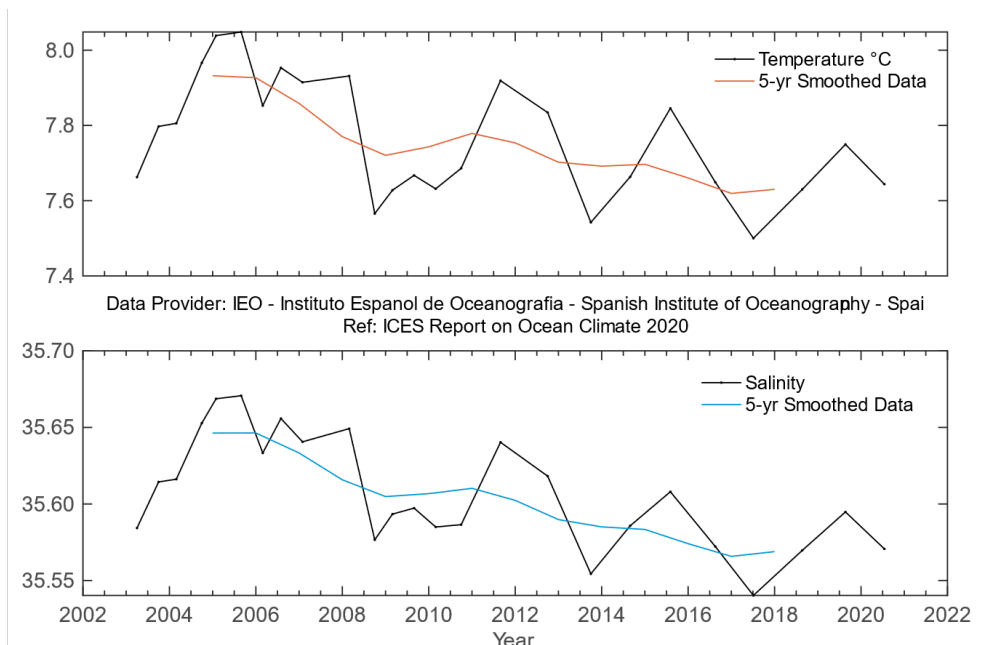
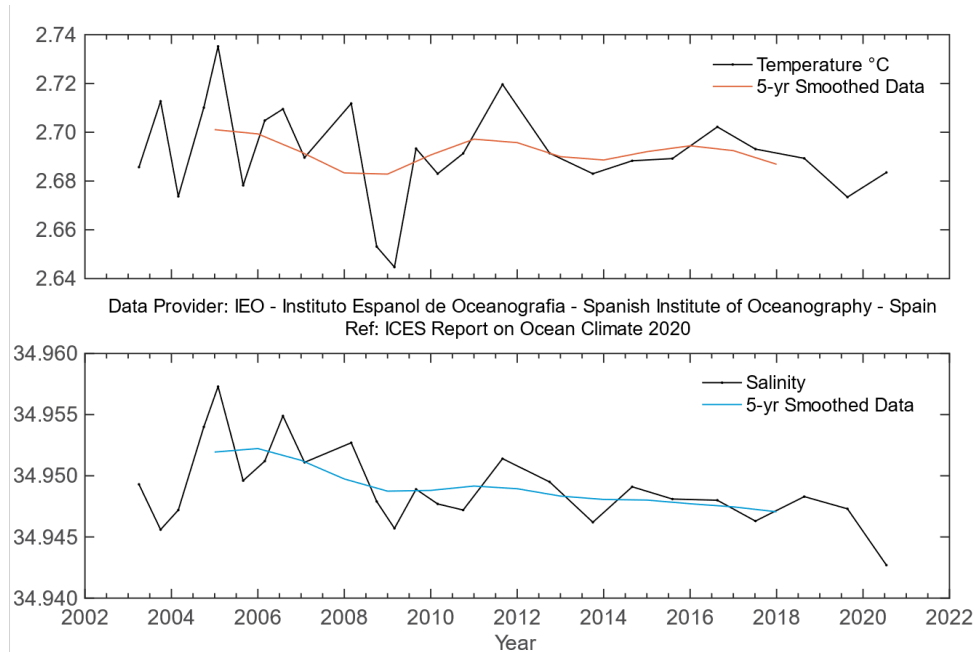


Figure 5.14. Western Iberian margin. Potential temperature (upper panel) and salinity (lower panel) for the 800–2000 m layer averaged across the Finisterre section.

The abyssal waters in this basin are NADW (composed of a mixture of all Arctic water masses) and what is known as Lower Deep Water, which reflects a signature of Antarctic-origin waters. Interannual variability for these abyssal waters within the monitored period has been weak ( $< 0.1^{\circ}\text{C}$  and 0.01 in salinity). A weak, but progressive, pattern of cooling and freshening has begun to emerge recently around 2000 to 3000 m. As a whole, temperature and salinity in the water layers between 2000 m and the bottom remain close to long-term mean values (Figure 5.15).



**Figure 5.15. Western Iberian margin. Potential temperature (upper panel) and salinity (lower panel) for the 2000–5500 m layer averaged across the Finisterre section.**



### 5.2.7 Gulf of Cadiz

*R. Sánchez-Leal*

The outer stations in the STOCA sections ([Figure 4.39](#)) sample the ENACW (100–300 m; [Figure 5.16](#)) and the Mediterranean Overflow Water (MOW, 300-m bottom; [Figure 5.17](#)).

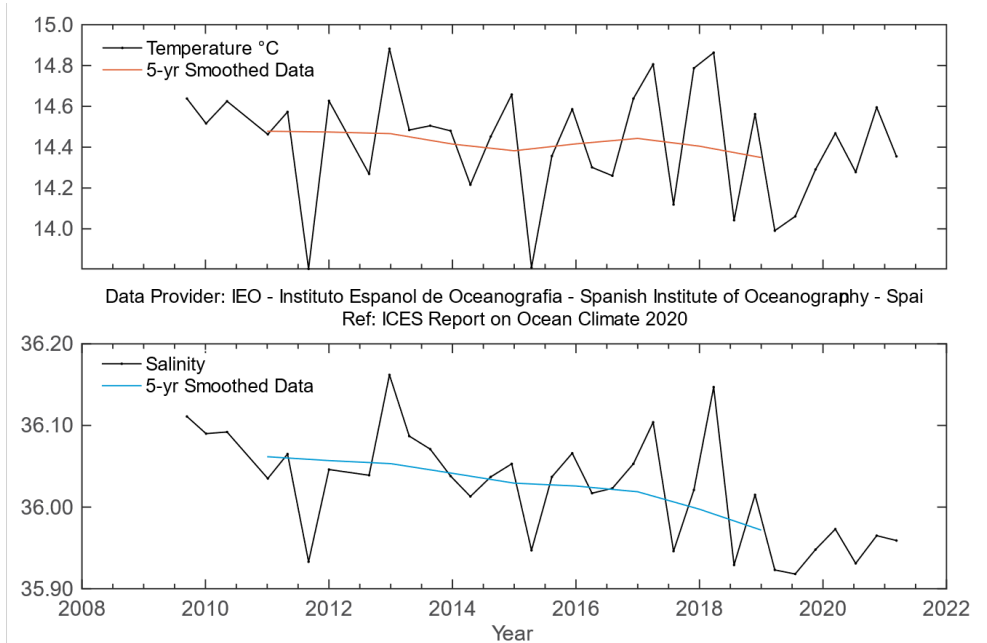


**Figure 5.16. Gulf of Cadiz. Potential temperature (upper panel) and salinity (lower panel) for the 100–300 m layer at STOCA SP6.**

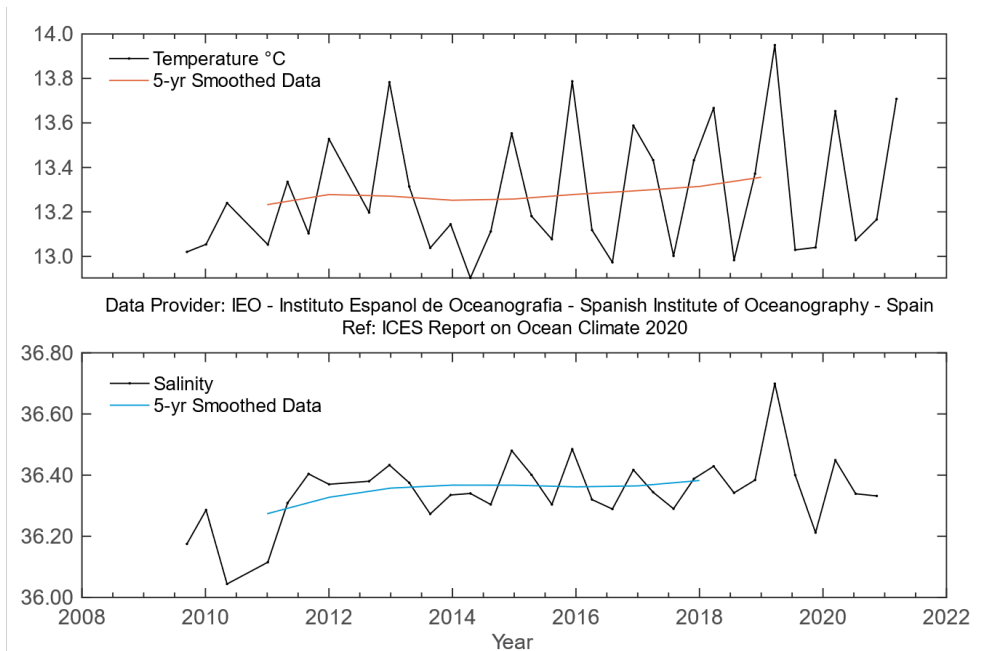


**Figure 5.17. Gulf of Cadiz. Potential temperature (upper panel) and salinity (lower panel) for the 300–600 m layer at STOCA SP6.**

The ENACW layer has been showing a statistically significant freshening trend since 2009 ( $-0.15 \text{ decade}^{-1}$ ). This freshening coincides with a non-statistically significant cooling trend ( $-0.31^\circ\text{C decade}^{-1}$ ). These trends have been sustained through time and were reinforced in 2020, when cooler- and fresher-than-average conditions prevailed.

The depth level occupied by the MOW (350–550 m) has been showing an opposing trend for salinity, with a statistically significant increase from 2009 to 2020 ( $0.13 \text{ decade}^{-1}$ ), peaking at about 400 m ( $0.2 \text{ decade}^{-1}$ ).

## 5.2.8 Canary Basin

*P. Vélez-Belchí*

As a unique observation in 2020 in the oceanic water stratum corresponding to intermediate waters (800–1400 m), a MW eddy (referred to as Meddie) was sampled. Therefore, the values measured for 2020 are not representative of the mean intermediate waters (Figure 5.18). Overall, since the 1990s, weak cooling and decreasing salinity trends have been observed. In the CTZ, the intermediate waters are dominated by the AAIW and show low, non-statistically significant increases in temperature ( $0.07 \pm 0.14^\circ\text{C decade}^{-1}$ ) and salinity ( $0.004 \pm 0.033^\circ\text{C decade}^{-1}$ ).

Both time-series show high variability due to the two very different intermediate water masses present in the region, i.e. the MW and the AAIW.

In the layer corresponding to the upper NADW (1700–2600 m), there is a long-term weak warming trend and a decrease in salinity that is not statistically significantly different from zero. However, in the stratum corresponding to the NADW (2600–3600 m), a marginally statistically significant freshening ( $-0.002 \pm 0.001 \text{ decade}^{-1}$ ) has been observed, consistent with the observation in the upper NADW, but no trend can be statistically confirmed for temperature ( $-0.005 \pm 0.01^\circ\text{C decade}^{-1}$ ; Figure 5.19).

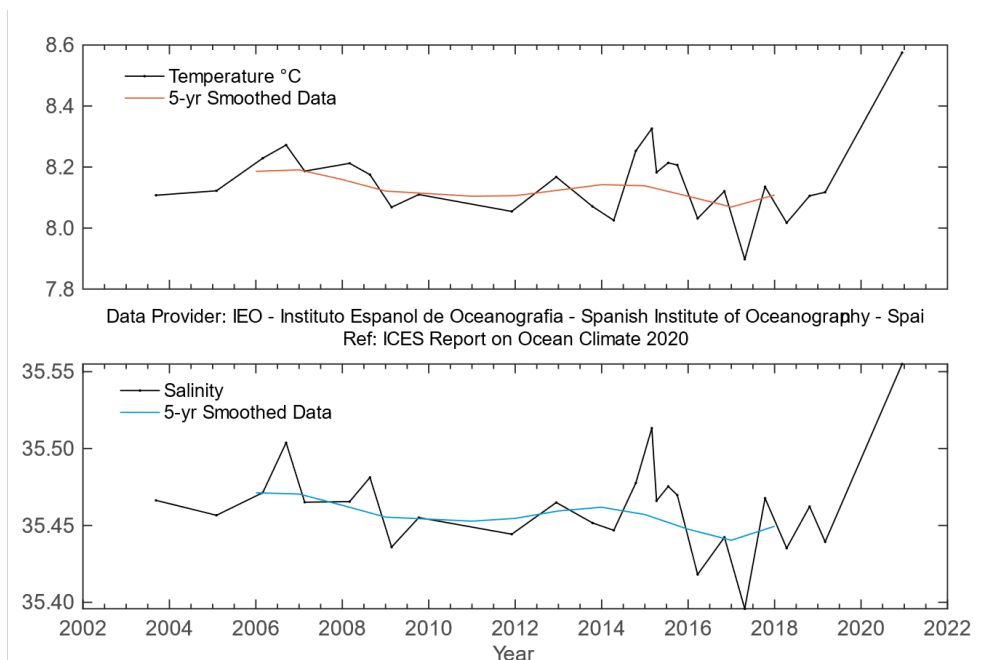
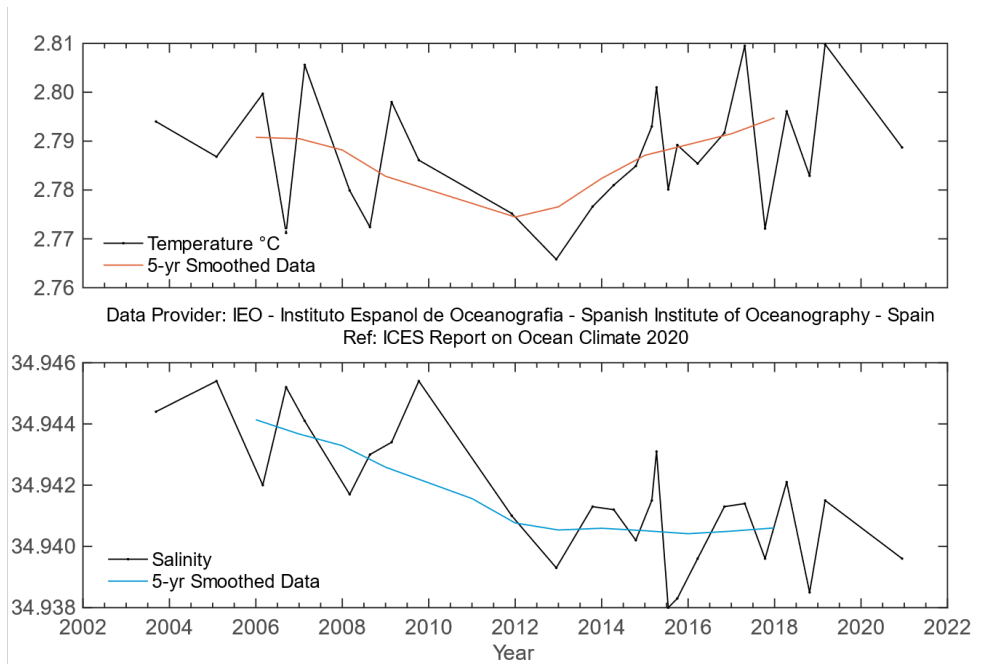


Figure 5.18. Canary Basin. Potential temperature (upper panel) and salinity (lower panel) for the 800–1400 m layer.



**Figure 5.19. Canary Basin. Potential temperature (upper panel) and salinity (lower panel) for the 2600–3600 m layer averaged across the Canaries section.**

## References

- Buckley, M. W., and Marshall, J. 2016. Observations, inferences, and mechanisms of the Atlantic Meridional Overturning Circulation: A review. *Reviews of Geophysics*, 54: 5–63. <https://doi.org/10.1002/2015RG000493>
- Cappelen, J. 2021. Greenland-DMI historical climate data collection 1784–2020, DMI Technical Report 21–04.
- de Boyer Montégut, C., Madec, G., Fischer, A. S., Lazar, A., and Iudicone, D. 2004. Mixed layer depth over the global ocean: An examination of profile data and a profile-based climatology. *Journal of Geophysical Research: Oceans*, 109 (C12). <https://doi.org/10.1029/2004JC002378>
- Delworth, T. L., Zeng, F., Vecchi, G. A., Yang, X., Zhang, L., and Zhang R. 2016. The North Atlantic Oscillation as a driver of rapid climate change in the Northern Hemisphere. *Nature Geoscience*, 9: 509–512. <https://doi.org/10.1038/ngeo2738>
- Duchez, A., Frajka-Williams, E., Josey, S. A., Evans, D. G., Grist, J. P., Marsh, R., McCarthy, G. D., *et al.* 2016. Drivers of exceptionally cold North Atlantic Ocean temperatures and their link to the 2015 European heat wave. *Environmental Research Letters*. 11 (7): 074004. <https://doi.org/10.1088/1748-9326/11/7/074004>
- Dunstone, N., Smith, D., Scaife, A., Hermanson, L., Eade, R., Robinson, N., Andrews, M., *et al.* 2016. Skilful predictions of the winter North Atlantic Oscillation one year ahead. *Nature Geoscience*, 9 (11): 809–814. <https://doi.org/10.1038/ngeo2824>
- Gaillard, F., Reynaud, T., Thierry, V., Kolodziejczyk, N., and von Schuckmann, K. 2016. *In situ*-based reanalysis of the global ocean temperature and salinity with ISAS: variability of the heat content and steric height. *Journal of Climate*. 29 (4): 1305–1323. <https://doi.org/10.1175/jcli-d-15-0028.1>
- González-Pola, C., Fratantoni, P., Larsen, K. M. H., Holliday, N.P., Dye, S., Mork, K.A., Beszczynska-Möller, A., *et al.* 2019. The ICES Working Group on Oceanic Hydrography: A bridge from *in-situ* sampling to the remote autonomous observation era. *Frontiers in Marine Science*, 6: 103. <https://doi.org/10.3389/fmars.2019.00103>
- González-Pola, C., Larsen, K. M. H., Fratantoni, P., and Beszczynska-Möller, A. (Eds.). 2020. ICES Report on Ocean Climate 2019. ICES Cooperative Research Reports, Vol. 350. 136 pp. <https://doi.org/10.17895/ices.pub.7537>
- González-Pola, C., Lavín, A., and Vargas-Yáñez, M. 2005. Intense warming and salinity modification of intermediate water masses in the southeastern corner of the Bay of Biscay for the period 1992–2003. *Journal of Geophysical Research*. 110: C05020. <https://doi.org/10.1029/2004JC002367>
- Häkkinen, S., and Rhines, P. B. 2004. Decline of subpolar North Atlantic circulation during the 1990s. *Science*, 304 (5670): 555–559. <https://doi.org/10.1126/science.1094917>
- Hátún, H., Azetsu-Scott, K., Somavilla, R., Rey, F., Johnson, C., Mathis, M., Mikolajewicz, U., *et al.* 2017. The subpolar gyre regulates silicate concentrations in the North Atlantic. *Scientific Reports*, 7: 14576. <https://doi.org/10.1038/s41598-017-14837-4>
- Hátún, H., and Chafik, L. 2018. On the recent ambiguity of the North Atlantic Subpolar Gyre Index. *Journal of Geophysical Research: Oceans*, 123 (8): 5072–5076. <https://doi.org/10.1029/2018JC014101>
- Hátún, H., Lohmann, K., Matei, D., Jungclaus, J. H., Pacariz, S., Bersch, M., Gislason, A., *et al.* 2016. An inflated subpolar gyre blows life toward the northeastern Atlantic. *Progress in Oceanography*, 147: 49–66. <https://doi.org/10.1016/j.pocean.2016.07.009>
- Hátún, H., Payne, M., Beaugrand, G., Reid, P., Sandø, A., Drange, H., Hansen, B., *et al.* 2009. Large biogeographical shifts in the north-eastern Atlantic Ocean: From the subpolar gyre, via plankton, to blue whiting and pilot whales. *Progress in Oceanography*, 80 (3): 149–162. <https://doi.org/10.1016/j.pocean.2009.03.001>

- Hátún, H., Sandø, A. B., Drange, H., Hansen, B., and Valdimarsson H. 2005. Influence of the Atlantic Subpolar Gyre on the Thermohaline Circulation. *Science*, 309 (5742): 1841–1844. <https://doi.org/10.1126/science.1114777>
- Hernández-Guerra, A., Espino-Falcón, E., Vélez-Belchí, P., Pérez-Hernández, M. D., Martínez- Marrero, A., and Cana, L. 2017. Recirculation of the Canary Current in fall 2014. *Journal of Marine Systems*, 174: 25–39. <https://doi.org/10.1016/j.jmarsys.2017.04.002>
- Holliday, N. P., Bersch, M., Berx, B., Chafik, L., Cunningham, S., Florindo-López, C., Hátún, H., *et al.* 2020. Ocean circulation causes the largest freshening event for 120 years in eastern subpolar North Atlantic. *Nature Communications*, 11 (1): 585. <https://doi.org/10.1038/s41467-020-14474-y>
- Holliday, N. P., Cunningham, S. A., Johnson, C., Gary, S. F., Griffiths, C., Read, J. F., and Sherwin, T. 2015. Multidecadal variability of potential temperature, salinity, and transport in the eastern subpolar North Atlantic. *Journal of Geophysical Research: Oceans*, 120: 5945–5967. <https://doi.org/10.1002/2015jc010762>
- Houpert, L., Cunningham, S., Fraser, N., Johnson, C., Holliday, N. P., Jones, S., Moat, B., and Rayner, D. 2020. Observed variability of the North Atlantic Current in the Rockall Trough from 4 years of mooring measurements. *Journal of Geophysical Research: Oceans*, 125 (10): 18. <https://doi.org/10.1029/2020JC016403>
- Hurrell, J. W., and Deser, C. 2010. North Atlantic climate variability: the role of the North Atlantic Oscillation. *Journal of Marine Systems*, 79: 231–244. <https://doi.org/10.1016/j.jmarsys.2009.11.002>
- Hurrell, J. W., Kushnir, Y., Ottersen, G., and Visbeck M. 2003. An overview of the North Atlantic oscillation. *In* The North Atlantic Oscillation: Climatic Significance and Environmental Impact Ed. by J. W. Hurrell, Y. Kushnir, G. Ottersen, and M. Visbeck. Wiley Online Library. <https://doi.org/10.1029/134GM01>
- Hurrell, J., and National Center for Atmospheric Research Staff (Eds). 2017. Climate Data Guide: Hurrell North Atlantic Oscillation (NAO) Index (station-based). <https://climatedataguide.ucar.edu/climate-data/hurrell-north-atlantic-oscillation-nao-index-station-based> Last accessed 4 July 2022.
- Josey, S. A., Hirschi, J. J.-M., Sinha, B., Duchez, A., Grist, J. P., and Marsh, R. 2018. The recent Atlantic cold anomaly: Causes, consequences, and related phenomena. *Annual Review of Marine Science*, 10 (1): 475–501. <https://doi.org/10.1146/annurev-marine-121916-063102>
- Kalnay, E., Kanamitsu, M., Kistler, R., Collins, W., Deaven, D., Gandin, L., Iredell, M., *et al.* 1996. The NCEP/NCAR 40-Year Reanalysis Project. *Bulletin of the American Meteorological Society*, 77: 437–471. [https://doi.org/10.1175/1520-0477\(1996\)077<0437:TNYRP>2.0.CO;2](https://doi.org/10.1175/1520-0477(1996)077<0437:TNYRP>2.0.CO;2)
- Kolodziejczyk, N., Prigent-Mazella, A., and Gaillard, F. 2017. ISAS-15 temperature and salinity gridded fields. SEANOE. <https://doi.org/10.17882/52367>
- Moffa-Sánchez, P., and Hall, I. R. 2017. North Atlantic variability and its links to European climate over the last 3000 years. *Nature Communications*, 8: 1726. <https://doi.org/10.1038/s41467-017-01884-8>
- National Center for Atmospheric Research Staff (Eds.). 2021. The climate data guide: Hurrell North Atlantic Oscillation (NAO) Index (PC-based). <https://climatedataguide.ucar.edu/climate-data/hurrell-north-atlantic-oscillation-nao-index-pc-based> Last accessed 4 July 2022.
- Paillet, J., and Mercier, H. 1997. An inverse model of the eastern North Atlantic general circulation and thermocline ventilation, Deep Sea Research Part I: Oceanographic Research Papers, 44 (8): 1293–1328. [https://doi.org/10.1016/s0967-0637\(97\)00019-8](https://doi.org/10.1016/s0967-0637(97)00019-8)
- Pingree, R. D. 1993. Flow of surface waters to the west of the British Isles and in the Bay of Biscay. Deep Sea Research Part II: Topical Studies in Oceanography, 40 (1–2): 369–388. [https://doi.org/10.1016/0967-0645\(93\)90022-f](https://doi.org/10.1016/0967-0645(93)90022-f)

- Pingree, R. D., and Le Cann, B. 1990. Structure, strength and seasonality of the slope currents in the Bay of Biscay region. *Journal of the Marine Biological Association of the UK*, 70(4): 857–885. <https://doi.10.1017/S0025315400059117>
- Prieto, E., González-Pola, C., Lavín, A., and Holliday, N. P. 2015. Interannual variability of the northwestern Iberia deep ocean: Response to large-scale North Atlantic forcing. *Journal of Geophysical Research: Oceans*, 120: 832–847. <https://doi.org/10.1002/2014jc010436>
- Robson, J., Sutton, R., Lohmann, K., Smith, D., and Palmer, M. 2012. Causes of the rapid warming of the North Atlantic Ocean in the mid-1990s. *Journal of Climate*, 25: 4116–4134. <https://10.1175/JCLI-D-11-00443.1>
- Scaife, A. A., Arribas, A., Blockley, E., Brookshaw, A., Clark, R. T., Dunstone, N. Eade, R., *et al.* 2014. Skillful long-range prediction of European and North American winters. *Geophysical Research Letters*, 41: 2514–2519. <https://doi.org/10.1002/2014gl059637>
- Scaife, A. A., Karpechko, A. Y., Baldwin, M. P., Brookshaw, A., Butler, A. H., Eade, R., Gordon, M., *et al.* 2015. Seasonal winter forecasts and the stratosphere. *Atmospheric Science Letters*, 17: 51–56. <https://doi.org/10.1002/asl.598>
- Somavilla, R., Gonzalez-Pola, C., Rodriguez, C., Josey, S. A., Sanchez, R. F., and Lavin, A. 2009. Large changes in the hydrographic structure of the Bay of Biscay after the extreme mixing of winter 2005. *Journal of Geophysical Research: Oceans*, 114 (C1). <https://doi.org/10.1029/2008jc004974>
- Taburet, G., Sanchez-Roman, A., Ballarota, M., Pujol, M-L, Legeais, J-F., Fournier, F., Faugere, Y., and Dibarboure, G. 2019. DUACS DT2018: 25 years of reprocessed sea level altimetry products. *Ocean Science* 15 (5): 1207-1224 <https://doi.org/10.5194/os-15-1207-2019>
- Tel, E., Balbin, R., Cabanas, J-M., Garcia, M-J., Garcia-Martinez, M. C., Gonzalez-Pola, C., Lavin, A., *et al.* 2016. IEOOS: the Spanish Institute of Oceanography Observing System. *Ocean Science*, 12 (2): 345–353, <https://doi.org/10.5194/os-12-345-2016>.
- van Aken, H. M. 2002. Surface currents in the Bay of Biscay as observed with drifters between 1995 and 1999. *Deep Sea Research Part I: Oceanographic Research Papers*, 49 (6): 1071–1086. [https://doi.org/10.1016/s0967-0637\(02\)00017-1](https://doi.org/10.1016/s0967-0637(02)00017-1)
- Vélez-Belchí, P., González-Carballo, M., Pérez-Hernández, M. D., and Hernández-Guerra, A. 2015. Open ocean temperature and salinity trends in the Canary Current Large Marine Ecosystem. *In* *Oceanographic and biological features in the Canary Current Large Marine Ecosystem*, pp. 201–213. Ed. by L. Valdés and I. Déniz-González. IOC Technical Series No. 115. IOC-UNESCO, Paris. 383 pp.
- Vélez-Belchí, P., Pérez-Hernández, M. D., Casanova-Masjoan, M., Cana, L., and Hernández-Guerra, A. 2017. On the seasonal variability of the Canary Current and the Atlantic Meridional Overturning Circulation. *Journal of Geophysical Research: Oceans*, 122 (6): 4518–4538. <https://doi.org/10.1002/2017jc012774>
- Yashayaev, I., and Loder, J. W. 2009. Enhanced production of Labrador Sea Water in 2008. *Geo-physical Research Letters*, 36 (1). <https://doi.org/10.1029/2008GL036162>
- Yashayaev, I., and Loder, J. W. 2016. Recurrent replenishment of Labrador Sea Water and associated decadal-scale variability. *Journal of Geophysical Research: Oceans*, 121 (11): 8095–8114. <https://doi.org/10.1002/2016JC012046>
- Yashayaev, I., and Loder, J. W. 2017. Further intensification of deep convection in the Labrador Sea in 2016. *Geophysical Research Letters*, 44 (3): 1429–1438. <https://doi.org/10.1002/2016gl071668>
- Yashayaev, I., van Aken, H. M., Holliday, N. P., and Bersch, M. 2007. Transformation of the Labrador Sea water in the subpolar North Atlantic. *Geophysical Research Letters*, 34 (22). <https://doi.org/10.1029/2007GL031812>

## Annex 1: Contact information for authors by section

Section	Area/topic	Authors	E-mail	Affiliation
<b>2. Summary of upper ocean conditions in 2018</b>				
2.3	Argo gridded temperature and salinity fields	Nicolas Kolodziejczyk	<a href="mailto:Nicolas.Kolodziejczyk@univ-brest.fr">Nicolas.Kolodziejczyk@univ-brest.fr</a>	University of Brest (UBO), CNRS, IRD, Ifremer, Laboratoire d'Océanographie Physique et Spatiale (LOPS, Laboratory for Ocean Physics and Satellite remote sensing), Brest, France
		Damien Desbruyères	<a href="mailto:Damien.Desbruyeres@ifremer.fr">Damien.Desbruyeres@ifremer.fr</a>	<a href="#">Laboratoire d'Océanographie Physique et Spatiale</a> (Ifremer/LOPS) Brest, France
2.4	Subpolar Gyre Index	León Chafik	leon.chafik@misu.su.se	Department of Meteorology (MISU), Stockholm University, Sweden
<b>3. The North Atlantic atmosphere</b>				
All		Stephen R. Dye	<a href="mailto:stephen.dye@cefas.co.uk">stephen.dye@cefas.co.uk</a>	Centre for Environment, Fisheries and Aquaculture Science (Cefas), Lowestoft, UK
<b>4. Detailed Area Descriptions, part I: The upper ocean</b>				
4.1	West Greenland	Boris Cisewski	<a href="mailto:boris.cisewski@thuener.de">boris.cisewski@thuener.de</a>	Thünen-Institut für Seefischerei (TI-SF, Thünen Institute of Sea Fisheries), Bremerhaven, Germany
4.2	Labrador Sea	Igor Yashayaev	<a href="mailto:Igor.Yashayaev@dfo-mpo.gc.ca">Igor.Yashayaev@dfo-mpo.gc.ca</a>	Fisheries and Oceans Canada (DFO), Bedford, Canada
4.3	Newfoundland-Labrador Shelf	Frédéric Cyr	<a href="mailto:Frederic.Cyr@dfo-mpo.gc.ca">Frederic.Cyr@dfo-mpo.gc.ca</a>	Fisheries and Oceans Canada (DFO), StJohn's, Newfoundland, Canada
		Peter Galbraith	<a href="mailto:Peter.Galbraith@dfo-mpo.gc.ca">Peter.Galbraith@dfo-mpo.gc.ca</a>	Maurice Lamontagne Institute, Fisheries and Oceans Canada

Section	Area/topic	Authors	E-mail	Affiliation
4.4	Gulf of Saint Lawrence	Peter Galbraith	<a href="mailto:Peter.Galbraith@dfo-mpo.gc.ca">Peter.Galbraith@dfo-mpo.gc.ca</a>	Maurice Lamontagne Institute, Fisheries and Oceans Canada
4.5	Scotian Shelf	David Hebert	<a href="mailto:David.Hebert@dfo-mpo.gc.ca">David.Hebert@dfo-mpo.gc.ca</a>	Fisheries and Oceans Canada (DFO), Bedford, Canada
		Chantelle Layton	<a href="mailto:Chantelle.Layton@dfo-mpo.gc.ca">Chantelle.Layton@dfo-mpo.gc.ca</a>	
		Peter Galbraith	<a href="mailto:Peter.Galbraith@dfo-mpo.gc.ca">Peter.Galbraith@dfo-mpo.gc.ca</a>	Maurice Lamontagne Institute, DFO, Canada
4.6	Northeast US continental shelf	Paula Fratantoni	<a href="mailto:paula.fratantoni@noaa.gov">paula.fratantoni@noaa.gov</a>	NOAA Fisheries, NEFSC, Oceans and Climate Branch, Woods Hole, MA, USA
4.7	Icelandic Waters	Solveig R. Ólafsdóttir	<a href="mailto:solveig.rosa.olafsdottir@hafogvatn.is">solveig.rosa.olafsdottir@hafogvatn.is</a>	Hafrannsóknastofnun (Marine and Freshwater Research Institute, MFRI), Reykjavík, Iceland
		Magnus Danielsen	<a href="mailto:magnus.danielsen@hafogvatn.is">magnus.danielsen@hafogvatn.is</a>	
4.8	Bay of Biscay and Iberian Coast	Almudena Fontán	<a href="mailto:afontan@azti.es">afontan@azti.es</a>	AZTI. Aquarium of San Sebastian (SOG) and Idalgo Meteorological Observatory (AEMet), San Sebastian, Spain
		Victor Valencia	<a href="mailto:vvalencia@azti.es">vvalencia@azti.es</a>	
		Cesar González-Pola	<a href="mailto:cesar.pola@ieo.es">cesar.pola@ieo.es</a>	
4.9	Gulf of Cadiz	Ricardo Sánchez-Leal	<a href="mailto:rleal@ieo.es">rleal@ieo.es</a>	Instituto Español de Oceanografía (IEO), Cádiz Oceanographic Centre, Cádiz, Spain
4.10	Canary Basin	Pedro Vélez-Belchí	<a href="mailto:pedro.velez@ieo.es">pedro.velez@ieo.es</a>	Instituto Español de Oceanografía (IEO, Spanish Institute of Oceanography), Canary Islands Oceanographic Centre, Tenerife, Spain
4.11	Southwest Approaches	Tim J. Smyth	<a href="mailto:TJSM@pml.ac.uk">TJSM@pml.ac.uk</a>	Marine Biological Association and Plymouth Marine Laboratory (PML), Plymouth, UK
4.12	Celtic Seas	Kieran Lyons	<a href="mailto:Kieran.lyons@Marine.ie">Kieran.lyons@Marine.ie</a>	Marine Institute/Met Eireann, Galway, Ireland
		Caroline Cusack	<a href="mailto:caroline.cusack@Marine.ie">caroline.cusack@Marine.ie</a>	

Section	Area/topic	Authors	E-mail	Affiliation
4.13	Rockall Trough	N. Penny Holliday	<a href="mailto:penny.holliday@noc.ac.uk">penny.holliday@noc.ac.uk</a>	National Oceanography Centre (NOC), Southampton UK
4.14	Hatton-Rockall Basin			
4.15	Iceland Basin	Sam Jones	<a href="mailto:Sam.Jones@sams.ac.uk">Sam.Jones@sams.ac.uk</a>	Scottish Association for Marine Science (SAMS), Oban, UK
4.16	Irminger Sea	M. Fremke de Jong	<a href="mailto:Femke.de.Jong@nioz.nl">Femke.de.Jong@nioz.nl</a>	Koninklijk Nederlands, Instituut voor Zeeonderzoek (NIOZ, Royal Netherlands Institute for Sea Research), Texel, Netherlands
4.17	Faroese Waters and the Faroe-Shetland Channel	Karin Margretha H. Larsen	<a href="mailto:karinl@hav.fo">karinl@hav.fo</a>	Havstovan (Faroe Marine Research Institute, FAMRI), Tórshavn, Faroe Islands
		Barbara Berx	<a href="mailto:Barbara.Berx@gov.scot">Barbara.Berx@gov.scot</a>	Marine Scotland Science (MSS), Aberdeen, UK
		Jenny Hindson	<a href="mailto:jennifer.hindson@gov.scot">jennifer.hindson@gov.scot</a>	
4.18	North Sea	Holger Klein	<a href="mailto:Holger.Klein@bsh.de">Holger.Klein@bsh.de</a>	Bundesamt für Seeschifffahrt und Hydrographie (BSH, Federal Maritime and Hydrographic Agency, Hamburg, Germany)
		Peter Loewe	<a href="mailto:peter.loewe@bsh.de">peter.loewe@bsh.de</a>	
		Manuela Köllner	<a href="mailto:manuela.koellner@bsh.de">manuela.koellner@bsh.de</a>	
		Katrin Latarius	<a href="mailto:katrin.latarius@bsh.de">katrin.latarius@bsh.de</a>	Institute of Marine Research (IMR), Bergen, Norway
		Kjell Arne Mork	<a href="mailto:kjell.arne.mork@hi.no">kjell.arne.mork@hi.no</a>	
		Jon Albretsen	<a href="mailto:jon.albretsen@hi.no">jon.albretsen@hi.no</a>	
4.19	Skaggerak, Kattegat and the Baltic Sea	Johanna Linders	<a href="mailto:johanna.linders@smhi.se">johanna.linders@smhi.se</a>	Swedish Meteorological and Hydrological Institute (SMHI), Göteborg, Sweden
		Tycjan Wodzinowski	<a href="mailto:tycjan@mir.gdynia.pl">tycjan@mir.gdynia.pl</a>	National Marine Fisheries Research Institute (MIR-PIB), Gdynia, Poland
		Taavi Liblik	<a href="mailto:taavi.liblik@taltech.ee">taavi.liblik@taltech.ee</a>	Tallinn University of Technology, Estonia

Section	Area/topic	Authors	E-mail	Affiliation
4.20	Norwegian Sea	Kjell-Arne Mork	<a href="mailto:kjell.arne.mork@hi.no">kjell.arne.mork@hi.no</a>	Institute of Marine Research (IMR), Bergen, Norway
4.21	Barents Sea	Alexander Trofimov	<a href="mailto:trofimov@pinro.ru">trofimov@pinro.ru</a>	Knipovich Polar Research Institute of Marine Fisheries and Oceanography (PINRO), Murmansk, Russian Federation
		Randi Ingvaldsen	<a href="mailto:randi.ingvaldsen@imr.no">randi.ingvaldsen@imr.no</a>	Institute of Marine Research (IMR), Bergen, Norway
4.22	Fram Strait	Agnieszka Beszczynska-Möller	<a href="mailto:abesz@iopan.gda.pl">abesz@iopan.gda.pl</a>	Institute of Oceanology, Polish Academy of Sciences (IOPAN), Sopot, Poland
		Wilken-Jon von Appen	<a href="mailto:Wilken-Jon.von.Appen@awi.de">Wilken-Jon.von.Appen@awi.de</a>	Alfred Wegner Institute, Helmholtz Centre for Polar and marine Research (AWI), Bremerhaven, Germany
<b>5. Detailed Area Descriptions, part II: The intermediate and deep ocean</b>				
5.1.1	Greenland Sea	Agnieszka Beszczynska-Möller	<a href="mailto:abesz@iopan.gda.pl">abesz@iopan.gda.pl</a>	Institute of Oceanology, Polish academy of sciences (IOPAN), Sopot, Poland
5.1.2	Norwegian Sea	Svein Østerhus	<a href="mailto:svos@norceresearch.no">svos@norceresearch.no</a>	Norwegian Research Institute (NORCE), Bergen
5.1.3	Iceland Sea	Sólveig R. Ólafsdóttir	<a href="mailto:solveig.rosa.olafsdottir@hafogvatn.is">solveig.rosa.olafsdottir@hafogvatn.is</a>	Hafrannsóknastofnun (Marine and Freshwater Research Institute, MFRI), Reykjavík, Iceland
		Magnus Danielsen	<a href="mailto:magnus.danielsen@hafogvatn.is">magnus.danielsen@hafogvatn.is</a>	
5.2.1	Iceland-Scotland Ridge overflow waters	Barbara Berx	<a href="mailto:Barbara.Berx@gov.scot">Barbara.Berx@gov.scot</a>	Marine Scotland Science (MSS), Aberdeen, UK
		Jenny Hindson	<a href="mailto:jennifer.hindson@gov.scot">jennifer.hindson@gov.scot</a>	
5.2.2	Iceland Basin	N. Penny Holliday	<a href="mailto:penny.holliday@noc.ac.uk">penny.holliday@noc.ac.uk</a>	National Oceanography Centre (NOC), Southampton UK
5.2.3	Rockall Trough	Sam Jones	<a href="mailto:Sam.Jones@sams.ac.uk">Sam.Jones@sams.ac.uk</a>	Scottish Association for Marine Science (SAMS), Oban, UK

Section	Area/topic	Authors	E-mail	Affiliation
5.2.4	Irminger Basin	M. Fremke de Jong	<a href="mailto:Femke.de.Jong@nioz.nl">Femke.de.Jong@nioz.nl</a>	Koninklijk Nederlands, Instituut voor Zeeonderzoek (NIOZ, Royal Netherlands Institute for Sea Research), Texel, Netherlands
5.2.5	Labrador Basin	Igor Yashayaev	<a href="mailto:Igor.Yashayaev@dfo-mpo.gc.ca">Igor.Yashayaev@dfo-mpo.gc.ca</a>	Ocean Monitoring and Observation Section, Oceans and Ecosystem Division, Bedford Institute of Oceanography, Fisheries and Oceans (BIO), Bedford, Canada
		Boris Cisewski	<a href="mailto:boris.cisewski@thuenen.de">boris.cisewski@thuenen.de</a>	Thünen-Institut für Seefischerei (TI-SF, Thünen Institute of Sea Fisheries), Bremehaven, Germany
5.2.6	Western Iberian Basin	Cesar González-Pola	<a href="mailto:cesar.pola@ieo.es">cesar.pola@ieo.es</a>	Instituto Español de Oceanografía (IEO, Spanish Institute of Oceanography), Gijón Oceanographic Centre, Gijón, Spain
5.2.7	Gulf of Cadiz	Ricardo Sánchez-Leal	<a href="mailto:rleal@ieo.es">rleal@ieo.es</a>	Instituto Español de Oceanografía (IEO, Spanish Institute of Oceanography), Cádiz Oceanographic Centre, Cádiz, Spain
5.2.8	Canary Basin	Pedro Vélez-Belchí	<a href="mailto:pedro.velez@ieo.es">pedro.velez@ieo.es</a>	Instituto Español de Oceanografía (IEO, Spanish Institute of Oceanography), Canary Islands Oceanographic Centre, Tenerife, Spain

## Annex 2: List of abbreviations and acronyms

<b>AAIW</b>	Antarctic Intermediate Waters
<b>AI</b>	Atlantic Inflow
<b>AIW</b>	Arctic Intermediate Water
<b>ARGO</b>	Not an acronym, but the name of a type of instrument used to collect data. The name ARGO is a reference to Greek mythology.
<b>Argo-GDAC</b>	Argo - Global Data Assembly Centres
<b>AW</b>	Atlantic Water
<b>BSH</b>	Bundesamt für Seeschifffahrt und Hydrographie (German Federal Maritime and Hydrographic Agency)
<b>CCLME</b>	Canary Current Large Marine Ecosystem
<b>CIL</b>	Cold Intermediate Layer
<b>CIRES</b>	Cooperative Institute for Research in Environmental Sciences, USA
<b>CTD</b>	Conductivity Temperature Depth
<b>CTZ</b>	Coastal Transition Zone
<b>DSOW</b>	Denmark Strait Overflow Water
<b>EGC</b>	East Greenland Current
<b>ENACW</b>	Eastern North Atlantic Central Waters
<b>GSDW</b>	Greenland Sea Deep Water
<b>ICES</b>	International Council for the Exploration of the Sea
<b>Ifremer</b>	Institut Français de Recherche pour l'Exploitation de la Mer (French Institute for Ocean Research)
<b>IROC</b>	ICES Report on Ocean Climate
<b>ISAS</b>	<i>In Situ</i> Analysis System
<b>ISOW</b>	Iceland Scotland Overflow Water
<b>LME</b>	Large marine ecosystem
<b>LSW</b>	Labrador Sea water
<b>MLD</b>	Mixed-layer depth
<b>MNAW</b>	Modified North Atlantic Water
<b>MOW</b>	Mediterranean Overflow Water
<b>MW</b>	Mediterranean Waters
<b>NAC</b>	North Atlantic Current
<b>NACW</b>	North Atlantic Central Waters
<b>NADW</b>	North Atlantic Deep Waters

<b>NAO</b>	North Atlantic Oscillation
<b>NAW</b>	North Atlantic Water
<b>NOAA</b>	National Oceanic and Atmospheric Administration (USA)
<b>NRT</b>	Near real time
<b>OI</b>	Optimal interpolation
<b>OISST.v2</b>	Optimum interpolation SST dataset version 2
<b>RAC</b>	Return Atlantic Current
<b>RAW</b>	Return Atlantic Water
<b>s.d.</b>	Standard deviation
<b>SLP</b>	Sea level pressure
<b>SST</b>	Sea surface temperature
<b>SSS</b>	Sea surface salinity
<b>UPDW</b>	Upper Polar Deep Water
<b>WGC</b>	West Greenland Current
<b>WGOH</b>	ICES Working Group Oceanic Hydrography
<b>WGWIDE</b>	ICES Working Group on Widely Distributed Stocks
<b>WOA5</b>	World Ocean Atlas 05